Virtual Energy Storage for Frequency and Voltage Control

Saif Sabah Sami

School of Engineering

Cardiff University

A thesis submitted for the degree of

Doctor of Philosophy

July 2017

A journey of a thousand miles begins with a single step

-Lao Tzu

The more you know, the more you know you do not know

-Aristotle

If we knew what it was we were doing; it would not be called research, would it?

-Albert Einstein

This work is dedicated to my beloved country…Iraq

Table of contents

Abstract

The secure and economic operation of the future power system is facing major challenges. These challenges are driven by the increase of the penetration of converter connected and distributed renewable generation and electrified demand. In this thesis, a new smart energy management paradigm, i.e. a Virtual Energy Storage System (VESS), to address these challenges was studied. A VESS aggregates energy storage and flexible demand units into a single entity which performs similarly to a large-capacity conventional energy storage system. A VESS mitigates the uncertainty of the response from flexible demand through coordination with a minimum capacity of costly energy storage systems.

Mathematical models of four components of a VESS were developed. Specifically, models of two types of energy storage, i.e. flywheel energy storage and battery energy storage, were developed. Thermodynamic models of two types of flexible demand units, i.e. domestic refrigerators and industrial bitumen tanks, were developed. These models were validated against the performance of similar equipment from the literature. Aggregated models, representing a population of units, for each of flywheels, batteries, refrigerators and bitumen tanks were developed. These aggregated models represent a randomly diversified population of units. These aggregated models were used to establish the frequency and the voltage control schemes of a VESS.

A frequency control scheme of the VESS was designed. The control scheme provides low, high and continuous frequency response services to the system operator. The centralised control scheme coordinates models of refrigerators and units of the flywheel energy storage system. Following frequency deviations, the local frequency controllers of refrigerators changed their power consumption. The local frequency controllers of the flywheel units cover the power mismatch between the change in refrigerators power consumption and the required response from the VESS. The required response from the VESS is determined by a droop control. Case studies were conducted to evaluate the frequency control scheme by connecting the VESS to a simplified GB power system. Results showed that the response from the frequency control scheme of the VESS was similar to that of only flywheel energy storage. Based on an economic evaluation, the VESS is estimated to obtain approximately 50% higher return compared with the case

that only uses flywheel energy storage system. These revenues are based on providing frequency response services to the system operator.

A voltage control scheme of the VESS was also designed. The control scheme facilitates the integration of distributed renewable energy generation by enhancing the voltage control of the distribution network. The control scheme coordinates models of bitumen tanks and battery energy storage system through different time delay settings of their voltage controllers. The local voltage controllers of bitumen tanks alter their power consumption following significant voltage deviations. If voltage violations continue, the distributed voltage controller of the battery energy storage system charges or discharges the battery using a droop setting obtained from voltage sensitivity factors. A case study was undertaken to assess the voltage control scheme by connecting the VESS, solar panels and wind farms to a UK Generic Distribution System (UKGDS) network. Results showed that the voltage control scheme made a significant improvement in the voltage and reduced tap changing actions of the on-load tap changing transformer and the voltage regulator by approximately 30 % compared with the base case where no VESS was used. Based on an economic evaluation, The VESS is an efficient solution to accommodate distributed renewable energy generation compared with network reinforcement.

Declaration

This work has not been submitted in substance for any other degree or award at this or any other university or place of learning, nor is being submitted concurrently in candidature for any degree or other award.

Signed ..Saif...Sabah.Sami.. (candidate) Date ..07/07/2017..

STATEMENT 1

This thesis is being submitted in partial fulfilment of the requirements for the degree of PhD.

Signed ..Saif...Sabah.Sami.. (candidate) Date ..07/07/2017..

STATEMENT 2

This thesis is the result of my own independent work/investigation, except where otherwise stated, and the thesis has not been edited by a third party beyond what is permitted by Cardiff University's Policy on the Use of Third Party Editors by Research Degree Students. Other sources are acknowledged by explicit references. The views expressed are my own.

Signed ..Saif...Sabah.Sami.. (candidate) Date ..07/07/2017..

STATEMENT 3

I hereby give consent for my thesis, if accepted, to be available online in the University's Open Access repository and for inter-library loan, and for the title and summary to be made available to outside organisations.

Signed ..Saif...Sabah.Sami.. (candidate) Date ..07/07/2017..

Acknowledgement

I am deeply thankful to God for His amazing grace, then to the following people, without whom this endeavour would not have been possible.

I would like to express my immense gratitude to my supervisors, Professor Jianzhong Wu and Professor Nick Jenkins, for providing me with the opportunity to carry out this highly interesting and relevant research, as well as for their continued supervision and support. Their vision and understanding of the key research challenges in this area have been invaluable for guiding my work.

I am indebted to my co-author and team member Dr Meng Cheng for the help she provided, not to mention the significant amount of time she spent discussing and purifying my ideas.

I am also indebted to my colleagues, Dr Yue Zhou, Dr Muditha Abeysekera, Dr Lee Thomas and Dr Chao Long for their support proofreading and reviewing the thesis.

My thanks also go out to all my colleagues in the smart grid group and the Centre for Integrated Renewable Energy Generation and Supply (CIREGS) for their support, encouragement and fruitful discussions during meetings and seminars, especially Mr Mazin T. Muhssin and Mr Zeyad A. Obaid.

I am particularly grateful to the advice of Professor Janaka Ekanayake and Dr Carlos Ugalde-loo, who in the early stages of this work helped me through discussions and suggestions.

I am eternally grateful for the financial support from the Higher Committee for Education Development in Iraq (HCEDiraq) through all my years of PhD studies.

Special thanks to Mrs Jeanette Whyte, Mrs Chris Lee, Mrs Aderyn Reid and Ms Sandra Chelmis for their motherly care and kindness throughout my three years in Cardiff.

Special thanks also to my B.Sc., M.Sc. and PhD colleague and friend Dr Ali Saad Al-Wakeel for his brotherly support throughout the years.

I would like to thank my parents, who have fostered my thirst for knowledge from the early childhood and have always taken great pride in my academic achievements, brother and sisters for their enormous love and support.

Finally, I would like to thank my wife and son for their steadfast patience and support and for putting up with anything but conventional working hours. Completing this thesis would have simply not been possible without them.

List of Figures

List of Tables

List of Abbreviations

BESS	Battery Energy Storage System
BT	Bitumen Tank
CADC	Coordinated Adaptive Droop Control
CAES	Compressed Air Energy Storage System
CCDC	Coordinated Constant Droop Control
CDC	Conventional Droop Control
CHP	Combined Heat and Power
DG	Distributed Generation
DNO	Distribution Network Operator
DR	Demand Response
DSM	Demand-Side Management
DSR	Demand-Side Response
EFR	Enhanced Frequency Response
ESS	Energy Storage System
EV	Electric Vehicle
FCDM	Frequency Control by Demand Management
FESS	Flywheel Energy Storage System
FFR	Firm Frequency Response
GB	Great Britain
HESS	Hydrogen-based Energy Storage System
ICT	Information and Communications Technology
Ofgem	Office for Gas and Electricity Markets
OLTC	On-Load Tap Changing transformer
PHES	Pumped Hydro Energy Storage
PLL	Phase-Locked Loop
PMSM	Permanent Magnet Synchronous Machine
PV	Photovoltaics
RTU	Remote Terminal Units
SoC	State of Charge
TESS	Thermal Energy Storage System
UK	United Kingdom
UKGDS	United Kingdom Generic Distribution System

VESS	Virtual Energy Storage System
VPP	Virtual Power Plant
VR	Voltage Regulator
VSC	Voltage Source Converter

CHAPTER 1

Introduction

1.1. Anticipated changes and challenges in the GB power system

The transition from fossil fuels based energy to renewable energy is driven by two reasons, the potential shortage of fossil fuels at reasonable prices and the emissions that come from burning them [1]. The United Kingdom (UK) of Great Britain (GB) and Northern Island (NI) is legally bound to provide the means for 15% of its energy needs to be met by renewable energy resources by 2020 [2], which includes the following targets:

- 30% of the UK electricity consumption is provided by renewable energy resources
- 10% of the UK energy used in transport is supplied by renewable energy resources
- 12% of the UK heat demand is supplied by renewable energy resources

Therefore, the Great Britain (GB) power system is facing challenges to fulfil the government's commitments to increase the proportion of energy consumption from renewable energy resources and accommodate electrified transport and heat demand. National Grid, the system operator in the GB power system, proposed four energy scenarios to outline the possible sources of and demand for electricity in the future. These future energy scenarios are [3]:

1. **Consumer Power**: which is a market-driven world, with limited government intervention. High levels of prosperity allow for high investment and innovation. New technologies are prevalent and focus on the desires of consumers over and above reducing greenhouse gas emissions. a wealthy and a market-driven world.
2. **Gone Green**: which is a world where policy interventions and innovation are both ambitious and effective in reducing greenhouse gas emissions. The focus on long-term environmental goals, high levels of prosperity and advanced European harmonisation ensure that the 2050 carbon reduction target is achieved. is a wealthy world where environmental sustainability is a top priority.

3. **No Progression**: which is a world where business as usual activities prevail. Society is focused on the short term, concentrating on affordability above green ambition. Traditional sources of gas and electricity continue to dominate, with little innovation altering how energy is used.
4. **Slow Progression**: which is a world where economic conditions limit society's ability to transition as quickly as desired to a renewable, low carbon world. Choices for residential consumers and businesses are restricted, yet a range of new technologies and policies develop. This results in some progress towards decarbonisation but at a slower pace than society would like.

In all but one of the GB future scenarios, i.e. No Progression, the installed capacity of renewable energy generation is expected to increase as shown in Fig. 1.1 [3]. Between March and June of this year (i.e. 2017), for dispersed days and a brief period, more than 50 % of the UK electricity was supplied by renewable energy resources, which include the wind, the solar, the hydro and the biomass energies [4, 5].

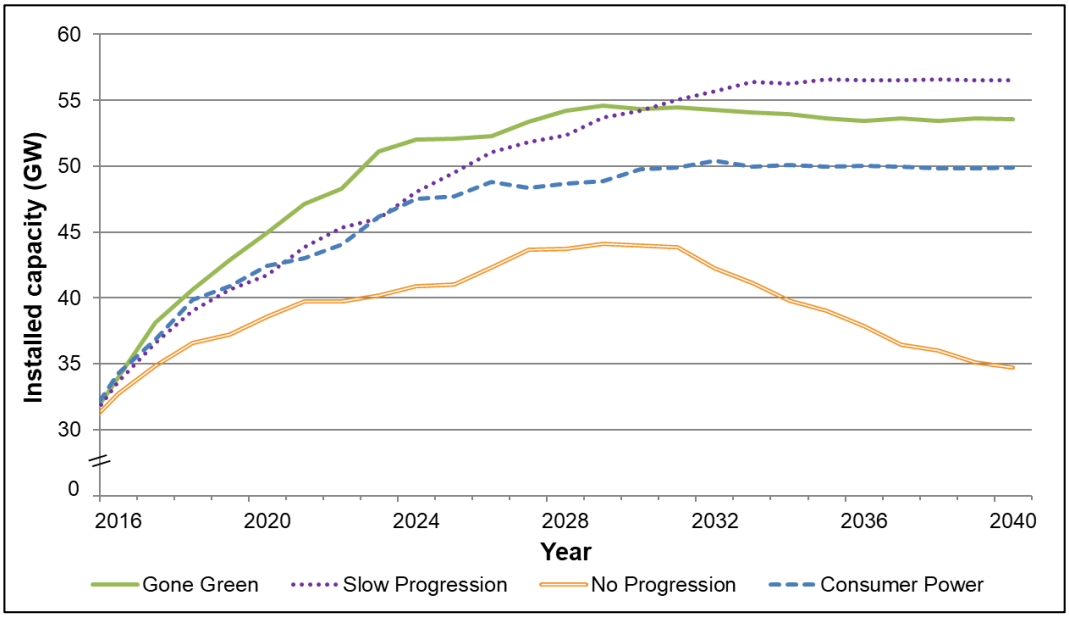

Fig. 1.1 Estimated percentages of the installed renewable energy generation in GB [3].

Increasing the penetration of renewable energy resources in the generation will give rise to two significant challenges. The intermittency associated with some renewable energy resources, e.g. the wind and the solar energies, poses a serious challenge for the operation and planning of the power system [6]. The second challenge is to maintain a sufficient inertia to confront any disturbance in the frequency. The system inertia is reduced when renewable energy generators displace synchronous generators in the generation [7].

The renewable energy generators include large-capacity units that are commonly connected to transmission networks and small-capacity units that are typically connected to distribution networks, i.e. part of Distributed Generation (DG). Distributed renewable energy generation bring some economic and technical benefits for the power system such as reducing the network losses, short construction times and lower capital costs of the smaller plant. However, a high penetration of distributed renewable energy generation leads to voltage changes, protection and power quality problems in the distribution networks [8]. Figure 1.2 shows the projected installed capacities percentage of the distributed renewable energy generation in the GB per four different future energy scenarios [3].

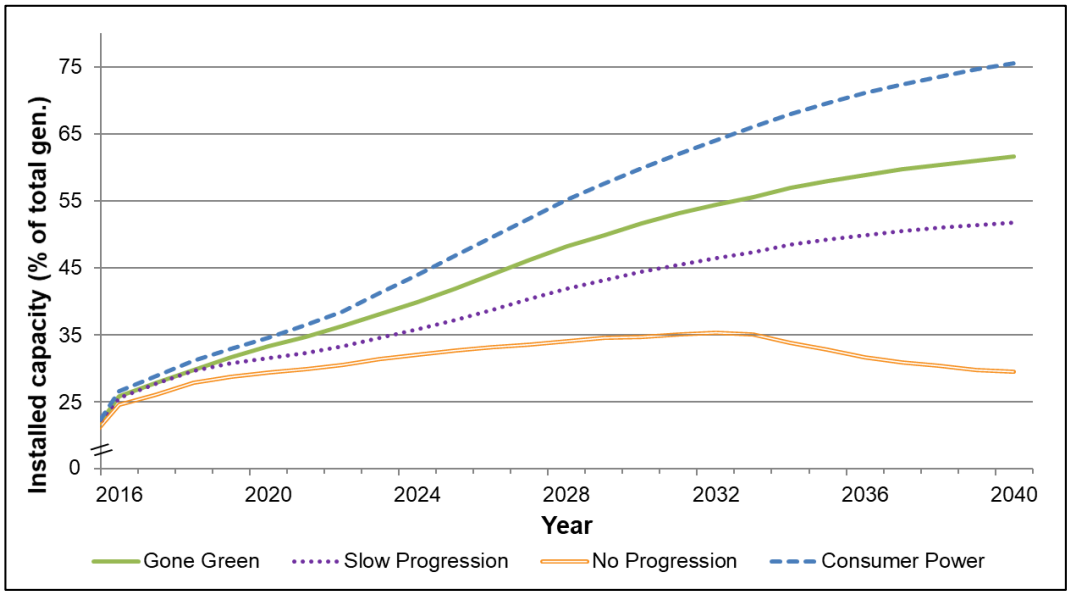

Fig. 1.2 Anticipated installed capacities of distributed renewable energy generation as a percentage of total generation in the GB power system for the four future energy scenarios [3].

The transport sector contributes just under a quarter of GB's greenhouse gas emissions [3]. As the number of Electric Vehicles (EVs) replacing combustion engine vehicles increases, the carbon emissions from the transport sector will decrease. When the number of electric vehicles increases in the GB, their estimated peak demand increases. Figure 1.3 shows the estimated peak demand of electric vehicles in GB for the different GB future energy scenarios [3]. Similarly, the replacement of fossil fuel heating systems with electric heating systems can reduce greenhouse gas emissions [9].

Accommodating the distributed renewable energy generation and the electrification of transport, e.g. electric vehicles, and heat demand, e.g. electric heat pumps, could lead to a high investment in the network reinforcement [10]. The Office for Gas and Electricity

Markets (Ofgem) estimated that the UK would need to invest as much as £53.4 billion in the electricity network between 2009 and 2025 [11]. The electrification of transport and heat demand could also lead to both thermal and voltage constraints violations in distribution networks [12].

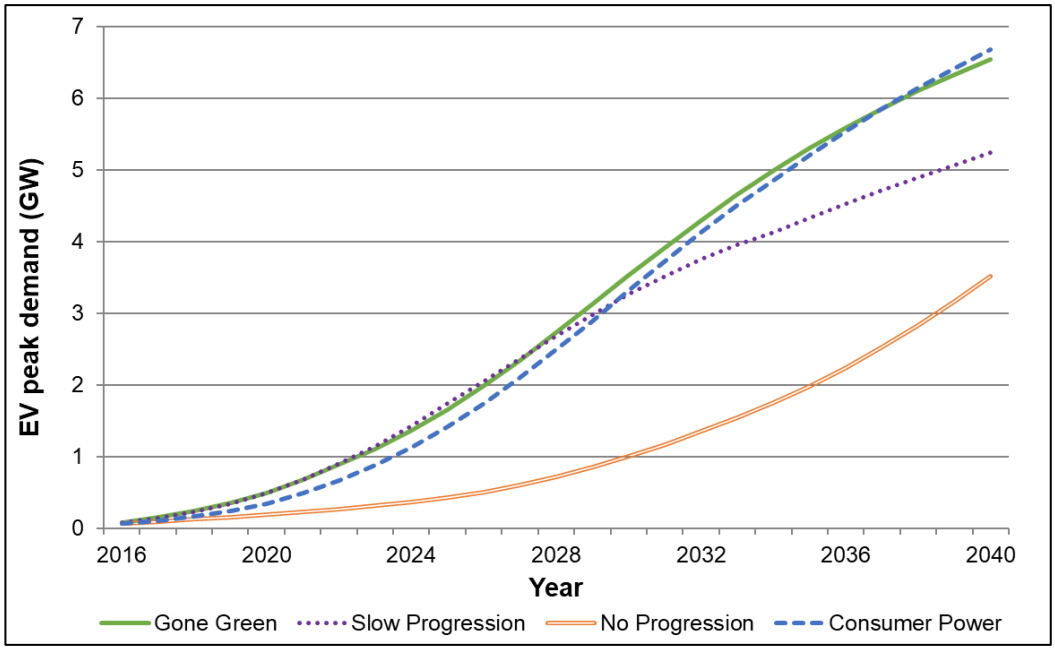

Fig. 1.3 Anticipated peak demand of electric vehicles in the GB [3].

1.2. Potential roles of energy storage systems and flexible demand in the GB power system

Energy Storage Systems (ESSs) can play a vital role in facilitating the transition to a power system with a high penetration of renewable energy generation through the improvement in the utilisation of renewable energy generation, the provision of flexible balancing services, and providing fast frequency response [13]. The installed capacity of energy storage systems is estimated to grow in the GB future energy scenarios as shown in Fig. 1.4 [3], where the pumped hydro energy storage systems were excluded from the estimation.

The management of flexible demand can provide various services to the power system by modifying the load consumption patterns. Such services include load shifting, peak load clipping and dynamic energy management [14]. It is estimated in [15] that the management of flexible demand has the potential to reduce the market size of energy storage systems by 50% in 2030.

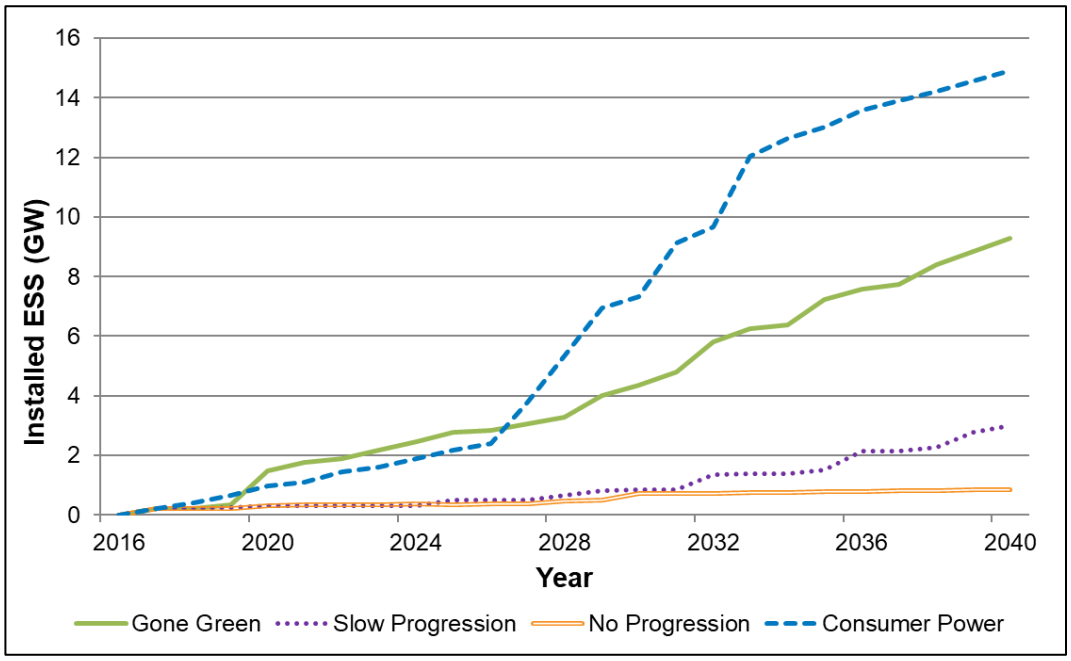

Fig. 1.4 Estimated new installed storage capacity (excluding pumped storage) in GB [3].

It is estimated in the Gone Green GB future energy scenario [3] that, flexible industrial and commercial demand can reduce their demand by approximately 5.7 GW and the flexible residential demand can reduce their demand by approximately 1.4 GW during peak time in 2030. This is equivalent to a peak reduction of approximately 10% from flexible commercial and industrial demand and approximately 2% from the flexible residential demand. Figure 1.5 shows the electricity demand of the GB power system by sector in 2015 [16]. As shown in Fig. 1.5, the domestic, industrial and commercial demand represent most of the electricity consumed in GB in 2015.

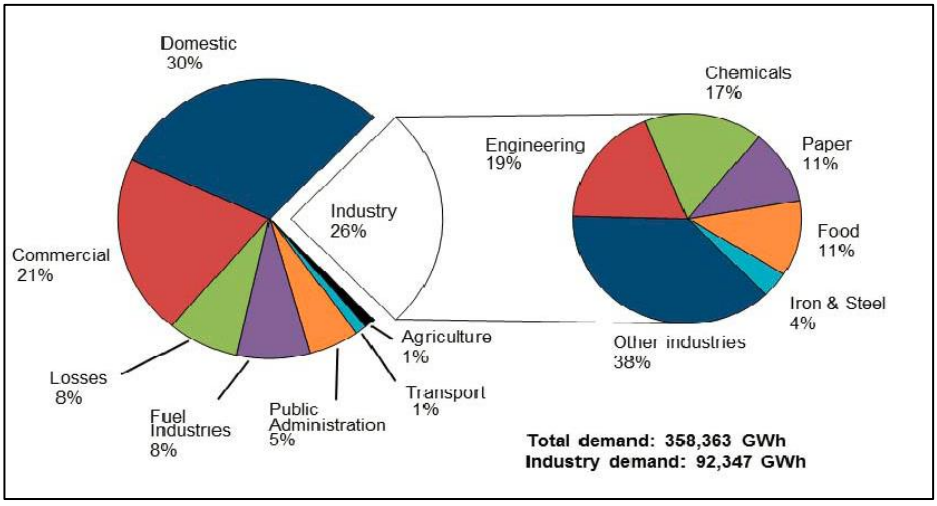

Fig. 1.5 The electricity demand of GB power system by sector in 2015 [16].

Most of the domestic consumption in 2012 was in lighting and appliances as shown in Fig. 1.6.a [17], which includes cold appliances (e.g. refrigerators) and wet appliances

(e.g. washing machine). Where the allocation of demand between different lighting and applications categories is shown in Fig. 1.6.b [17].

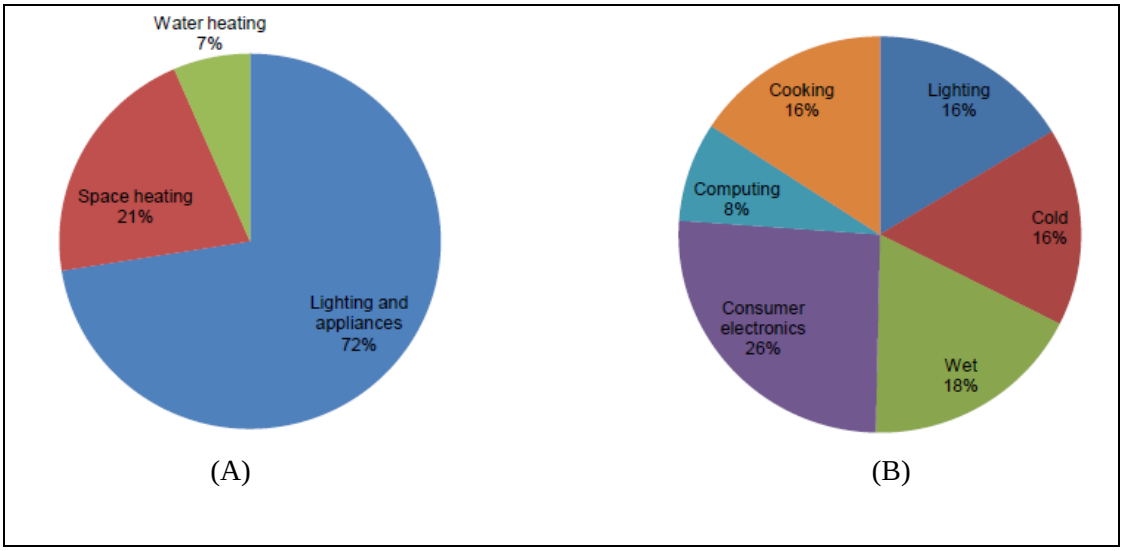

Fig. 1.6 (A) GB annual electricity demand in 2012 and (B) the domestic demand – lighting and appliances in 2012 [17].

1.3. Research motivation

The transition to a GB power system that is able to achieve the targets listed in section 1.1 is by no means straightforward. The challenges raised due to this transition, e.g. the reduction in the whole power system inertia and the voltage problems in distribution networks, were the focus of many studies. Several studies proposed the use of energy storage systems or flexible demand to address these challenges. However, the cost and regulations are the key challenges for a significant deployment of energy storage systems [3]. Moreover, the challenges facing the response from flexible demand, include the uncertainty of the response and the consequent reduction in the diversity amongst the demand response units [18].

While other researchers presented either energy storage systems or flexible demand as a potential solution, comparatively little research was conducted to coordinate both of them for a better performance and reduced costs to tackle those challenges. Control schemes that coordinate energy storage and demand response units to address the challenges above are the subject investigated in this research and reported in this thesis.

1.4. Research objectives

The objective of this research is to investigate the development of a mathematical model of a new smart management scheme of energy storage systems and demand response units and to demonstrate two of its potential applications, i.e. provide frequency

and voltage support. This new smart management scheme is called Virtual Energy Storage System (VESS). A VESS is able to provide services to the power system in a similar way to a conventional energy storage system with lower costs.

The aims of the research conducted and presented in this thesis were:

- **To develop the concept of a virtual energy storage system.**

  A virtual energy storage system mitigates the uncertainty of the response from flexible demand through the coordination with a minimum capacity of the costly energy storage systems.

- **To develop the mathematical models of the components of the virtual energy storage system**.

  The mathematical models of energy storage systems and demand response units are the components which form the virtual energy storage system. The choice of these models should reflect the diversity of the existing energy storage systems and the available types of flexible demand.

- **To investigate the use of a virtual energy storage system for frequency control.**

  A frequency control scheme of a virtual energy storage system is developed, providing frequency response services to the GB power system operator. The frequency control scheme delivers a certain amount of low, high and continuous frequency response at a lower cost compared with an equal capacity of only energy storage systems.

- **To investigate the use of a virtual energy storage system for voltage control.**

  A voltage control scheme of a virtual energy storage system to support voltage control in distribution networks is developed. The voltage control scheme facilitates the connection of more distributed generation through the coordination with the existing voltage control equipment.

1.5.Contributions of this thesis

This research contributions can be highlighted as

• The development of the concept of the Virtual Energy Storage System (VESS) to minimise demand response uncertainty and reduce the capacity of the costly energy storage system.

• The development of two energy storage systems mathematical models, i.e. flywheel and battery, and two demand response units' mathematical models, i.e. refrigerators and bitumen tanks, as components of the VESS.

• The development of the frequency control scheme of the VESS to provide low, high and continuous frequency response services to the power system operator with higher revenues compared with using only the flywheel energy storage system.

• The development of the voltage control scheme of the VESS to support distribution networks to accommodate more DG without violating the voltage constraint and upgrading network infrastructure.

This research has resulted in the following publications:

• Cheng, M., Sami, S.S. and Wu, J., "Virtual Energy Storage System for Smart Grids," Energy Procedia, vol. 88, pp.436-442, 2016.

• Sami, S.S., Cheng, M. and Wu, J., "Modelling and control of multi-type grid-scale energy storage for power system frequency response," In IEEE Power Electronics and Motion Control Conference, pp. 269-273. 2016.

• Cheng, M., Sami, S.S. and Wu, J., "Benefits of using virtual energy storage system for power system frequency response," Applied Energy, vol. 194, pp. 376-385, 2017.

• Sami, S.S., Cheng, M., Wu, J. and Jenkins, N., "Virtual energy storage system for voltage control of distribution networks," CSEE Journal of Power and Energy Systems, accepted for publication, 2017.

1.6. Thesis structure

Figure 1.7 shows the outline of this thesis. This thesis has six chapters.

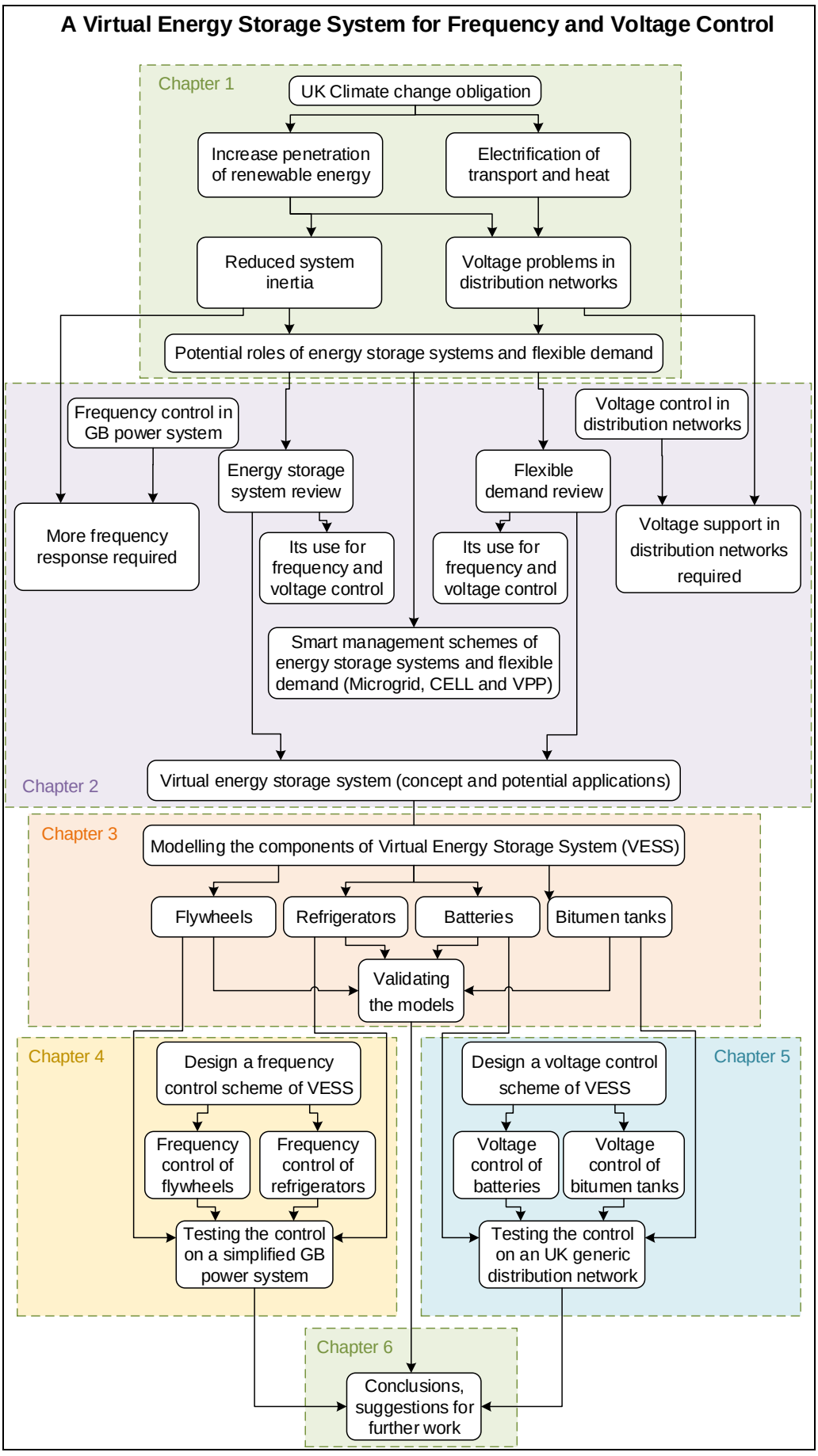

Fig. 1.7 The thesis outline.

Chapter 2 presents the literature review which covers the following areas:

- The frequency control in the GB power system and the voltage control in distribution networks in GB.
- The challenges facing the frequency control and the voltage control.
- Existing smart management schemes of distributed energy resources, e.g. energy storage and demand response units, namely Microgrid, CELL and VPP.
- Types of energy storage systems used in the power system and previous studies that propose using it for the frequency control and the voltage control.
- The definition of demand-side integration and previous studies that propose using it for the frequency control and the voltage control.
- The definition of the Virtual Energy Storage System (VESS), its potential applications in the power system and the difference between the VESS and other smart management schemes of distributed energy resources presented earlier.

Chapter 3 presents the mathematical modelling and validating the models of the components of the virtual energy storage system which include:

- Developing the simplified model of a flywheel energy storage system.
- Developing the simplified model of a battery energy storage system.
- Developing a thermodynamic model of a domestic refrigerator.
- Developing a thermodynamic model of an industrial bitumen tank.
- Validating the developed models.
- Developing the aggregated model of a population of flywheels, the aggregated model of a population of batteries, the aggregated model of a population of refrigerators, the aggregated model of a population of bitumen tanks.

Chapter 4 presents the design and the assessment of a frequency control scheme of a virtual energy storage system which include:

- Developing the outline of the frequency control scheme.
- Developing the distributed frequency control of the refrigerator.
- Developing the distributed frequency control of the flywheel energy storage system.
- Demonstrating the effectiveness of the control scheme through a test system which includes a population of refrigerators and a population of flywheels connected to a simplified GB power system.

- Assessing the control scheme through three case studies which are a low-frequency response, a high-frequency response and a contentious frequency response.
- Presenting a simple economic evaluation of the frequency control scheme.

Chapter 5 presents the design and the evaluation of a voltage control scheme of a virtual energy storage system which include:

- Developing the outline of the voltage control scheme.
- Developing the distributed voltage control of the bitumen tank.
- Developing the distributed voltage control of the battery energy storage system.
- Demonstrating the effectiveness of the control scheme through a test system which includes the wind and the solar energy generation, a population of bitumen tanks and a battery energy storage system connected to a UK generic distribution network.
- Evaluating the control scheme through a case study that covers different seasons of the year.
- Presenting a simple economic evaluation of the voltage control scheme.

Chapter 6 presents the research findings and conclusions which include:

- Presenting the conclusions that are drawn from the research conducted in this thesis.
- Presenting the contributions and achievements of this research in terms of publications.
- Introducing the suggestions for further work on the virtual energy storage system.

CHAPTER 2

Literature review

2.1. Frequency control in the GB power system

Power system frequency is a continuously changing variable that indicates the real-time balance between the system demand and the total generation [19]. National Grid, the system operator of the Great Britain (GB) power system, is responsible for maintaining the frequency within the operational limits of ±0.2 Hz (i.e. 49.8 Hz to 50.2 Hz) and statutory limits of ±0.5 Hz (i.e. 49.5 Hz and 50.5 Hz) [20]. Under normal operation conditions, the frequency control is provided by large-capacity synchronous generators [21, 22]. Under significant frequency drop, i.e. below 49.2 Hz, the frequency control is provided by both generators and demand disconnection by low-frequency relays. Table 2.1 describes the frequency containment policy in the GB power system specified by the regulations [23].

TABLE 2.1 THE FREQUENCY CONTAINMENT POLICY OF THE GB POWER SYSTEM [23]

Frequency Deviation	Description
±0.2 Hz	System frequency under normal conditions and the maximum frequency change for the loss of generation or the connection of demand up to ±300 MW
±0.5 HZ	Maximum frequency change for the loss of generation greater than ±300 MW and less than or equal to ± 1320 MW
-0.8 Hz	Maximum frequency change for the loss of generation greater than 1320 MW and less than or equal to 1800 MW. The frequency must be restored to at least 49.5 Hz within 1 minute

National Grid procures a variety of balancing services, i.e. reserve services and system security services, frequency response services, to maintain the frequency within limits and restore the frequency after sudden changes in the generation or the demand. Both the generation and the demand are involved in these services [19].

The frequency response services include [19] Mandatory Frequency Response (MFR), Firm Frequency Response (FFR), Enhanced Frequency Response (EFR) and Frequency Control by Demand Management (FCDM).

- **Mandatory Frequency Response** is an automatic change in the active power output in response to a frequency change. All large-capacity generators[1][24] connected to the transmission system are obligated [21] to provide this service. These generators operate with a speed droop between 3% to 5% and a frequency dead-band of 0.03 Hz or smaller. Mandatory Frequency Response is achieved by using one or more of *Primary response, Secondary response* and *High frequency responses.*

  Primary response is an automatic increase in the active power output in response to a frequency fall. This increase is released within 10 seconds from the frequency fall and it is sustainable for a further 20 seconds.

  Secondary response is an automatic increase in the active power output in response to a frequency fall. The power output must be fully available within 30 seconds from the frequency fall and it is sustainable for a further 30 minutes.

  High frequency response is an automatic reduction in the active power output in response to a frequency rise. This reduction is released within 10 seconds from the frequency rise and it is sustainable indefinitely.
- **Firm Frequency Response** is the provision of a dynamic or a non-dynamic response to changes in the frequency. National Grid acquire this service from generators (i.e. excluded from the mandatory frequency response) or the demand through a competitive tender process. Tenders can be for low-frequency events, high-frequency events or both [25].
- **Frequency Control by Demand Management** is the provision of a response through the interruption of the demand, where a low-frequency value automatically triggers a relay which interrupts the demand. This service is required to manage large deviations in the frequency where the demand may be interrupted for 30 minutes [26].
- **Enhanced Frequency Response** is the provision of 100% of the active power output at 1 second (or less) of measuring a frequency deviation and it is sustainable for 15 minutes [27]. This new service is triggered when the frequency exceeds the dead-band (i.e. ±0.015 Hz) to improve the frequency management of the system. Figure 2.1 shows the envelope of the expected response (i.e. the Gray area) from the enhance frequency response providers [28]. Any delivery outside the envelope (i.e. over-delivery or under-delivery in Fig. 2.1) will be penalised by a reduction in this

[1] All generators with capacity equal or larger than 100 MW in England and Wales and equal or larger than 10 MW in Scotland.

service payment. The under-delivery may not arrest the fall in the frequency to prevent a low-frequency event and the over-delivery could result in a high-frequency event [28]. National Grid recently contracted a total of 201 MW of energy storage system from different providers, most of which are estimated to start providing the service by the end of 2017 [19].

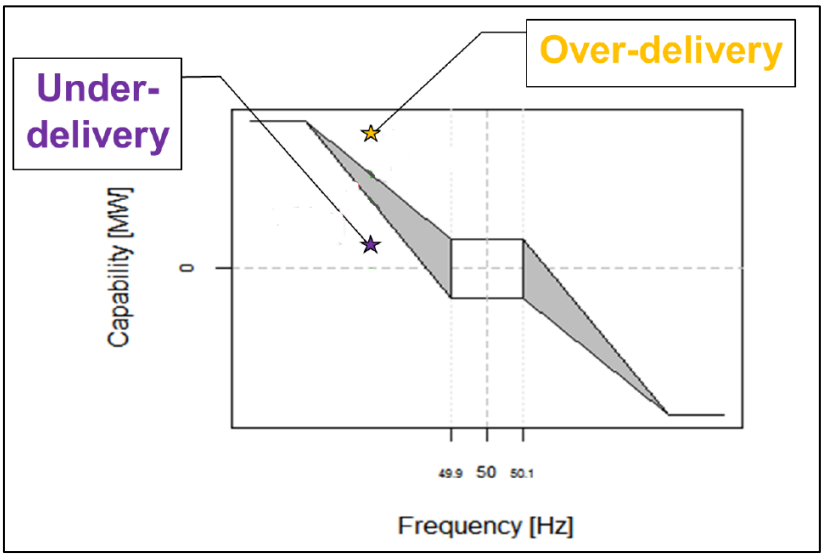

Fig. 2.1 The delivery envelope of the enhanced frequency response service [28].

Figure 2.2 illustrates the mandatory and the enhanced frequency response services with respect to time in the GB power system [7].

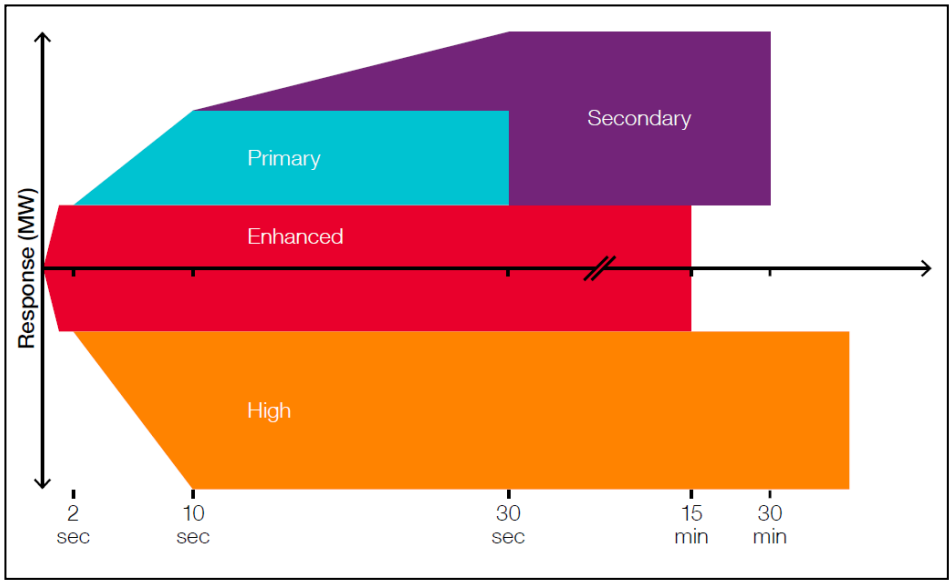

Fig. 2.2 The timescale of mandatory and enhanced frequency response services in the GB power system [7].

National Grid, at the present, is instructing conventional generators to run even if they are out of economic merit since they are part-loaded. This creates a minimum inertia

level to secure an adequate capacity for frequency response [7]. However, this capacity is expected to increase by 30-40% in the next 5 years in the GB power system [29]. These generators are therefore expensive to operate and produce large amounts of greenhouse gas emissions.

The capacity required from firm frequency response service is higher over the summer than the other seasons. This is because the demand is relatively lower in the summer and hence fewer synchronous generators are committed to supply the demand. The minimum daily capacity required varies between approximately 400 MW to 700 MW for the primary response and approximately 1200 MW to 1450 MW for the secondary response and approximately 0 MW to 150 MW for the high-frequency response [25]. Therefore, payments for frequency response services are varying as well. Table 2.2 shows these payments for July 2016 and January 2017 [30].

TABLE 2.2 PAYMENTS FOR DIFFERENT FREQUENCY RESPONSE SERVICES BY NATIONAL GRID IN JULY 2016 AND JANUARY 2017 [30]

Services	July 2016	January 2017
Mandatory response (Primary, Secondary and High response)	£2.4milion	£2.33milion
Firm Frequency Response and Frequency Control by Demand Management	£8.86milion	£7.71milion

2.2. Voltage control in distribution networks

The voltage in distribution networks varies with the variation of demand. Therefore the Distribution Network Operator (DNO) is obligated to keep the voltage variations within limits. Because electrical devices are designed to operate optimally at the nominal voltage and thus any deviation from this value can result in decreased efficiency, damage or severely reduced life of these devices [31].

For low voltage networks (voltages up to 1 kV), voltage variations should not exceed 10% above or 6% below the nominal value [32]. For high voltage networks (voltages from above 1 kV to 132 kV), voltage variations should not exceed ±6% of the nominal value [32]. For higher voltage networks (voltages from 132 kV and higher), voltage variations should not exceed ±10% of the nominal value [32].

The available methods and devices for voltage control in distribution networks include [33-35]:

- **On Load Tap Changers (OLTC) transformers**: The voltage on the secondary side of the transformer is kept within a certain dead-band by using an automatic tap changer that alters the transformer ratio.
- **Voltage Regulators (VR):** These devices are fundamentally autotransformers with many taps, and the desired voltage is obtained by automatically changing these taps.
- **Capacitors:** Shunt or switched capacitors supply a reactive power to the network, hence improving the voltage.

2.3. Challenges for frequency and voltage control

The key factors that pose challenges to the power system frequency and the voltage control in distribution networks are discussed hereafter in brief:

- **The reduction in the system inertia**

The growing capacity of renewable energy generators, presented in section 1.1, that displace synchronous generators in the generation leads to reduced system inertia. The system inertia determines the response of the power system to frequency disturbances due to a sudden loss of generation or load [36]. The system inertia defines how much energy is available in the rotating masses of all machines that are directly coupled to the system [7]. Approximately, 70% of the system inertia in the GB power system is provided by large-capacity synchronous generators. While smaller synchronous generators and synchronous demand provide the rest. The absence of direct coupling between the machine and the power system in some renewable energy resources, e.g. the wind and the solar energies, prevent them from contributing to the system inertia [7]. Figure 2.3 shows the frequency drop and the frequency response capacity needed of a simulated GB power system by National Grid with 20 GW of demand during a generation loss of 500 MW and different values of the system inertia [7]. As shown in Fig. 2.3, when the system inertia decrease, frequency response services procured are increased [7] to maintain an acceptable security level.

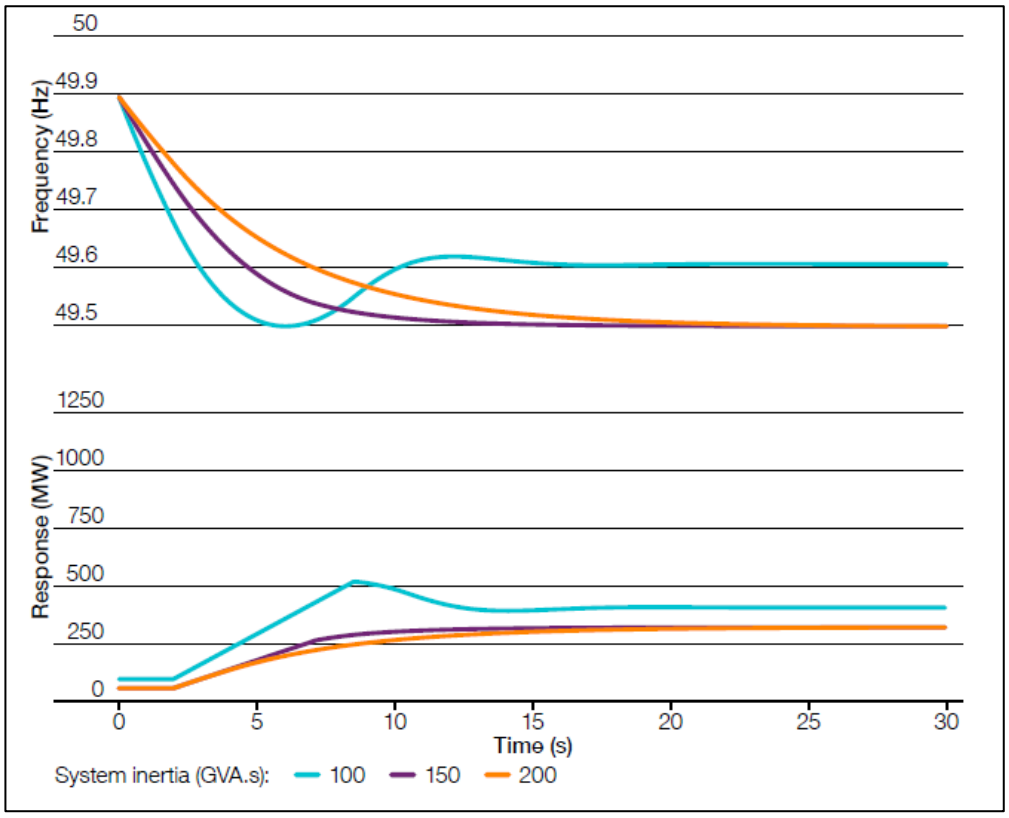

Fig. 2.3 The frequency containment and the required response capacity of a simulated GB power system [7].

- **The high penetration of distributed renewable generation**

The expected high penetration of renewable energy generation in distribution networks (i.e. shown in Fig. 1.2) also leads to high voltage problems, increased transient voltage variations and harmonic distortions [37]. Moreover, a large penetration affects the protection of distribution networks and the supplied energy quality [35, 38].

- **Electrification of the transport and heat demand**

The large deployment of Electric Vehicles (EV) may lead to low voltage problems and a low phase diversity, which will result in voltage and current imbalances in distribution networks [39]. Also, a massive deployment of EV may increase transformers degradation [40] in distribution networks. Consequently, more advanced strategies are needed to control the voltage in distribution networks [41].

The proliferation of low carbon heating systems may negatively impact the voltage and thermal limits of distribution networks [3]. Specifically, low voltage and high thermal limits problems may occur due to the high penetration levels of heat pumps in distribution networks [42, 43].

2.4. Smart management of distributed energy resources

In the research reported in this thesis, a new smart management scheme of distributed energy resources, i.e. virtual energy storage system, was investigated. As a background to the research that was carried out, the main existing smart management schemes of distributed energy resources are presented hereafter.

Distributed energy resources include Distributed Generation (DG), energy storage systems and demand response units. Several approaches were proposed to effectively manage a coordinated operation of distributed energy resources under constrained operation conditions. These approaches are aimed to integrate distributed energy resources into distribution networks rather than just connect them through the traditional passive manner existed in GB (i.e. fit and forget approach), in order to achieve a secure and more economic operation.

One approach to actively manage distributed energy resources is to break a distribution network into smaller entities such as Microgrids or wider unit control areas called CELLs [44], both of which are aimed to coordinate distributed energy resources to supply the local demand. Another approach is to establish a Virtual Power Plant (VPP) which aims to aggregate different distributed energy resources into a portfolio to participate in the wholesale market [44].

- **Microgrid**

A Microgrid is a small distribution network with distributed energy resources and it can operate in a non-autonomous way when connected to the grid, or in an autonomous way when disconnected from the main grid [45].

The control of a Microgrid involves controlling the voltage and the frequency. The coordinated operation of distributed energy resources can provide distinct benefits to the overall system performance, such as [44, 45] reducing feeder losses, supporting local voltages, accommodating the fluctuation of intermittent distributed renewable energy generation and improving the power quality.

- **CELL**

The concept of “CELL” was proposed to tackle the challenges of high penetration of DG, e.g. higher than 50% of total generation capacity in the Danish system, and its

intermittency impact on the power system [44, 46]. A CELL is defined as a wide area in a distribution network, in which a collection of distributed energy resources can be controlled [44].

The control of a CELL would involve the voltage and the frequency control both in normal and islanded modes. The CELL is defined to achieve the following objectives [44, 46]:

1. In normal operation, a CELL manages the distributed energy resources in it effectively.
2. In a case of regional emergency, e.g. a high risk of a blackout, as a high ambition objective, a CELL disconnects itself from the main grid and transfers to an islanded operation. In the moderate ambition objective, a CELL is expected to black-start itself after the system blackout to an islanded operation.

- **Virtual Power Plants**

A virtual power plant aggregates DG into a single entity that can be controlled by the system operator and then their energy output is traded [14]. Through aggregating the distributed energy resources into a portfolio, they become visible to the system operator and can be actively controlled [47].

The aggregated output of a virtual power plant is arranged to have similar commercial and technical roles as a central generation unit [14]. The activity of market participation, e.g. energy supplier, drives the commercial virtual power plant role, while the technical virtual power plant role is driven by the activity of the system management and support [47].

2.5. Energy storage systems

As an important components of a virtual energy storage system studied in this thesis, the existing studies on the application of Energy Storage Systems (ESSs) in the frequency control and the voltage control in distribution networks are reviewed below.

2.5.1. Types of energy storage systems

Fig. 2.4 shows the different types of ESSs utilised in the power system [48, 49]. In terms of the stored energy form, ESSs are classified into electrochemical, mechanical,

electrical and thermal energy storage systems. In terms of the power and the energy densities or ratings, ESSs are classified into high power density ESSs and high energy density ESSs. The high-power density ESSs include flywheels ESS, superconducting magnetic ESS and super-capacitor ESS, which are often used for power management applications. In contrast, the high-energy density ESSs include compressed air ESS, hydrogen-based ESS, thermal ESS and pumped hydro ESS, which are typically used for energy management applications. Many types of battery ESS acquire high power and energy densities, which make it suitable for both power and energy management applications [50].

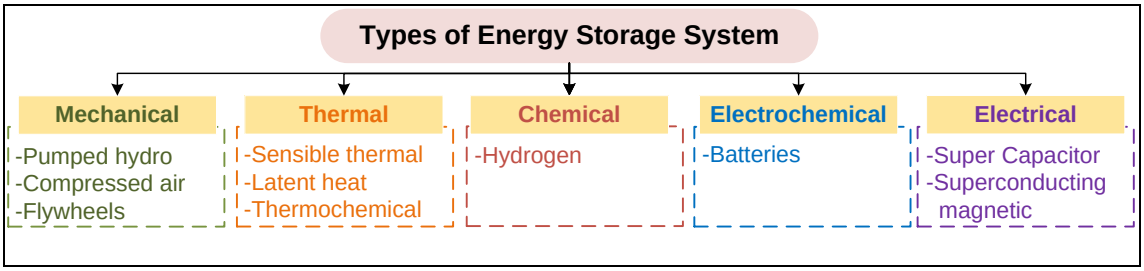

Fig. 2.4 Types of energy storage systems used in the power system [48, 49].

The number of types of ESSs is increasing, driven by the growing need to a medium to store the surplus energy and utilise it later for electrical power systems, electrified transport systems, and smart appliances. Two summary tables were made by the researcher, i.e. Table 2.3 and Table 2.4. Table 2.3 shows a brief description of different types of ESSs which reached the commercial or early commercial stage. Table 2.4 presents a simple comparison between different ESSs. Figure 2.5 shows briefly the capital cost of different ESSs [51].

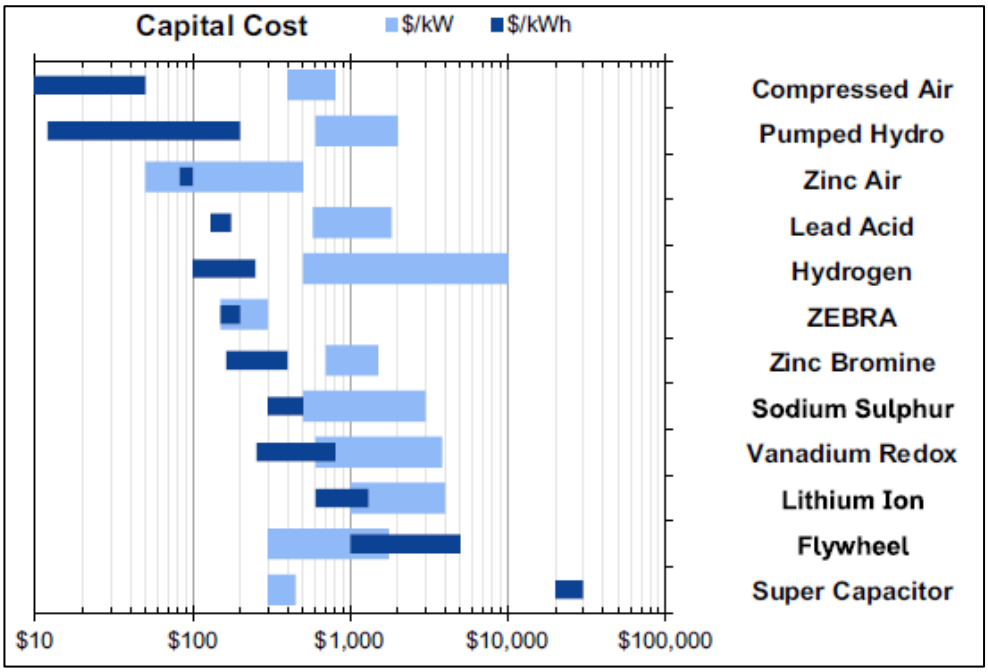

Fig. 2.5 A brief comparison of the power in kW and the energy in kWh costs in US dollars for various types of energy storage systems (Zinc Air, Lead Acid, ZEBRA, Zinc Bromine, Sodium Sulphur and Lithium Ion are types of batteries) [51].

TABLE 2.3 MAIN TYPES OF ENERGY STORAGE SYSTEMS USED IN POWER SYSTEMS

Type	Structure	Advantage/disadvantage
Pumped Hydro Energy Storage (PHES)	The system is typically comprised of an upper reservoir, waterways, a pump/turbine, a synchronous motor/generator and a lower reservoir. The energy is stored in the system by pumping water from lower reservoir to the upper reservoir. The energy is released when the stored water is discharged through the turbine. The energy stored depends on the height difference between the reservoirs [50, 52]	The system has advantages of zero emissions, a long life, a large storage scale, a fast reaction and a low maintenance, while the geographical constraint and the capital costs are the main disadvantages [15]
Compressed Air Energy Storage System (CAES)	The system uses a piston to compress air (i.e. the medium of storage) typically in the underground salt caverns to store energy. The energy is recovered by a combustion gas turbine where the stored air is decompressed and heated. The second generation of CAES is either above-ground or under the sea. It would typically be smaller than underground CAES but more expensive to build [53, 54]	The system has the advantage of large storage scale. The main disadvantages are the necessity of a fuel source and the geographical constraint for the underground CAES [53, 54]
Flywheel Energy Storage System (FESS)	The system stores energy mechanically be rotating a flywheel coupled with an electrical machine. By accelerating the velocity of the machine the electrical energy is converted to mechanical energy. The electrical energy is retrieved by decelerating the velocity [52]	The system has a long life, i.e. regarding the number of charging and discharging cycles, and a fast response. The high self-discharge is the main disadvantage of FESS [55]
Thermal Energy Storage System (TESS)	The system stores energy in the forms of heat, cold or their combination. The TESS is classified based on physical principles to: 1-sensible thermal energy storage, based on the temperature difference. 2-latent heat storage, based on the phase change materials. 3-thermochemical energy storage [49, 56]	The system has low costs and no geographical constraints. Yet it has moderate efficiencies [49, 56]
Hydrogen-based Energy Storage System (HESS)	The system is composed of an electrolyser and fuel Cells. The operation principles of the electrolyser are similar to fuel cells. However, instead of generating electricity, they decompose water into hydrogen and oxygen[57, 58]	The HESS produces zero harmful emissions and has a separate process for generation, storage and deployment, which can contribute to its future applications such as dividing the system into two distanced parts that are connected through pipelines caring the hydrogen. The main disadvantage is the low overall efficiency [57, 58]
Lithium-Ion Battery Energy Storage System (BESS)	The most conventional structure of Lithium-Ion battery contains a graphite anode, a cathode made of a Lithium metal oxide and an electrolyte consisting of a solution of a Lithium salt in a mixed organic solvent embedded in a separator felt [59]	The Li-Ion batteries have high power, high permissible depth of discharge, yet a high cost. However, the cost declined rapidly in the last years [29]

Lead-Acid Battery Energy Storage System (BESS)	Lead-Acid batteries are made of stacked cells, immersed in a dilute solution of sulphuric acid (H_2SO_4) as an electrolyte. The positive electrode of each cell is composed of lead dioxide (PbO_2), while the negative electrode is sponge lead (Pb) [60]	Lead-Acid batteries are the cheapest BESS. The main disadvantages include having a low permissible depth of discharge, considerable sensitivity to the temperature of surrounding medium and a limited cycling capability [61, 62]
Sodium–Sulphur Battery Energy Storage System (BESS)	The Sodium–Sulphur batteries operate at a temperature of about 300°C to keep the electrode materials in a molten state, thereby reducing resistance to the sodium ions flow through the β-alumina solid (β-Al_2O_3) electrolyte [63]	The Sodium–Sulphur batteries have a high efficiency and a low maintenance requirement. However, thermal management and safety are the main disadvantages [64]
Nickel Battery Energy Storage System (BESS)	Research on Alkaline rechargeable batteries represented by Nickel–Cadmium (Ni–Cd) battery and Nickel–Metal Hydride (Ni–MH) battery had been carried out since 1950. [70]. The main components of Ni–Cd batteries are nickel and cadmium, which are used as the active materials of the positive and negative electrodes respectively. Aqueous alkali solution acts as the electrolyte [65]	Despite of the good technical characteristics of the Ni–Cd battery, it has not had a major commercial success, due to its considerable costs, their toxicity and the fact that they suffer from the memory effect [60]
Flow Battery Energy Storage System (BESS)	In these batteries, the electrolyte contains one or more dissolved electroactive materials flowing through a power cell/reactor in which the chemical energy is converted to electricity. The three major types of flow batteries are; Vanadium Redox Battery (VRB), Zinc Bromine Battery (ZBB) and Polysulphide Bromide Battery (PSB), since their operation is based on reduction and oxidation reactions of the electrolyte solutions. These types of batteries are also called redox flow batteries [50, 66]	The main advantage is the ability to deliver long-term charging or discharging for more than 8 hours [61] and a negligible self-discharge. The moderate efficiency, due to the energy needed to circulate the electrolyte, and losses, due to chemical reactions, are the main disadvantages [50, 60, 66]
Super or ultra-capacitors energy storage system	Super-capacitors are based on two conductor electrodes and an insulator (electrolyte and a porous membrane). The energy stored in the capacitors is directly proportional to their capacity and the square of the voltage between the terminals [52]	The super or ultra-capacitor has a long service life, no limitations on the depth of its discharge and relatively high power capacity, but essentially a small energy capacity and a high cost [61]
Superconducting Magnetic Energy Storage (SMES)	The system stores energy in the magnetic field generated by the direct current flowing through a coiled wire. A conductor at cryogenic temperature (near absolute zero or 0 Kalvin) becomes a superconductor, thus nearly having no resistive losses as it produces the magnetic field [67, 68]. The energy stored is proportional to the coil self-inductance and the square of the current circulating in the coil [69]	The system has high energy storage efficiency and a rapid response (within a few milliseconds) but for short periods of time. Despite the high cost, the continuous energy required to cool the coil and environmental issues associated with strong magnetic field are the main disadvantages [50, 67]

TABLE 2.4 A COMPARISON BETWEEN ENERGY STORAGE SYSTEMS

Parameter / Type of ESS		Response time [70]	Discharge time [70]	Rated capacity (MW) [64]	Depth of discharge % [61]	Cycle lifetime [61, 64]	Efficiency % [61]	Technology maturity [64]	Typical applications [64]	Installed projects example
Pumped hydro		min	hours	100-5000	100	More than 3000 (30-60Y)	70-80	Mature& Commercial	Large grid	3,003 MW-USA [71]
Compressed air		min	hours	50-300	70-90	(20-40Y)	70-89	Commercial	Large grid	321 MW - Germany [72]
Flywheel		ms	sec to min	0.4-20	70-90	More than 100000 (15-20Y)	95	Early commercial	Small grid/House/EV	200*0.1 MW-USA [73]
Hydrogen		sec to min	hours	10-200	100	Up to 3000 (5-20Y)	30-40	demo	Grid/EV/ Commercial UPS	10 KW –Norway [74]
Super-capacitor		ms	sac to min	0-10	100	Up to 10^6 (8-20+Y)	Up to 95	Research/ early demo	Small grid/house/EV	
Superconducting magnetic		ms	sec to min	0.1-10	70-90	10^6 (20-30Y)	95	Demo/ Early commercial	Small grid/ Commercial UPS	3 MW- USA [75]
Batteries	**Lead-Acid**	ms	sec to hours	0-40	30-80	600-10000 (5-20Y)	85	commercial	Small grid/ Commercial UPS	8.5 MW-Germany [50]
	Lithium-Ion	ms	ms to hours	1-100	70-95	Up to 10^4 (5-15Y)	85-95	commercial	Small grid/ Commercial UPS	30 MW/120MWh [76]
	Redox flow	sec	sec to hours	0.03-3	100	5000-20000 (5-30+Y)	80	Research/ Early commercial	Small grid/ Commercial UPS	4 MW-Japan [77]
	Sodium-Sulfur	sec	sec to hours	0.05-34	92	2500-4500 (5-15Y)	70 -95	Demo/ Early commercial	Small grid/ Commercial UPS	2*17 MW-Japan [78]

In this thesis, two types of ESSs, i.e. flywheels as a high-power density ESS and batteries as a high-energy density ESS, were selected as a part of the development of the virtual energy storage system. Therefore, further information on flywheels and batteries is provided henceforth.

- **Flywheel Energy Storage System (FESS)**

The main components of the FESS are the electrical machine and the AC/DC power electronic converters which are required to connect the machine that runs with variable speeds to the power system.

Figure 2.6 shows a commercial FESS [55]. The flywheel is placed in a vacuum to rotate in high tangential speeds, i.e. store higher energy. The aerodynamic drag increases considerably with the increase in the velocity, the density and the pressure of the gas surrounding the flywheel [55, 79]. To address the problem of the rotor heat extraction in a vacuum atmosphere, a Permanent Magnet Synchronous Machine (PMSG) is used [80]. The PMSM have a higher efficiency and a smaller size than other types of motor/generator with a similar rating [81].

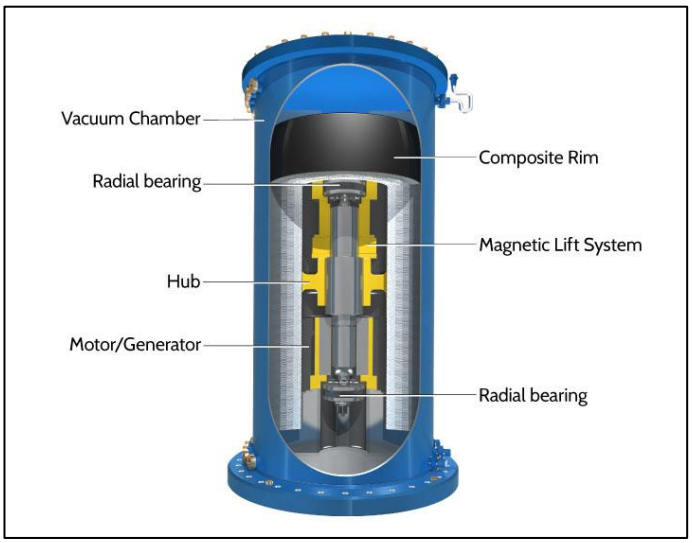

Fig. 2.6 A commercial flywheel energy storage unit by Beacon power co. [55].

The energy E (joule) stored in the FESS is [82]

$$E = KJ{\omega_{max}}^2 \tag{2.1}$$

where K is the flywheel shape factor (K=0.93 for a constant stress disc and K=0.5 for a thin rim), J (kg.m^2) is flywheel moment of inertia which is determined by the mass and the shape of the flywheel and ω_{max} (rad) is the maximum velocity.

For a flywheel of radius r (m) and a mass m_F (kg) concentrated in the rim (K=0.5), the energy stored is [52]

$$E = 0.5 \times r^2 \times m_F \times {\omega_{max}}^2 \quad (2.2)$$

The energy density stored E_{vol} can be expressed per unit volume (Joule/m^3) as [52]

$$E_{vol} = 0.5 \times \rho \times r^2 \times {\omega_{max}}^2 \quad (2.3)$$

where ρ (kg/m^3) is the mass density. The tensile stress σ (N/m) in the rim is given by [52]

$$\sigma = \rho \times {\omega_{max}}^2 \times r^2 \quad (2.4)$$

The maximum velocity depends on the density and the strength of the material of the flywheel [83]. Therefore, the maximum kinetic energy stored per unit volume (joule/m^3) will be [52]

$$E_{vol\ max} = 0.5 \times \sigma_{max} \quad (2.5)$$

A mix of a carbon fibre and a fibreglass composite was used in the commercial FESS shown in Fig. 2.6 [55]. This commercial FESS of 20 MW/6 MWh provides frequency regulation services to the system operator in New York/USA. The system is comprised of 200 flywheels, each with a storage capacity of 100 kW/30 kWh [84].

In GB, the largest power rated FESS is used to support the experiments of the European Atomic Energy Community (EURATOM) within the Joint European Torus (JET) project. These experiments typically last 20 s and draw more than 1000 MW. The FESS is consisting of two large flywheels, each flywheel is capable of supplying up to 400 MW for 30 seconds. The flywheels are charged up from the grid for several minutes, then quickly discharged into the required loads. Hence, distribution network congestion is avoided by reducing the demand on the grid during experiments [84].

- **Battery Energy Storage System (BESS)**

A BESS stores energy in a set of multiple cells, connected in series or in parallel or both to obtain the desired voltage and capacity [52]. The installed capacity of BESSs worldwide is estimated to grow from 1.5 GW in 2015 to over 14 GW by 2020 [85]. Many of these BESSs are Lithium-Ion battery based, due to the rapid reduction in their cost. Lithium-Ion batteries cost decreased from more than $3,000/kWh in 1990 to less than $200/kWh in early 2016 [29]. Figure 2.7 shows a commercial BESS scheme [86]. The system control unit directs the operation of the system, while the battery management

system monitors the state of charge, the voltage, and the temperature of the individual battery modules [86].

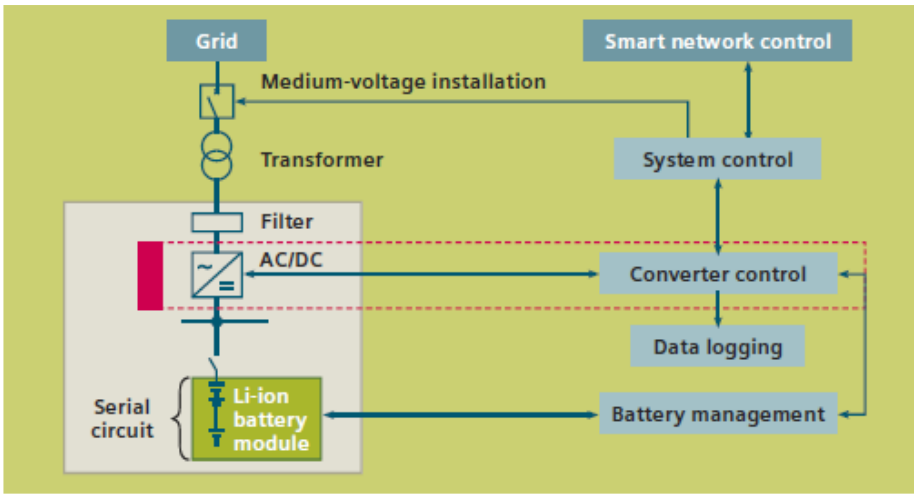

Fig. 2.7 A schematic diagram of a commercial battery energy storage system [86].

2.5.2. **Energy storage systems for frequency response**

The use of different high-power rating or density ESSs, e.g. superconducting magnetic [87], ultra-capacitor [88], battery [89] and flywheel [90], for frequency regulation was reported in the literature. This type of ESS was proposed due to the non-geographical constraints and the high controllability provided by the fast power for frequency droop control, i.e. 1% or 2% droop setting, through the power electronic interface with the power system [87-90].

In the GB power system, the pumped hydro ESS is being used for secondary frequency response [91] for decades. While the large-scale deployment of BESSs will be started through the 201 MW capacity recruited for enhanced frequency response service (presented in Section 2.1). To utilise the existing infrastructure and reduce the overall cost, a 49 MW Lithium-Ion based BESS for enhanced frequency response will be built at the site of a former coal and gas power plant in the GB [92].

2.5.3. **Energy storage systems for voltage control in distribution networks**

The use of ESSs to support the voltage control of distribution networks, i.e. through the exchange of the active and the reactive powers with the reactive power priority, was proposed in the literature [93]. A centralised voltage control [94] of multiple BESSs and an OLTC transformer was proposed to solve over-voltage and voltage unbalance problems caused by DG. However, this method does not involve a coordination among

batteries. In [95], a coordinated control of multiple BESSs for voltage control of low-voltage networks was presented. This coordinated centralised controller determines which batteries will be used to solve voltage problems based on the state of charge of all batteries and voltage sensitivity factors.

In the GB power system, several small-scale capacities, i.e. 1-2 MW capacity, demonstration projects used an ESS to provide voltage support in distribution networks [96]. In 2014 a 6 MW/10 MWh capacity of a BESS was installed in a GB distribution network to provide voltage support and defer the substation upgrade, i.e. adding a 38 MVA transformer, to cap with the increased demand [96].

2.6. Flexible demand

2.6.1. Demand-side integration

Demand-Side Integration (DSI) is a set of measures to use loads and local generation to support network management and improve the quality of power supply [27]. According to [27], the term demand-side integration can be used to refer to all aspects of the relationships between the electric power system, energy supply and end-user load, which include Demand-Side Management (DSM), Demand Response (DR) and Demand-Side Response (DSR). The potential of demand-side integration depends on the availability and the timing of the information provided to consumers, the duration and the timing of their demand response, the performance of the ICT infrastructure, metering, automation of end-use equipment and pricing/contracts [44].

Demand-side integration can be applied through two types of programs, incentive-based programs and price-based programs [97, 98]. Incentive-based programs are provided through interruptible or curtailment contracts, in which consumers are paid to reduce or shift their energy consumption. By contrast in the price-based programs, consumers adjust their energy consumption to changes in the electricity market price [97].

A final report of a demand-side integration project in the GB estimated that the demand-side integration programs are more commercially viable for distribution network operators at the medium-voltage (i.e. 33 kV and above) than lower voltage levels in term of deferring capital investment needed [99].

It is important to stress that the application of demand-side integration techniques tends to disturb the natural diversity of loads and create some undesirable effects. For example, the amount of energy recovered after the provision of response may exceeds the amount of load curtailed [100].

2.6.2. **The use of flexible demand for frequency control**

Using flexible industrial and public buildings demand such as steelworks [101], water supply companies [102], wastewater treatment industry, hospitals and universities [103] to provide frequency response services is well established and growing in the GB power system. The estimated flexibility from commercial and educational buildings during peak hours is 2.5 GW in the GB power system in 2012 as shown in Table 2.3 [104].

TABLE 2.5 ESTIMATED DEMAND FLEXIBILITY DURING PEAK HOUR OF A WINTER DAY [104]

Sector	Capacity (GW)
Retail	0.7
Education	0.3
Commercial	0.3
Other non-domestic sectors	1.2
total	2.5

Both centralised and decentralised control of demand response units to provide frequency support to the power system were studied in the literature. Among flexible loads, those with thermal storage showed suitable characteristics for the provision of frequency response [101, 105-107].

Centralised control of the demand response units relies on the Information and Communications Technology (ICT) infrastructure to establish communications between the demand response units and the centralised controller, which can be managed by an aggregator [108]. A centralised frequency controller in [109] sends a turn OFF or ON signal to domestic air conditioning units and water heaters after a frequency rise or dip event. Although a centralised controller reduces the uncertainty of demand response, the establishment of extensive communication remains the main obstacle.

To tackle the problems associated with the ICT such as costs and the latency, decentralised frequency controllers were investigated. A decentralised controller in [106] regulates the temperature set-points of refrigerators to vary in line with the frequency deviations and therefore controls the power consumption of a refrigerator. A dynamic decentralised controller was developed in [105], which changes the aggregated power consumption of refrigerators in linear with the frequency changes. The controller aims not to undermine the primary cold supply function of refrigerators and the impact of the grid-scale DSI on the grid frequency control was investigated. Similar local frequency controllers were developed to provide frequency support from industrial bitumen tanks [101] and melting pots [110].

Considering the availability of refrigerators to provide frequency response depicted by [18], it is estimated that 20 MW of response requires approximately 1.5 million refrigerators with the total cost of frequency controllers added in each of these refrigerators of roughly £3 m (i.e. each controller costs £2) in 2007 according to [106].

2.6.3. **The use of flexible demand for voltage control in distribution networks**

When a DSI technique reduces the demand in a distribution network, the active and reactive powers flowing through feeders decrease and the voltage rise. Consequently, several studies were undertaken investigating the flexible demand ability to support voltage control and reduce peak demand, hence deferring reinforcement in the distribution network. Both centralised and distributed control strategies were proposed to integrate DSI with the conventional voltage control of distribution network.

In [111], a centralised voltage control scheme was proposed. The control monitors the busbar voltage through Remote Terminal Units (RTU) and determines the required flexible load curtailment and the tap position of the OLTC transformer in a distribution network based on voltage sensitivity factors. In [112] a Genetic Algorithm based optimisation technique was developed to reduce voltage deviation and feeder losses using flexible demand under dynamic electricity pricing regime. The main drawback of centralised control systems is the costs of communications.

A decentralised voltage control of demand response units was proposed in [113]. The controller uses a normalised voltage deviation value, i.e. to compensate for the effect of loads' own consumption on the measured voltage, to produce a signal indicating the desired power consumption. Then, this desired power is linearly mapped into an offset with respect to the temperature set-point of the flexible demand, i.e. a load with a thermal storage. However, such flexible demand control scheme may face a high stress which leads to the result that the flexible energy exhausted.

2.7. Virtual energy storage system

In this thesis, the concept of a new smart management scheme of distributed energy resources called Virtual Energy Storage System (VESS) is presented. A VESS aggregates various controllable components of distributed energy resources, which include conventional energy storage systems and demand response units, to form a single high-capacity energy storage system with reasonable capital costs. Other distributed energy resources such as DG and multi-vector energy resources can be included in the VESS as

well, which are out of the scope of this thesis. The aggregation of small-capacity energy storage and demand response units eliminates the uncertainty of the response of the flexible demand and reduces the capital cost of energy storage systems. A VESS, which can be enabled by an aggregator or a distribution network operator, allows the small-capacity flexible demand and energy storage systems to access to the wholesale market and to provide system and distribution level services to the power system.

Different from the virtual power plant, a VESS aggregates distributed energy resources to act as a single large capacity energy storage system, which aims to store the surplus electricity or release the electricity according to the system needs. Unlike Microgrid and CELL, the VESS is not limited to a geographical area, although the participation in some services may require managing distributed energy resources within an electric-geographical area.

A VESS is able to form a synthetic energy storage system at both transmission and distribution levels with different capacities as a result of the aggregation. The potential capabilities of the VESS include:

1. Provide ancillary services

   A VESS is technically feasible to provide ancillary services, such as frequency response services, because it is able to provide faster response, higher ramp rates and higher flexibilities than the conventional generation units.

2. Facilitate the integration of intermittent DG in the distribution networks

   A VESS charges or discharges to smooth the variations of the power output of intermittent DG, e.g. the wind and the solar energy resources. Additionally, it increases the hosting capacity for DG in distribution networks, where the integration of DG is limited by the voltage and thermal constraints.

3. Reduce generation margins

   A VESS can reduce the required spinning reserve capacity and increase the generators loading capacity, since available VESS capacity can be reported to the system operator in advance and every control cycle (e.g. every minute).

The first two capabilities were investigated in this thesis, while the third capability is suggested as a future work.

Several studies presented centralised or distributed coordinated control schemes of energy storage and demand response units for different applications. Centralised control schemes of Microgrids were developed to smooth the power fluctuations of renewable DG [114] or to maximise the production of DG and minimise power exchanges with the main distribution grid [115, 116]. In [117], a distributed control scheme was developed to maximise the profits of DG and minimise the disutility of flexible demand in a Microgrid. In [118], a centralised control scheme was developed to support the voltage control of distribution networks. However, in the above-mentioned studies, the uncertainty of flexible demand was not addressed and/or reducing the costly energy storage units was overlooked.

Several studies presented other definitions for the term "virtual energy storage system" to refer to a single flexible demand unit, e.g. a building [119] or an aggregation of flexible demand units (such as air-conditioning loads) [120]. These definitions are out of the scope of this thesis.

In the project "hybrid urban energy storage" [121], different distributed energy resources in buildings (e.g. heat pumps or combined heat and power systems) and centralised and distributed energy storage systems are coordinated to create a VESS. Unfortunately, little information was found on this project.

A UK based company aggregates energy stored in systems that end-users own (e.g. uninterruptible power supplies (UPS), solar PV systems (solar panels), electric vehicles (EV) and domestic heating systems) to create a "Virtual Energy Store" that provides services to the power system such as spinning reserve [122].

2.8. Summary

National Grid, the system operator in the GB power system, is obligated to maintain the frequency deviations within limits by procuring various services, e.g. frequency response services.

The distribution network operator is obligated to keep the voltage variations within limits, it typically utilises on-load tap changing transformers and voltage regulators for voltage control in distribution networks.

The high penetration of renewable energy generation and the electrification of heat and transport sectors are important factors affecting the frequency control of power system and the voltage control in distribution networks. The increase proportion of

renewable energy generation that replaces synchronous generators reduces system inertia and therefore requires a large-capacity of frequency response services. The growing penetration of renewable energy generation in distribution networks may cause several problems such as high voltage. The electrification of heat and transport, e.g. electric vehicles, in large capacities may lead to a low voltage and thermal limits problems in distribution networks.

Several approaches were proposed in the literature to manage distributed energy resources, which include Distributed Generation (DG), energy storage system and demand response units. Microgrid, CELL and virtual power plant were among these distributed energy resources smart management schemes.

In the GB power system, pumped hydro ESSs are used for frequency response and battery ESSs was recruited recently for frequency response as well. Several demonstration projects of ESSs to provide voltage support in distribution networks were established. The use of different types of flexible demand for frequency response is well established in the GB power system, while their use of for voltage control remains an active field of research.

The concept of a new smart management scheme called Virtual Energy Storage System (VESS) is presented. A VESS aggregates various controllable components of distributed energy resources, e.g. conventional energy storage systems and demand response units. Although several studies were proposed to coordinate different distributed energy resources, yet there are still some important issues that remain to be tackled, including eliminating the uncertainty of the flexible demand and reducing the capital cost of energy storage systems. Moreover, the aim of the coordination in these studies was not to form a synthetic large-capacity energy storage system, which is the main purpose of the VESS.

Unlike VPP, the VESS forms a synthetic large-capacity energy storage system to store or release the electricity according to the system needs. Different from Microgrid and CELL, the VESS allows the small-capacity energy storage systems and demand response units to access to the wholesale market to provide services. The VESS capability of providing frequency response services, and the VESS capability of facilitating the integration of DG through supporting the voltage control of distribution networks will be investigated in this thesis in Chapters 4 and 5.

CHAPTER 3

Modelling the components of the virtual energy storage system

Models of two types of energy storage system (i.e. flywheel and battery) and two types of demand response units (i.e. refrigerator and bitumen tank) were developed. For validation, results of these models were compared to results reported in the literature. All models were developed in Matlab®/Simulink using a PC with a hardware specifications of CPU Intel i7-3.1 GHz and 16 GB of RAM.

3.1. Models of a flywheel energy storage system

An average model and a simplified model of a flywheel energy storage system were developed. Figure 3.1 shows the average model of a flywheel energy storage system. The essential elements of the system are an electrical machine and a DC interface to the power system. The DC interface consists of a DC busbar connecting back to back converters. A more detailed model would include a representation of switches (e.g. IGBT) and their pulse-width modulation technique, which increases the computational burden. Instead, an average model provides a similar behaviour and a dynamic response by replicating the average response of switching devices using ideal controlled sources. The grid side converter controls the DC busbar voltage and the reactive power flow to the grid. While the machine side converter controls the exchanged active and reactive powers between the machine and the grid.

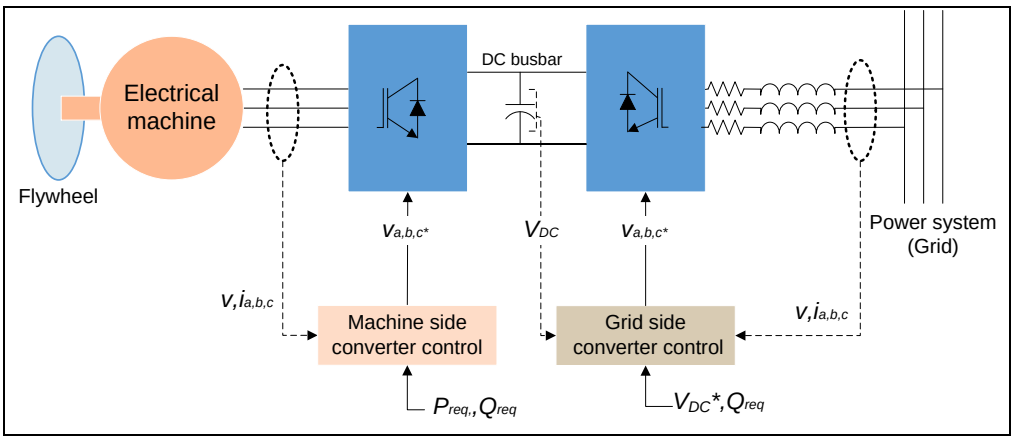

Fig. 3.1 The diagram of an average model of a flywheel energy storage system.

The electrical machine and power electronic converters, i.e. the important elements in the average model, were simplified in the simplified model. The average model was used to gain an understanding of how the flywheel energy storage system works and to develop the simplified model. The simplified model significantly reduces the simulation time and facilitates system-level studies which consider many units. To simulate the operation of a flywheel energy storage system for 3600 seconds, the average model requires 5425 seconds while the simplified model requires only one second. Also, the simulation time increases linearly with the increase in the number of units of the average model. In the simplified model, the simulation time increases slightly with the increase in the number of units.

3.1.1. **The average model of a flywheel energy storage system.**

The modelling and the control of the average model (i.e. shown in Fig. 3.1) were presented in Appendix A. Appendix A is divided to two parts, the first part presents the modelling and control of the DC busbar and the grid side converter. The second part of the Appendix A presents the modelling and control of the machine side converter and the electrical machine. In this research, the flywheel is modelled as an additional mass added to the mass of the rotor of electrical machine.

3.1.2. **The simplified model of a flywheel energy storage system**

Figure 3.2 shows the simplified model of the flywheel energy storage system. The simplified model includes the model of power electronic converters, and the model of the electromechanical parts (i.e. the machine and the coupled flywheel).

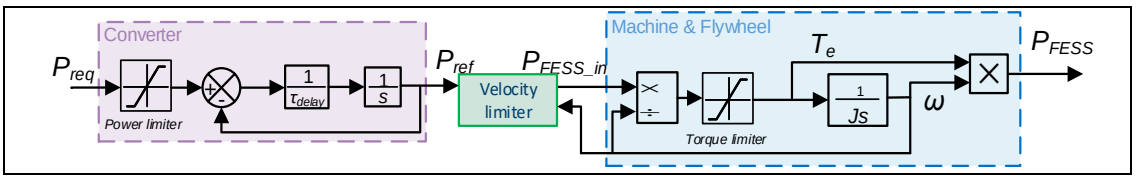

Fig. 3.2 A simplified model of a flywheel energy storage system.

Power electronic converters were modelled as a first order lag system. This model represents the delays in the control of converters on a given required power P_{req} (W). This required power is limited to the converter capacity by a power limiter. The power output from the simplified converter is P_{ref} (W) and the power input to the electromechanical part is P_{FESS_in} (W). The analytical equation of the simplified converter is given by

$$P_{ref} = P_{req}[\frac{1}{1+s\times\tau_{delay}}] \tag{3.1}$$

where τ_{delay} (s) is the time constant of the power converter control loops.

The electromechanical part is modelled using the electromechanical equation (A.24), where P_{FESS_in} (W) is the power input to the simplified electrical machine, T_e is electromagnetic torque developed by the machine (N.m), J is the inertia of the machine's rotor plus the flywheel (kg.m^2) and ω is the mechanical velocity of the machine (rad/s). The equation (A.24) can be rewritten as:

$$T_e = J\times\frac{d\omega}{dt} \tag{3.2}$$

Figure 3.3. shows the velocity limiter of the simplified flywheel energy storage system model which is embedded in Fig. 3.2. The limiter ensures that the machine does not exceeds its velocity limits (i.e. the maximum velocity (ω_{max}) and the minimum velocity (ω_{min})). The velocity limiter employs logic gates to generate a switching signal $FESS_{state}$ which govern the power input to the electromechanical parts, when the velocity is within limits $P_{ref.}$ equal P_{FESS_in} otherwise it is zero.

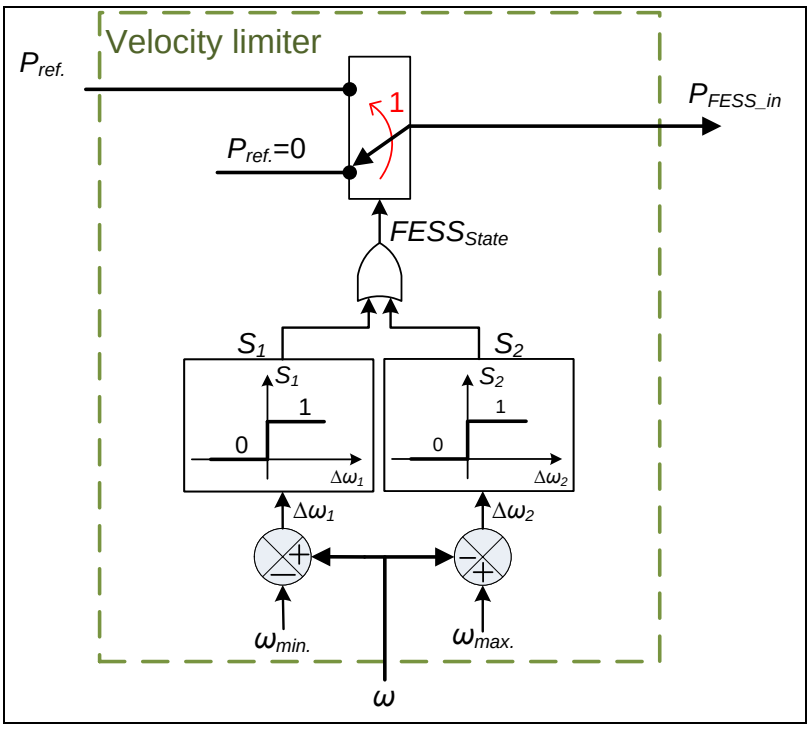

Fig. 3.3 The velocity limiter of the simplified flywheel energy storage system model.

The parameters of the simplified model are listed in Table 3.1. These parameters represent a machine model [123] which has a rated power of 50 kW and an energy density of 1 kWh (i.e. 50 kW for approximately one minute). The power output of the simplified model was limited to 1.6 kW to last for 35 minutes and scaled up to 50 kW by multiplying it by a factor of 31.25 to reproduce the commercial flywheel energy storage system in [55].

TABLE 3.1 PARAMETERS OF THE SIMPLIFIED FLYWHEEL ENERGY STORAGE SYSTEM MODEL

Parameter	Value
Rated Power (kW)	1.6 (scaled up to 50)
Energy stored (kWh)	1 (scaled up to 31.25)
Rotating disc inertia (kg.m^2)	0.862
Converter time constant (sec)	0.001

3.2.The simplified model of the battery energy storage system

Figure 3.4 shows the simplified model of the battery energy storage system. The model consists of a generic battery model [124] and a simplified power electronic converters model. Different types of batteries can be represented in this model, such as Lead-Acid, Lithium-Ion, Nickel-Cadmium and Nickel-metal hybrid.

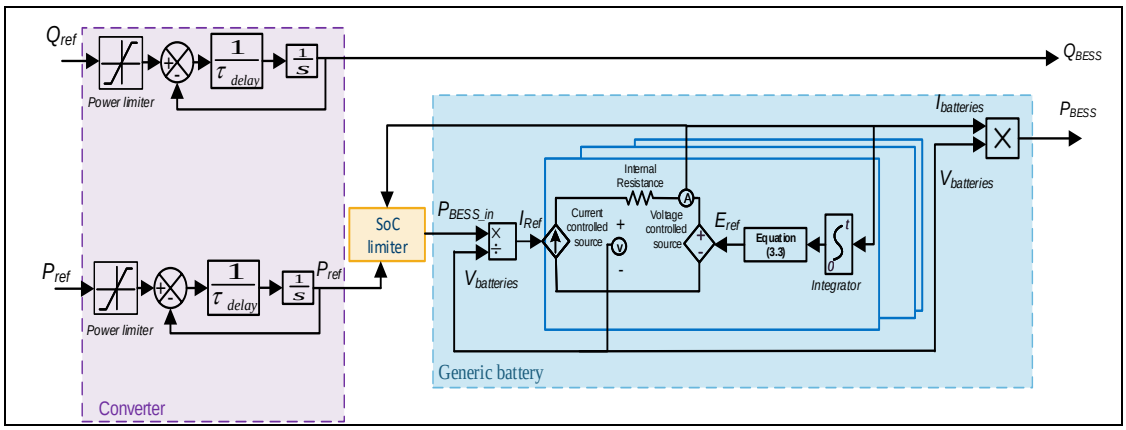

Fig. 3.4 A model of a battery energy storage system.

The power electronic converters were modelled as a first-order lag system to represent the delays (τ_{delay} in seconds) in the converters control loop. Assuming that voltage source converters were used, the active and the reactive power are controlled independently and only the active power passes to the batteries and therefore affects the stored energy.

The generic battery model is composed of a controllable voltage source, a controllable current source and a resistance connected in series [124]. The battery no load voltage (E_{ref}) is a function of the battery current (i) as following:

$$E_{ref} = E_0 - K\times\frac{Q}{Q-\int i.dt} + A\times e^{-(B\times\int i.dt)} \quad (3.3)$$

where:

E_o: The battery constant voltage (V).

K: The polarisation voltage (V).

Q: The battery capacity (Ah).

A: The exponential zone amplitude of the battery (V).

B: The inverse of the exponential zone time constant (Ah^{-1}).

The following assumptions were made [124];

1) A constant internal resistance value was used during the charging and discharging cycles.

2) The parameters were extracted from manufacturer's charts of the discharging cycle and assumed identical to the charging cycle.

3) Temperature effects on the model were neglected.

4) The battery has no memory effect.

The model parameters to represent different types of batteries are listed in Table 3.2 [124].

TABLE 3.2 THE GENERIC BATTERY MODEL PARAMETERS TO REPRESENT DIFFERENT TYPES OF BATTERIES [124]

Type / Parameter	Lead-Acid (12V / 1.2Ah)	Nickel-Cadmium (1.2V / 1.3Ah)	Lithium-Ion (3.6V / 1Ah)	Nickel-Metal-Hybrid (1.2V / 6.5Ah)
E_0(V)	12.6463	1.2505	3.73458	1.2848
R(Ω)	0.25	0.023	0.09	0.0046
K(v)	0.33	0.00852	0.008876	0.01875
A(V)	0.66	0.144	0.468	0.144

Figure 3.5. shows the State of Charge (SoC) limiter of the battery energy storage system model. The SoC limiter guarantees that the generic battery model does not exceeds its state of charge high and low limits (i.e. SoC_{high} and SoC_{low}), it uses logic gates to generate a switching signal $BESS_{state}$ which govern the power input to the generic battery model, when the SoC is within limits $P_{ref.}$ equal P_{BESS_in} otherwise it is zero. The battery current was used to obtain the state of charge [125]:

$$SoC = 1 - \frac{\int i.dt}{Q} \tag{3.4}$$

The factor (η) was introduced to the state of charge computation (Fig. 3.5) to reflect a more realistic system efficiency. For example, if the battery has an efficiency of 90%, then η equals 0.95.

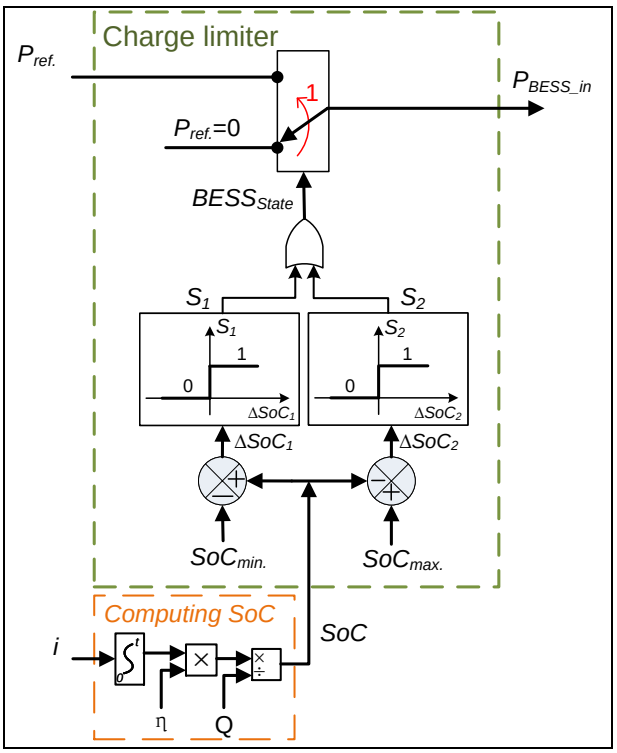

Fig. 3.5 The state of charge limiter of the battery energy storage system model.

3.3. The model of a refrigerator

Figure 3.6 shows the diagram of a domestic refrigerator. A refrigerator is composed of a cavity and an evaporator. Food is stored in the cavity under cold conditions. The cavity has thermal contact with both the room and the evaporator. The heat transferred from the ambient room to the cavity increases the cavity temperature. The cavity temperature controls the compressor ON/OFF state [105]. When the compressor is ON, it compresses the refrigerant gas, raising its pressure, and pushes it into the condenser coils outside of the refrigerator. The refrigerant gas heat dissipated into the ambient room and the refrigerant gas becomes a liquid. By flowing through the evaporator, this high-pressure liquid absorbs the heat from the cavity and evaporates to a gas. The refrigerant gas flows back to the compressor and the refrigeration cycle starts all over [126].

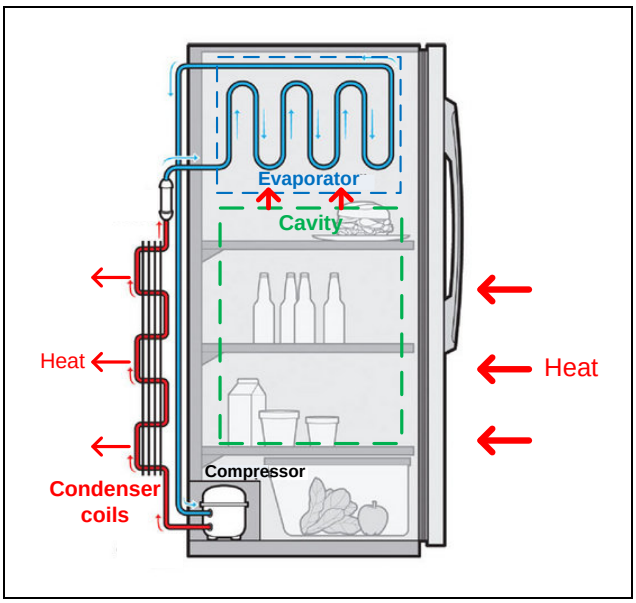

Fig. 3.6 A diagram of a refrigerator and its refrigeration cycle (a modified figure based on [126]).

A thermodynamic model of a refrigerator was adopted from [18, 105]. The model depicts the temperature variations in a refrigerator using two thermal equations. The two equations describe the heat transfer function between the cavity and the room, and the cavity and the evaporator [105].

In the cavity, the heat is transferred from the ambient room and released to the evaporator. This heat transfer causes the cavity temperature to vary; the variation is captured in the form of a differential equation:

$$\frac{dT_{Ca}(t)}{dt} = \frac{U^{Ca\_Amb} \times A^{Ca\_Amb}}{c_v^{Ca} \times m^{Ca}} (T_{Amb} - T_{Ca}(t)) - \frac{U^{Ca\_Ev} \times A^{Ca\_Ev}}{c_v^{Ca} \times m^{Ca}} (T_{Ca}(t) - T_{Ev}(t)) \quad (3.5)$$

where

$_{Ca\_Amb}$: The thermal contact between the cavity and the ambient room.

$_{Ca\_Ev}$: The thermal contact between the cavity and the evaporator.

T_{Ca}: The cavity temperature (ºC).

T_{Amb}: The ambient room temperature (ºC).

T_{Ev}: The evaporator temperature (ºC).

U^{Ca_Amb}: The heat transfer coefficient of the thermal contact between the cavity and the ambient room ($Wm^{-2}ºC^{-1}$).

A^{Ca_Amb}: The area of the thermal contact between the cavity and the ambient room (m^2).

U^{Ca_Ev}: The heat transfer coefficient of the thermal contact between the cavity and the evaporator ($Wm^{-2}ºC^{-1}$).

A^{Ca_Ev}: The area of the thermal contact between the cavity and the evaporator (m^2).

c_v^{Ca}: The specific heat capacity of the cavity ($Jkg^{-1o}C^{-1}$).

m^{Ca}: The mass of the cavity (kg).

In the evaporator, the heat transferred from the cavity and released to the ambient room by the compressor is represented by a differential equation:

$$\frac{dT_{Ev}(t)}{dt} = \frac{U^{Ca\_Ev} \times A^{Ca\_Ev}}{c_v^{Ev} \times m^{Ev}} (T_{Ca}(t) - T_{Ev}(t)) - \frac{P_{cr} \times S_T}{c_v^{Ev} \times m^{Ev}} \quad (3.6)$$

where

$_{Ca\_Ev}$: The thermal contact between the cavity and the evaporator.

T_{Ca}: The cavity temperature (ºC).

T_{Ev}: The evaporator temperature (ºC).

U^{Ca_Ev}: The heat transfer coefficient of the thermal contact between the cavity and the evaporator ($Wm^{-2o}C^{-1}$).

A^{Ca_Ev}: The area of the thermal contact between the cavity and the evaporator (m^2).

c_v^{Ev}: The specific heat capacity of the evaporator ($Jkg^{-1o}C^{-1}$).

m^{Ev}: The mass of the evaporator (kg).

P_{cr}: The power consumption of the compressor (W).

S_T: The compressor switching state (S_T=1 if the compressor is ON, S_T=0 if the compressor is OFF).

Figure 3.7 shows the diagram of the cavity temperature and the compressor state of a refrigerator [18]. Each refrigerator is equipped with a temperature controller as shown in Fig. 3.8. The controller continuously measures the cavity temperature (T_{Ca}) and compares it with set-points T_{low} and T_{high}. If the cavity temperature reaches T_{high} (point A in Fig.3.7), the controller switches ON the compressor and the evaporator starts absorbing heat from the cavity. Due to the process of heat transfer through the thermal contact between the evaporator and the cavity, the cavity temperature takes time before starting to drop (point B in Fig.3.7). When the cavity temperature reaches T_{low} (point C in Fig.3.7), the controller switches OFF the compressor. However, this heat transfer process causes a further drop in the cavity temperature before its starts to rise (point D in Fig.3.7). The compressor remains OFF until the cavity temperature reaches T_{high} again.

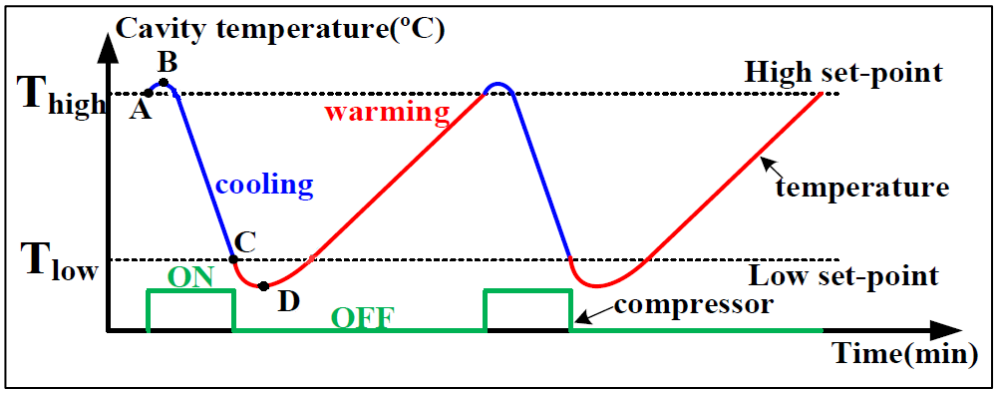

Fig. 3.7 The cavity temperature and compressor state diagram of a refrigerator [18].

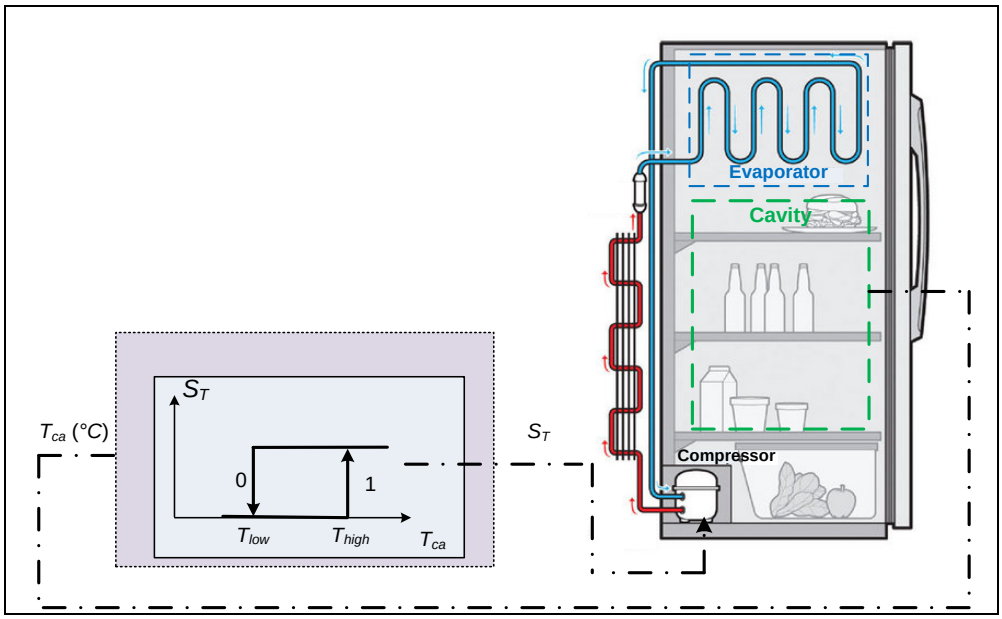

Fig. 3.8 The temperature control of a refrigerator.

The parameters of the refrigerator model were provided by Open Energi. These parameters and any related materials (e.g. figures, charts) are not included in this thesis, due to non-disclosure agreement signed by Cardiff University and Open Energi.

3.4.The model of a bitumen tank

Bitumen is a material extracted mainly from petroleum and used in road constructions [127]. Figure 3.9 shows the diagram of an industrial bitumen tank. The tank stores bitumen in hot conditions using an electrical heater. When it is ON, the heater provides heat at a rate of P_{supply} (W) to the bitumen in the tank. The bitumen loses heat to the surrounding at a rate of P_{loss} (W).

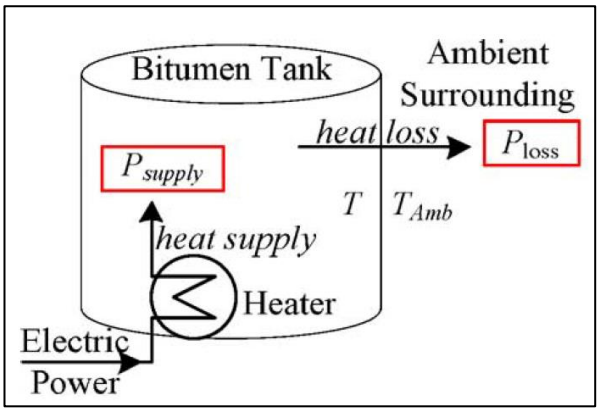

Fig. 3.9 A diagram of a bitumen tanks and its heat transfer process [101].

A thermodynamic model of a bitumen tank was adopted from [101]. The net rate of heat transfer P_{net} (W) is the difference between the supplied and lost heat rates as shown in (3.7)-(3.9):

$$P_{supply} = P_h \times S_h \tag{3.7}$$

$$P_{loss} = U_h \times A_h \times (T(t) - T_{Amb}) \tag{3.8}$$

$$P_{net} = P_{supply} - P_{loss} \tag{3.9}$$

where

P_h: The power consumption of the heater (W).

S_h: The heater state (S_h=1 if the heater is ON and S_h=0 if the heater is OFF).

U_h: The overall heat transfer coefficient ($Wm^{-2}\,{}^oC^{-1}$).

A_h: The surface area of the tank (m^2).

T: The internal temperature of the tank (ºC).

T_{Amb}: The ambient temperature (ºC).

The net rate of heat transfer results in the internal temperature variations of the tank:

$$P_{net} = c_v^h \times m_h \times \frac{dT(t)}{dt} \tag{3.10}$$

where:

$c_v{}^h$: The specific heat capacity ($Jkg^{-1}\,{}^oC^{-1}$).

m_h: The mass of a bitumen tank (kg).

Combining (3.7)-(3.10) results in a first order differential equation for the internal tank temperature:

$$\frac{dT_b(t)}{dt} = \frac{P_h \times S_h}{c_v^h \times m_h} - \frac{U_h \times A_h \times (T(t) - T_{Amb})}{c_v^h \times m_h} \tag{3.11}$$

Based on the heater state, Equation (3.11) has two possible solutions. Assuming a bitumen tank with an ON-period of 150 minutes and OFF-period of 300 minutes, the internal temperature of the tank is [101]:

For the ON-period (S_h=1)

$$T(t) = 184.68 - 34.68 \times e^{\frac{-t}{74.91}} \quad (3.12.a)$$

$$0 \leq t \leq 150\ minutes$$

For the OFF-period (S_h=0)

$$T(t) = 145.32 - 34.68 \times e^{\frac{-(t-150)}{149.81}} \quad (3.12.b)$$

$$150 \leq t \leq 450\ minutes$$

Figure 3.10 shows the diagram of internal temperature and heater states of a bitumen tank [101]. Each bitumen tank has an internal temperature controller to keep the stored bitumen within a range of high temperatures as shown in Fig. 3.11. The controller continuously measures the internal temperature and compares it with a set-points T_{BT_low} and T_{BT_high}. When the temperature is lower than T_{BT_low}, the controller switches ON the heater; when the temperature is higher than T_{BT_high}, the controller switches OFF the heater. The low and high temperatures (T_{BT_low} and T_{BT_high}) were set to 150º and 180º [101].

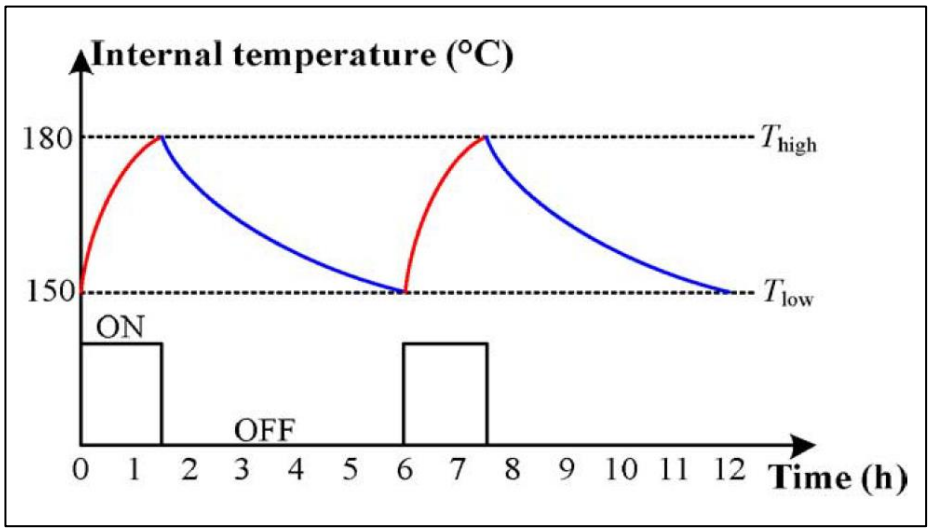

Fig. 3.10 The temperature and heater state diagram of a bitumen tank [101].

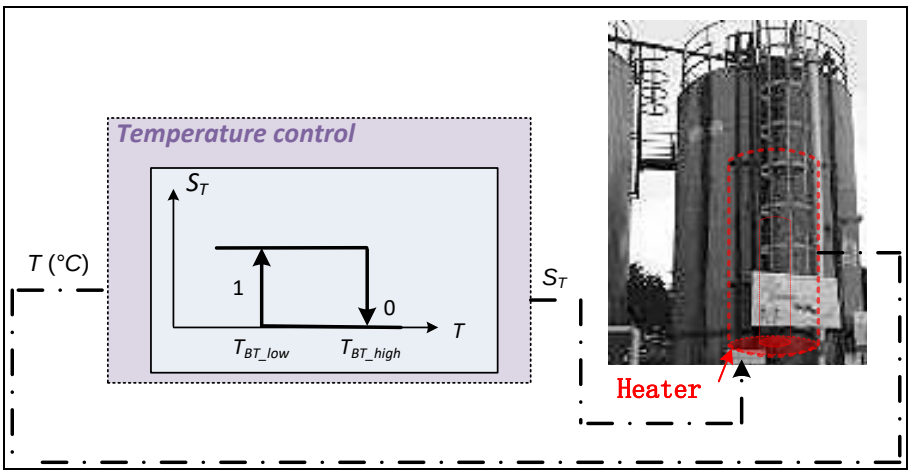

Fig. 3.11 The temperature control of a bitumen tank.

3.5. Validation of the models

3.5.1. Validating the models of a flywheel energy storage system

A. Validation of the average model

To observe the behaviour of the grid side converter and the DC busbar model, a reference power of a ±5kW unit-step was applied to the DC busbar and the output power to the grid was measured as shown in Fig. 3.12. Following changes in the polarity of reference power, percentage overshoots of the output power to the grid were less than 0.4 % of the reference value. The output power to the grid was settled to 2% of the final value within 1 second. The percentage overshoot of the DC voltage was approximately 0.1% of the nominal voltage value (i.e. 650 V) as shown in Fig. 3.13.

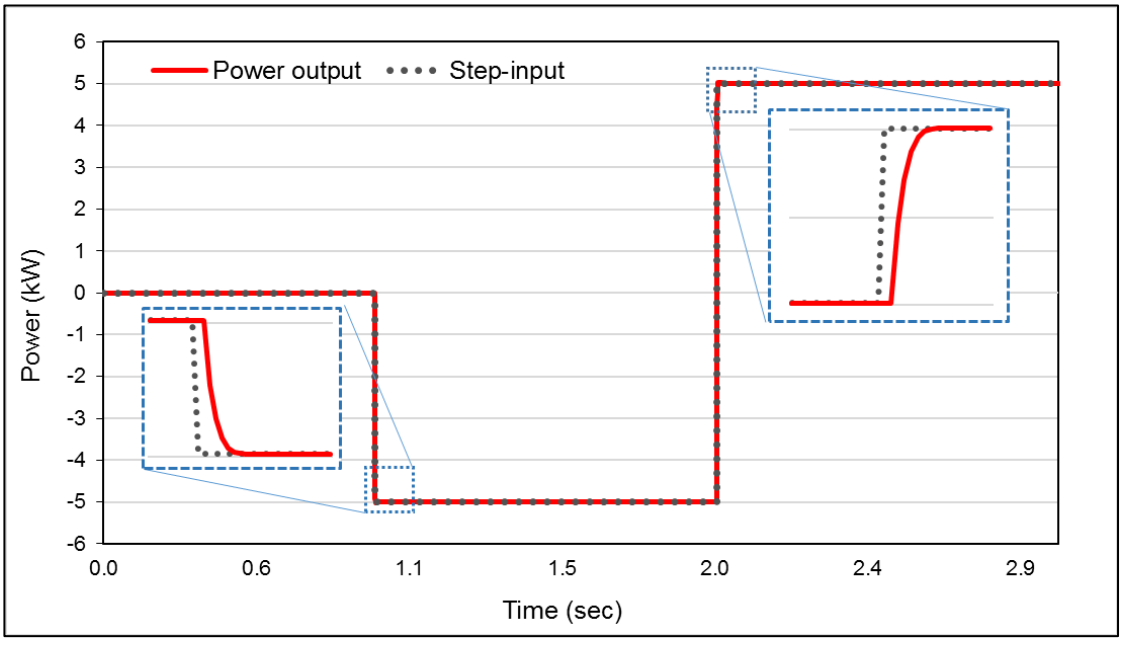

Fig. 3.12 The grid side converter and DC busbar model power output.

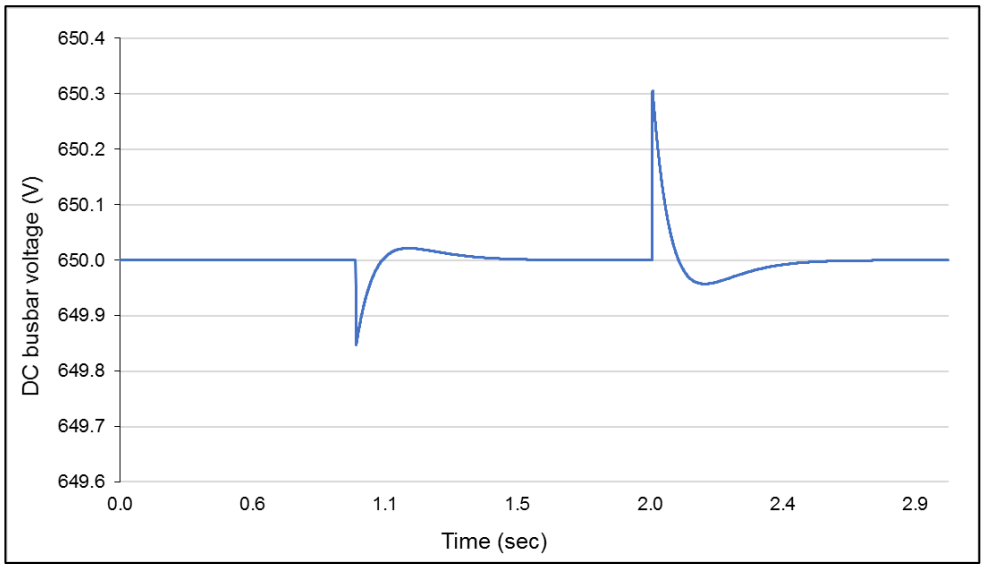

Fig. 3.13 The DC busbar voltage in response to unit-step.

The electrical machine model was validated against results in [123] by comparing the power output and the velocity in response to a reference power of a ± 50kW unit-step as shown in Fig. 3.14 and Fig. 3.15. Following changes in the polarity of reference power, the percentage overshoot obtained in the electrical machine model was less than (0.1 %) of the reference value. Figures 3.14 and 3.15 show a very little discrepancy between the developed model and the model presented in [123].

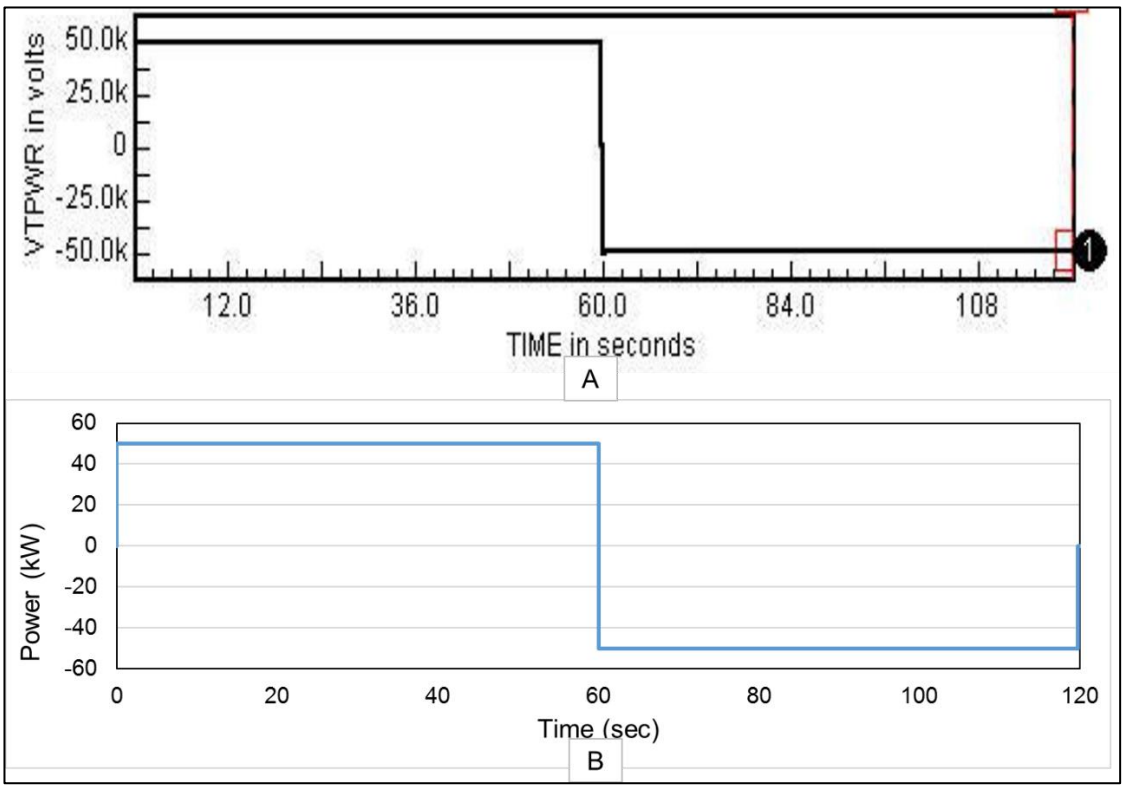

Fig. 3.14 (A) The power output from the model in [123], (B) the electrical machine model power output.

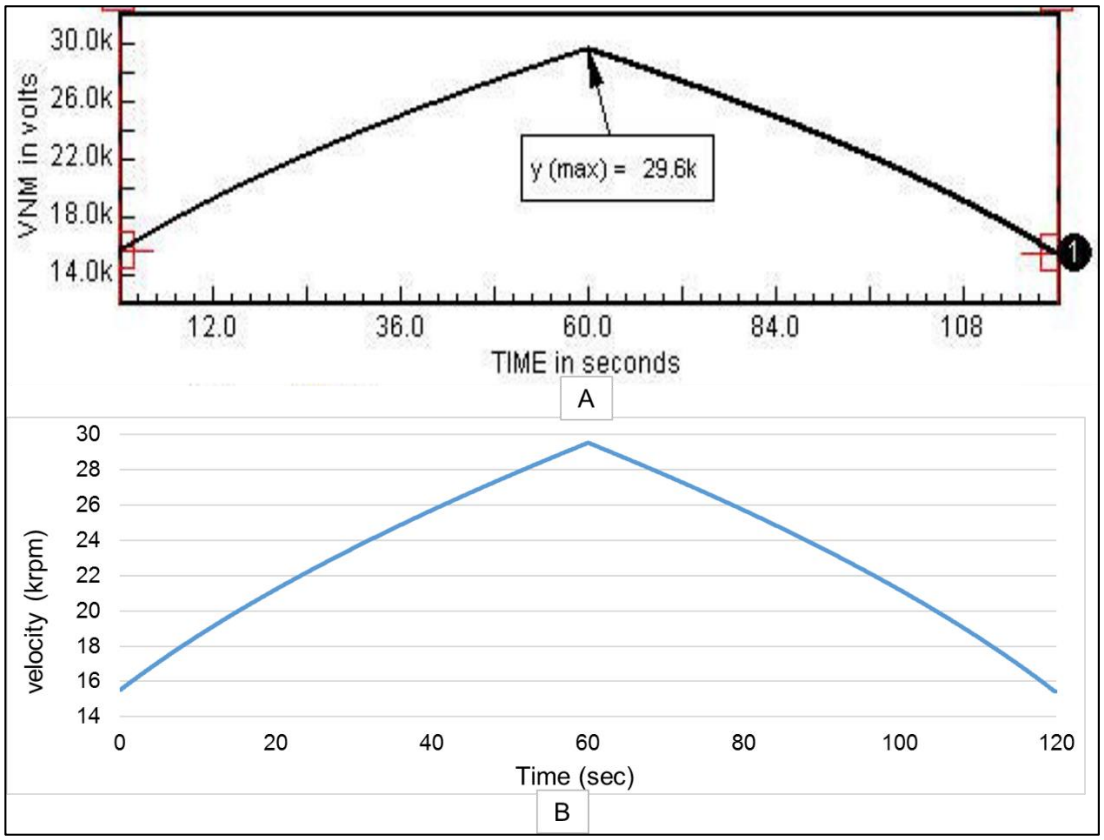

Fig. 3.15 (A) The velocity from the model in [123], (B) the electrical machine model velocity.

B. Validation of the simplified model

The simplified model was validated against the results in [123] by comparing the power output and the velocity in response to a reference power of a ± 50kW unit-step as shown in Fig. 3.16 and Fig. 3.17. Figures 3.16 and 3.17 show that the power output and the velocity of the simplified model are similar to that of the model presented in [123].

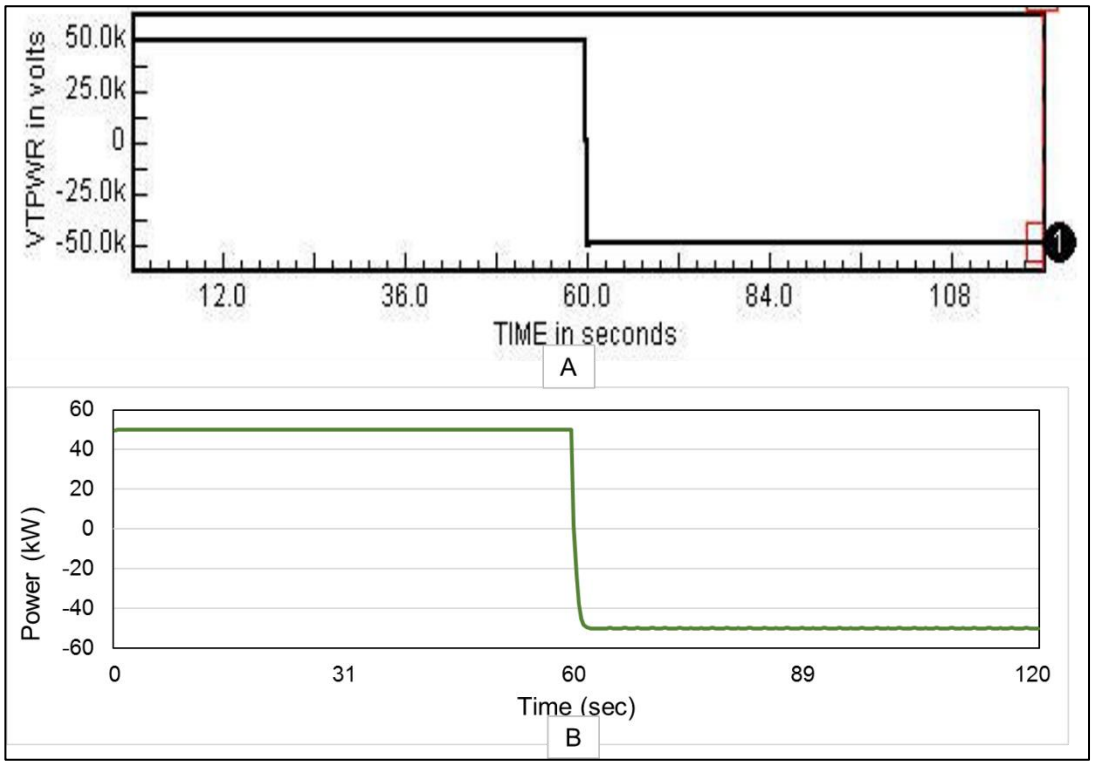

Fig. 3.16 (A) The power output from the model in [123], (B) the simplified model power output.

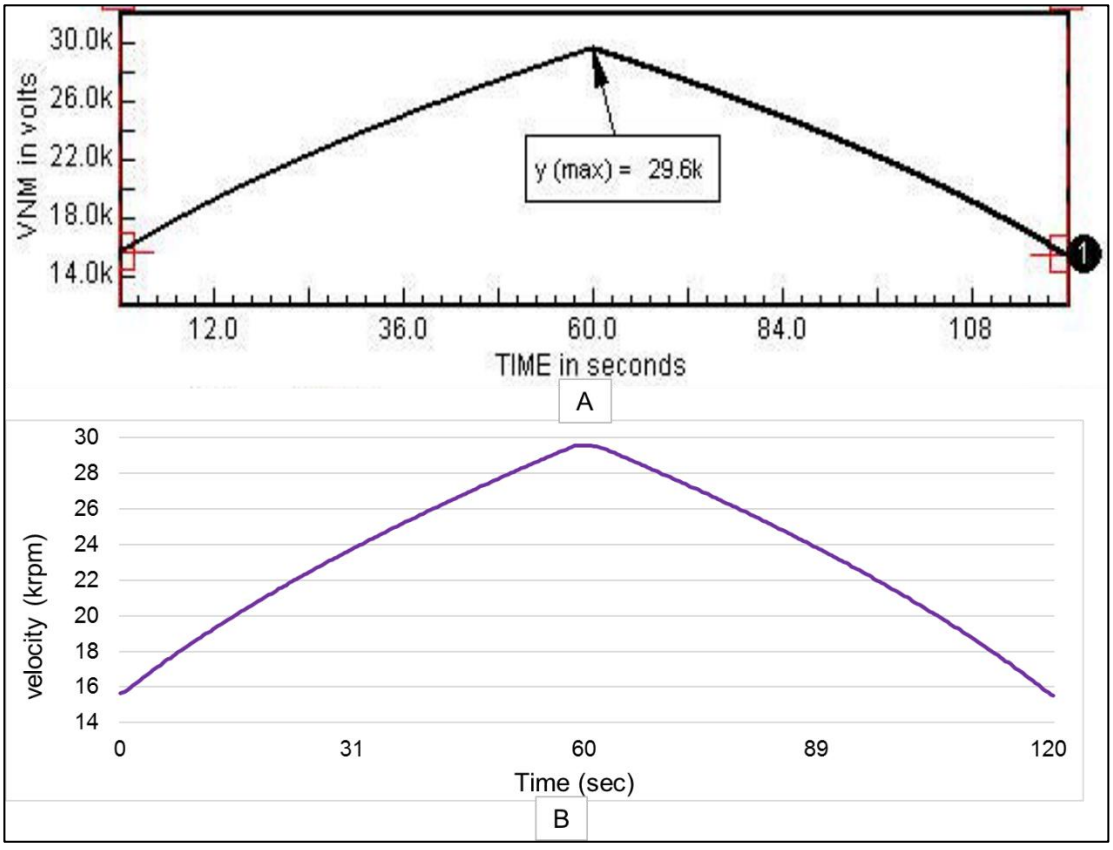

Fig. 3.17 (A) The velocity from the model in [123], (B) the simplified model velocity.

Figure 3.18 shows the performance of the simplified model against the average model of a flywheel energy storage system when responding to a reference power of a ± 5kW unit-step. The simplified model provided a similar response to the average model.

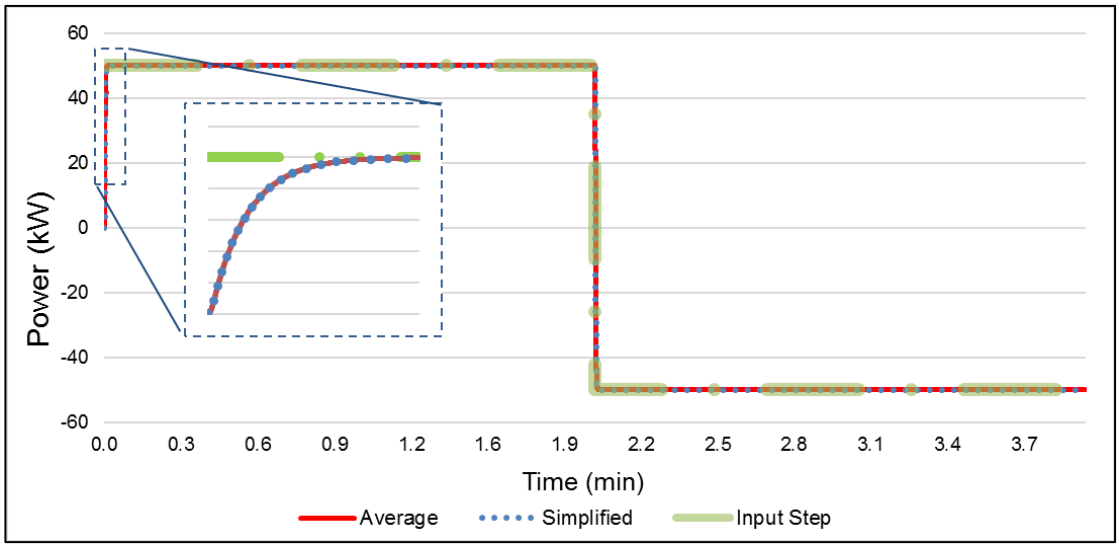

Fig. 3.18 Average and simplified models of the flywheel energy storage system tracking reference signal.

3.5.2. **Validating the model of a battery energy storage system**

The battery energy storage system model was validated by comparing discharging curves against a Nickel-Metal-Hybrid battery manufacturer discharging chart [128] and the Lithium-Ion battery diagram in [124]. The model performance (in both types of batteries) matches closely to the manufacturers charts as shown in Fig.3.19 and Fig. 3.20 at different discharging currents.

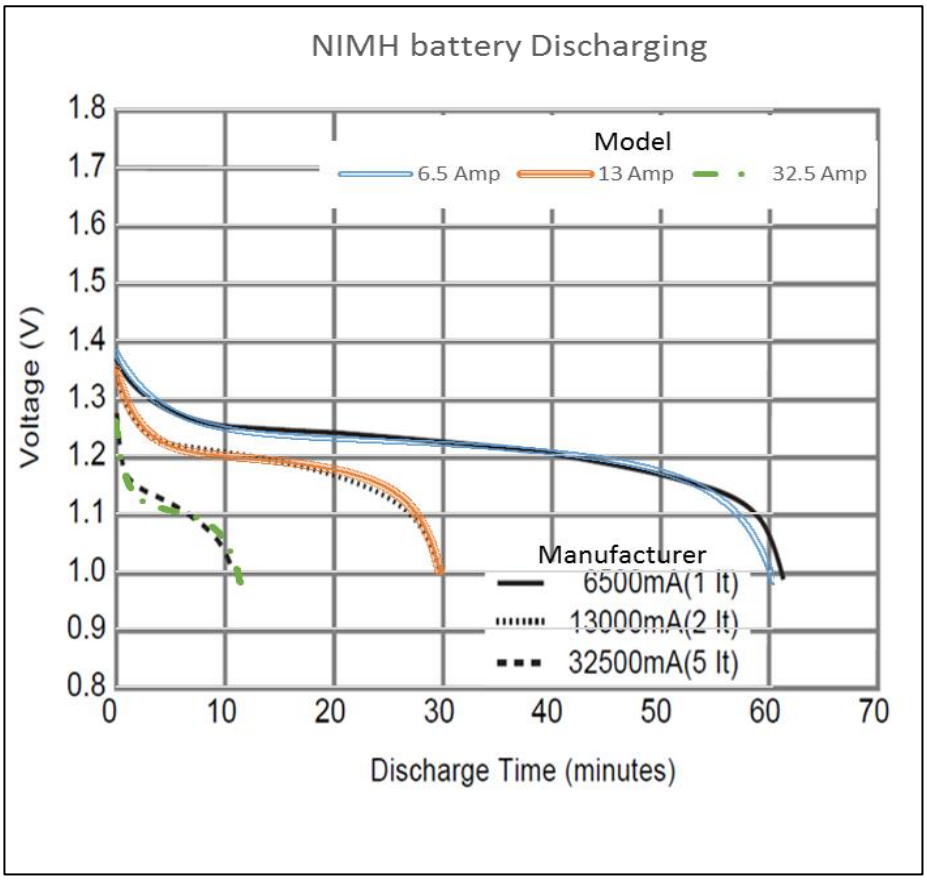

Fig. 3.19 A generic battery model validation against a Nickel-Metal-Hybrid Panasonic battery discharging chart [128].

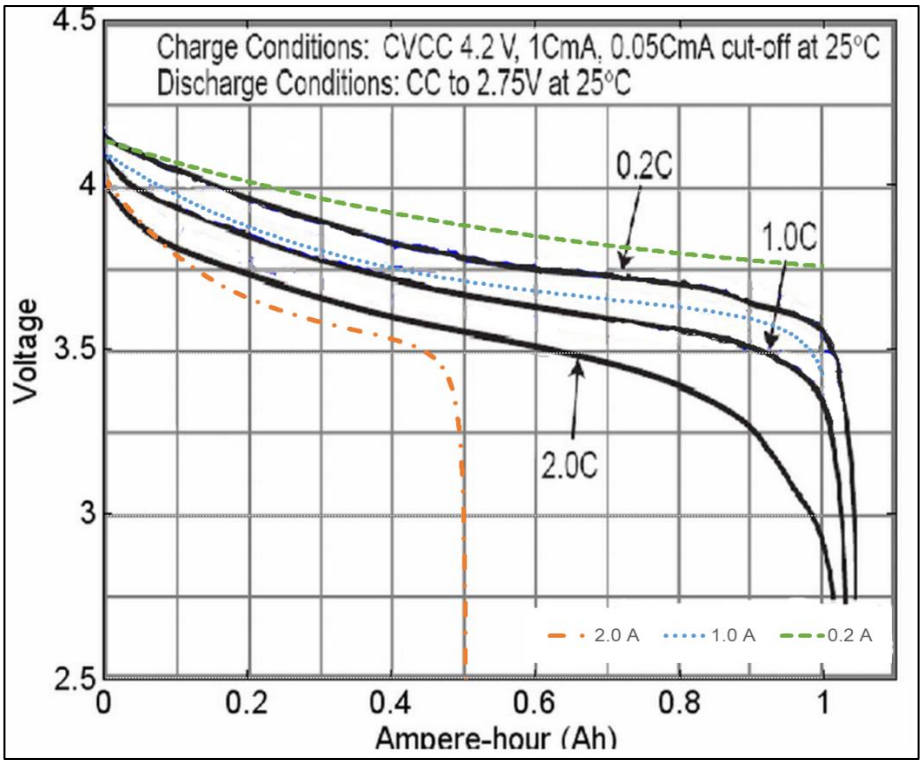

Fig. 3.20 A generic battery model validation against a Lithium-Ion battery discharging chart from [124].

3.5.3. **Validating the model of a refrigerator**

Figure 3.21 shows the validation by comparison of the cavity temperature and the compressor states of the refrigerator against the diagram in [18]. The result in Fig. 3.21.B depicts more accurately the cavity temperature than the diagram in Fig. 3.21 (A). The cavity temperature remains lower than T_{low} for approximately half of the refrigeration cycle. During this time, the evaporator temperature rises from its low to high temperatures absorbing the heat from the cavity.

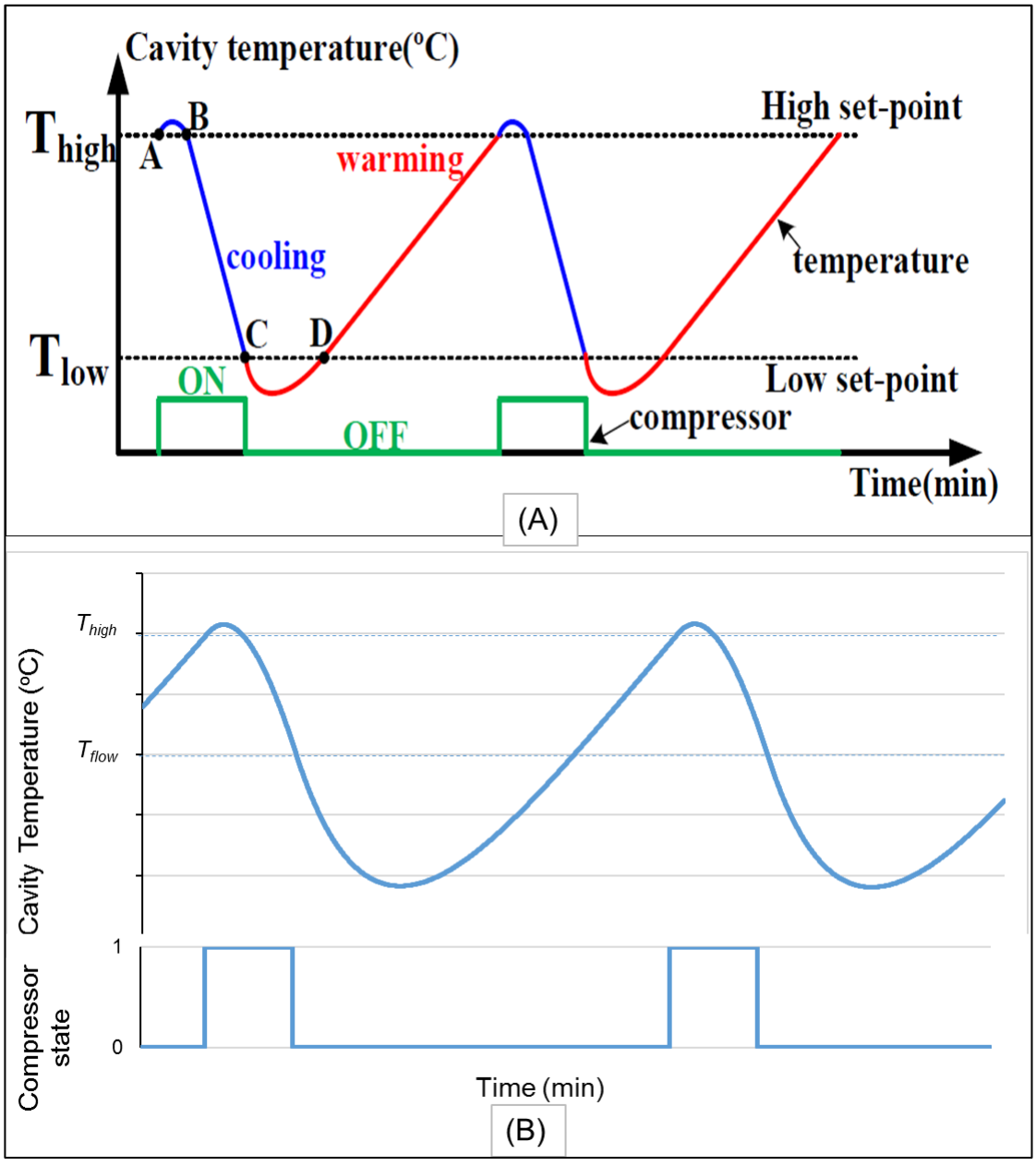

Fig. 3.21 (A) The diagram of cavity temperature and compressor state of a refrigerator from [18], (B) the cavity temperature and compressor state of the refrigerator model.

3.5.4. **Validating the model of a bitumen tank**

Figure 3.22 shows the validation of the bitumen tank model by comparing its internal temperature and heater states against the diagram in [101]. Figure 3.22 (B) shows a bitumen tank model with ON/OFF periods of 150/300 min. Similar temperature variations were observed for other ON/OFF periods.

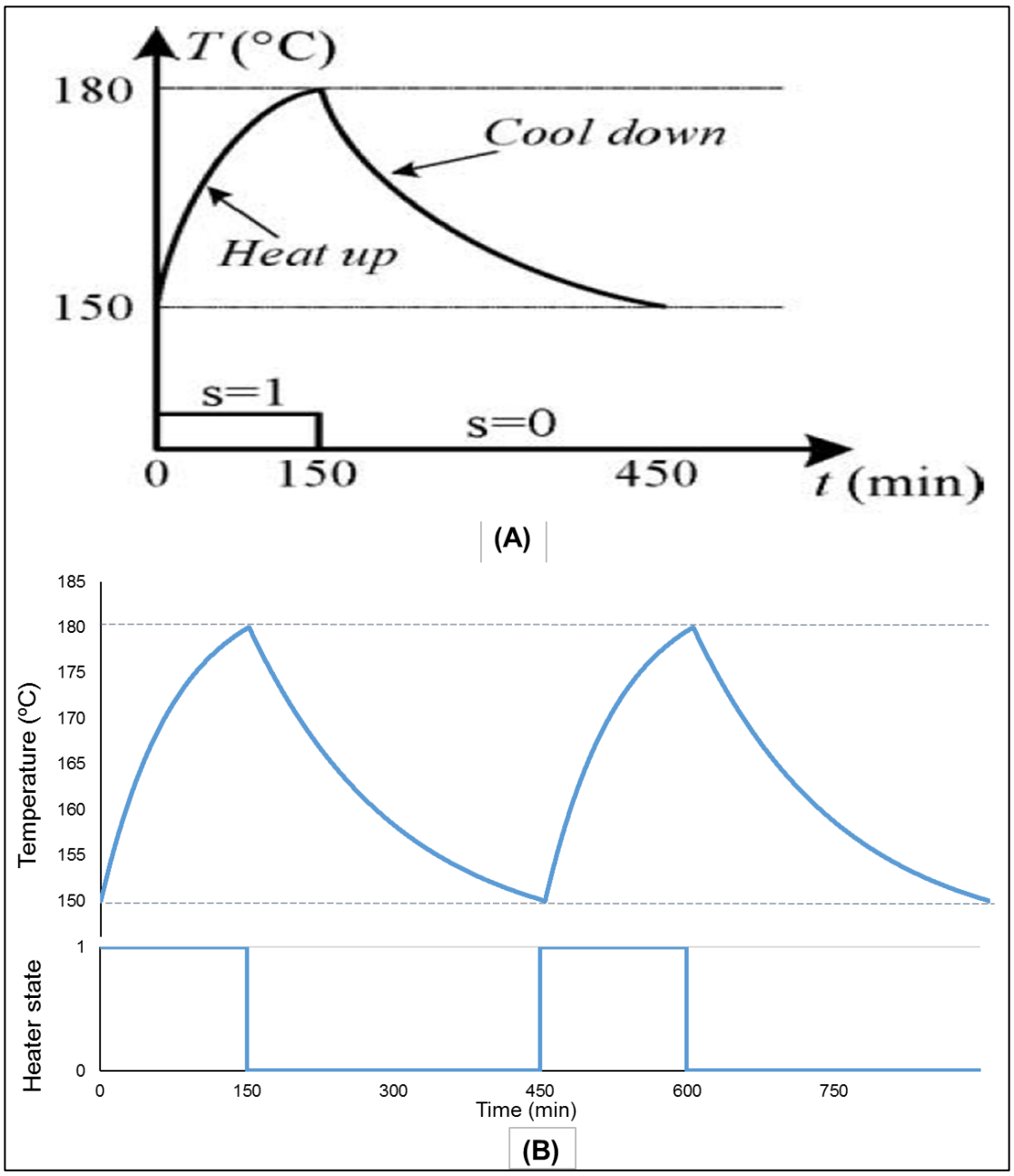

Fig. 3.22 (A) The diagram of temperature and heater state of a bitumen tank from [101], (B) the temperature and heater state of the bitumen tank model.

3.6. Modelling a population of units

For a population of units, the internal temperatures of refrigerators or bitumen tanks are determined not only by their inherent dynamics but also by their usage. Therefore, it is unlikely that all units have a similar level of temperatures. Similarly, the state of charge of a population of flywheel or battery energy storage systems varies over their permitted range. In this research, the diversity amongst a population of units is preserved by assigning a different initial state of charge and temperature to different units.

3.6.1. Modelling of a population of units of a flywheel energy storage system

Figure 3.23 (A) shows the power output of an aggregated model of a population of the units (i.e. four units) of the simplified flywheel energy storage system. While Fig. 3.23 (B) shows the velocity of the aggregated model. Initial velocities were randomly distributed between the maximum and minimum velocities (i.e. ω_{max} and ω_{min}). Figures 3.23 (A) and 3.23 (B) show that unit 2 had reached its maximum velocity at minute 9, consequently its power input reduced to zero. Similarly, unit 3 had reached its minimum velocity at minute 26 and its power output reduced to zero accordingly. As illustrated in Figs. 3.15 and 3.16, the velocity limiter efficiently prevented flywheel energy storage system units from exceeding their velocity limits.

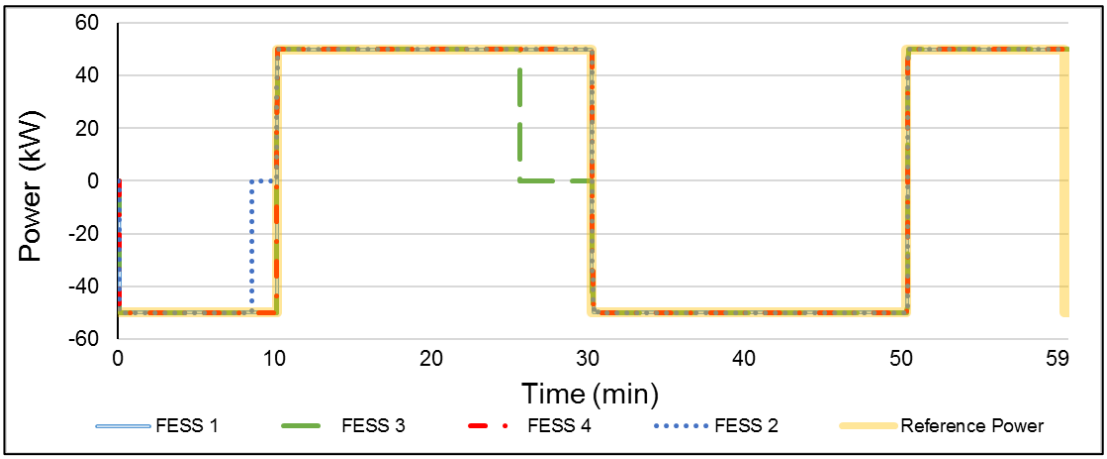

(A)

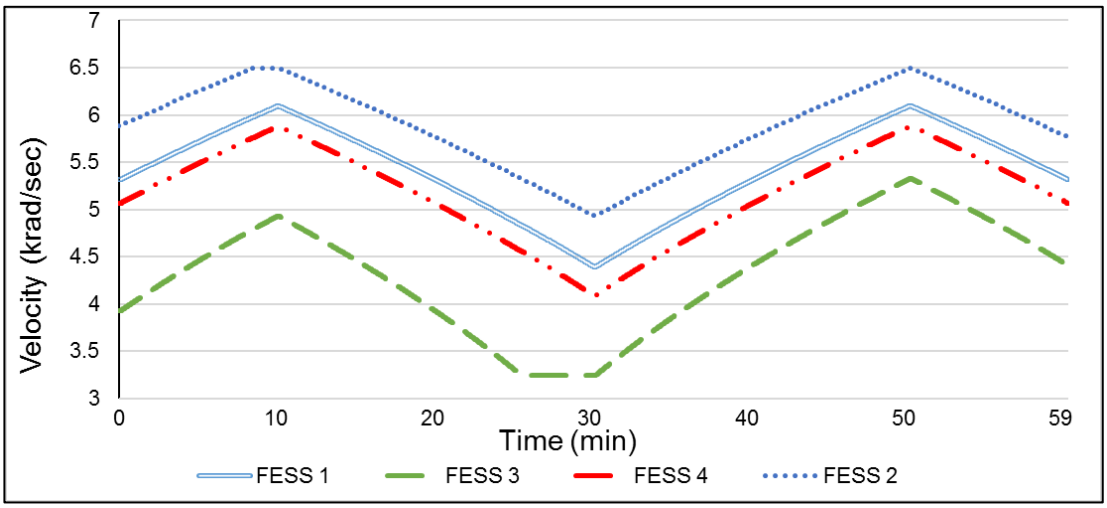

(B)

Fig. 3.23 (A) The power output of a population of units of the simplified flywheel energy storage system model, (B) velocities of a population of units of the simplified flywheel energy storage system model.

3.6.2. **Modelling of a population of units of a battery energy storage system**

Figure 3.24 (A) shows the power output of an aggregated model of a population of units (i.e. four units) of the battery energy storage system. Figure 3.24 (B) shows the states of charge of a population of units of the battery energy storage system. The initial states of charge of the population were randomly distributed between the minimum and the maximum values (i.e. 0%-100%). As a promising type of battery in terms of efficiency and price, the Lithium-Ion-based model was used in this simulation. Figures 3.24 (A) and 3.24 (B) show that units 1 and 2 had reached its maximum and minimum velocities respectively. Consequently, unit 1 power input and unit 2 powers output reduced to zero. These figures demonstrate the ability of the charge limiter to maintain charging/discharging actions of units within limits.

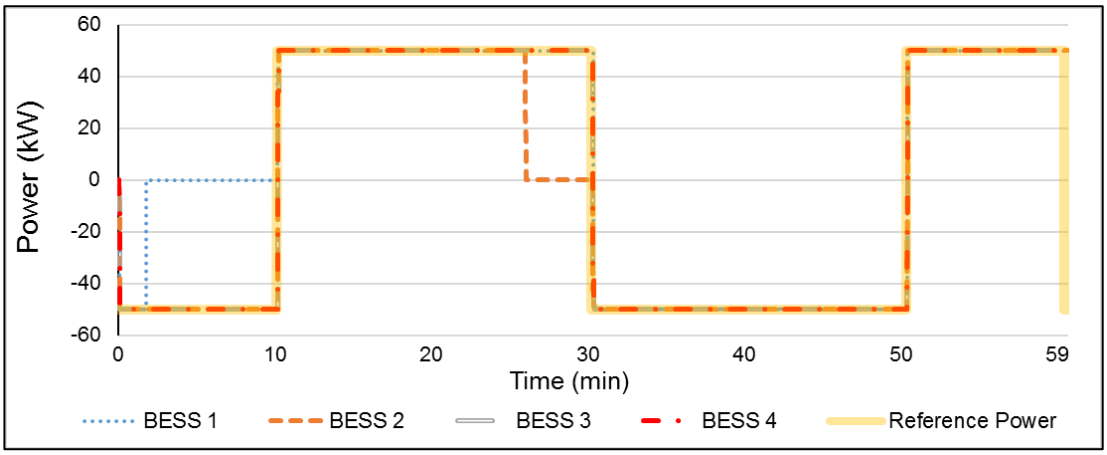

(A)

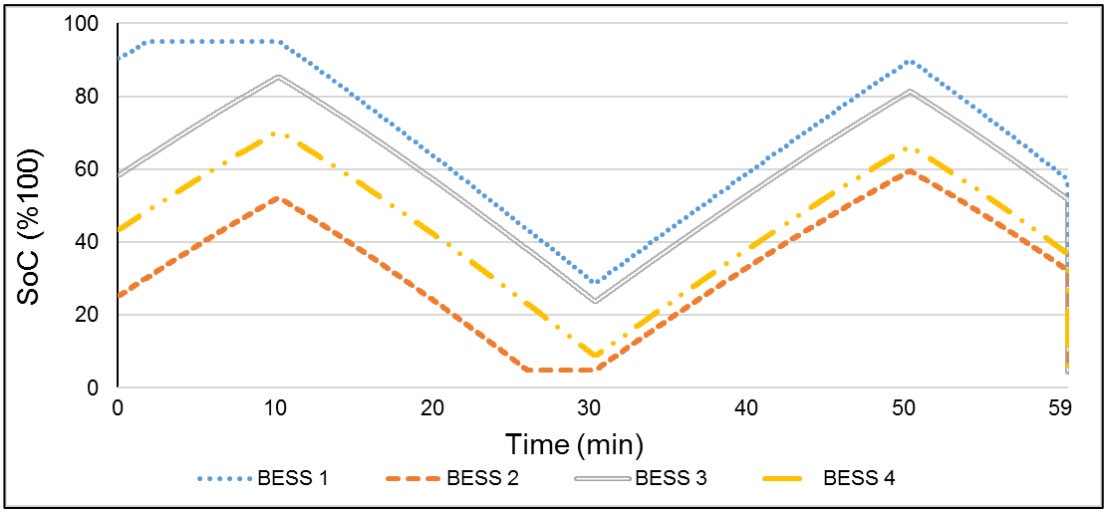

(B)

Fig. 3.24 (A) The power output of a population of units of the battery energy storage system model, (B) the state of charge of a population of units of the battery energy storage system model.

3.6.3. **Modelling of a population of refrigerators**

Figure 3.25 shows the cavity temperature and the compressor states of an aggregated model of a population of refrigerators (i.e. four refrigerators). Initial cavity temperatures were randomly distributed between T_{low} and T_{fhigh} set-points. The compressor states of refrigerators in Fig. 3.25 were initiated randomly of 30% ON and 70% OFF [18]. According to [18], this percentage varies widely over the day and from summer to winter, because the ON/OFF cycle of refrigerators is strongly affected by the ambient temperature. Hence, the ON cycle in summer is longer than that in winter. A power consumption of 100 W was considered for all refrigerator [18].

3.6.4. **Modelling of a population of bitumen tanks**

Figure 3.26 shows the temperature and heater states of an aggregated model of a population of bitumen tanks. Initial temperatures of tanks were randomly distributed

between T_{BT_high} and T_{BT_low}. According to the field tests in [8], the population of bitumen tanks were randomly distributed with ON-periods within the range of 30 min to 360 min and OFF-periods within the range of 60 min to 1140 min. States of tank heaters in Fig. 3.26 were initiated randomly of 30% ON and 70% OFF [18]. The main factor that influences the ON/OFF state of bitumen tanks is the electricity price, the bitumen tank owners switch ON tanks when the price is low in the early morning [18]. Consequently, the percentage of ON state is higher when the electricity price is lower. In this research, bitumen tanks have a typical power consumption of 40 kW and 150 ºC of low-temperature set-point (T_{BT_low}) and 180 ºC of high-temperature set-point (T_{BT_high}).

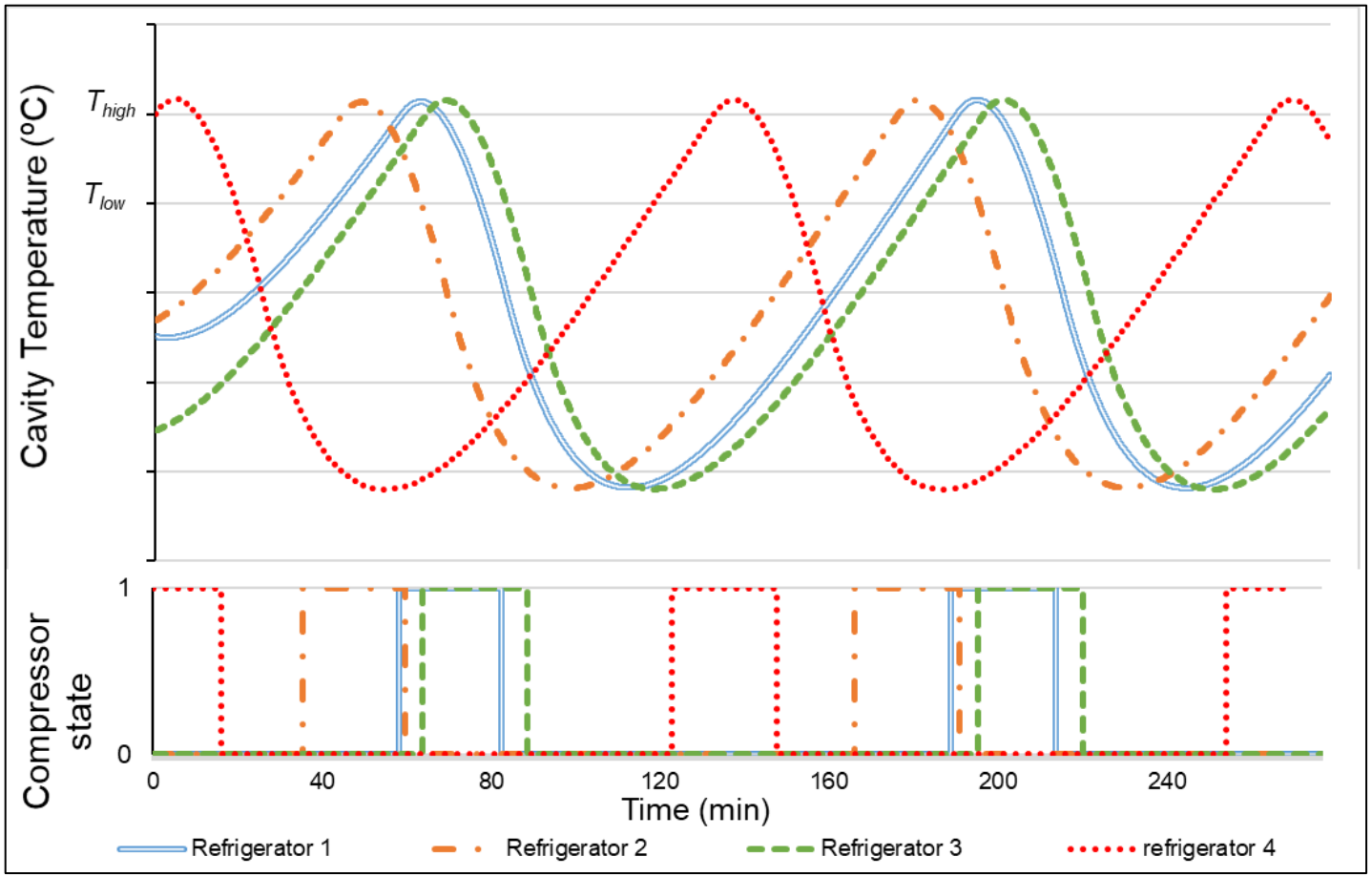

Fig. 3.25 The cavity temperature and compressor states of a population of refrigerators population of refrigerators models.

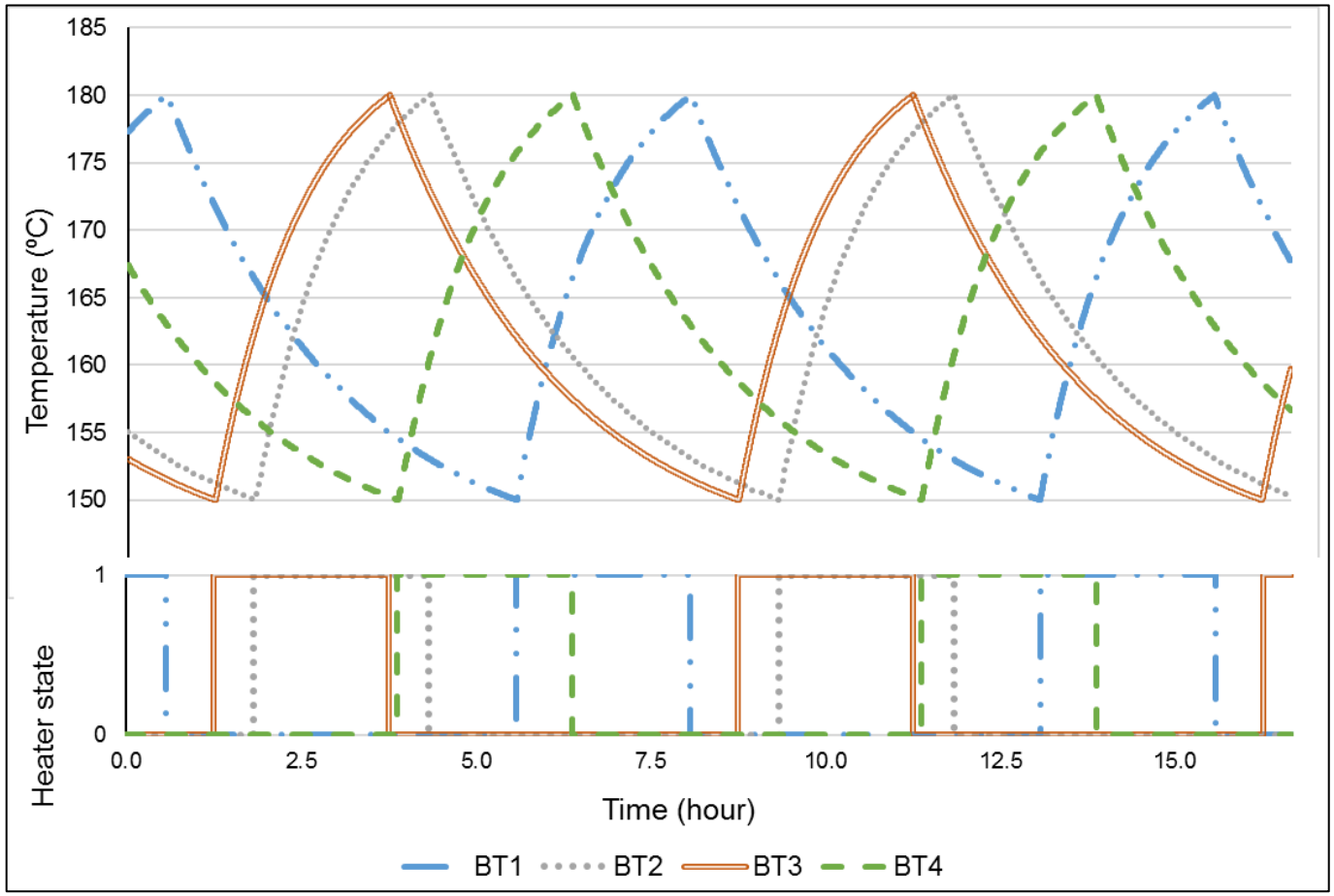

Fig. 3.26 The temperature and compressor states of a population of refrigerators population of bitumen tanks models.

3.7. Summary

Mathematical models of four components of the VESS were developed and validated in this chapter. Two types of energy storage system (i.e. flywheels and batteries) were modelled, and two types of demand respond units (i.e. refrigerators and bitumen tanks) were modelled based on literature. These models will be used to implement control schemes of the VESS in the next two chapters.

An average and a simplified models of a flywheel energy storage system were developed. The average model presents more accurately than the simplified model the system dynamic performance, while the simplified model facilitates the simulation of a large number of units due to a shorter simulation time required. The simplified model simulated one hour the operation of a flywheel energy storage system in one second, while the average model required an hour and a half to finish the same simulation. A battery energy storage system model was developed. The model is able to characterise different types of batteries, i.e. Lead-Acid, Lithium-Ion, Nickel-Cadmium and Nickel-hybrid. The model also facilitates grid scale studies with many units. To avoid exceeding the state of charge limits, a velocity limiter of the flywheel model and a state of charge limiter of the battery model were developed. The average and simplified models of flywheel energy storage system were validated against the performance of a similar model from the literature. The model of a battery energy storage system was validated against a manufacturer discharging chart.

Two types of demand response units were modelled. These models mimic the thermodynamic behaviour of refrigerators and the bitumen tanks by considering their internal temperature variations. These models are used to simulate populations of demand response units. Temperature controllers were included in the refrigerator and bitumen tank models. These controllers continuously measure the cavity temperature in refrigerators and the internal temperature in bitumen tanks to preserve their primary function, i.e. cold supply of refrigerators and hot supply of bitumen tanks. Models of refrigerator and bitumen tanks were validated against the performance of similar models in [101, 105].

Aggregated models, representing a population of units, of the four components of the virtual energy storage system were developed. The temperatures and compressor states of refrigerators and the internal temperatures and heater states of bitumen tanks were all

randomly initialised to present the diversity amongst a population of refrigerators and a population of bitumen tanks. Similarly, the velocities and states of charge of a population of flywheels and a population of batteries energy storage systems units were randomly initialised to simulate diversified populations.

Modelling the components of the VESS helped to identify the more suitable components for different applications of the VESS. Indeed, flywheels, which has a very long life in terms of the number of charging cycles, and refrigerators have short-duration responses are more suitable for frequent and short duration applications, such as frequency response services. In context, batteries, which has a moderate life in terms of the number of charging cycles, and bitumen tanks have long-duration responses therefore suitable for long duration applications, such as support the voltage control in distribution networks.

CHAPTER 4

A Frequency control scheme to provide frequency response services

Frequency control scheme of a Virtual Energy Storage System (VESS) to provide high, low and continuous frequency responses was designed. The VESS aggregates refrigerators and flywheel energy storage system modelled in Chapter 3.

The frequency control scheme of the VESS coordinates refrigerators and the flywheel energy storage system to deliver a certain amount of frequency response at a lower cost compared with an equal capacity of only flywheel energy storage systems. The control scheme was implemented using Matab®/Simulink on the same PC utilized to develop the models in Chapter 3.

4.1. The frequency control scheme of a virtual energy storage system

The frequency control scheme of the VESS is shown in Fig. 4.1. Following changes in frequency (Δf), the required response from the VESS (ΔP_{VESS_req}) is determined by a droop control (R_{VESS}). Both refrigerators and the flywheel energy storage system have local controllers. The frequency controller of refrigerators responds to the grid frequency f. The power mismatch between the change in refrigerators' power consumption ($\sum \Delta P_{Refrigerators}$) and ΔP_{VESS_req} is covered by the flywheel energy storage system ($\sum \Delta P_{FESS\text{-}req.}$). Hence, it compensates for the uncertain response of refrigerators.

It is assumed that an aggregator is responsible for receiving the power consumption of refrigerators, and then calculating and sending the power mismatch between the change in refrigerators' power consumption and the required response from the VESS to the flywheel energy storage system. A fast (i.e. not more than 1 second latency) two-way communication network is assumed to be available for measuring the power consumption of refrigerators and sending the power mismatch to the flywheels energy storage system.

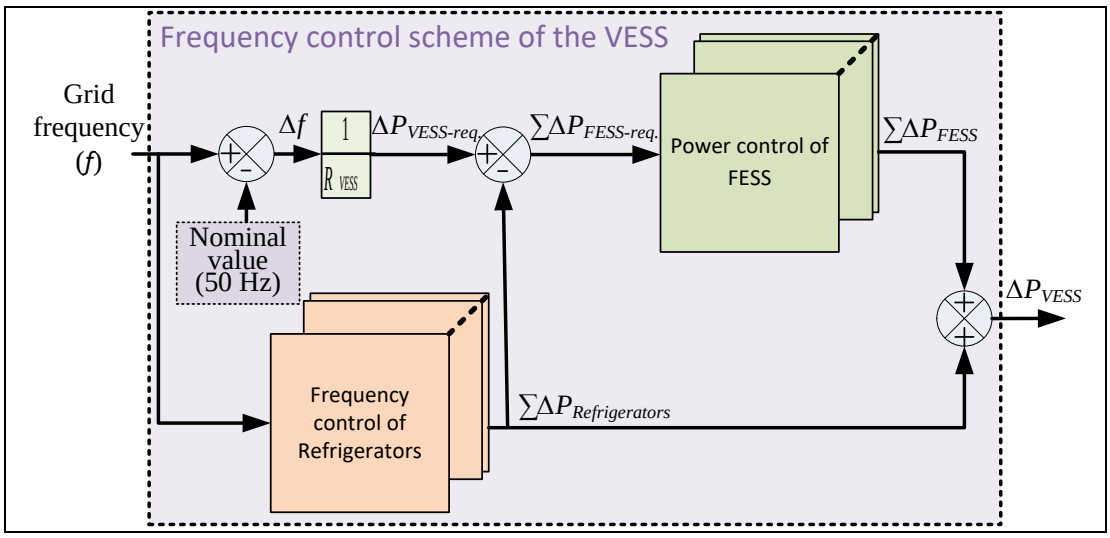

Fig. 4.1 The frequency control scheme of a VESS.

4.1.1. **The frequency control of a refrigerator**

The control scheme of each refrigerator is depicted in Fig. 4.2. In addition to the existing inherent temperature controller of the refrigerator presented in Chapter 3, a frequency controller was added. The temperature controller measures the cavity temperature (T_{ca}) of a refrigerator and generates a temperature state signal (S_T). S_T is 1 if T_{ca} is higher than the high temperature limit (T_{high}), and S_T is 0 if T_{ca} is lower than the low-temperature limit (T_{low}). The frequency controller also measures T_{ca} and defines a pair of frequency set points (e.g. F_{ON} and F_{OFF}) based on T_{ca}. It compares the measured frequency (f) to these set points to determine the state signals (S_{HF} and S_{LF}). The frequency controller switches ON/OFF the refrigerator in response to the frequency deviation. The frequency controller continuously compares f with F_{ON} and F_{OFF}. If f is higher than F_{ON}, the frequency controller sets the high-frequency state signal (S_{HV}) to 1, else to 0. On the contrary, if f is lower than F_{OFF}, the frequency controller sets the low-frequency state signal (S_{LF}) to 1, otherwise to 0. The temperature and the frequency controllers are connected to the compressor through logic gates, therefore these logic gates produce the final signal (S_{final}) to the compressor. The logic gates prioritise the temperature controller signal (S_T) above the frequency control signals (S_{HF} and S_{LF}) to maintain the cold supply function of refrigerators.

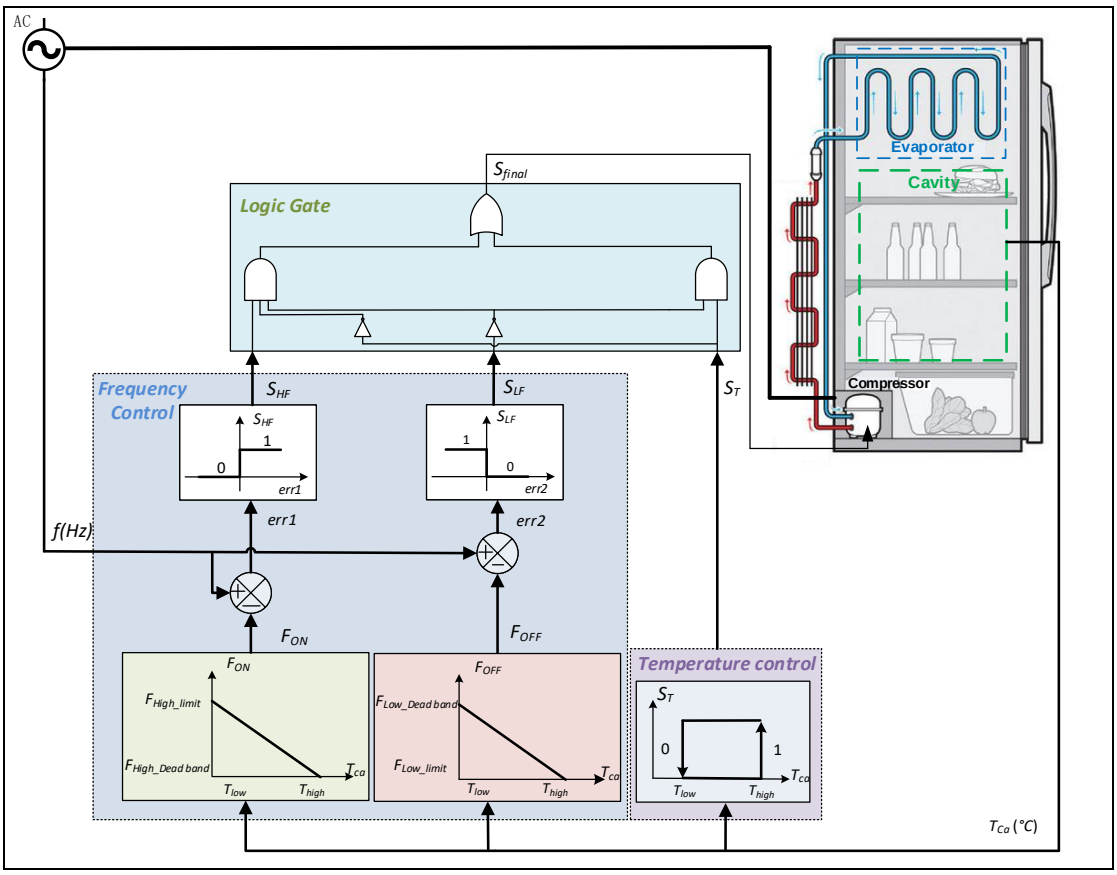

Fig. 4.2 The control scheme of the refrigerator.

Table 4.1 shows the truth table of the logic gates (shown in Fig. 4.2). In rows 1 and 5, the normal refrigeration cycle (presented in Chapter 3) is kept since f is higher than F_{OFF} and lower than F_{ON}. Rows 2 and 6 represent high-frequency states. In row 2, the refrigerator responds to the high frequency by switching ON. Rows 3 and 7 represent low-frequency states, and in row 7 the refrigerator responds to the low frequency by switching OFF. Since the grid frequency cannot be higher and lower than nominal frequency value simultaneously, rows 4 and 8 are not possible states.

TABLE 4.1 THE TRUTH TABLE OF LOGIC GATES IN FIG. 4.2

Row	S_T	S_{LF}	S_{HF}	S_{final}
1	0	0	0	0
2	0	0	1	1
3	0	1	0	0
4	0	1	1	-
5	1	0	0	1
6	1	0	1	1
7	1	1	0	0
8	1	1	1	-

A population of refrigerators is considered. A refrigerator having a lower temperature than others will have a lower F_{ON} and a higher F_{OFF} values as indicated in Fig. 4.2 If f

drops, refrigerators will start switching OFF from the refrigerator with the lowest *T*, because it will take the longest time to reach the high-temperature limit. In contrast, refrigerators will start switching ON from the refrigerator with the highest *T* when *f* rises above the nominal frequency value. The higher the frequency variation is, the larger number of refrigerators will be committed to respond. The number of refrigerators committed increases linearly with the increase in frequency variations, and consequently their aggregated power consumption will be larger.

In this study, a nominal frequency of 50 Hz was assumed (i.e. grid frequency in Great Britain (GB)). For frequency response services provision (presented in Chapter 2), a population of refrigerators must deliver a full change in power consumption when the frequency reaches/exceeds the limits of ± 0.5 Hz of the nominal value (i.e. 49.5 Hz-50.5 Hz) [23]. The frequency controller of refrigerators has dead-bands of ± 0.015 Hz of the nominal value (i.e. 49.985 Hz-50.015 Hz) [129].

4.1.2. **The frequency control of a flywheel energy storage system**

A simple active power controller of a flywheel energy storage system is shown in Fig. 4.3. The total power required is divided equally among the flywheel units. The required change in power of each unit (*i*) of the flywheel energy storage system ($\Delta P_{FESS\text{-}req\_i}$) is therefore calculated using (4.1)

$$\Delta P_{FESS-req\_i} = \frac{\sum \Delta P_{FESS-req.}}{no.of\ FESS\ units} \quad (4.1)$$

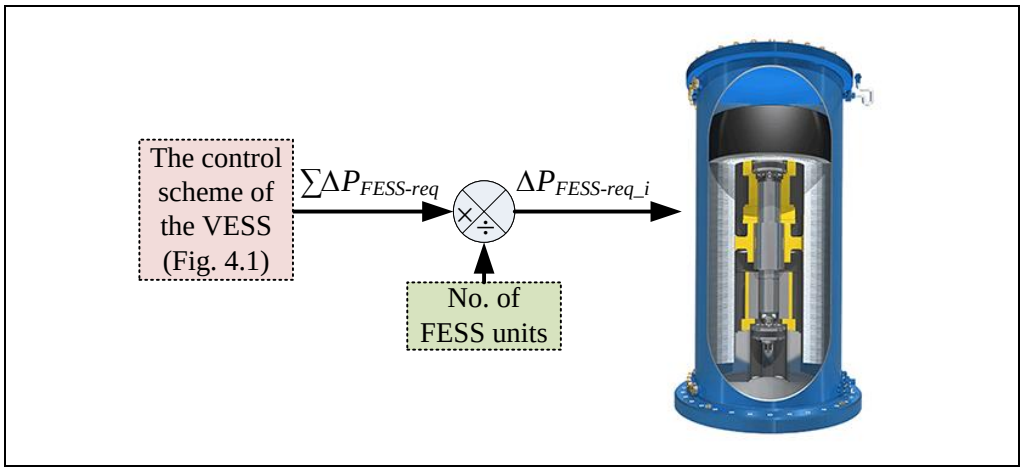

Fig. 4.3 The power control of a flywheel energy storage system unit.

To investigate the possibility of reducing the number of units responding to small frequency variations, hence extending the life of each of flywheel energy storage system

units, a profile recording the frequency of GB power system was used. Intuitively, a Conventional Droop Control (CDC) was used to determine the power output of the units.

A. Conventional Droop Control

Figure 4.4 shows a conventional droop control of a flywheel unit, all units are committed to provide frequency response. This control uses a droop setting (R_{FESS}) to determine the unit's power output (4.2):

$$R_{FESS} = \frac{\Delta f^{max}}{P^{rated}{}_{FESS}} \tag{4.2}$$

where Δf^{max} is the maximum frequency deviation from the nominal value (set to 0.5 Hz), and $P^{rated}{}_{FESS}$ is the rated power of the flywheel unit.

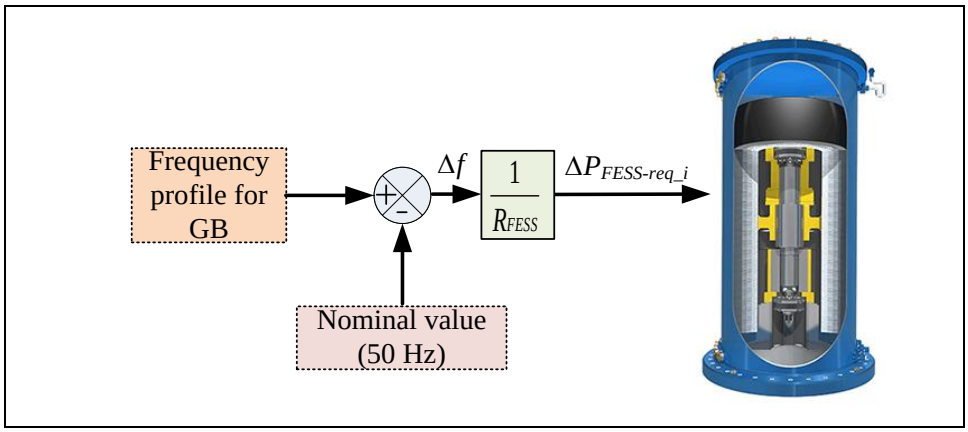

Fig. 4.4 The conventional droop control of a flywheel energy storage system unit.

Figure 4.5 shows the aggregated power of the population of units of the flywheel energy storage system responding to a historical frequency profile of the GB power system. 400 identical units, each unit have a power capacity of 50 kW and an energy capacity of 30 kWh, were used.

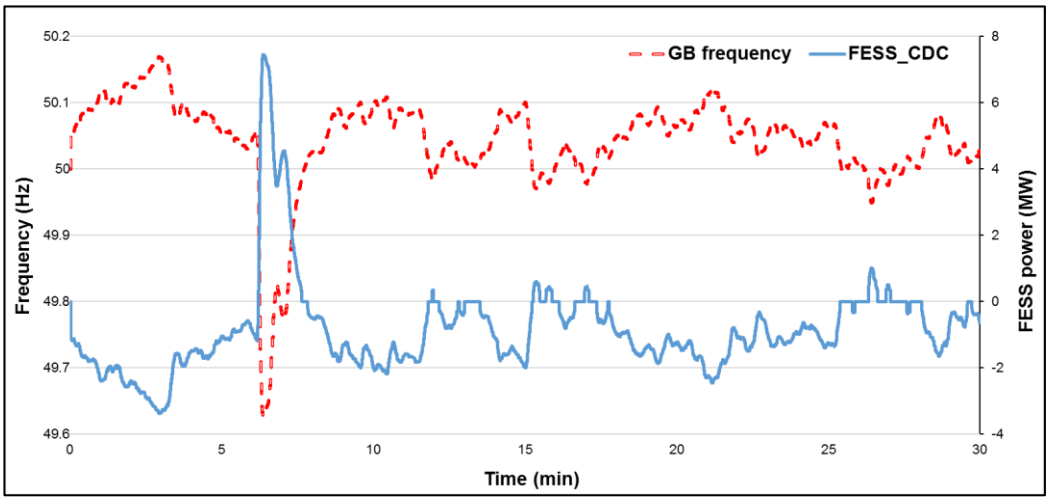

Fig. 4.5 The aggregated power of flywheel energy storage system units responding to frequency variations.

Influenced by the frequency control of refrigerators to reduce the number of units committed, the coordinated constant droop control was proposed.

B. Coordinated Constant Droop Control (CCDC)

The coordinated constant droop control of a flywheel energy storage system is shown in Fig. 4.6. The local controller consists of a coordinated controller and a constant droop control. The coordinated controller determines which unit to commit, while the droop control regulates the power output of the committed units.

The coordinated controller assigns a pair of frequency set points (e.g. F_{Chrg} and $F_{Dischrg}$) ~~based on~~ which varies linearly with the units' velocity (ω). A flywheel having a higher velocity than other flywheels will have higher F_{Chrg} and $F_{Dischrg}$ values than others. The controller compares the frequency f to these set points to determine the state signals (S_{Chrg} and $S_{Dischrg}$). If f is higher than F_{Chrg}, the controller sets the charging state signal (S_{Chrg}) to 1, else S_{Chrg} is 0. Otherwise, if f is lower than $F_{Dischrg}$, the controller sets the discharging state signal ($S_{Dischrg}$) to 1, otherwise $S_{Dischrg}$ is 0. Both state signals are connected to an OR-logic gate, the logic gate output ($FESS_{state}$) governs the switch which determines the required power output from the flywheel unit (illustrated in Fig 4.6). The required power output of the flywheel energy storage system is determined by a droop control constant value (R_{FESS}) with respect to the received f.

Flywheels will start committing (and charge) from the flywheel with the lowest ω when f rises above the nominal frequency value. Similarly, flywheels will start committing (and discharge) form the flywheel with the highest ω when f drop below the nominal frequency value. The number of flywheels committed increases linearly with the increase in frequency deviations.

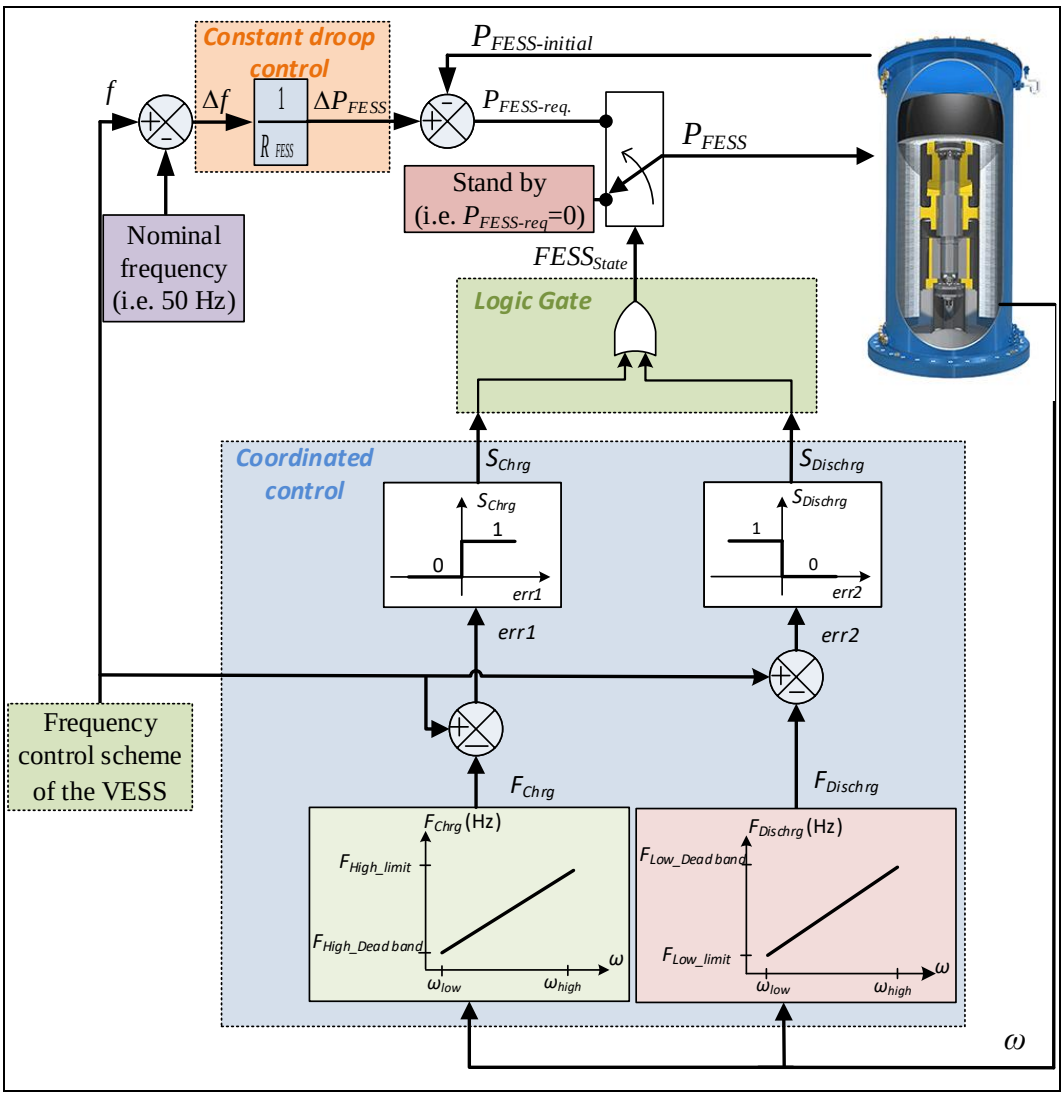

Fig. 4.6 The coordinated constant droop control of a flywheel energy storage system.

This control reduces significantly the number of charging and discharging cycles, hence prolonging the lifetime of units. However, when the frequency variation (Δf) is small, the aggregated power output from the population of units will be smaller than that using Conventional Droop Control (CDC) strategy presented earlier in Fig. 4.7. Because only a few units are committed to the frequency variation compared to the whole population committed in conventional droop control strategy.

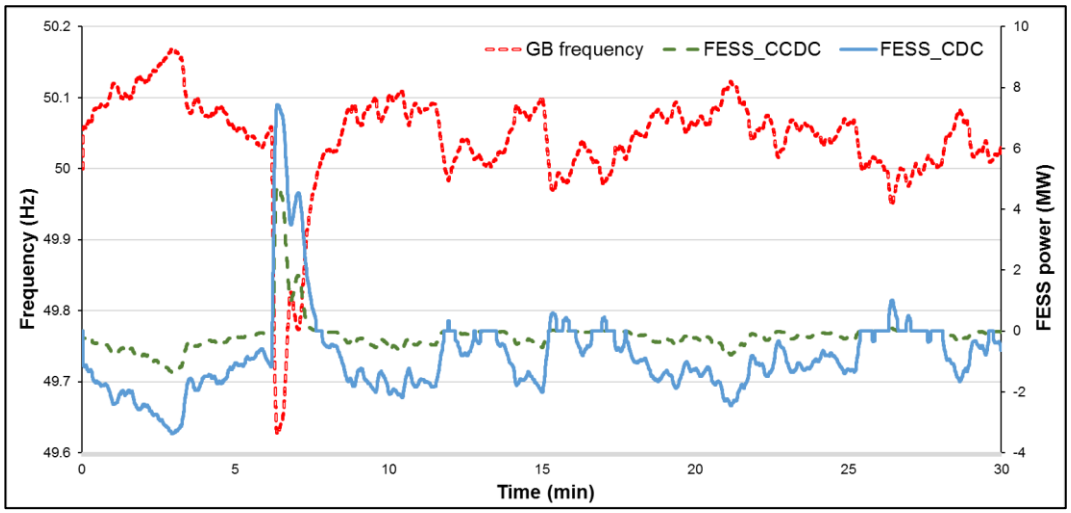

Fig. 4.7 The aggregated power of flywheel units responding to frequency variations under the two control strategies.

A test frequency varying between below 49.5 Hz and 50 Hz was used to examine the number of committed units, which are controlled by the coordinated constant droop control, responding to frequency variations. Figure 4.8 shows the correlation between the number of flywheel units and the test frequency. The test validates that the number of committed units varies linearly with the frequency changes, and this feature was used in the following proposed control.

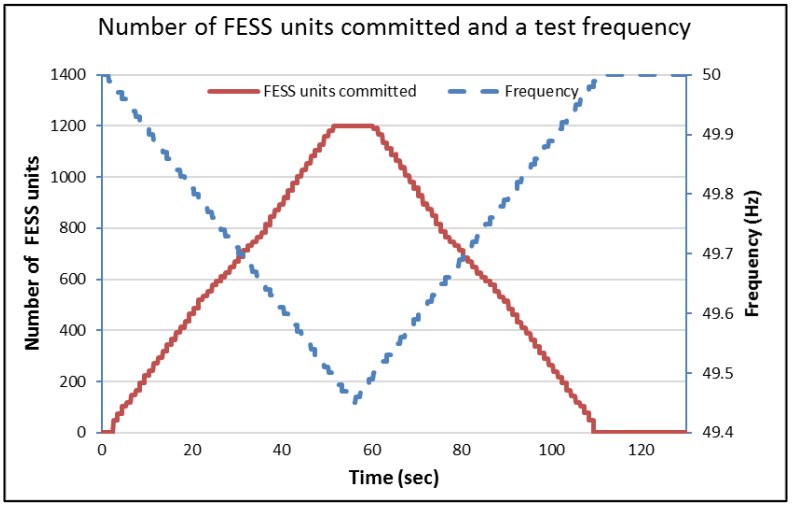

Fig. 4.8 The number of units committed of a flywheel energy storage system and the test frequency.

C. Coordinated Adaptive Droop Control (CADC)

To provide a similar level of frequency response to Conventional Droop Control (CDC) while reducing the number of committed units, a Coordinated Adaptive Droop Control (CADC) was developed. The coordinated adaptive droop control of a flywheel energy storage system is depicted in Fig. 4.9. Instead of the constant droop setting used

in the coordinated constant droop control, an adaptive droop control value ($R_{adaptive}$) is defined, being inversely proportional to frequency deviations (Δf) as shown in (4.3).

$$R_{adaptive} = \frac{\Delta f^{max}}{\Delta f} \times R_{FESS} \tag{4.3}$$

Since a small frequency deviation (Δf) triggers only a small number of units to commit, a droop value $R_{adaptive}$ greater than the conventional droop value R_{FESS} is required. When the frequency deviation increases and reaches the maximum frequency deviation (i.e. Δf^{max}) and all units are triggered to commit, the droop value $R_{adaptive}$ equals to R_{FESS}.

Figure 4.10 shows the aggregated power output of the population of units of the flywheel energy storage system in the three control strategies. Figure 4.11 shows the number of charging/discharging times the flywheel units respond to the GB frequency profile variations in the three control strategies. When the frequency deviations are small (Fig.4.10), the aggregated power output under the CDC or the CADC are higher than that with the CCDC. The aggregated power output with either CDC or CADC was similar while only less than a quarter of units respond in the CADC strategy compared with the CDC strategy (see Fig. 4.11). Therefore, the CADC strategy is preferable to extend the lifetime of the costly flywheel units. In the case of a large frequency deviation, the aggregated power of the units with all control strategies presented, i.e. the CDC, the CCDC and the CADC, will have equal aggregated power outputs and all units will respond.

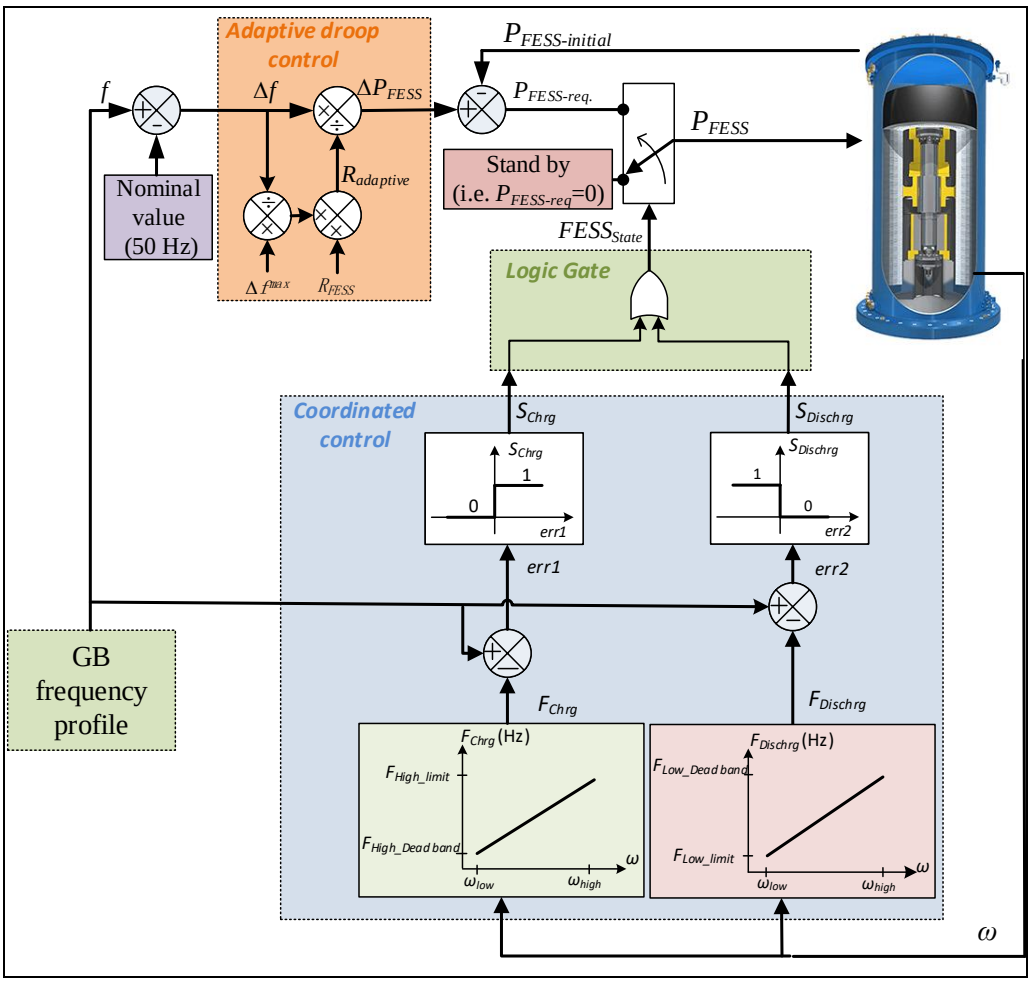

Fig. 4.9 The coordinated adaptive droop control of a flywheel energy storage system.

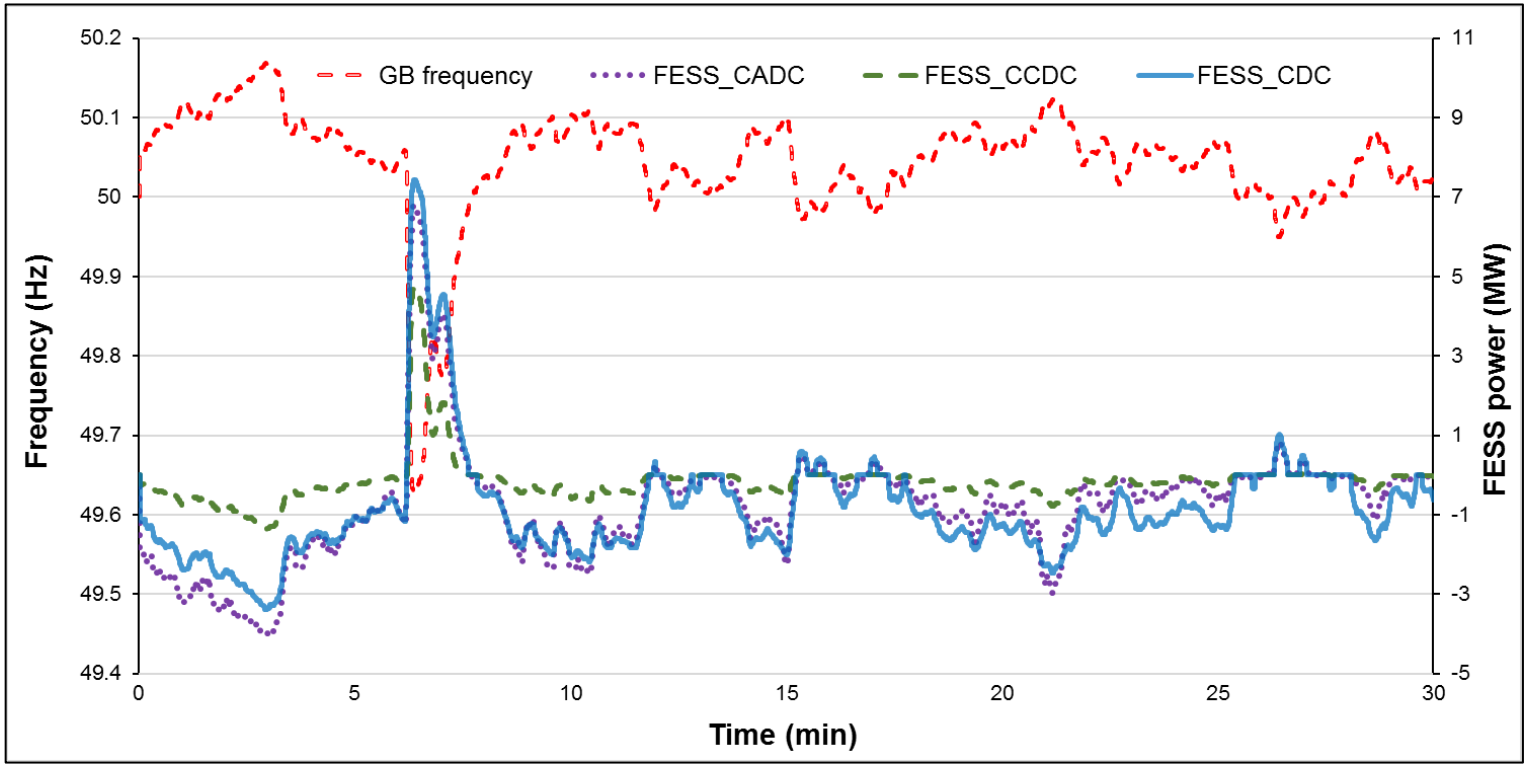

Fig. 4.10 The aggregated power of flywheel units responding to frequency variations for the three control strategies.

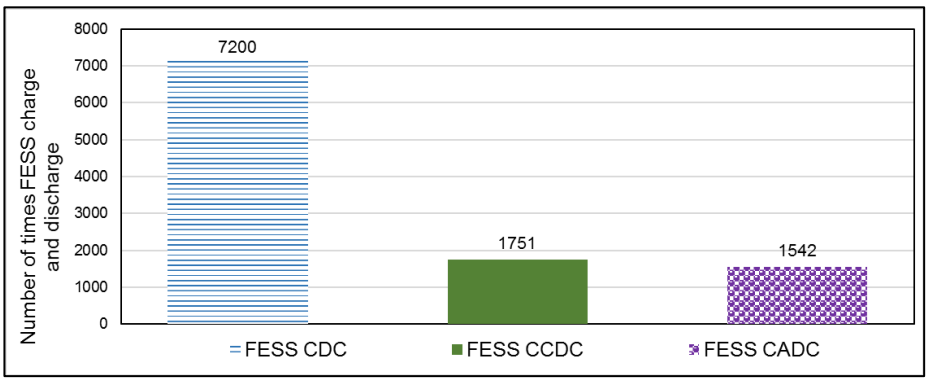

Fig. 4.11 The number of times the flywheel units responded to frequency variations under different control strategies.

Based on the results in Fig. 4.10 and Fig. 4.11, the CADC control strategy was adopted to control the population of the flywheel units within the VESS. The frequency control scheme of the VESS, presented in section 4.2, has therefore updated accordingly. Figure 4.12 shows the updated, i.e. based on Fig. 4.1 shown earlier, frequency control scheme of the VESS. The required flywheel energy storage system ($\sum\Delta P_{FESS\text{-}req}$) is converted to a modified frequency change value ($\Delta f'$) through a droop control setting ($R_{\sum FESS}$) as shown in (4.4).

$$R_{\sum FESS} = \frac{\Delta f^{max}}{\sum P^{rated}{}_{FESS}} \tag{4.4}$$

The aggregator sends the modified frequency f' to the units of the flywheel energy storage system, and then the local frequency control (i.e. CADC) of the units responds to f'.

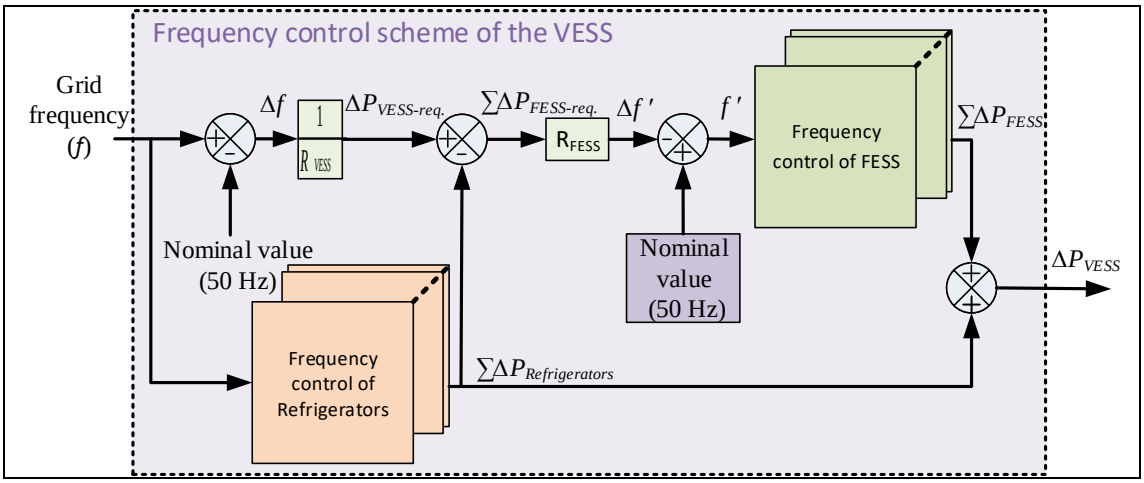

Fig. 4.12 The updated frequency control scheme of a VESS.

4.2. The test system

The performance of the frequency control scheme of the VESS was evaluated by a series of simulations. It was assumed that an aggregator located in London was responsible for aggregating refrigerators and dispersed flywheel energy storage system units to provide frequency response services to the GB power system.

4.2.1. The simplified GB power system

The simplified GB power system was adopted from [101, 130] to assess the performance of the VESS frequency control scheme (Fig. 4.13). The active and the reactive power flows in the transmission networks are assumed relatively independent from each other. Since frequency control is related to active power control, only active power is concerned in this study.

All large scale generators connected to the GB power system are required to provide primary frequency response [21]. Also, most of these generators have an obligation to provide secondary frequency response as well. To simulate this, two generators were modelled. Generator 1 only provides primary frequency response while generator 2 provides both primary and secondary frequency response services. It was assumed that 80% of the generators provide both primary and secondary response services (i.e. K_F=0.2 in Fig 4.13). Therefore, an additional integral control loop was added to the model of generator 2. This integral control loop with parameter (K_I=0.01) is responsible for restoring the grid frequency to 50 Hz.

In both generators, the synchronous power plants' characteristics such as coal, gas and hydro were modelled as a governor and a turbine transfer functions [131]. Their frequency response was presented by droop control. The damping effect of frequency dependent loads was modelled through the system inertia (H_{eq}) and a damping factor (D) [131, 132].

Based on [133], the equivalent system inertia (H_{eq}) was estimated to be 4.5 s and the equivalent droop control (R_{PS}) was 9% in both generators. Assuming that, the inertia constant for coal, gas, nuclear and other power plants as 4.5, 6.0, 3.0 and for wind and interconnectors as 0.0, H_{eq} was calculated using (4.5) [133] based on the operating capacity of each power plant in 2008 in the GB power system. H_{eq} calculation is presented in Table 4.2 [133]. In both generators, a governor dead-band of ± 0.015 Hz [21] was assumed and the time constants of the governor, the turbine and the load damping constant

were set as follows: T_{gov}=0.2 s; T_1=2 s; T_2=12 s; T_{turb}=0.3 s; D=1. The parameters of the model were calibrated with a real frequency record following a 1,220 MW loss of generation on the GB power system [130].

$$H_{eq} = \sum_{i=coal,gas,\dots} H_i * \frac{S_i}{S_{sys}} \quad (4.5)$$

where H_i is the inertia constant of power plant i (sec), S_i is the capacity of power plant i (MVA) and S_{sys} is the total capacity of all operating power plants (MVA).

TABLE 4.2 The equivalent system inertia on the system base of 70 MVA in 2008 [133]

Power plant type	Installed capacity (GW)	Operating capacity (GW)	Hi
Coal	29.40	23.52	1.51
Gas	29.40	23.52	2.01
Nuclear	10.60	10.60	0.45
Interconnector	2.00	2.00	0.00
Wind	3.70	1.48	0.00
Other	12.00	9.12	0.58
Total	87.10	70.24	4.55

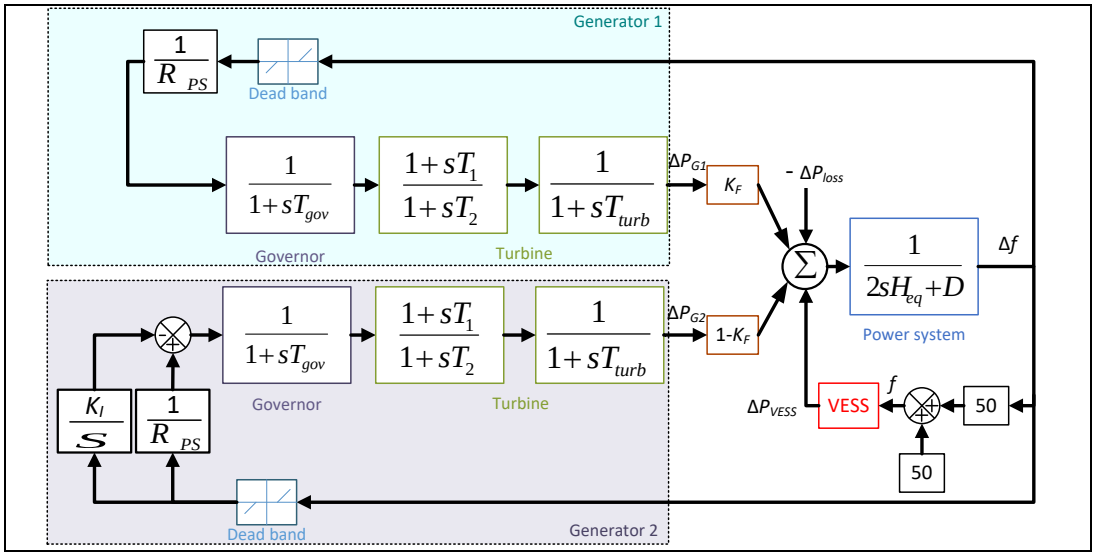

Fig. 4.13 A simplified GB power system.

4.2.2. The VESS capacity

A) Refrigerators capacity

There are 3,220,300 households in London in 2014 [134]. It is assumed that the refrigerator (0.1 kW) in each household is equipped with the frequency controller presented in section 4.2.1. This results in 322 MW of controllable loads in London.

The amount of frequency response from refrigerators varies over the day [18] (see Fig. 4.14). The maximum reduction in power consumption (i.e. the red lower dotted line

in Fig 4.14) is 18.5% at 18:00 and the minimum reduction is 13.2% at 6:00. Considering the number of refrigerators in London, a maximum power reduction of 60 MW and minimum power reduction of 40 MW is expected. Similarly, the maximum and minimum increase in power consumption (i.e. the blue upper dotted line in Fig 4.6) is approximately 50% to 56%. Based on the number of refrigerators in London, a minimum power increase of approximately 160 MW and a maximum power increase of approximately 180 MW. Consequently, refrigerators have more potential to provide a response to the frequency rise than to the frequency drop. In summary, refrigerators can provide (40-60 MW) power reduction for the low-frequency response, and they can provide (160-180 MW) power increase for the high-frequency response.

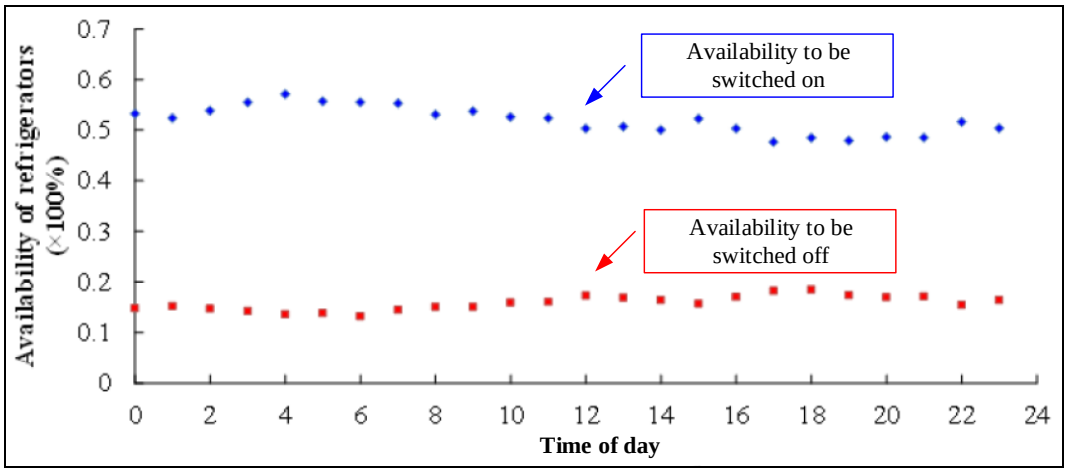

Fig. 4.14 The availability of refrigerators to be switched ON/OFF over a day based on field measurements [18].

The VESS is therefore planned to provide a linear dynamic frequency response of a maximum of 60 MW when frequency drops to 49.5 Hz or lower and of 180 MW when frequency rises to 50.5 Hz or higher over a day. For periods of the day in which the refrigerators cannot provide the required response from VESS, the flywheel energy storage system is used. The flywheel energy storage system can support the required response from VESS for 30 minutes.

B) Flywheels energy storage system capacity

The flywheels are required to cover a maximum power mismatch between the planned power output from the VESS (i.e. 60 MW) and the minimum reduction in refrigerators power consumption (i.e. 40 MW). Consequently, 20 MW of flywheel units' capacity was used. This 20 MW of flywheels consists of 400 units, with each unit has a power capacity of 50 kW and an energy capacity of 30 kWh.

4.3. Case studies

Three case studies were carried out to assess the VESS ability to provide low, high and continuous frequency response services. In Cases 1 and 2, the VESS is recruited to provide low and high-frequency responses services by connecting it to the simplified GB power system. The GB power system demand was 20 GW representing a summer night, and the following three scenarios were compared:

"**No FESS/VESS' Scenario 1**

"**Only FESS" Scenario 2** (60 MW flywheel energy storage system is used)

"**VESS" Scenario 3** (all refrigerators in London and 20 MW flywheel energy storage system are used).

In Case 3, the VESS is recruited to provide a continuous frequency response in proportion to frequency changes. The simulation was implemented by injecting a historical frequency profile from the GB power system, presented in section 4.2.2, into the VESS.

4.3.1. **Case 1 (Low-frequency response)**

The VESS is procured to provide primary and secondary low-frequency response services (described in Chapter 2) following a loss of a generation of 1.8 GW.

Figure 4.15 shows the frequency variation of the simplified GB power system after the loss of generation under the three scenarios. Since the VESS is injecting active power into the power system, this case depicts the discharging phase of the VESS.

Figure 4.16.A shows the power output change of the VESS and only the flywheel energy storage system in Scenario 3 and 2 respectively, while Fig. 4.16.B shows the change of power consumption of refrigerators and power output of flywheel energy storage system in the VESS. Both the VESS in Scenario 3 and only the flywheel energy storage system in Scenario 2 responded to the frequency deviation with 60 MW response.

Since the 60 MW response is small in a 20 GW system, the improvement in frequency was approximately 0.01 Hz and seems hardly noticeable. If the installed capacity of the VESS is higher, the frequency drop will be significantly reduced. The number of units of the flywheel energy storage system in the VESS (i.e. Scenario 3) was only one-third of that in Scenario 2, however, the VESS provided a similar amount of frequency response to that of only the flywheel energy storage system in Scenario 2. The reduced capacity of

the flywheel energy storage system in Scenario 3 will reduce the cost significantly compared to Scenario 2.

Figure 4.17 shows the change of power output of generators in the three scenarios. It can be seen that, with the flywheel energy storage system only (i.e. Scenario 2) or the VESS (Scenario 3), the required capacity of the costly frequency-responsive generators is reduced.

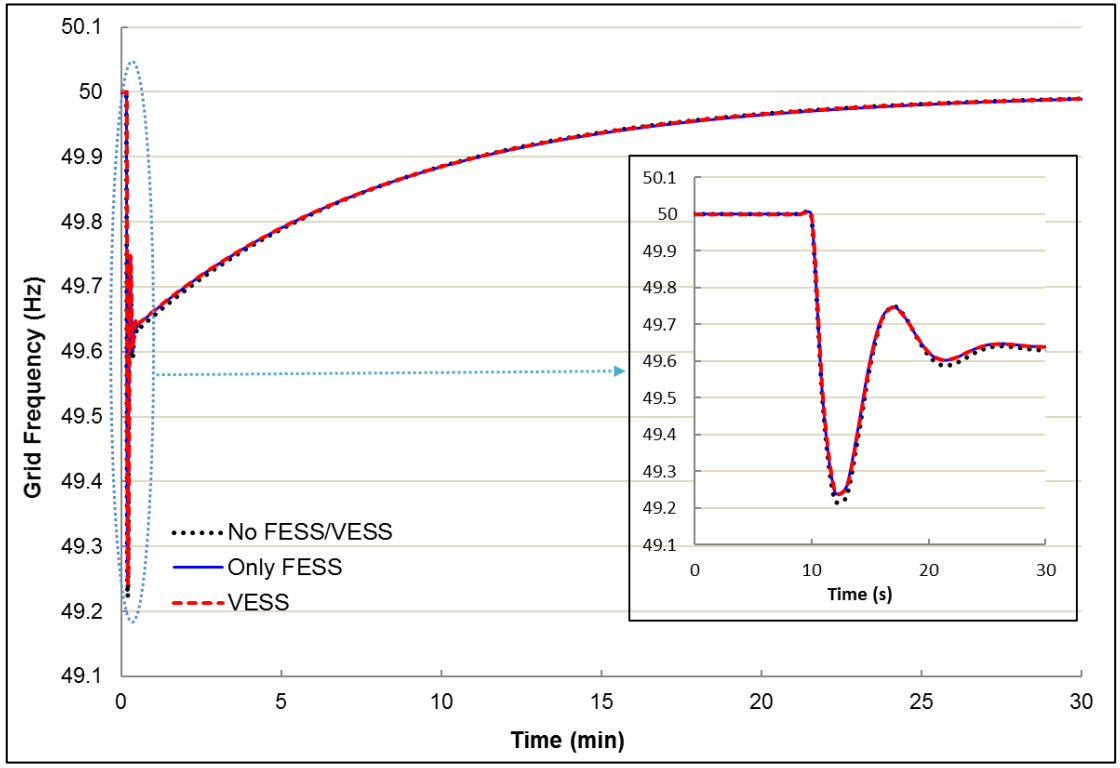

Fig. 4.15 The variation of the system frequency after the loss of generation.

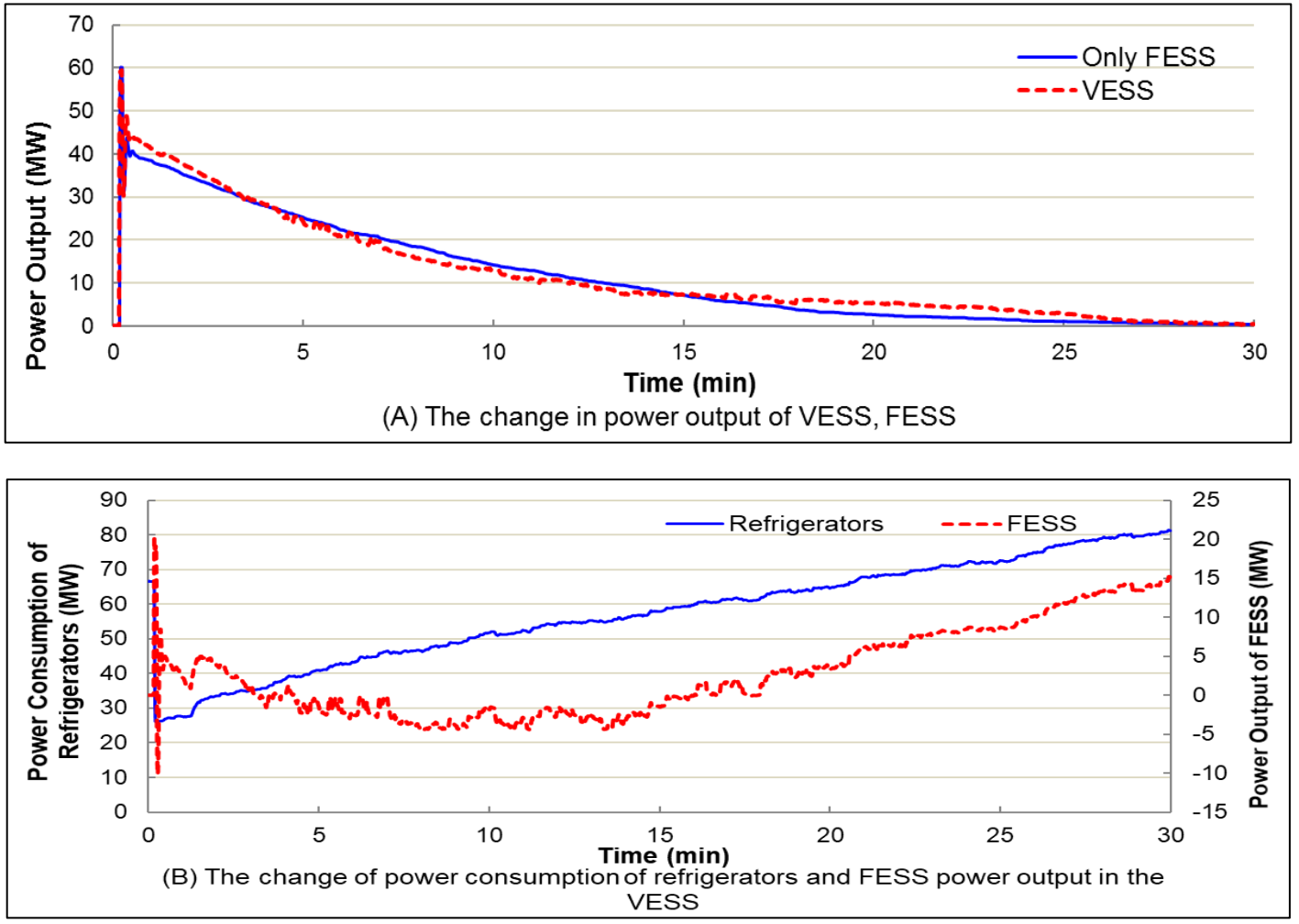

Fig. 4.16 (A) The change in power output of the VESS and FESS, (B) the change of power consumption of refrigerators and FESS power output in the VESS.

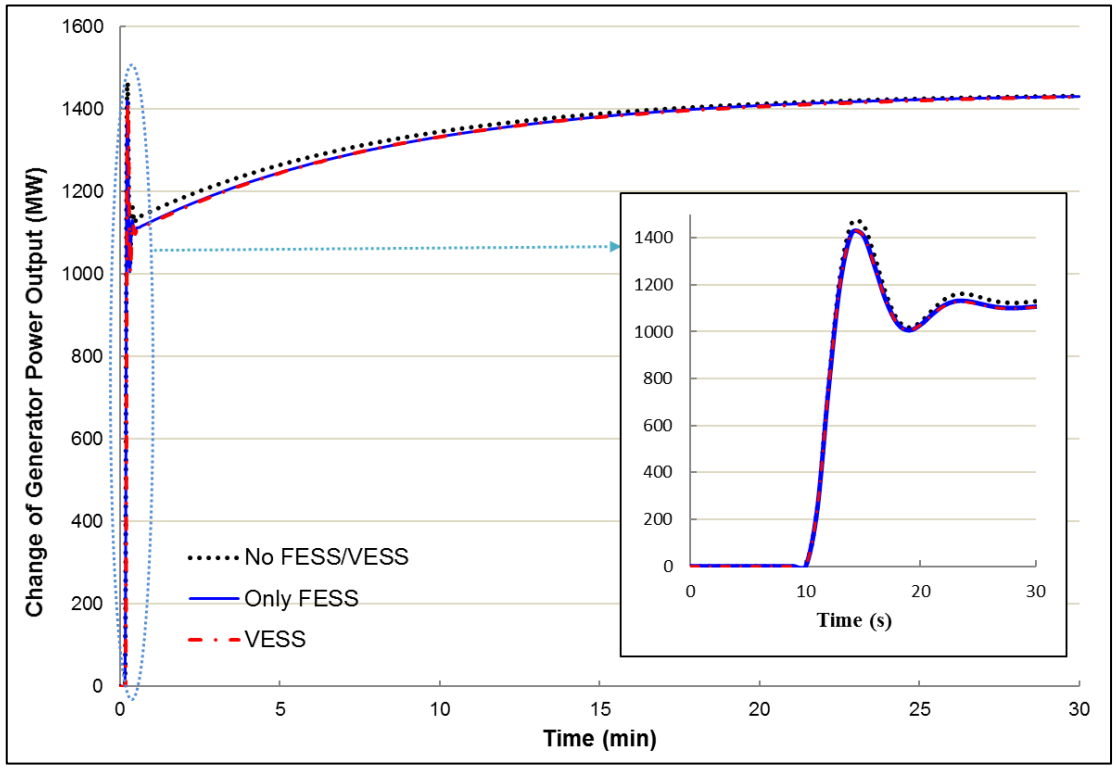

Fig. 4.17 The change of power output of generators after the loss of generation.

4.3.2. **Case 2 (High-frequency response)**

The VESS is acquired to provide a high-frequency response service (described in Chapter 2) following a loss of demand of 1 GW.

Figure 4.18 shows the frequency variation of the simplified GB power system after the loss of generation under the three scenarios. Since the VESS is absorbing active power for the power system, this case represents the charging phase of the VESS.

Figure 4.19.A shows the change in power output of the VESS and only the flywheel energy storage system in Scenario 3 and 2 respectively, while Fig. 4.19.B shows the change of power consumption of refrigerators and the power output of the flywheel energy storage system in the VESS in Scenario 3. Since the frequency rise did not reach the 50.5 Hz, the flywheel energy storage system in Scenario 2 provided approximately 45 MW response and the maximum frequency rise was slightly reduced by 0.01 Hz compared with Scenario 1. However, the VESS in Scenario 3 provided approximately 140 MW after the sudden loss of demand which is much higher than the response of the flywheel energy storage system in Scenario 2 and the frequency rise was reduced by 0.05 Hz. This 140 MW response from the VESS was approximately 120 MW increase in the power consumption of refrigerators plus 20 MW power output of the flywheel energy storage system.

Figure 4.20 shows the change of power output of generators in the three scenarios. The required capacity of the costly frequency-responsive generators was reduced with the flywheel energy storage system only (i.e. Scenario 2) or the VESS (Scenario 3).

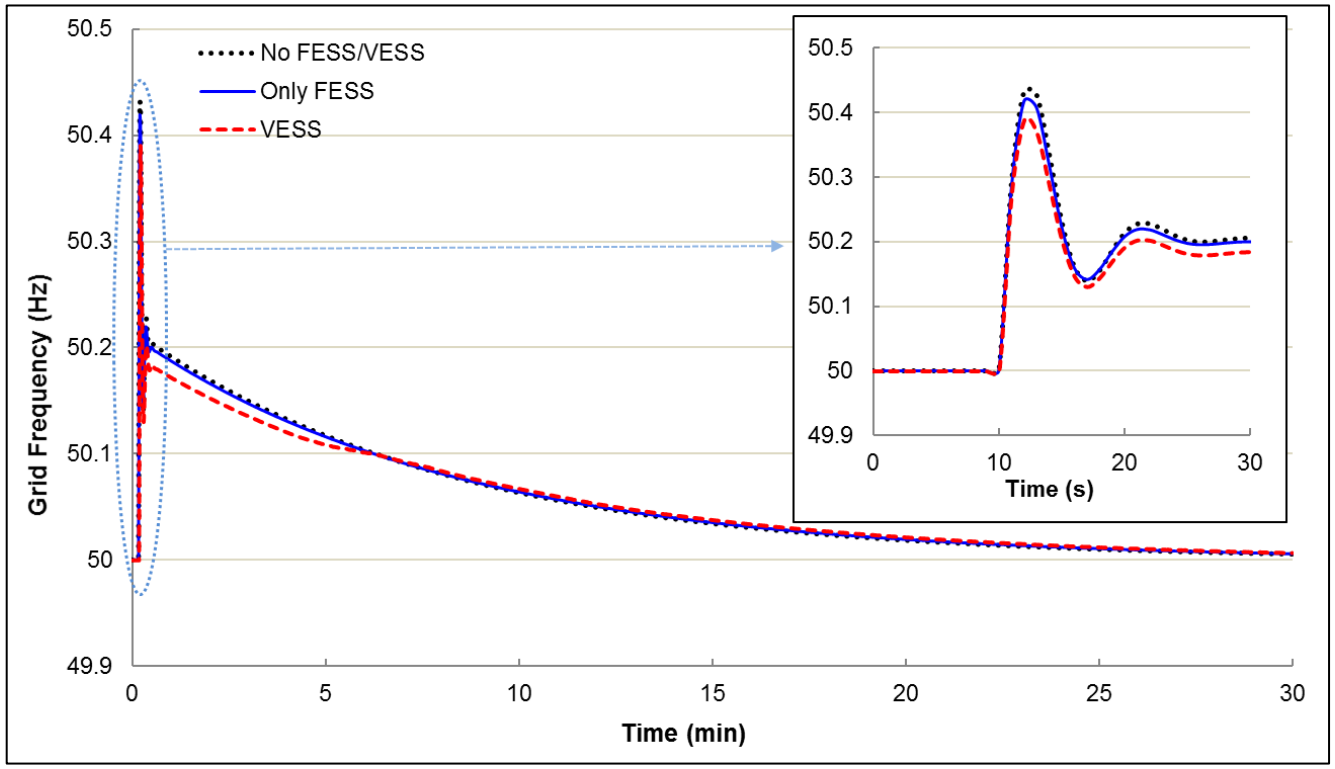

Fig. 4.18 The variation of the system frequency after the loss of demand.

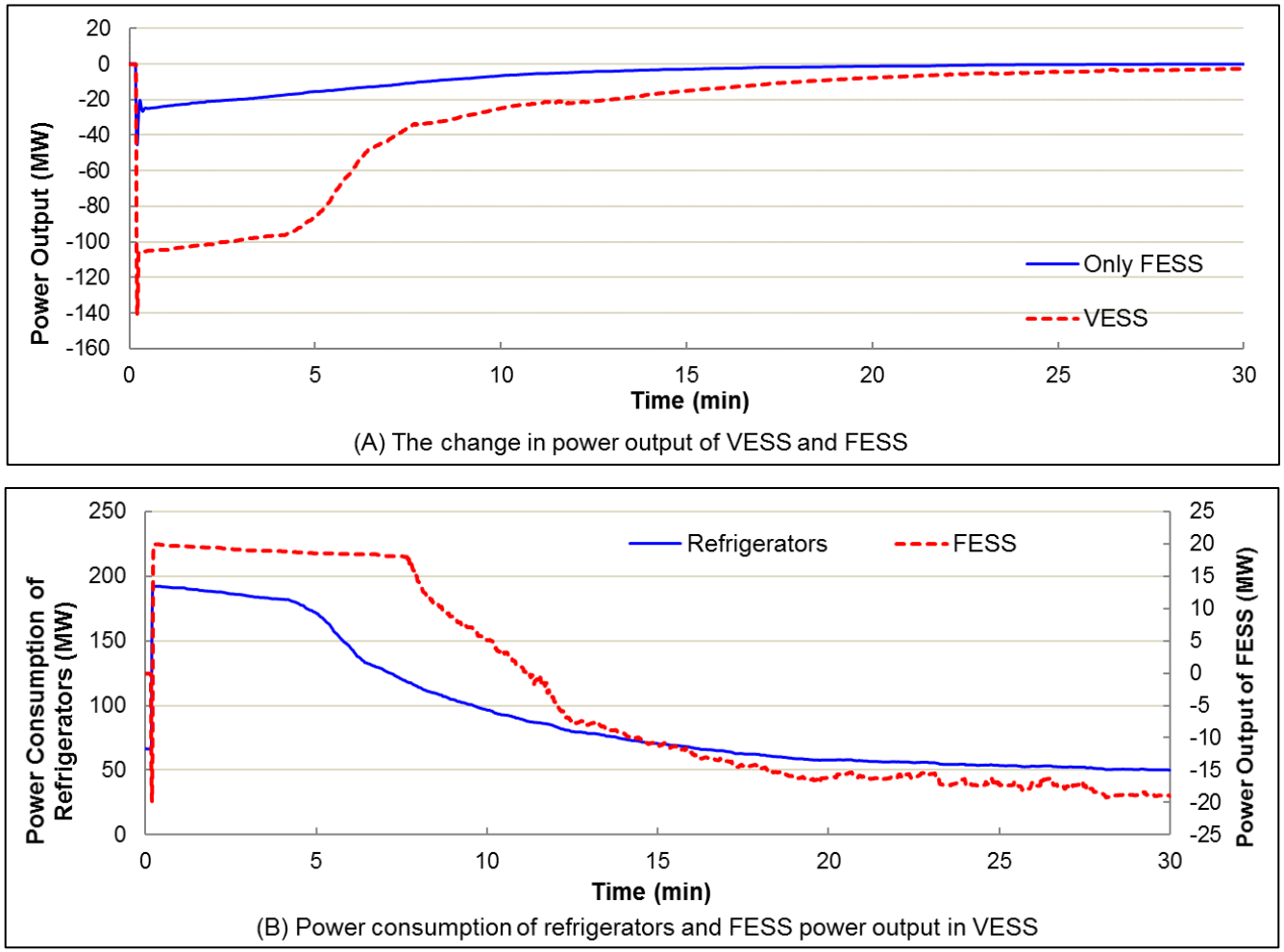

Fig. 4.19 (A) The change in power output of the VESS and FESS, (B) the power consumption of refrigerators and FESS power output in VESS.

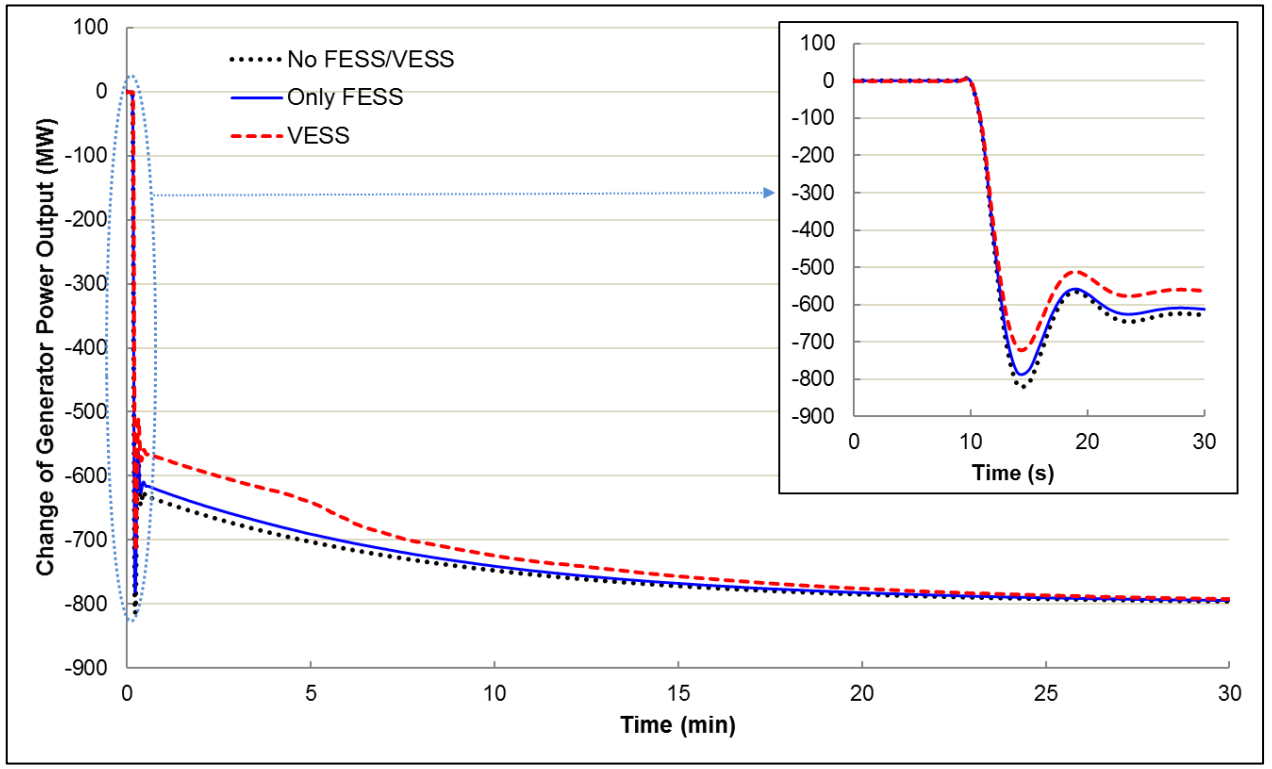

Fig. 4.20 The change of power output of generators after the loss of generation.

Since some refrigerators were switched ON following the frequency rise, their temperature started to drop. It had taken several minutes before the temperature reached the low set point and refrigerators began to switch OFF (Fig. 4.19.B). Therefore, the flywheel energy storage system changes from charging (i.e. absorbing power) to discharging (i.e. injecting power) following the frequency recovery. Because of the limitation in the flywheel energy storage system capacity (i.e. only 20 MW), the total response from the VESS was not linear with the frequency recovery. However, the VESS in Scenario 3 provides much more response following the frequency rise than that of the flywheel energy storage system in Scenario 2, which is specifically critical for the future power system with a low inertia. The VESS provides much more response following the frequency rise than that of the only flywheel energy storage system.

4.3.3. **Case 3 (Continuous frequency response)**

The VESS is recruited to provide enhanced frequency response service described in Chapter 2. Figure 4.21 Shows the behaviour of the VESS in response to the continuous fluctuations of frequency.

The power output of the VESS dynamically changes following the frequency deviations. Because the refrigerators have a greater capability to be switched ON than to be switched OFF, the VESS can provide greater high-frequency response than low-frequency response as depicted by Fig. 4.21.

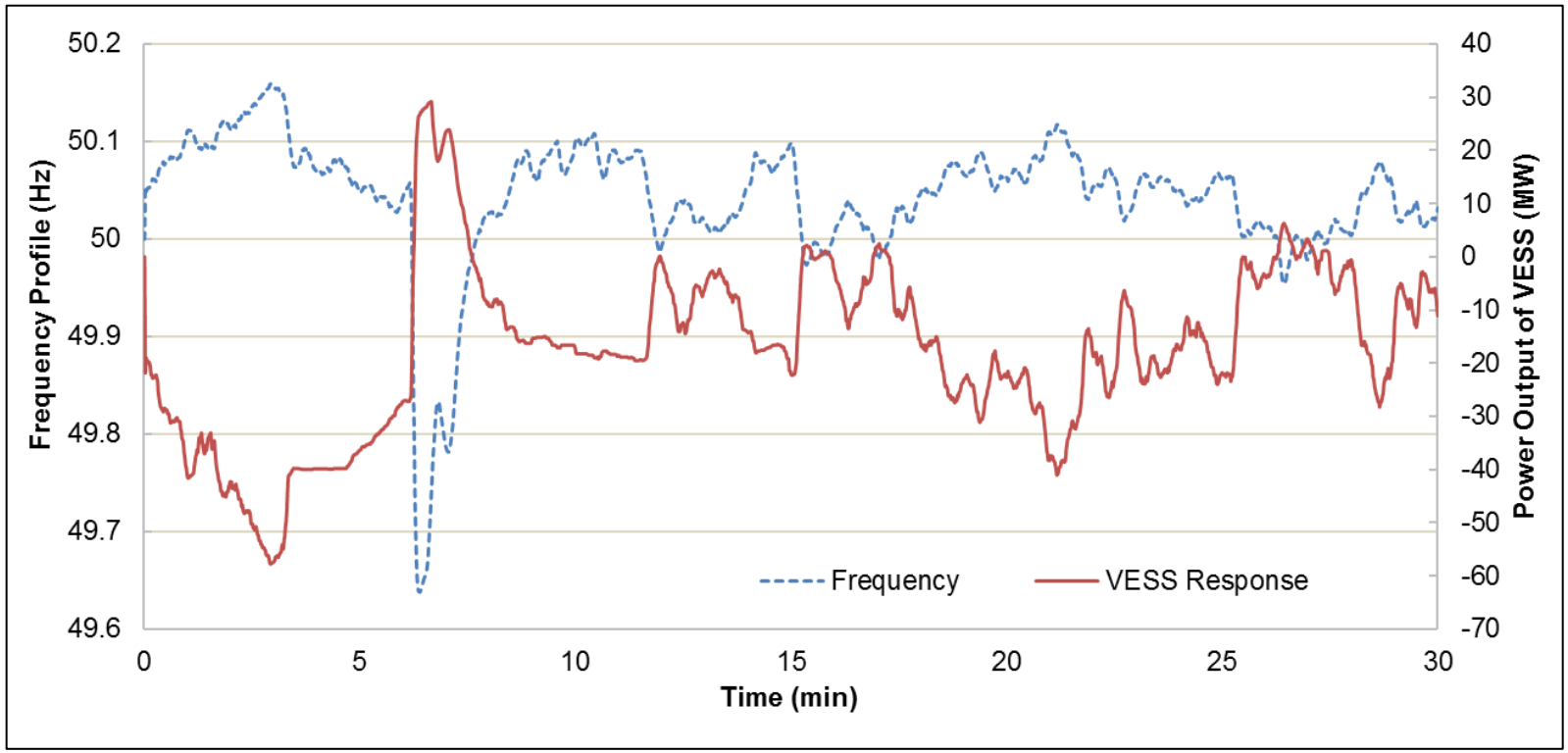

Fig. 4.21 The variation in the system frequency and the VESS response.

4.4. The economic evaluation

The investment cost of the VESS is briefly estimated. Then, the benefits of the VESS for the provision of frequency response services are calculated as an example.

Table 4.2 shows the roughly estimated investment cost of the flywheel energy storage system and the VESS. It is assumed that the lifetime of a flywheel energy storage system is approximately 20 years and the lifetime of refrigerators is 13 years [135]. Considering a timescale of 20 years and using the investment costs shown in Table 4.1, the investment cost of the flywheel energy storage system in Scenario 2 providing 60 MW response is estimated to be approximately **£75m-£84m** [15]. The investment cost of the VESS in Scenario 3 providing 60 MW response includes the cost of installing controllers on 3,220,300 refrigerators, which is approximately £9.66m [106] for 13 years and therefore will be approximately £14.86m for 20 years. Also, the cost of the flywheel energy storage system in the VESS providing 20 MW response is approximately £25m-£28m. Therefore, the investment cost of the VESS in Scenario 3 is approximately **£39.8m-£42.8m** which is less costly compared with the cost of the flywheel energy storage system in Scenario 2. However, establishing the VESS communications was not considered in the VESS total investment costs.

TABLE 4.3 INVESTMENT COSTS FOR DIFFERENT SCENARIOS

Scenario	VESS unit	Unit price	Capacity or no. of units	Total investment cost for 20 years	
S2	FESS	£1.25m-£1.4m/MW [7]	60 MW	**£75m-£84m**	
S3	FESS	£1.25m-£1.4m/MW [7]	20 MW	**£25m-£28m**	**£39.8m - £42.8m**
	Refrigerator 's controller	£3 [9]	3,220,300	▪ £9.66m for 13 years lifetime ▪ **£14.86m** for 20 years lifetime (£9.66m×20year/13year)	

Economic incomes of using the flywheel energy storage system alone or the VESS for frequency response services are calculated based on the existing regulation of the GB frequency response market. The payment of participating in the firm frequency response service [136, 137] consists of the availability fee per day and the utilisation fee per day. The availability fee (£/MWh) is the payment to the service provider that makes a certain amount of response service available for the tendered hours of a day. The utilisation fee (£/MWh) is the payment to the service provider for the utilisation volume during the tendered hours of a day. The utilisation volume is the amount of response that has been delivered to the system and depends on the system frequency changes.

The payments of both the flywheel energy storage system alone in Scenario 2 and the VESS in Scenario 3 are calculated by (4.6) for the availability fee and by (4.7) for the utilisation fee. The parameters values used in (4.6) and (4.7) were calculated based on [13,14] over the year 2014. Table 4.3 provides the average unit price of the availability fee and the utilisation fee, the average response periods and the meaning of all parameters used in (4.6) and (4.7). It is assumed that the availability and utilisation time periods are the same (i.e. the nominated period in Table 4.4) for simplicity. However, in fact the availability period is stated in the provider tender [13] submitted the system operator (e.g. 24 hours) while the utilisation period is the actual period that the provider delivers the service to the system operator (e.g. 1 hour).

$$Availability\_fee = MW_{primary} \times t_{primary\_nominated} \times availability\_unit\_price_{primary} + MW_{secondary} \times t_{secondary\_nominated} \times availability\_unit\_price_{secondary} + +MW_{high} \times t_{high\_nominated} \times availability\_unit\_price_{high} \quad (4.6)$$

$$Utilization\_fee = MW_{primary} \times t_{primary\_nominated} \times utiliztion\_unit\_price_{primary} + MW_{secondary} \times t_{secondary\_nominated} \times utilization\_unit\_price_{secondary} + +MW_{high} \times t_{high\_nominated} \times utilization\_unit\_price_{high} \quad (4.7)$$

TABLE 4.4 PARAMETERS AND VALUES OF CALCULATING THE INCOME OF PROVIDING FREQUENCY RESPONSE SERVICES IN THE GB POWER SYSTEM

Parameters	Meaning	Value	Unit
$MW_{primary}$	Amount of primary response	60	MW
$MW_{secondary}$	Amount of secondary response	60	MW
MW_{high}	Amount of high response	60 (FESS) or 180 (VESS)	MW
$t_{primary\_nominated}$	Nominated hours of primary response per day	15.97	h
$t_{secondary\_nominated}$	Nominated hours of secondary response per day	11.53	h
$t_{high\_nominated}$	Nominated hours of high response per day	18.66	h
$Availability\_unit\_price_{primary}$	Unit price of available primary response per day	8.7791	£/MWh
$Availability\_unit\_price_{secondary}$	Unit price of available secondary response per day	8.7791	£/MWh
$Availability\_unit\_price_{high}$	Unit price of available high response per day	4.3896	£/MWh
$Utilisation\_unit\_price_{primary}$	Unit price of utilised primary response per day	4.4204	£/MWh
$Utilisation\_unit\_price_{secondary}$	Unit price of utilised secondary response per day	4.4204	£/MWh
$Utilisation\_unit\_price_{high}$	Unit price of utilised high response per day	2.2102	£/MWh

Based on (4.5) and (4.6), the income of the flywheel energy storage system in Scenario 2 providing 60 MW of primary, secondary and high response is £29.168k/day. For 20-year time scale, the total income is hence **£213m**. Similarly, the revenue of the VESS to provide 60 MW of primary and secondary response and 180 MW of high response is £43.946k/day. Therefore, the total income for a 20-year timescale is **£321m** in Scenario 3 which is 50% higher than Scenario 2.

4.5. Summary

A frequency control scheme of a VESS was developed. A VESS is formed by coordinating domestic refrigerators and units of the flywheel energy storage system to provide functions similar to a conventional flywheel energy storage system, but with higher capacity and lower costs. In the VESS, refrigerators change their power consumption immediately following the frequency deviations. While units of the flywheel energy storage system cover the power mismatch between the required response from the VESS and refrigerators response. The required response from the VESS was determined using a droop control.

The frequency controller was designed and added to the internal temperature controller of refrigerators. The integrated frequency and the temperature control scheme maintains the primary function of refrigerators and mitigates the impact of the reduction in load diversity amongst the population.

Two frequency control schemes of the flywheel energy storage system were designed, namely, the Coordinated Constant Droop Control (CCDC) and the Coordinated Adaptive Droop Control (CADC). These control schemes can be used for other types of energy storage systems. These control strategies reduce the number of committed units when frequency deviations are small compared to the Conventional Droop Control (CDC) where all units must be committed. Therefore, prolong the lifetime of each unit of the energy storage system by minimising their charging/discharging cycles. Since the CADC strategy provides a similar level of aggregated response to the CDC, the CADC strategy was adopted.

Case studies were undertaken to evaluate the performance of the frequency control scheme of the VESS. The VESS was connected to a simplified GB power system to provide a low-frequency response after a loss of generation, a high-frequency response following the loss of demand and an enhanced frequency response service. In the low-

frequency case (Case 1), the VESS delivered a similar aggregated response compared with the strategy using flywheel energy storage system alone, but used only one-third of the flywheel units. In the high-frequency case (Case 2), the aggregated response from the VESS was approximately three times larger than the response of only using flywheel energy storage system. In Continuous frequency response case (Case 3), the frequency control scheme of the VESS provided dynamic frequency response. In summary, the response from the frequency control scheme of the VESS was 60 MW when the frequency dropped to 49.5 Hz and 140 MW when the frequency rose to approximately 50.4 Hz.

Capital costs were briefly estimated, and then the economic benefits of using only the flywheel energy storage system and the VESS to provide frequency response services were approximately calculated. The VESS is estimated to obtain higher profits compared with the case that only uses the flywheel energy storage system.

CHAPTER 5

A voltage control scheme to support the integration of distributed generation

A coordinated voltage control scheme of a Virtual Energy Storage System (VESS) to support voltage control of a medium voltage distribution network was designed to accommodate Distributed Generation (DG).

The VESS is an aggregation of Demand Response (DR) units and Energy Storage Systems (ESSs). An industrial bitumen tank model as a demand response unit and a battery energy storage system model were used to demonstrate the performance of the voltage control scheme. Models of the bitumen tank and the battery energy storage system were presented in Chapter 3. The control scheme was established using Matab®/Simulink on the same PC utilized to develop the models in Chapter 3.

5.1. The voltage control scheme of a virtual energy storage system

The voltage control scheme of the VESS is shown in Fig. 5.1. Demand response units used a local voltage controller, which does not require communication with other units and hence is not affected by communication latency or loss of connection. However, challenges facing the implementation of this local control of flexible demand are the uncertainty of the amount and the duration of the response. The energy storage system used a voltage control relying on remote voltage measuring devices. These devices were connected only to vulnerable busbars with respect to voltage violations. Consequently, the energy storage system is expected to eliminate any voltage violations following the provision of demand response. Therefore, the VESS allows the demand response to mitigate the voltage deviation first which reduces the required capacity of the energy storage system.

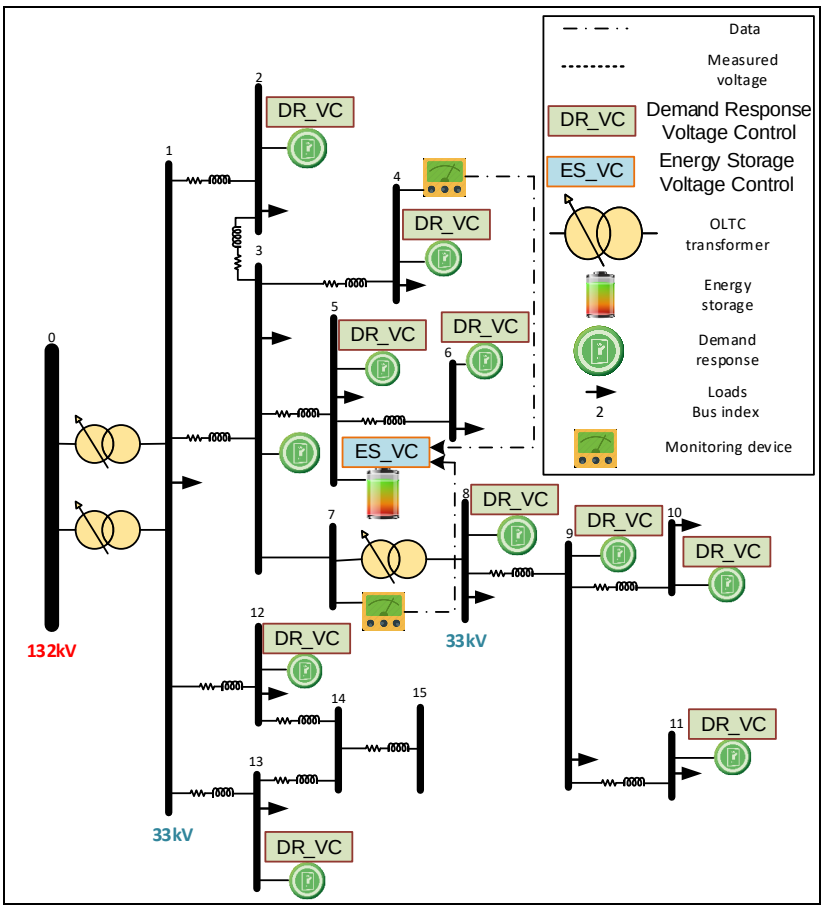

Fig. 5.1 The voltage control scheme of a VESS.

Since the aim of this study is to support the voltage control, it is assumed that the voltages at all busbars are measured every 1 min. and voltage controllers of the VESS components are pre-set time delays before taking action. Table 5.1 shows the time delay settings for the VESS components and also for the existing network voltage control strategy, which are voltage controllers of the On-Load Tap Changing (OLTC) transformer and the Voltage Regulator (VR). The coordination between the aforementioned voltage control mechanisms is achieved by setting the voltage controllers with different time delay settings.

The voltage control of demand response units have a small time delay setting (i.e. τ_{DR}) while the voltage control of the energy storage system has a longer time delay setting (i.e. τ_{ESS}). Hence demand response units respond before the energy storage system, because demand response units have larger aggregated capacity compared with energy storage unit and they are distributed over the network. To avoid any voltage hunting problem between the voltage control scheme of the VESS and the voltage control of the OLTC transformer and the VR, they were assigned different delay settings (i.e. τ_{OLTC} and τ_{VR}). The voltage control scheme assigns longer time delay settings for the OLTC

transformer and VR to avoid frequent tap changing actions, or to reduce the number of actions required.

TABLE 5.1 THE TIME DELAY SETTINGS OF THE VESS AND TRANSFORMERS FOR VOLTAGE CONTROL

Controller	Time Delay (min.)
Demand response units (τ_{DR})	1
Energy storage system (τ_{ESS})	2
Voltage regulator transformer (τ_{VR})	3
On load tap changing transformer (τ_{OLTC})	4

5.1.1. The voltage control of a bitumen tank

The control scheme of the bitumen tank is shown in Fig. 5.2. In addition to the existing inherent temperature controller presented in Chapter 3, the voltage controller was added to the control scheme of the bitumen tank. The temperature control measures the temperature (T) of a tank and generates a temperature state signal (S_T). The voltage control measures the busbar voltage (V) and generates high and low voltages state signals (S_{HV}) and (S_{LV}). The final switching signal (S_{final}) to the heater is then determined by logic gates, which ensures the priority of the temperature control. In this way, the voltage control will not undermine the hot storage function of the bitumen tank.

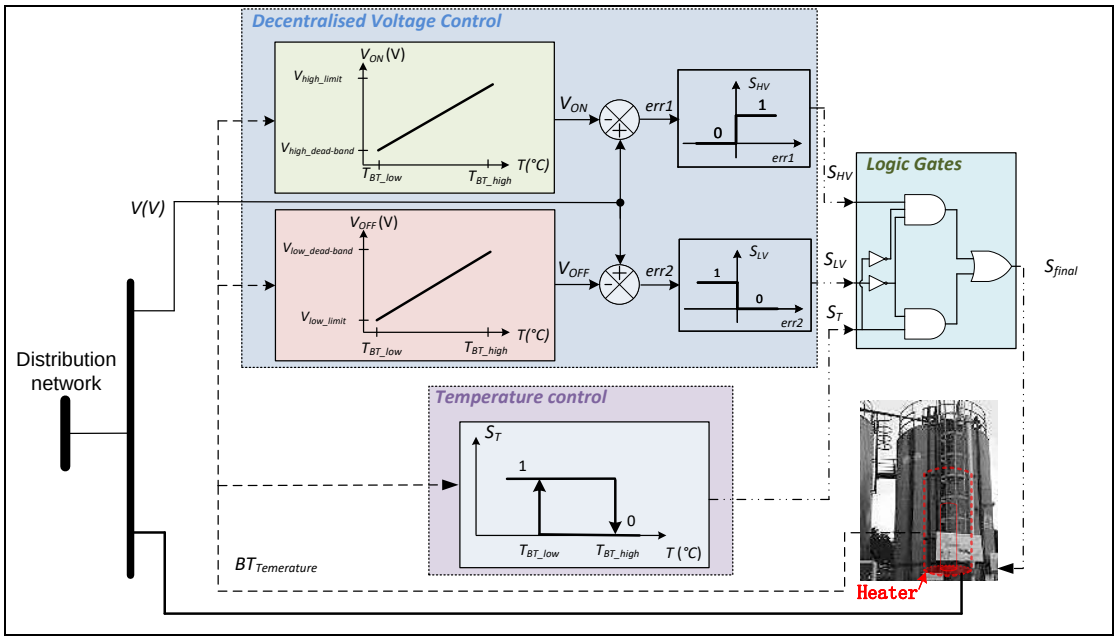

Fig. 5.2 The voltage control of a bitumen tank.

If T is lower than the low-temperature limit (T_{BT_low}) the temperature state signal (S_T) is 1, and if the T is higher than the high temperature limit (T_{BT_high}) the temperature state

signal (S_T) is 0. The voltage controller switches ON/OFF the bitumen tank in response to voltage deviations. The controller assigns a pair of voltage set-points, namely (V_{ON}) and (V_{OFF}), which dynamically and linearly varies with the temperature of the bitumen tank as shown in Fig. 5.2. The voltage controller continuously compares the measured voltage V with the voltage set-points. If V is higher than V_{ON}, the voltage control generates a high voltage state signal (S_{HV}) of 1 and the bitumen tank is switched ON, alternatively S_{HV} is 0. In contrast, if V is lower than V_{OFF}, the voltage control generates a low voltage state signal (S_{LV}) of 1 and the bitumen tank is switched OFF, otherwise S_{LV} is 0.

Table 5.2 shows the truth table of the logic gates (illustrated in Fig. 5.2). Rows 2 and 6 represent high voltage states, and in row 2 the bitumen tank responds to the high voltage by switching ON. Rows 3 and 7 represent low voltage states, and in row 7 the bitumen tank responds to the low voltage by switching OFF. In rows 1 and 5, the main function of the tank is not disturbed because measured V are higher than V_{OFF} and lower than V_{ON}. Rows 4 and 8 are not feasible states because the busbar voltage cannot be higher and lower than a reference value simultaneously. A 25 seconds minimum ON/OFF switching time was applied to each tank, to avoid frequent switching actions caused by the voltage control which may damage the heater.

TABLE 5.2 THE TRUTH TABLE OF LOGIC GATES IN FIG. 5.2

Row	S_T	S_{LV}	S_{HV}	S_{final}
1	0	0	0	0
2	0	0	1	1
3	0	1	0	0
4	0	1	1	-
5	1	0	0	1
6	1	0	1	1
7	1	1	0	0
8	1	1	1	-

In a population of bitumen tanks, a bitumen tank having a higher temperature than others will have a higher V_{ON} and a lower V_{OFF} values as indicated in Fig. 5.2. If the voltage drops, the bitumen tank with the highest temperature will be first to switch OFF because its temperature is the closest to the high temperature limit). As a result, it has the longest potential response (i.e. requires the longest time to reach the low-temperature limit). On the contrary, bitumen tanks will be switched ON in response to a voltage rise starting from the bitumen tank with the lowest temperature. Therefore, the number of bitumen tanks committed to respond to voltage deviations increases linearly with the increase in voltage deviations and hence the power consumption. Thus, all the demand

response units are committed if the voltage accessed the limits.

In this study, it was assumed that the distribution network voltage limits are ± 6% of nominal value (i.e. 0.94 p.u.-1.06 p.u.) [32]. Also, it is assumed that the voltage control dead-bands are ± 3% of the nominal value (i.e. 0.97 p.u.-1.03 p.u.). These dead-band values allow bitumen tanks to perform their primary function of hot supply under small voltage deviations.

5.1.2. **The voltage control of a battery energy storage system**

As a part of the setup of the voltage controller of the battery energy storage system, locations of the most vulnerable busbars with respect to the voltage violation were identified. These busbars are often the ones loaded heavily or with a large DG connection capacity. Remote monitoring devices were installed to these busbars to measure and send the voltage to the voltage controller of the battery energy storage system.

Figure 5.3 shows the voltage controller of the battery energy storage system. The controller initially determines the most deviated busbars (i.e. V_{MD1} and V_{MD2}). Then, through Table 5.3, selects the designated busbar. Droop controls set the required active and reactive powers injection/absorption from the energy storage system using the voltage of the designated busbar. The high and the low voltage limits (i.e. V_{high_limit} and V_{low_limit}) in Fig. 5.3 were set to 1.06 p.u. and 0.94 p.u. based on [32], the droop control settings (N_{i_ESS} and M_{i_ESS}) were obtained from voltage sensitivity factors.

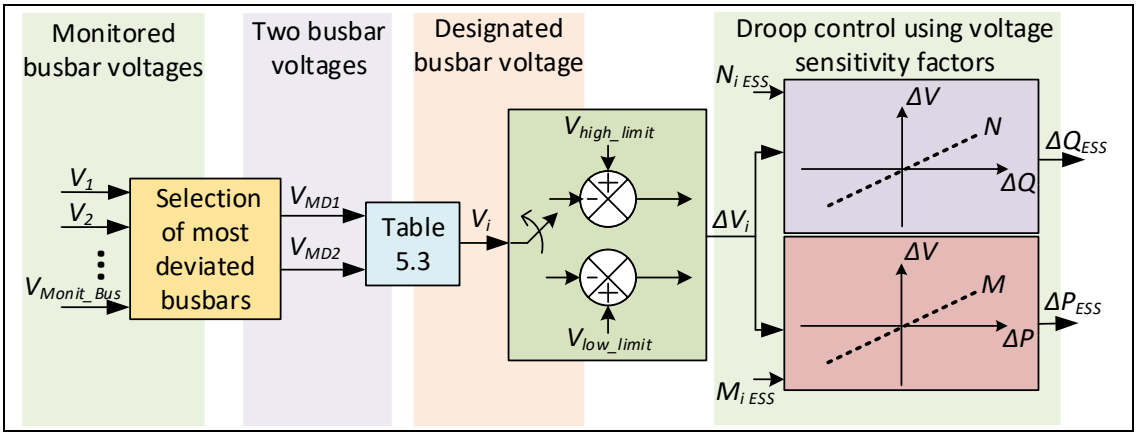

Fig. 5.3 The voltage control of a battery energy storage system.

The voltage controller of the battery energy storage system classifies the received voltages from the monitored busbars into zones as illustrated in Fig. 5.4.

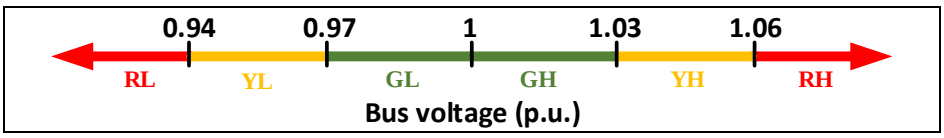

Fig. 5.4 The busbar voltage zones.

The received voltages fall under one of the following zones:

1. Red zones (RH and RL) represent the **voltage violation** ranges, i.e. busbar voltage violates (exceeds) the ± 6% limits of the nominal value (i.e. 1 p.u.).
2. Yellow zones (YL and YH) represent the **severe voltage deviation** ranges, i.e. busbar voltage deviates largely (i.e. equal or larger than ± 3% of the nominal value) from the nominal value yet within the limits of ± 6%.
3. Green zones (GL and GH) represent the **slight voltage deviation** ranges, i.e. busbar voltage deviates marginally (i.e. smaller than ± 3% of the nominal value) from the nominal value.

In the worst case, the network will suffer from high voltage deviations in both the high and the low voltage directions (i.e. two directions). To address this case, the voltage controller selects the two busbars with the largest voltage deviations, of which the voltage deviations may or may not exceed the limits. Then, these selected two busbars' voltages are placed on the MD1-axis and the MD2-axis of Table 5.3 to identify the designated busbar and its target voltage. In the case of having more than two monitored busbars with voltage violations, by mitigating the extreme cases, the less severe voltage violations will also be released.

The designated busbar is the busbar which the battery energy storage system aims to regulate its voltage by charging/discharging the active and the reactive powers and is determined by the following rules:

- If no voltage violation occurs, i.e. all monitored busbar voltages are within limits, no designated busbar is assigned and the battery energy storage system takes no action.
- If the two busbars have opposite directions of voltage violations, no designated busbar is assigned and the battery energy storage system takes no action.
- If both busbars have a similar direction of voltage deviations (i.e. voltages of both busbars are above/below a nominal value), the designated busbar is the busbar with a higher voltage violation (RH or RL). The battery energy storage system will then

charge/discharge to bring the voltage of the designated busbar back to the voltage limit (i.e. high or low voltage limits).

- If the two busbars have opposite directions of voltage deviation (i.e. one busbar voltage is above a nominal value and the other is below it), the designated busbar is the one not violating voltage limits (YL or YH). The battery energy storage system will charge or discharge to push the voltage of the designated busbar to the voltage limit (i.e. high or low voltage limits), therefore reduce the other busbar's voltage violation.

TABLE 5.3 THE VOLTAGE CONTROL SETTING OF THE ENERGY STORAGE SYSTEM

	A high voltage deviation MD2-axis busbar				
0	$MD1_L$	$MD2_H$	$MD2_H$	$MD2_H$	$MD2_H$ / $MD1_H$
$MD2_H$	0	0	0	0	$MD1_H$
$MD1_L$	0	0	0	0	$MD1_H$
$MD1_L$	0	0	0	0	$MD1_H$
$MD2_L$	0	0	0	0	$MD2_L$
$MD1_L$ / $MD2_L$	$MD1_L$	$MD2_L$	$MD2_L$	$MD1_H$	0

A high voltage deviation MD1-axis busbar

where:

$MD1_H$: The designated busbar is the MD1-axis busbar, its target voltage is the High voltage limit (i.e. 1.06 p.u.).

$MD1_L$: The designated busbar is the MD1-axis busbar, its target voltage is the Low voltage limit (i.e. 0.94 p.u.).

$MD2_H$: The designated busbar is the MD2-axis busbar, its target voltage is the High voltage limit.

$MD2_L$: The designated busbar is the MD2-axis busbar, its target voltage is the Low voltage limit.

0 : No action from the battery energy storage system.

A) The droop control of the battery energy storage system

The voltage controller of the battery energy storage system responds to the voltage deviation of the designated busbar (*i*) through a droop control (5.1). The required change in the voltage of the designated busbar *i* (ΔV_i in p.u.) was determined through Table 5.3. This required change in the voltage is the difference between its measured value and its target value. Then, the required changes in the active power (ΔP_{ES} in p.u.) and the reactive power (ΔQ_{ES} in p.u) of the battery energy storage system were calculated using (5.1).

$$\Delta V_i = M_{i\_ESS} \times \Delta P_{ESS} + N_{i\_ESS} \times \Delta Q_{ESS} \tag{5.1}$$

where M_{i_ESS} is the voltage sensitivity factor (in voltage p.u./power p.u.) which relates the change in the active power of the battery energy storage system to the change in the voltage of busbar *i* and N_{i_ESS} is the voltage sensitivity factor (in voltage p.u./power p.u.) which relates the change in the reactive power of the battery energy storage system to the change in the voltage of busbar *i*. The value of M_{i_ESS} and N_{i_ESS} is determined as illustrated below in section B.

B) The voltage sensitivity factors matrices

A large voltage sensitivity factor implies that a change in the active and/or the reactive powers at a busbar drives a large change in the voltage at the corresponding busbar [138]. The voltage sensitivity factors matrices (5.3) - (5.4) were extracted from the Jacobian matrix in (5.2):

$$\begin{bmatrix} \Delta P \\ \Delta Q \end{bmatrix} = \begin{bmatrix} \frac{\partial P}{\partial \delta} & \frac{\partial P}{\partial V} \\ \frac{\partial Q}{\partial \delta} & \frac{\partial Q}{\partial V} \end{bmatrix} \begin{bmatrix} \Delta \delta \\ \Delta V \end{bmatrix} \tag{5.2}$$

where

$$M = \left[\frac{\partial P}{\partial V} - \frac{\partial P}{\partial \delta} \cdot \left[\frac{\partial Q}{\partial \delta} \right]^{-1} \cdot \frac{\partial Q}{\partial V} \right]^{-1} \tag{5.3}$$

$$N = -M \cdot \frac{\partial P}{\partial \delta} \cdot \left[\frac{\partial Q}{\partial \delta} \right]^{-1} \tag{5.4}$$

where:

$\frac{\partial P}{\partial \delta}$ is the partial derivative of the active power with respect to voltage angle.

$\frac{\partial P}{\partial V}$ is the partial derivative of the active power with respect to voltage magnitude.

$\frac{\partial Q}{\partial \delta}$ is the partial derivative of the reactive power with respect to voltage angle.

$\frac{\partial Q}{\partial V}$ is the partial derivative of the reactive power with respect to voltage magnitude.

ΔV is the change in voltage magnitude.

$\Delta \delta$ is the change in voltage angle.

The reactive power of the energy storage system is prioritised over its active power in order to minimise the charging or discharging of the battery. The required reactive power was obtained by setting the active power to zero in (5.1). If the required reactive power was higher than its rated value, the battery energy storage system would then provide both the active and the reactive powers supports. Accordingly, the reactive power is set to its rated value to calculate the required active power value in (5.1).

A detailed step-by-step example of how the voltage controller works is given hereafter; assuming that there are three busbars A, B, C that are the most vulnerable busbars with monitoring devices. The received values from the three busbars are 1.0654 p.u., 1.0661 p.u. and 1.0614 p.u..

1- The received voltage values (i.e. 1.0654 p.u., 1.0661 p.u. and 1.0614 p.u.) from the monitored busbars A, B and C are all classified into the red zone (RH).
2- Busbar A and busbar B are selected to be placed on Table 5.3 axes. Busbar A is placed on the MD1-axis and busbar B is placed on the MD2-axis arbitrarily.
3- Since both busbars have voltage violations (i.e. RH) and busbar B has the larger voltage violation, the intersected cell identifies the MD2-axis busbar (i.e. busbar B) as the designated busbar and its target voltage is the high voltage limit (i.e. Y_H).
4- The response from the battery energy storage system is expected to bring the voltage of busbar B back to the limit (i.e. the target voltage is 1.06 p.u.). A smaller value of the target voltage of 1.0585 p.u. is used to compensate for any changes in voltage sensitivity factors. Values of voltage sensitivity factors may change slightly due to changes in loading conditions or DG generations. Therefore, the change in busbar B voltage is calculated:

$$\Delta V_B = 1.0661 - 1.0585 = 0.0076 \ p.u.$$

5- Equation (5.1) is used to calculate the required response for the battery energy storage system. To find the required change in reactive power, the active power

component is set to zero in (5.1). Assuming that M_{B_ESS} equals to 0.0806 voltage p.u./power p.u. and N_{B_ESS} equals to 0.326 voltage p.u./power p.u. in (5.1). Therefore:

$$0.0076 = 0 \times 0.0806 + 0.326 \times \Delta Q \Longrightarrow \Delta Q = 0.0233\, p.u.$$

The rated reactive power is assumed to be 0.0184 p.u. in this example, hence the calculated value is larger than the rated reactive power. Therefore, both the active and the reactive powers are required. Setting the change in reactive power to the rated value and solve for the change in active power in (5.1):

$$0.0076 = \Delta P_{ESS} \times 0.0806 + 0.326 \times 0.0184 \Longrightarrow \Delta P_{ESS} = 0.0198\, p.u.$$

C) **The State of Charge control of the battery energy storage system**

The state of charge control of the battery energy storage system maintains the state of charge value within a certain range from the midpoint (i.e. 50%±10%). Consequently, any forthcoming charging or discharging requirements are expected to be met.

Figure 5.5 shows the State of Charge (SoC) control of the battery energy storage system. When the voltage of all monitored busbars are in the green zones and the state of charge is outside the 10% range from the 50% value, the controller charges/discharges the battery energy storage system to bring back the state of charge to that range. The voltage of the monitored busbar which is having the largest Voltage Sensitivity Factor (VSF) is regulated to absorb/deploy the active power of the battery energy storage system. This ensures that deploying or absorbing battery energy storage system power will not cause voltage violations.

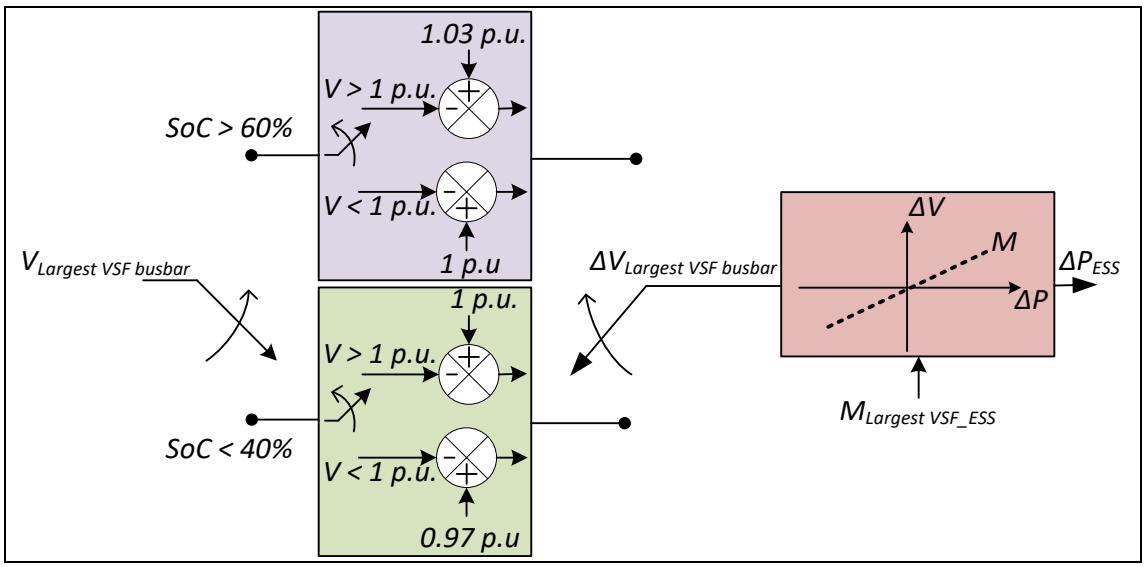

Fig. 5.5 The state of charge control of a battery energy storage system.

5.2. The test system

5.2.1. The UK generic distribution system

The network studied in this research, i.e. one of the networks of the United Kingdom Generic Distribution System (UKGDS) project, is illustrated in Fig. 5.6. Models of several distribution networks were developed in the UKGDS project, which are representative of the typical distribution networks in the UK, to support the analysis of network related issues and the assessment of the impact/benefits of new technologies. The network used in this research is a simplified representation of a rural, low customer density distribution network. This network has long lines and all loads at the 11 kV voltage level were lumped to the 33 kV busbars for simplicity [139]. The 33 kV radial network was used to evaluate the voltage control scheme of the VESS. The network supplied by two identical 33 MVA On-Load Tap Changing (OLTC) (132/33 kV) transformers, has 15-busbars and supplies a peak load of 38.94 MVA with a power factor of 0.98. A Voltage Regulator (VR) and a sub-sea cable are connecting busbar 8 to busbar 7. Half-hourly loads and DG profiles were used [139]. Based on the load profiles, the network minimum load is 4.74 MVA.

A 3% of the UKGDS energy demand was considered as an Electric Vehicles (EV) charging demand consistently with the projection of the energy demand for electric vehicles in the year 2030 in the UK [3]. Electric vehicles loads were assumed to be

distributed in proportion to the peak load at each load busbar. An electric vehicle charging profile was obtained from [3].

In the UK, the connection of DG is traditionally limited to levels that allows the operation of DG at rated power during the outage of the highest rated distribution circuit which is often the transformer, this is known as firm DG connection arrangement [140]. Accordingly, the UKGDS firm connection is 37.74 MVA (i.e. 33 KVA transformer capacity plus 4.74 MVA minimum load).

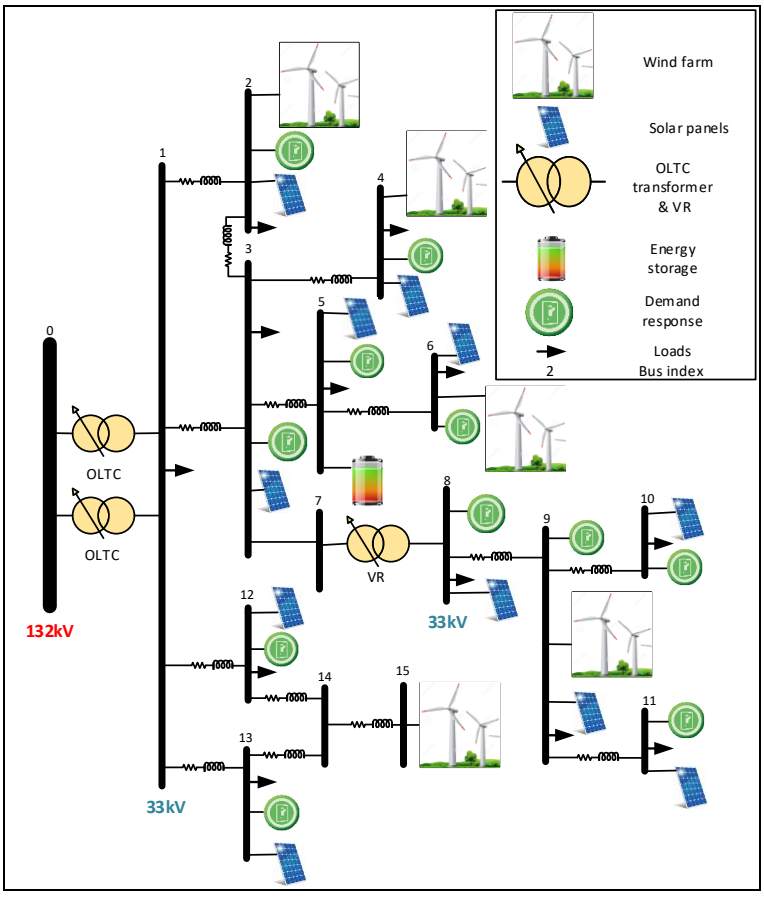

Fig. 5.6 The UK Generic Distribution System (UKGDS) network.

5.2.2. **Locations and capacities of distributed generation**

A) Locations and capacities of solar photovoltaics

The first type of distributed generation (DG) connected to the UKGDS was the solar panels (i.e. Photovoltaic (PV)). Solar panels were connected to 11 busbars, i.e. it were connected to all load busbars excluding the main busbar (i.e. busbar no. 1 in Fig. 5.6). Solar panels were assumed to be distributed in proportion to the maximum load at each busbar. The penetration level of solar panels at each busbar (e.g. $PV\%_i$ at busbar i) was set according to (5.5). 10% and 20% penetration levels of solar panels were assumed.

$$PV\%_i = \frac{P_{PV\_i}^{rated}}{Pl_i^{max}} \quad (5.5)$$

where $P^{rated}_{PV\_i}$ is the aggregated rated power of all solar panels connected to busbar *i* and Pl^{max}_i is the maximum total load of busbar *i*.

B) Locations and capacities of wind farms

The second type of DG connected to the studied network was the wind farms. In addition to the existing wind farm at busbar 15, four new wind farms were connected to the network. All wind farms were located far from the substation and at the end of individual feeders. The capacities of these wind farms were optimised using a developed Genetic Algorithm (GA).

The network hosting capacity for DG is the total DG capacity allowed into the network without violating network constraints under the minimum loading condition. The network constraints considered are the thermal limits of branches and the voltage limits. The UKGDS hosting capacity for DG was optimised by using GA.

Based on the locations of solar panels and wind farms presented early, Genetic Algorithm maximises the total capacity of the wind farms at a given penetration level of solar panels. Genetic Algorithm iteratively modifies a population of individual solutions (Fig. 5.7). For each GA solution, MATPOWER [141] was employed to find load flow solution and hence violations of the voltage and the thermal constraints were checked. The optimisation objective function and constraints are described in (5.6)-(5.7). The parameters of GA used are listed in Table 5.4.

The objective function

$$max\ (\sum_{i=1}^{N_w} P_{wi}\ ) \quad (5.6)$$

Subject to:

$$T_i^{min} \le T_i \le T_i^{max} \quad i \in N_{transformers} \quad (5.7.a)$$

$$S_{ij} \le S^{max}{}_{ij} \quad i,j \in N_{bus} \quad (5.7.b)$$

$$V_i^{min} \le V_i \le V_i^{max} \quad i \in N_{bus} \quad (5.7.c)$$

where:

N_w: No. of wind farms considered

P_{wi}: Power capacity of wind farm *i* (MW)

T_i: Tap ratio of a transformer *i* (i.e. OLTC and VR)

T_i^{max},T_i^{min}: Maximum and minimum tap ratio of a transformer i (i.e. OLTC and VR)

S_{ij}: Appetent power flow between busbar i and busbar j (MVA)

S_{ij}^{max}: Thermal limit the branch connecting bus i to busbar j (MVA)

V_i : Voltage of busbar i (kV)

V_i^{max},V_i^{min}: Maximum and minimum voltages limits at busbar i (kV)

TABLE 5.4 PARAMETERS OF THE GENETIC ALGORITHM

Parameter	Value
Number of generations (iterations)	60
Population size	120
Elitism size	120
Tournament selection probability	100%
Single point crossover probability	100%
Heuristic mutation probability	10%

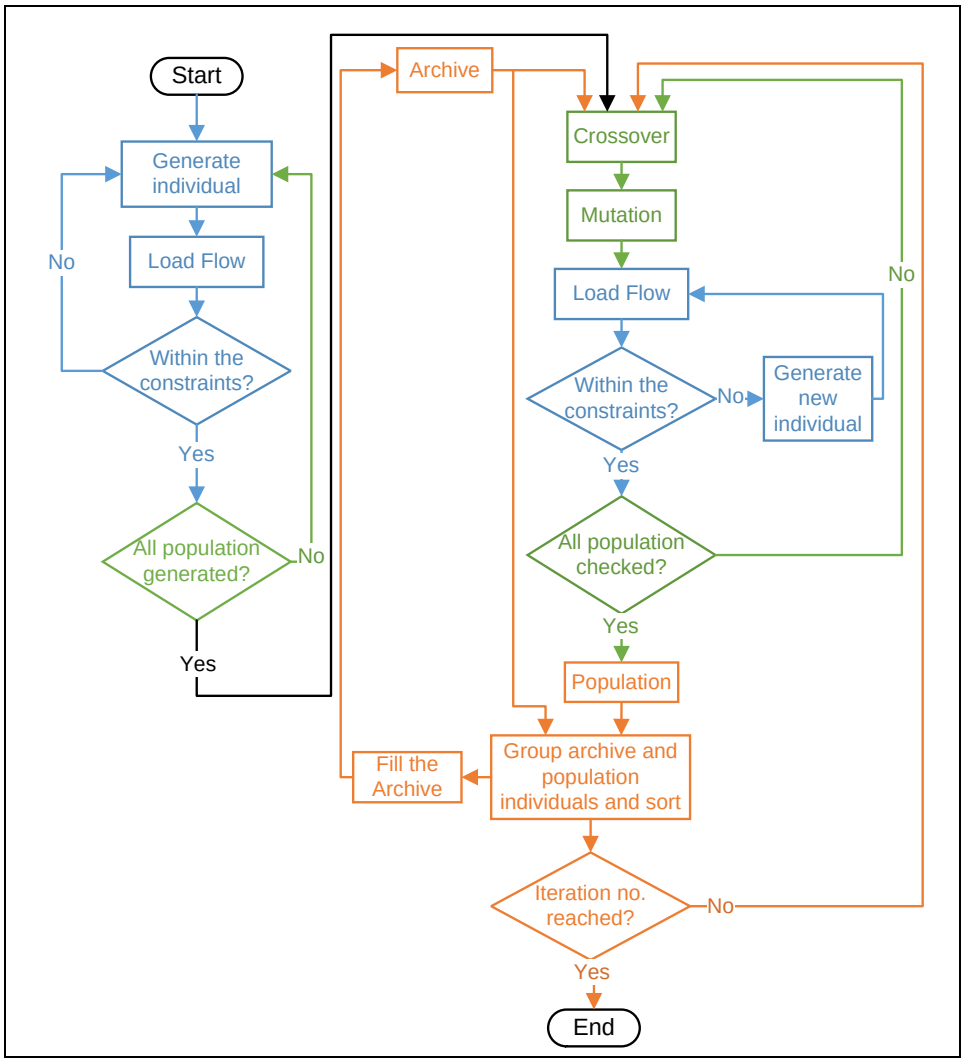

Fig. 5.7 The flowchart of the Genetic Algorithm developed.

Table 5.5 shows the distribution network hosting capacity for DG evaluated by the optimisation for different penetration levels of solar panels. As solar panels penetration level increased, the total capacity of wind farms allowed into the UKGDS decreased. Any rise in the solar panels penetration level increases the network voltage further, which leaves a smaller permissible voltage deviation to be caused by the wind farms.

TABLE 5.5 THE UKGDS HOSTING CAPACITY FOR DG

PV penetration level	PV total capacity (MW)	Wind farms total capacity (MW)	Total DG capacity (MW)
0	0	45.8	45.8
10%	3.28	43.8	47.63
20 %	6.55	41.9	48.45

5.2.3. Locations and capacities of the virtual energy storage system components

A) Locations and capacities of the demand response units

It was assumed that 11 busbars of the UKGDS had flexible loads and the power consumption of non-flexible loads was not affected by voltage variations. The penetration level of demand response at each busbar (e.g. $DR\%_i$ at busbar i) was defined in (5.8)

$$DR\%_i = \frac{Pl_{DR\_i}^{max}}{Pl_i^{max}} \tag{5.8}$$

where $Pl^{max}{}_{DR\_i}$ is the aggregated maximum power of all demand response units connected to busbar i and $Pl^{max}{}_i$ is the maximum total load of busbar i.

Under 30% demand response penetration level, 9.8 MW of demand response aggregated capacity was connected to the UKGDS. Assuming all bitumen tanks have a typical power consumption of 40 kW, 245 bitumen tanks are connected in the UKGDS network.

In the presence of the flexible (i.e. controllable) demand, the UKGDS hosting capacity for DG was increased, because the total minimum load used to calculate the hosting capacity was increased by the addition of the flexible loads. The hosting capacity for DG in the presence of the flexible demand was obtained by genetic algorithm presented earlier. Table 5.6 shows the hosting capacity for DG with different Demand Response (DR) penetration levels obtained by Genetic Algorithm at 20% solar panels penetration levels. For instance, with a 30% demand response penetration level (i.e. 9.8 MW of aggregated capacity), 60.25 MW of DG capacity is allowed into the network. This

60.25 MW of DG capacity is composed of, 6.55 MW of total solar panels capacity (i.e. 20% solar panels penetration level) and 53.70 MW of total wind farms capacity.

TABLE 5.6 THE UKGDS HOSTING CAPACITY FOR DG WITH DEMAND RESPONSE

DR penetration level	DR total capacity (MW)	Total DG capacity (MW)
10 %	3.28	52.15
20%	6.55	56.45
30 %	9.83	60.25

B) Location and capacity of the battery energy storage system

The battery energy storage system was connected to the busbar having largest values of voltage sensitivity factors with respect to the monitored busbars, which are the most vulnerable busbars with respect to voltage violation. Therefore, the vulnerable busbars of the UKGDS should be identified first.

Intuitively, busbar 4 and busbar 7 might suffer for a large voltage deviation, because busbar 4 have the largest proportion of the network load and busbar 7 connects VR with several busbars. A simple test was carried out to identify the most vulnerable busbars with respect to the voltage violation. For the DG capacity of 60.25 MW and 20% rather than 30% penetration level of demand response, busbars 4, 6, and 7 violated voltage limits as shown in Table 5.7. Therefore, busbar 4 and busbar 7 were nominated to be monitored by the voltage controller of the battery energy storage system. Table 5.7 shows the studied network voltage sensitivity factors for the change in the voltage at a busbar due to the change in the active power output at the corresponding busbar. While Table 5.8 shows the studied network voltage sensitivity factors for the change in the voltage at a busbar due to the change in the reactive power output at the corresponding busbar.

Based on the voltage sensitivity factors, busbar 5 had the largest voltage sensitivity factors with respect to busbars 4, 6, and 7. Consequently, the battery energy storage system was connected to busbar 5, hence it monitors busbar 5 voltage. Since busbars 5 and 6 are located on the same feeder, no remote monitoring device was connected to the vulnerable busbar 6.

In summary, the voltage control of the battery energy storage system monitors the voltage of busbars 4, 7 and 5. It utilises the voltage sensitivity factors values shown in Table 5.9 as droop control gains.

TABLE 5.7 THE DISTRIBUTION NETWORK VOLTAGE AND VOLTAGE SENSITIVITY FACTORS WITH RESPECT TO THE ACTIVE POWER

Busbar voltage (p.u.)	Busbar	1	2	3	4	5	6	7	8	9	10	11	12	13	14	15
1.014936	**1**	-0.0072	-0.0251	-0.0237	-0.0249	-0.0242	-0.0249	-0.0245	-0.0248	-0.0275	-0.0272	-0.0271	-0.0090	-0.0094	-0.0107	-0.0136
1.05364	**2**	-0.0070	0.0877	0.0227	0.0196	0.0212	0.0195	0.0203	0.0194	0.0130	0.0139	0.0139	-0.0087	-0.0092	-0.0104	-0.0132
1.055432	**3**	-0.0070	0.0203	0.0834	0.0786	0.0810	0.0784	0.0795	0.0782	0.0688	0.0702	0.0700	-0.0087	-0.0092	-0.0104	-0.0132
1.06186	**4**	-0.0070	0.0202	**0.0829**	**0.1065**	**0.0805**	0.0779	0.0791	0.0778	0.0683	0.0698	0.0696	-0.0087	-0.0091	-0.0103	-0.0131
1.059144	**5**	-0.0070	0.0202	0.0831	0.0783	0.5661	0.5578	0.0793	0.0780	0.0685	0.0700	0.0698	-0.0087	-0.0091	-0.0104	-0.0132
1.062776	**6**	-0.0070	0.0202	**0.0829**	0.0781	**0.5642**	**0.9243**	0.0790	0.0777	0.0683	0.0697	0.0695	-0.0087	-0.0091	-0.0103	-0.0131
1.064147	**7**	-0.0070	0.0202	**0.0831**	0.0783	**0.0807**	0.0781	**0.4900**	0.4864	0.4603	0.4650	0.4638	-0.0087	-0.0091	-0.0104	-0.0132
1.024445	**8**	-0.0067	0.0194	0.0798	0.0752	0.0775	0.0750	0.4707	0.5381	0.5092	0.5144	0.5130	-0.0083	-0.0088	-0.0099	-0.0126
1.033995	**9**	-0.0067	0.0193	0.0792	0.0746	0.0769	0.0744	0.4672	0.5341	1.0125	1.0226	1.0199	-0.0083	-0.0087	-0.0099	-0.0125
1.031089	**10**	-0.0067	0.0193	0.0794	0.0748	0.0771	0.0746	0.4685	0.5356	1.0154	1.9444	1.0228	-0.0083	-0.0087	-0.0099	-0.0126
1.03322	**11**	-0.0067	0.0193	0.0793	0.0748	0.0771	0.0746	0.4681	0.5351	1.0145	1.0246	2.5655	-0.0083	-0.0087	-0.0099	-0.0126
1.021524	**12**	-0.0072	-0.0249	-0.0236	-0.0248	-0.0241	-0.0247	-0.0243	-0.024	-0.0274	-0.0270	-0.0270	0.1673	0.0634	0.1214	0.1094
1.023176	**13**	-0.0072	-0.0249	-0.0236	-0.0248	-0.0241	-0.0247	-0.0243	-0.024	-0.0273	-0.0270	-0.0270	0.0644	0.3016	0.1519	0.1377
1.029828	**14**	-0.0071	-0.0248	-0.0234	-0.0246	-0.0240	-0.0246	-0.0242	-0.024	-0.0272	-0.0269	-0.0268	0.1268	0.1567	0.2869	0.2649
1.04885	**15**	-0.0070	-0.0243	-0.0230	-0.0242	-0.0235	-0.0241	-0.0237	-0.024	-0.0267	-0.0264	-0.0263	0.1246	0.1540	0.2819	0.6320

TABLE 5.8 THE DISTRIBUTION NETWORK VOLTAGE AND VOLTAGE SENSITIVITY FACTORS WITH RESPECT TO THE REACTIVE POWER

Busbar voltage (p.u.)	Busbar	1	2	3	4	5	6	7	8	9	10	11	12	13	14	15
1.014936	**1**	-0.125	-0.127	-0.127	-0.127	-0.127	-0.127	-0.127	-0.127	-0.128	-0.128	-0.128	-0.126	-0.126	-0.126	-0.126
1.05364	**2**	-0.122	-0.368	-0.249	-0.249	-0.249	-0.249	-0.249	-0.249	-0.250	-0.250	-0.250	-0.122	-0.122	-0.122	-0.122
1.055432	**3**	-0.122	-0.248	-0.327	-0.327	-0.327	-0.328	-0.327	-0.328	-0.328	-0.329	-0.328	-0.122	-0.122	-0.122	-0.122
1.06186	**4**	-0.121	-0.247	-0.325	-0.353	-0.326	-0.326	-0.326	-0.326	-0.326	-0.327	-0.326	-0.121	-0.121	-0.122	-0.122
1.059144	**5**	-0.122	-0.248	-0.326	-0.326	-0.682	-0.682	-0.326	-0.326	-0.327	-0.327	-0.327	-0.122	-0.122	-0.122	-0.122
1.062776	**6**	-0.121	-0.247	-0.325	-0.325	**-0.679**	-1.007	-0.325	-0.325	-0.326	-0.326	-0.326	-0.121	-0.121	-0.121	-0.121
1.064147	**7**	-0.122	-0.247	-0.326	-0.326	-0.326	-0.326	-0.695	-0.695	-0.697	-0.698	-0.697	-0.122	-0.122	-0.122	-0.122
1.024445	**8**	-0.117	-0.238	-0.313	-0.313	-0.313	-0.313	-0.668	-0.769	-0.771	-0.772	-0.771	-0.117	-0.117	-0.117	-0.117
1.033995	**9**	-0.116	-0.236	-0.311	-0.311	-0.311	-0.311	-0.663	-0.764	-1.476	-1.478	-1.475	-0.116	-0.116	-0.116	-0.116
1.031089	**10**	-0.116	-0.237	-0.312	-0.312	-0.312	-0.312	-0.664	-0.766	-1.480	-2.120	-1.479	-0.116	-0.116	-0.116	-0.116
1.03322	**11**	-0.116	-0.236	-0.311	-0.311	-0.311	-0.312	-0.664	-0.765	-1.479	-1.481	-2.649	-0.116	-0.116	-0.116	-0.116
1.021524	**12**	-0.125	-0.126	-0.127	-0.127	-0.127	-0.127	-0.127	-0.127	-0.127	-0.127	-0.127	-0.348	-0.231	-0.292	-0.292
1.023176	**13**	-0.125	-0.126	-0.126	-0.126	-0.126	-0.126	-0.127	-0.127	-0.127	-0.127	-0.127	-0.231	-0.446	-0.336	-0.336
1.029828	**14**	-0.124	-0.126	-0.126	-0.126	-0.126	-0.126	-0.126	-0.126	-0.126	-0.126	-0.126	-0.290	-0.334	-0.453	-0.453
1.04885	**15**	-0.122	-0.123	-0.123	-0.123	-0.123	-0.124	-0.124	-0.124	-0.124	-0.124	-0.124	-0.285	-0.328	-0.445	-0.723

TABLE 5.9 VOLTAGE SENSITIVITY FACTORS (VOLTAGE P.U./POWER P.U.)

	Busbar 4 Voltage	Busbar 5 Voltage	Busbar 7 voltage
ESS Active Power	0.0805	0.564	0.0806
ESS Reactive Power	0.325	0.681	0.326

The power and the energy capacities of the battery energy storage system were determined by a time series load flow analysis. This analysis was conducted using the UKGDS with DG at different periods of the year. Whenever a voltage violation occurs, the required active and reactive powers values from battery energy storage system were calculated to eliminate that violation. These required power values were calculated according to (5.1) using voltage sensitivity factors listed in Table 5.7.C. As a result, the power capacity of the battery energy storage system is the maximum value of active power values. Whereas, its energy capacity was the integration of consecutive deployed/absorbed active power values. For 9.83 MW capacity of demand response and 60.25 MW capacity of DG and utilising one summer week, one winter week and one spring day periods, the energy storage system rated power and energy capacities were calculated to be 2.3 MW and 1.4 MWh. The maximum reactive power of the battery energy storage system was limited to 0.8 times of the rated active power, similar to the battery energy storage system installed in the CLNR project [94] to reduce the size of the converter installed.

5.3. Case study

The performance of the voltage control scheme of the VESS was assessed against a base case of no VESS. The assessment was conducted using the UKGDS network with a connected DG capacity of 60.25 MW. The VESS components capacities used were 9.8 MW of bitumen tanks and 2.3 MW of a battery energy storage system. Half-hourly generation and non-flexible demand profiles [139] were used.

In the base case, the voltage of the UKGDS was only controlled by the electronic On-Load Tap Changing (OLTC) transformer and a Voltage Regulator (VR). Controllers of the electronic OLTC transformer and the VR change discretely the tap position to regulate the transformer secondary voltage with a corresponding set-point and a bandwidth. Both the OLTC transformer and the VR had 20 tap positions (i.e. -0.85 +0.05 as a per unit nominal value). When the secondary voltage deviates outside the bandwidth for a time longer than the controller time delay setting (τ_{OLTC} or τ_{VR}), the controller takes

action to return the voltage to the set-point. The controller changes the transformer tap position in proportion to the voltage deviation.

The voltage set-points of the OLTC transformer and the VR are listed in Table 5.10. These values allow network voltage levels close to the nominal value when no DG connected to the distribution system (except the existing wind farm at busbar 15). One winter week and one summer week load profiles were adopted to identify these set-points and bandwidths.

TABLE 5.10 THE CONTROL SETTINGS OF THE OLTC TRANSFORMER AND THE VR

Transformer	Parameter	Value (p.u.)
OLTC	Voltage set-point/winter	1.0265
	Voltage set-point /summer	1.02
	Bandwidth	0.011
VR	Voltage set-point /all year	1.02
	Bandwidth	0.013

In the VESS case, non-flexible loads, which form 70 % of the loads, follow half hourly profiles. Whereas, 30% of loads profiles was the power consumption of the flexible loads (i.e. bitumen tanks).

A simple analysis aims to investigate the robustness of the voltage control scheme of the VESS against different DG penetration levels was carried out. Results were depicted in Fig. 5.8. Figure 5.8 shows the effect of different DG penetration levels (i.e. 0%-200% of the UKGDS hosting capacity for DG) on the UKGDS network maximum voltage deviation considering the cases with and without the voltage control scheme of the VESS. The 100% DG penetration level indicates the UKGDS hosting capacity for DG of 60.25 MW. Under low DG penetration levels (i.e. less than 60%), the maximum voltage deviation in the UKGDS network with and without the control scheme of the VESS were similar. Under high DG penetration levels (i.e. 60% to 100%), the voltage control scheme of the VESS controlled the maximum voltage deviation to remain within the voltage limit (i.e. 0.06 p.u.) while the maximum voltage deviation exceeded the voltage limit without the VESS voltage control scheme. When the DG penetration level is higher than the network DG hosting capacity (i.e. higher than 100%), the maximum voltage deviation in the UKGDS network with and without the control scheme of the VESS were both breaching the voltage limits. With DG penetration levels higher than 100 % however, the voltage control scheme of the VESS reduced the maximum voltage violation more than

the base case. Figure 5.8 therefore, shows that the voltage control scheme of the VESS is able to reduce voltage violations caused by DG penetration levels higher than the UKGDS network hosting capacity (i.e. 100% or 60.25 MW).

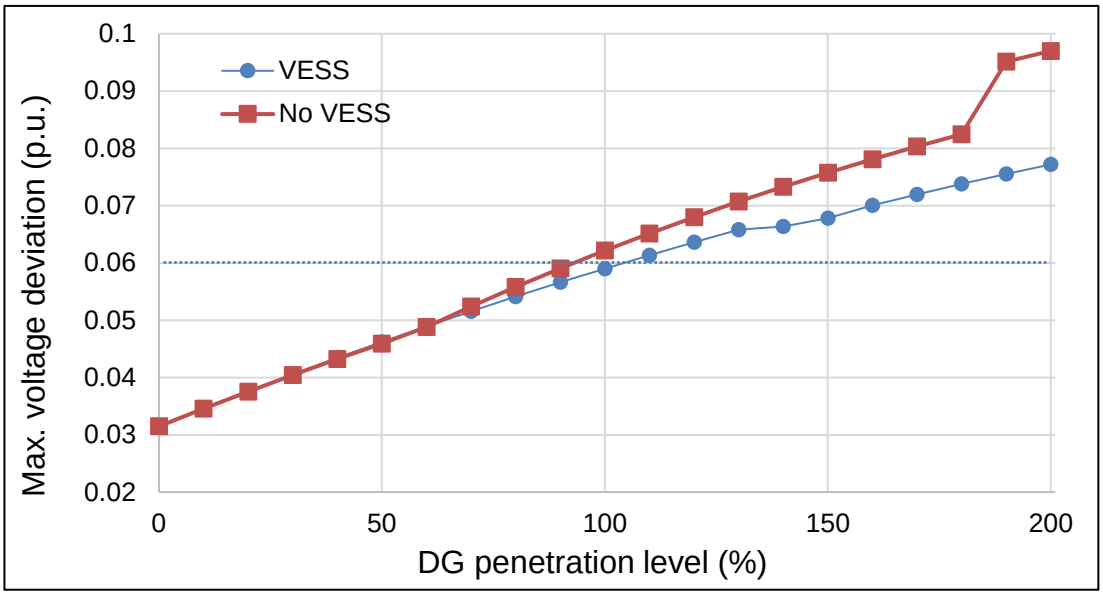

Fig. 5.8 UKGDS maximum voltage deviations at different DG penetration levels.

The performance of the voltage control scheme of the VESS was evaluated using the following four test time periods, which covers all seasons of the year. The first test period was a spring day with high wind and solar generation and low demand. The second test period was a winter week with a high wind energy generation. The third test period was a summer week with a high solar generation. The fourth test period was an autumn week with high solar and wind generation. All time intervals were chosen with the aim of obtaining representative test periods of the different seasons of the year. These time intervals show to some extent the worst-case scenarios of high DG outputs and low demand. The first test period aims to simulate the scenario of a persistent high DG output and a low demand over several hours. Second, third and fourth test periods aim to investigate the impact of the voltage control scheme on the existing OLTC transformer and VR. Results were compared with the base case. A 1 minute resolution of load flow analysis was carried out using MATPOWER. The OLTC transformer and VR controllers were implemented using MATLAB.

1) First test period (a spring day)

Figure 5.9 shows the total load, the wind and the solar generation for this test period.

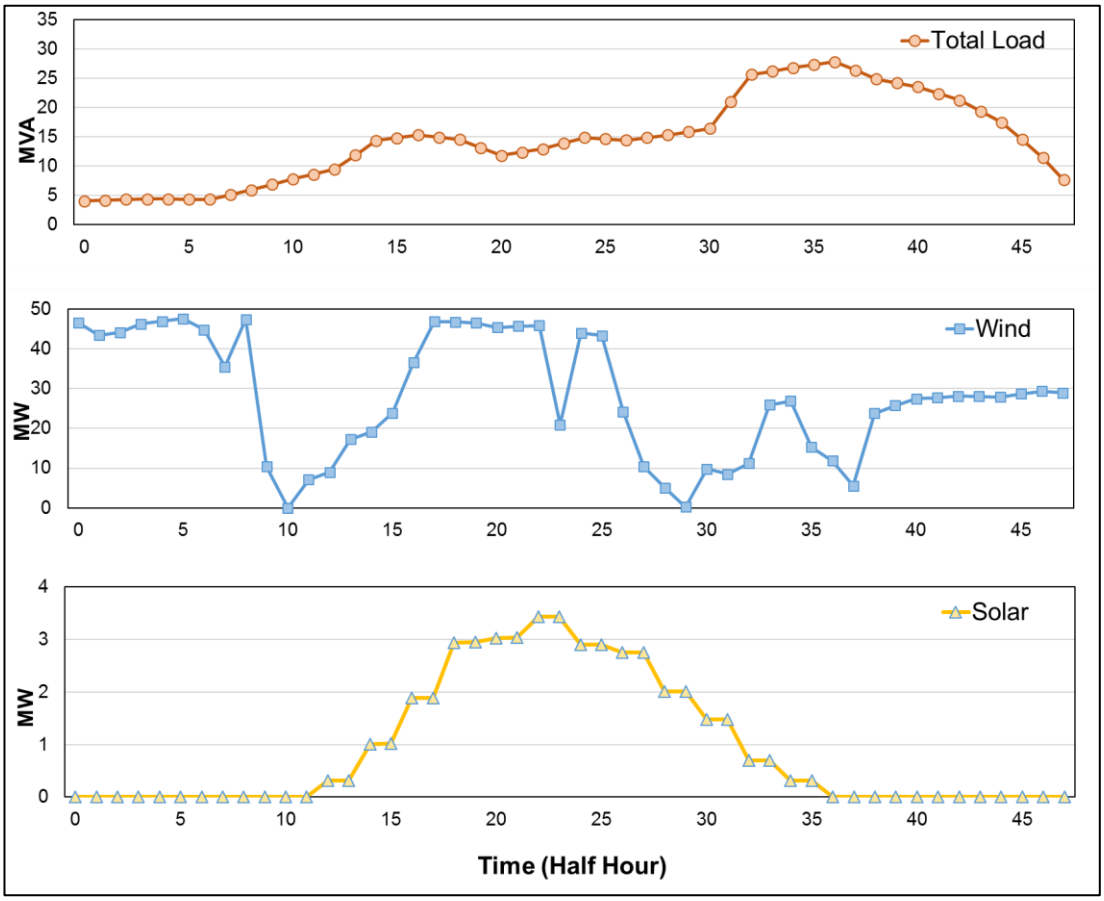

Fig. 5.9 The load, the wind and the solar generation in the first test period (a spring day).

The coincidence of a high DG output and a low demand led to a voltage violation in the first five hours of the day (see Fig. 5.10).

The voltage control of the Demand Response (DR) units responded to the significant voltage deviation by switching ON a proper number of bitumen tanks (Fig. 5.11). A half hour later, those flexible loads started switching OFF due to reaching their high-temperature limits. To mitigate limitations in the demand response, the battery energy storage system started charging to bring back monitored busbar voltages to limits. As a result, all busbar voltages were within limits (Fig. 5.12).

Figure 5.13 shows the distribution of busbars voltages over the spring day. The number of samples is 720 (i.e. 15 busbars over 48-time intervals). Figure 5.13 shows that with the VESS voltage control scheme, the voltage violations were eliminated and all busbars with very high voltages were reduced to the voltage permissible limit (i.e. 1.06

p.u.). With the VESS voltage control scheme, the number of busbars with permissible high voltages was increased (i.e. between 1.03-1.06 p.u.). However, the ability of UKGDS network to host a greater DG generation capacity (i.e. 48.45 MW without the VESS to 60.25 MW with the VESS) was not affected since all busbars voltages were controlled to remain within limits.

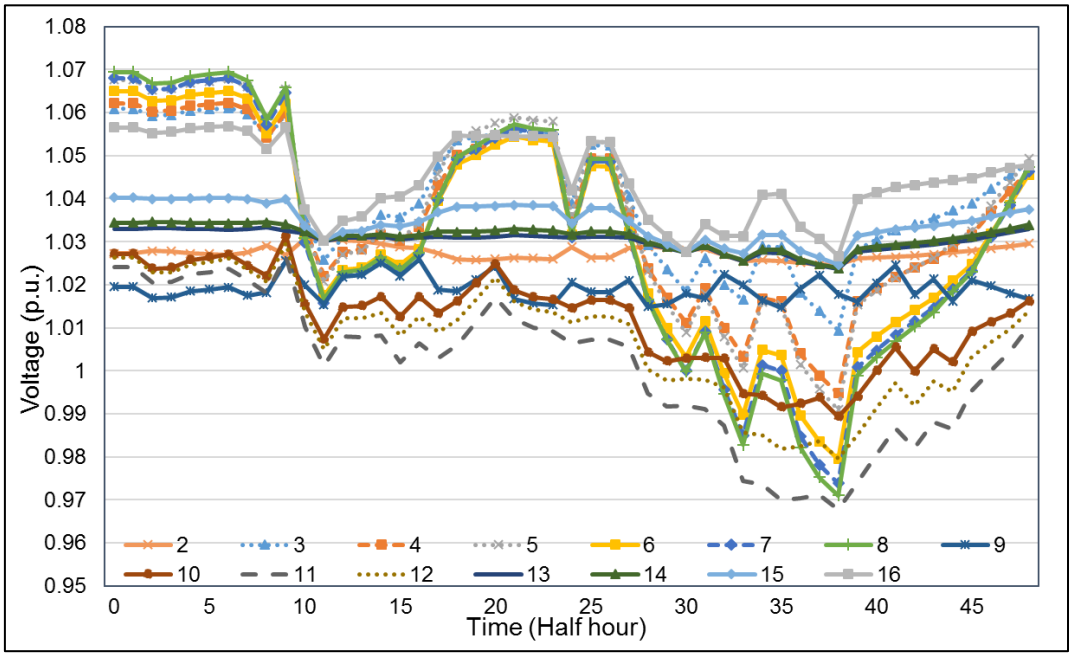

Fig. 5.10 UKGDS busbar voltages without the VESS (base case) in the first test period (a spring day).

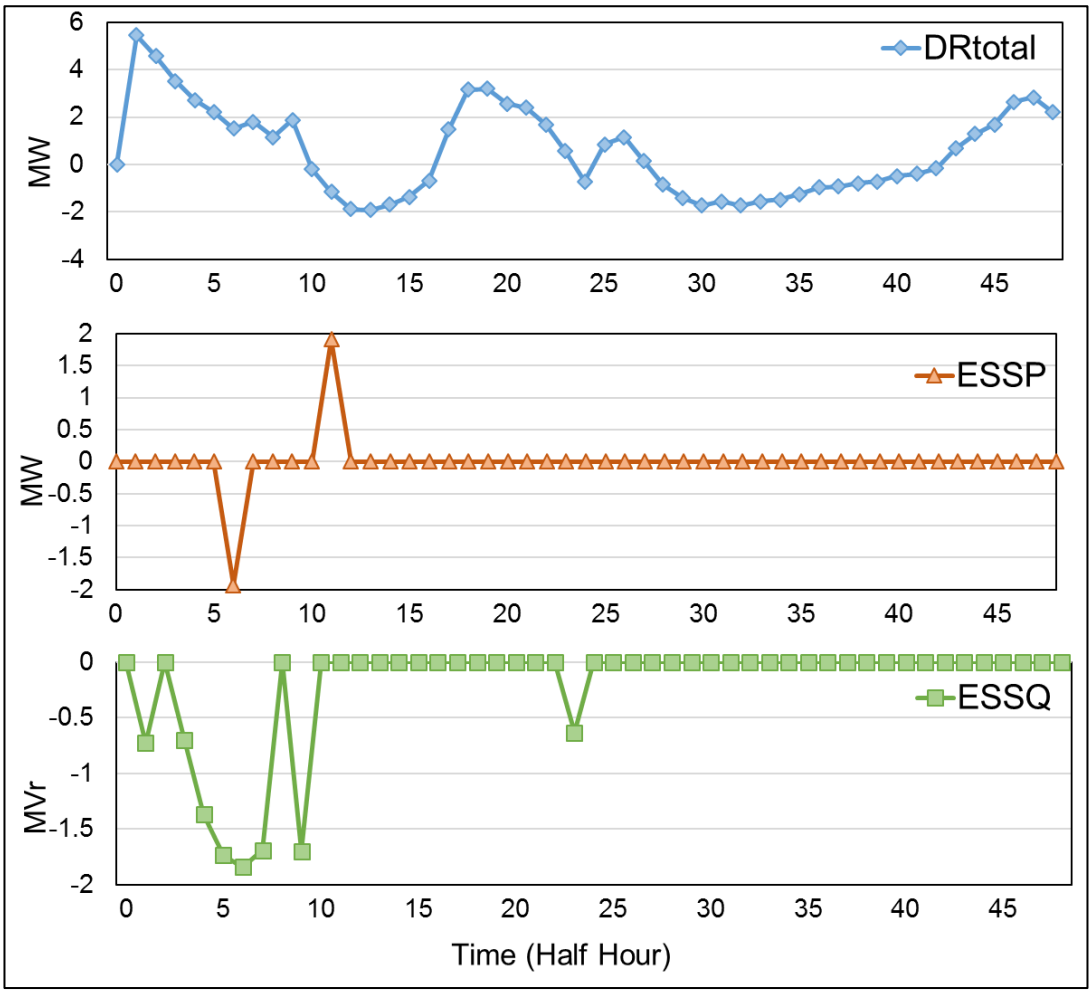

Fig. 5.11 The response from different VESS components in the first test period (a spring day).

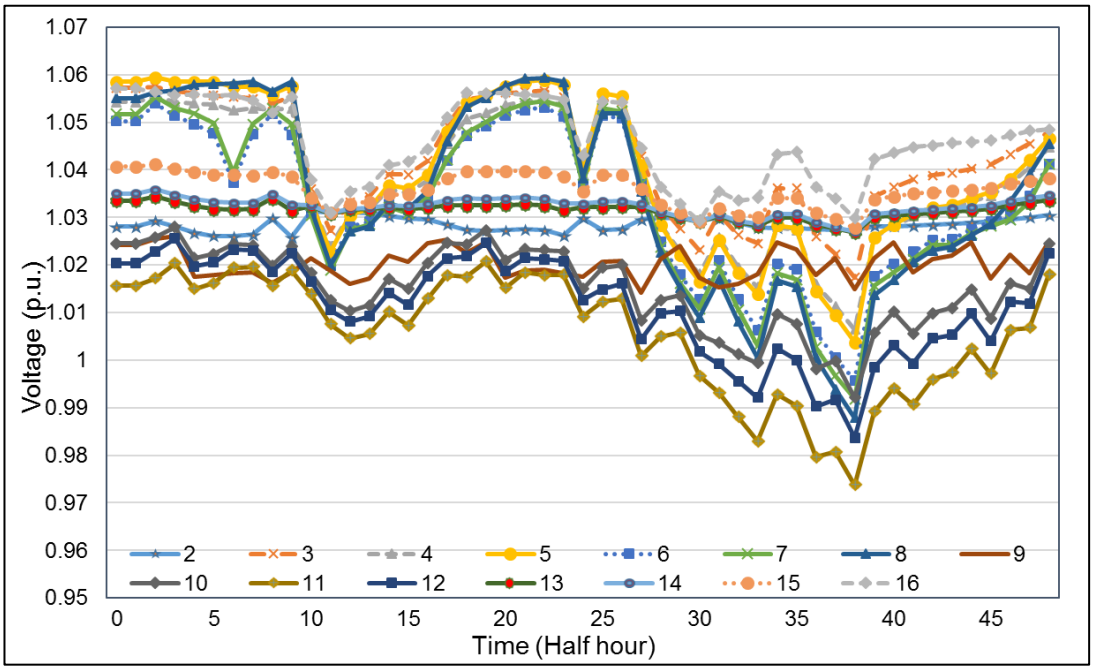

Fig. 5.12 UKGDS busbar voltages with the VESS in the first test period (a spring day).

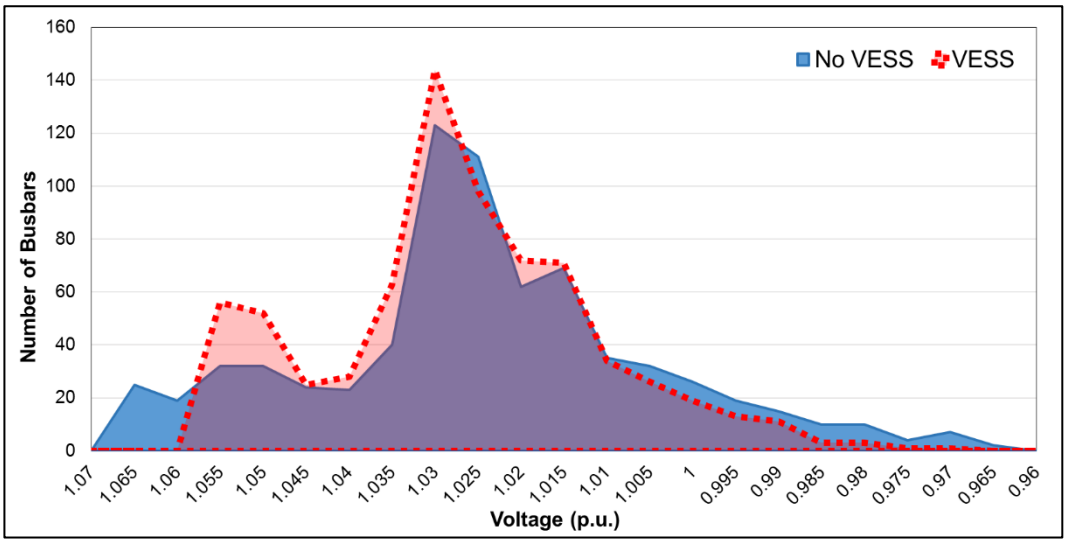

Fig. 5.13 The distribution of the UKGDS busbars voltages in the first test period (a spring day).

Figure 5.14 shows the state of charge of the battery energy storage system in the first test period. Succeeding an active power absorption from the network, the State of Charge (SoC) control of the battery energy storage system (ESS) restored the SoC value into the midpoint area (i.e. 50%±10%).

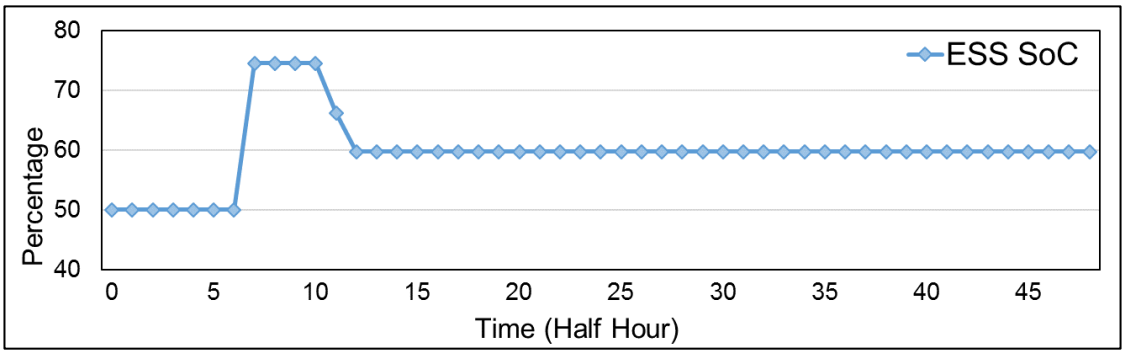

Fig. 5.14 The state of charge of the energy storage system.

2) Second test period (a winter week)

Figure 5.15 shows the total load, wind and solar generations for this time interval. A high wind generation and a high demand consumption compared with the rest of the year characterise this test period. The high wind generation and the low demand in two different half hours led to voltage violations (Fig. 5.16). Figure 5.17 shows the voltage of the UKGDS busbars with the VESS, all voltage violations were eliminated and all busbars with very high voltages were reduced to the permissible voltage limit. Figure 5.18 shows the response from different VESS components. The number of actions of the OLTC transformer and the VR with the voltage control scheme of the VESS decreased compared with the base case.

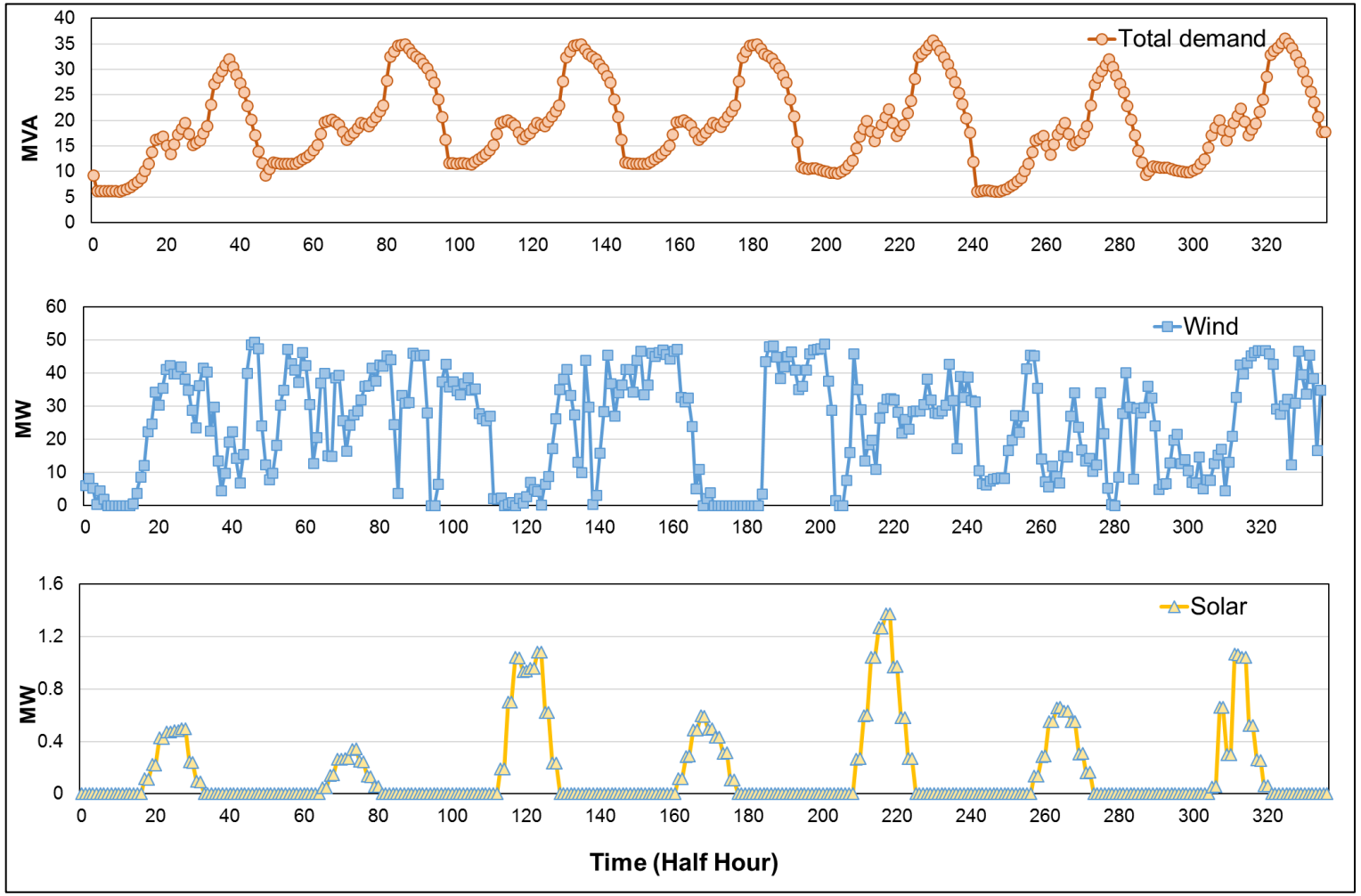

Fig. 5.15 The load, the wind and the solar generation in the second test period (winter week).

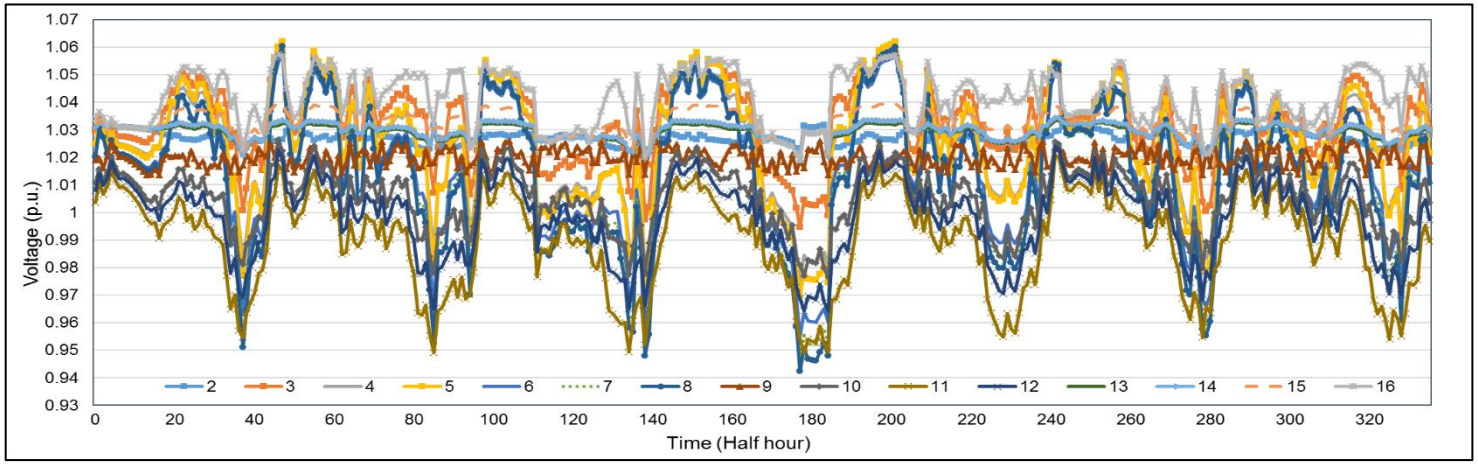

Fig. 5.16 UKGDS busbar voltages without the VESS (base case) in the second test period (winter week).

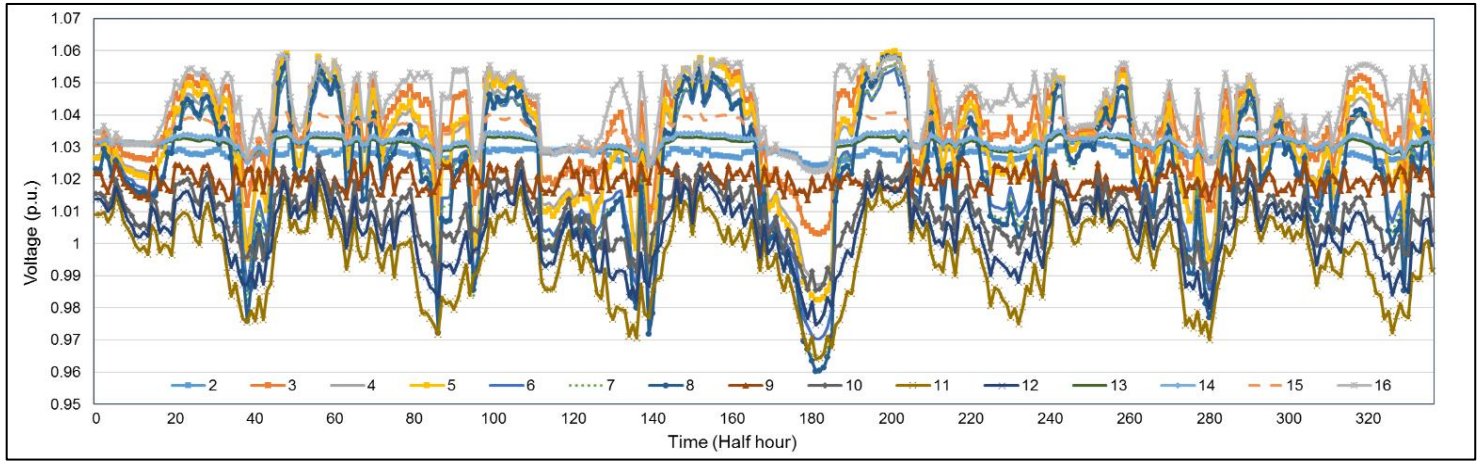

Fig. 5.17 UKGDS busbar voltages with the VESS in the second test period (winter week).

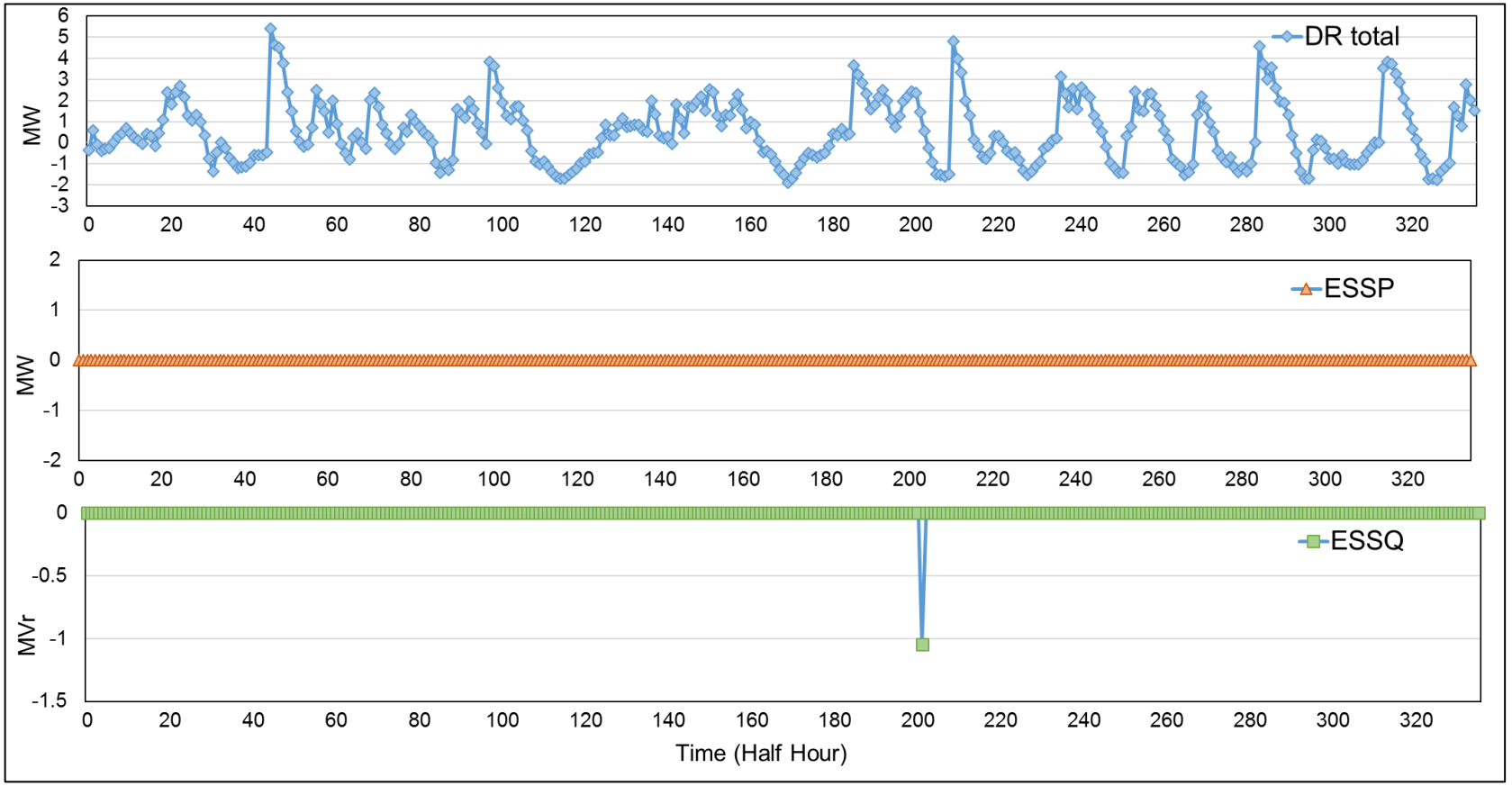

Fig. 5.18 the response from different VESS components in the second test period (winter week).

Figure 5.19 shows the distribution of busbars voltages with respect to voltage over this winter week. The number of samples is 5040 (i.e. 15 busbars over 336-time intervals).

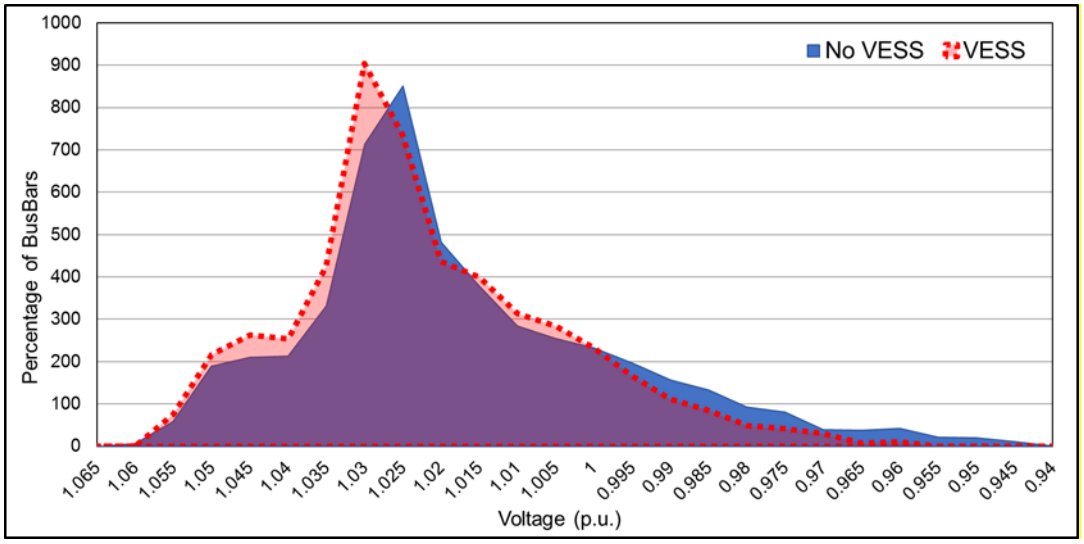

Fig. 5.19 The distribution of the UKGDS busbar voltages in the second test period (winter week).

3) Third test period (a summer week)

Figure 5.20 shows the total load, the wind and the solar generation for this test period. A high solar generation and a low demand consumption compared with the rest of the year characterise this test period. As shown in Fig. 5.21, the high wind and the solar generation with a low demand led to voltage violations in two busbars. Figure 5.22 shows the voltage of the busbars of UKGDS with the VESS, where all voltage violations were eliminated, and Fig. 5.23 shows the response from different VESS components. Figure 5.24 shows the distribution of busbars voltages with respect to voltage over this week. The number of samples is 5040 (i.e. 15 busbars over 336-time intervals).

The number of tap changes of the VR with the voltage control scheme of the VESS increased slightly during the summer week compared with the base case, due to the increase in voltage variations with the voltage control scheme. An equivalent capacity of loads (i.e. 30% of the total load) in the base case was replaced by bitumen tanks for demand response in the VESS. Therefore, the response of bitumen tanks combined with the low demand (i.e. summer week demand) from the remaining loads (i.e. non-flexible loads) led to a higher total load variation than the base case. This higher total load variation triggered slightly different voltage variations than the base case, which caused the slightly more numbers of tap changing actions.

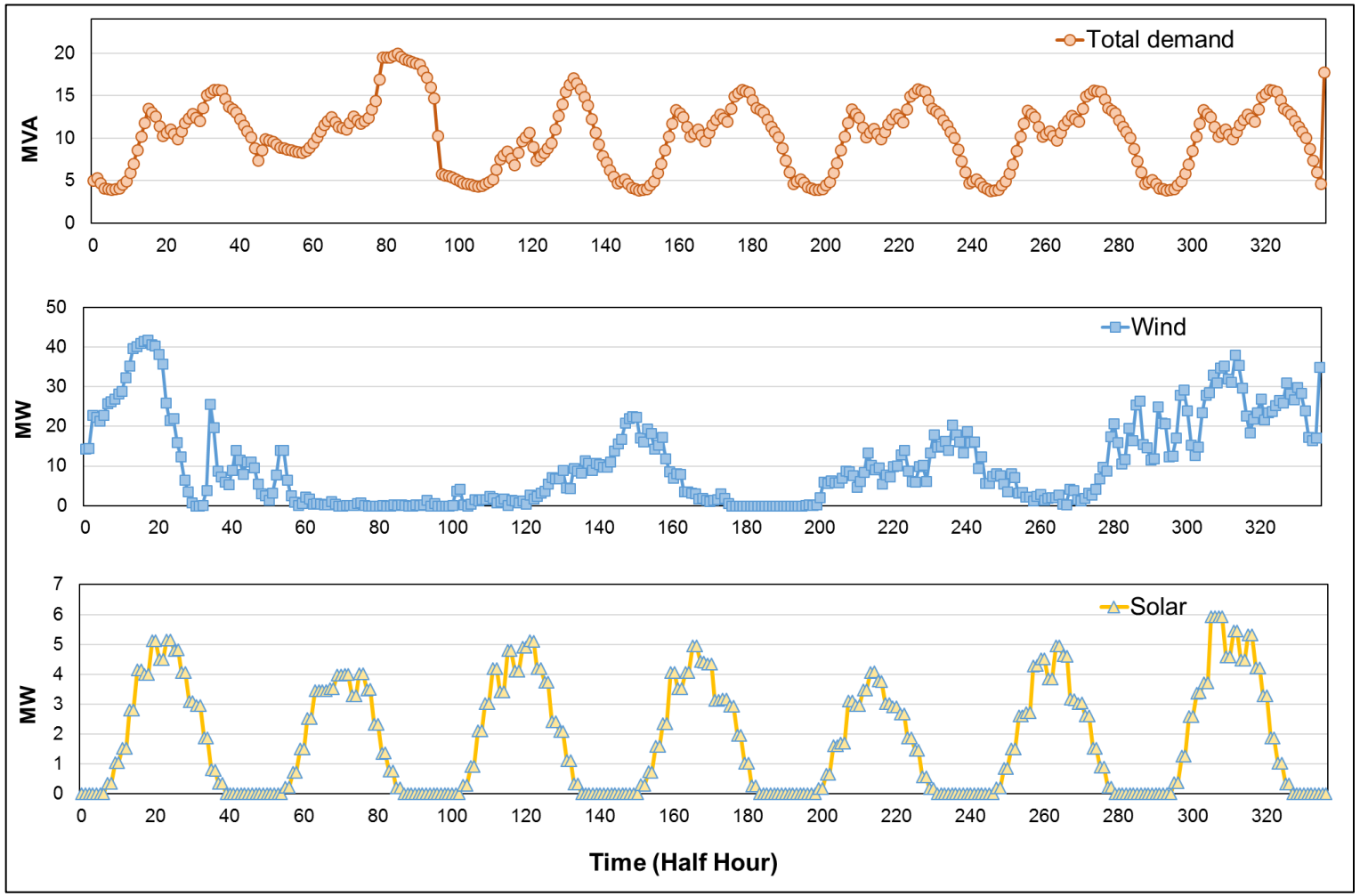

Fig. 5.20 The load, the wind and the solar generation in the third test period (summer week).

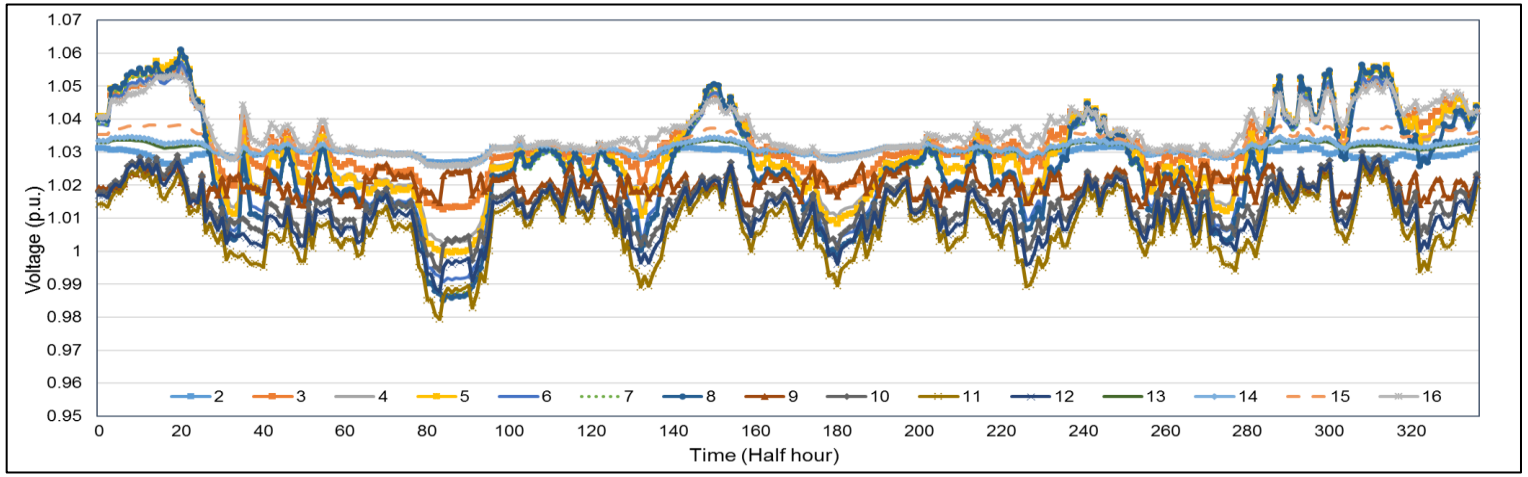

Fig. 5.21 UKGDS busbar voltages without the VESS (base case) in the third test period (summer week).

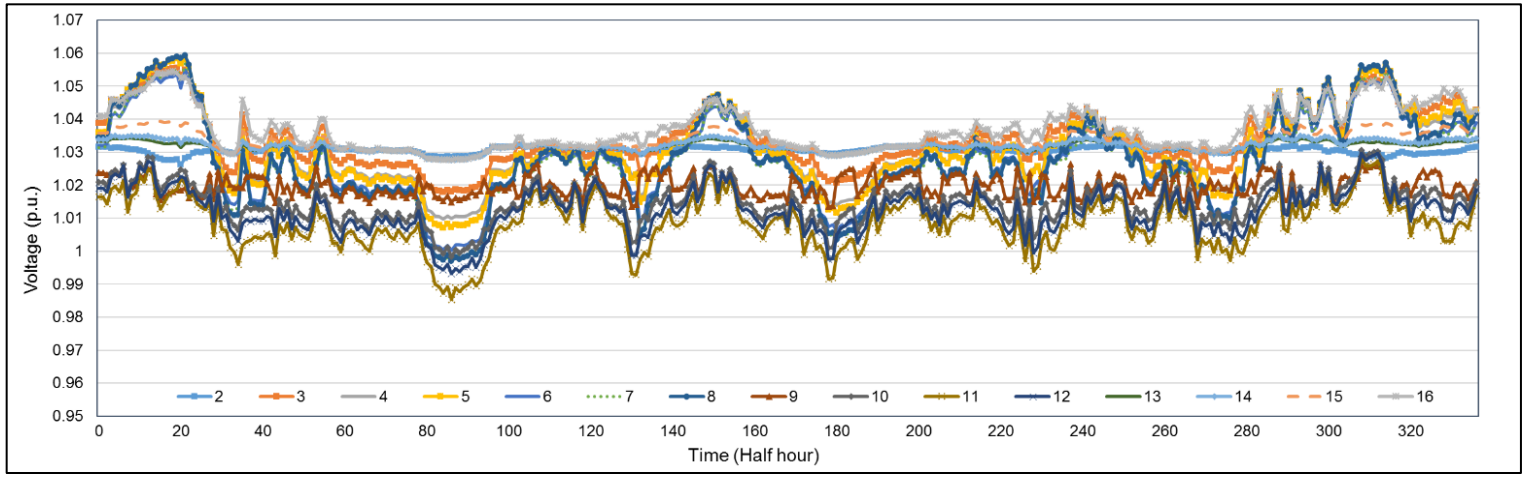

Fig. 5.22 UKGDS busbar voltages with the VESS the third test period (summer week).

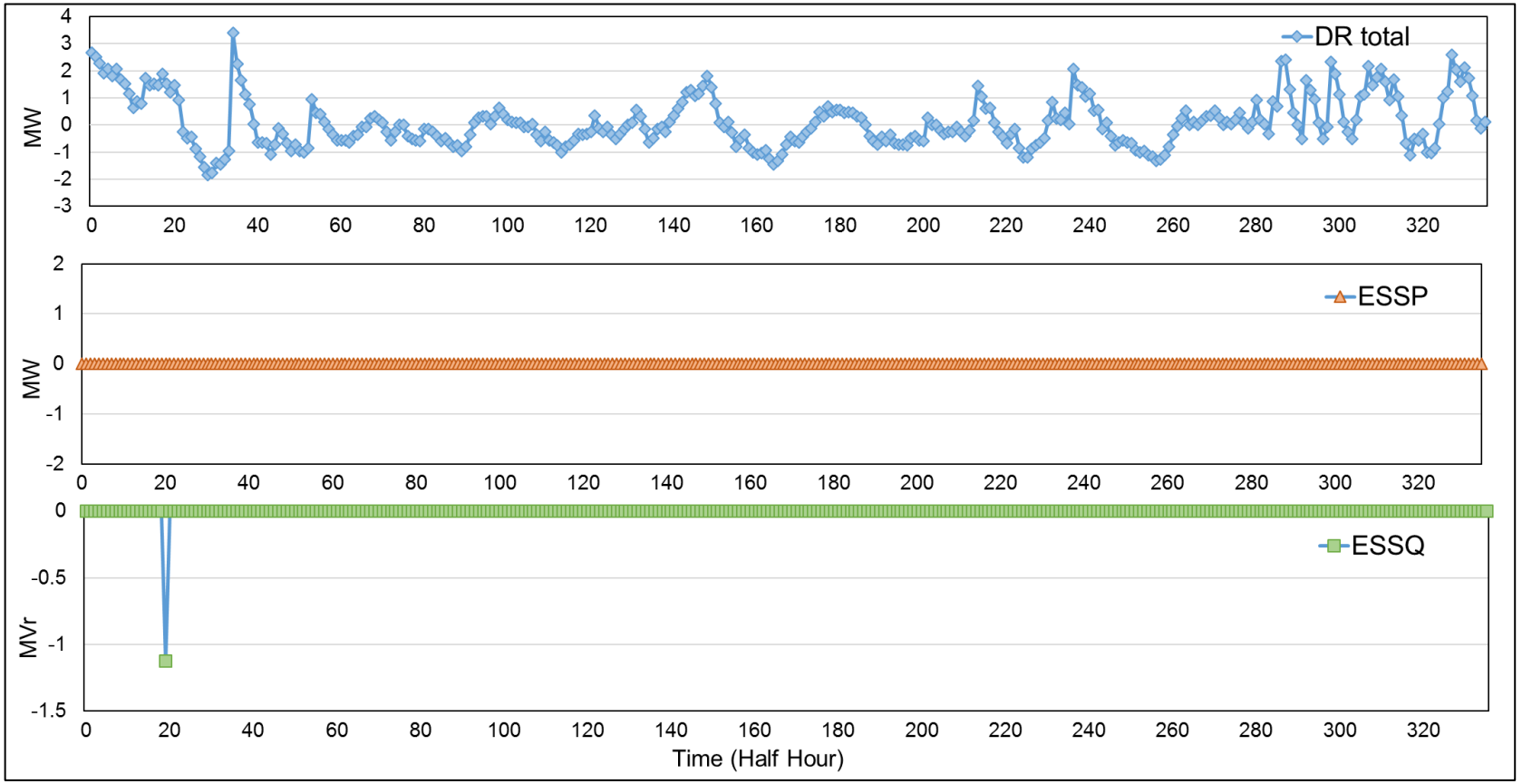

Fig. 5.23 The response from different VESS components in third test period (summer week).

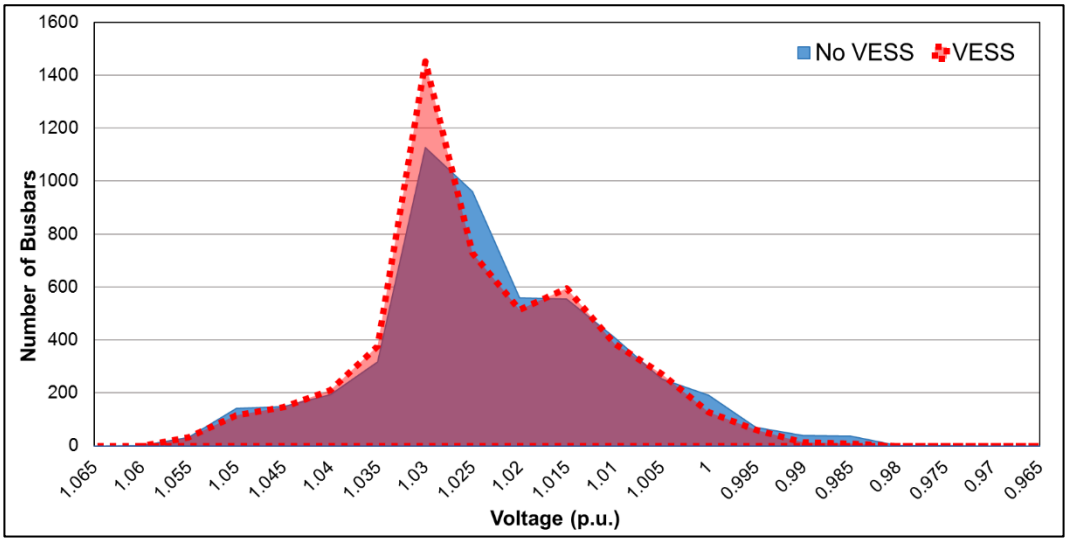

Fig. 5.24 The distribution of the UKGDS busbar voltages in the third test period (summer week).

4) Fourth test period (an autumn week)

Figure 5.25 shows the total load, the wind and the solar generation for this time interval. A High wind and solar generation and a medium demand consumption compared with winter and summer weeks characterise this test period.

A high wind generation and a low demand in an early morning hour led to a voltage violation (Fig. 5.26). Figure 5.27 shows the voltage of the UKGDS busbars with the VESS, where all voltage violations were eliminated, and Fig. 5.28 shows the response from different VESS components. The response from the flexible loads (i.e. bitumen tanks) was sufficient to mitigate high voltage deviations and the early morning hour voltage violation, no energy storage system actions told place.

Figure 5.29 shows the distribution of busbar voltages with respect to voltage over this winter week. In Fig. 5.29, the number of samples is 5040 (i.e. 15 busbars over 336-time intervals). Figure 5.29 Indicates a noticeable improvement in the voltage profile with the control scheme of the VESS than the base case.

Similar to the spring day and the winter week test periods, the number of actions of the VR with the voltage control scheme of the VESS decreased compared with the base case.

In summary, the voltage control scheme of the VESS reduces the OLTC transformer and the VR actions in all cases except the number of VR tap changes in the summer week

as listed in Table 5.11. Hence the voltage control scheme of the VESS reduces transformers maintenance requirements. Moreover, the reactive power of the battery energy storage system was sufficient to counteract voltage violations caused by the high DG output and the limited demand response most of the time in the tested periods.

TABLE 5.11 THE PERFORMANCE ANALYSIS OF THE VOLTAGE CONTROL SCHEME OF A VESS

Test period	Performance Indicator	No VESS	With VESS
Spring Day First period	No. of voltage violation	44	0
	No. of VR tap changes	32	21
	No. of OLTC tap changes	0	0
Winter Week Second period	No. of voltage violation	7	0
	No. of VR tap changes	191	162
	No. of OLTC tap changes	4	0
Summer Week Third period	No. of voltage violation	2	0
	No. of VR tap changes	79	83
	No. of OLTC tap changes	0	0
Autumn week Case Four	No. of voltage violation	2	0
	No. of VR tap changes	101	72
	No. of OLTC tap changes	0	0

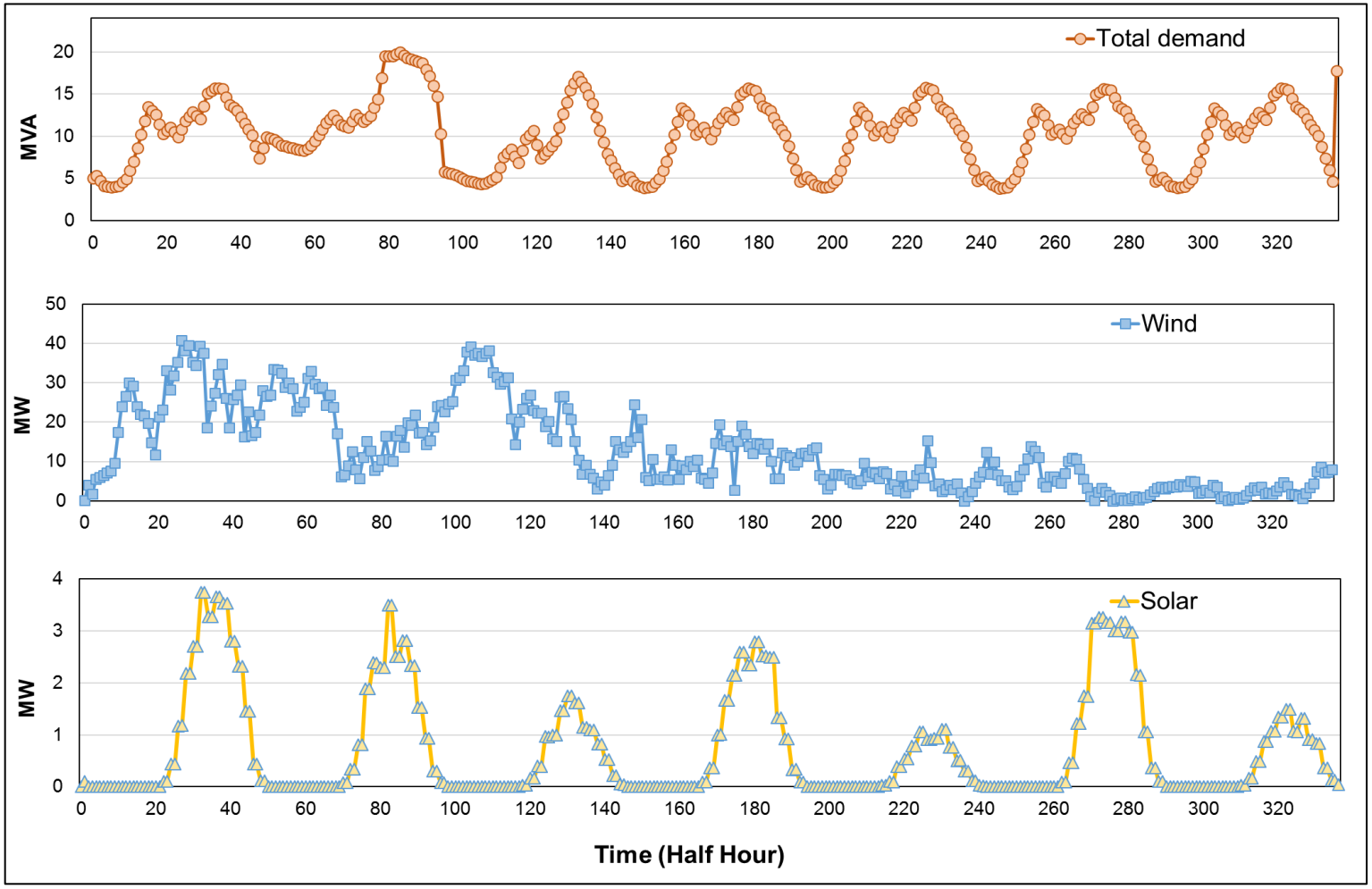

Fig. 5.25 The load, the wind and the solar generation in the fourth test period (autumn week).

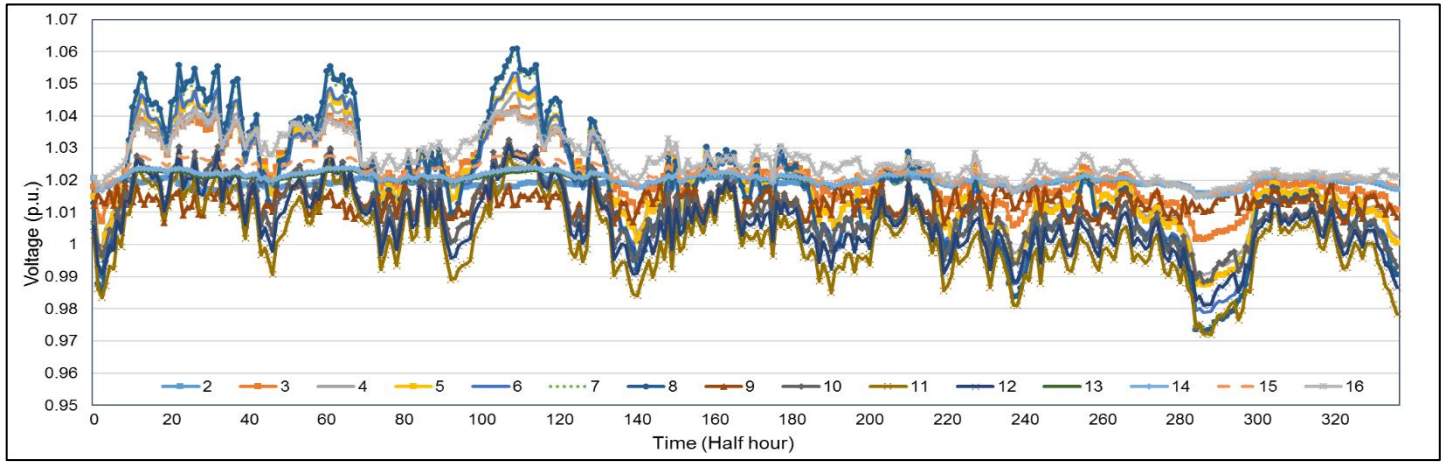

Fig. 5.26 UKGDS busbar voltages without the VESS (base case) in the fourth test period (autumn week).

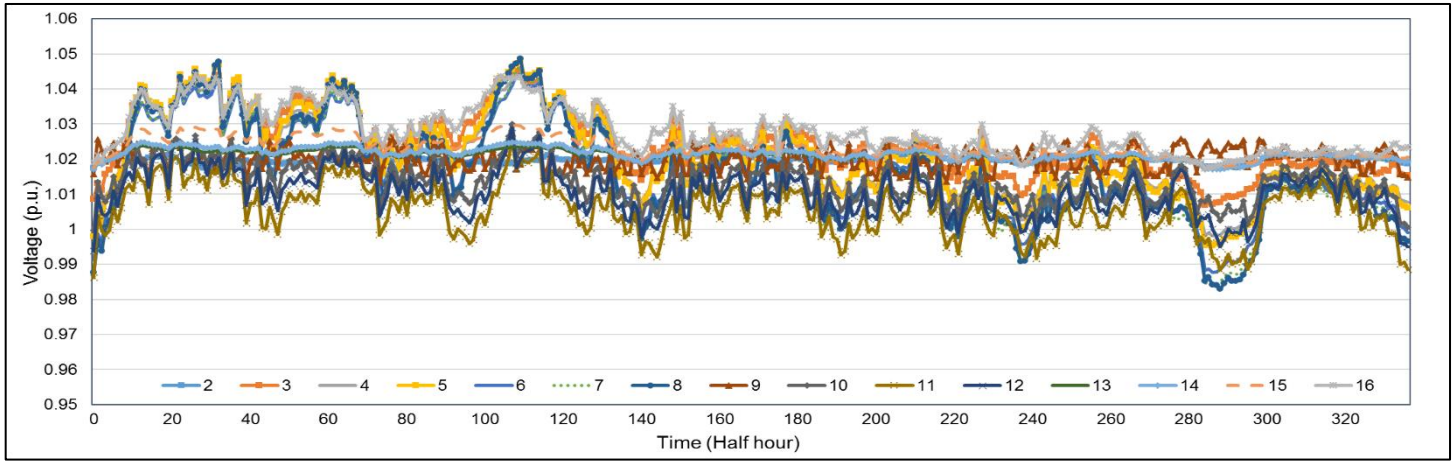

Fig. 5.27 UKGDS busbar voltages with the VESS in the fourth test period (autumn week).

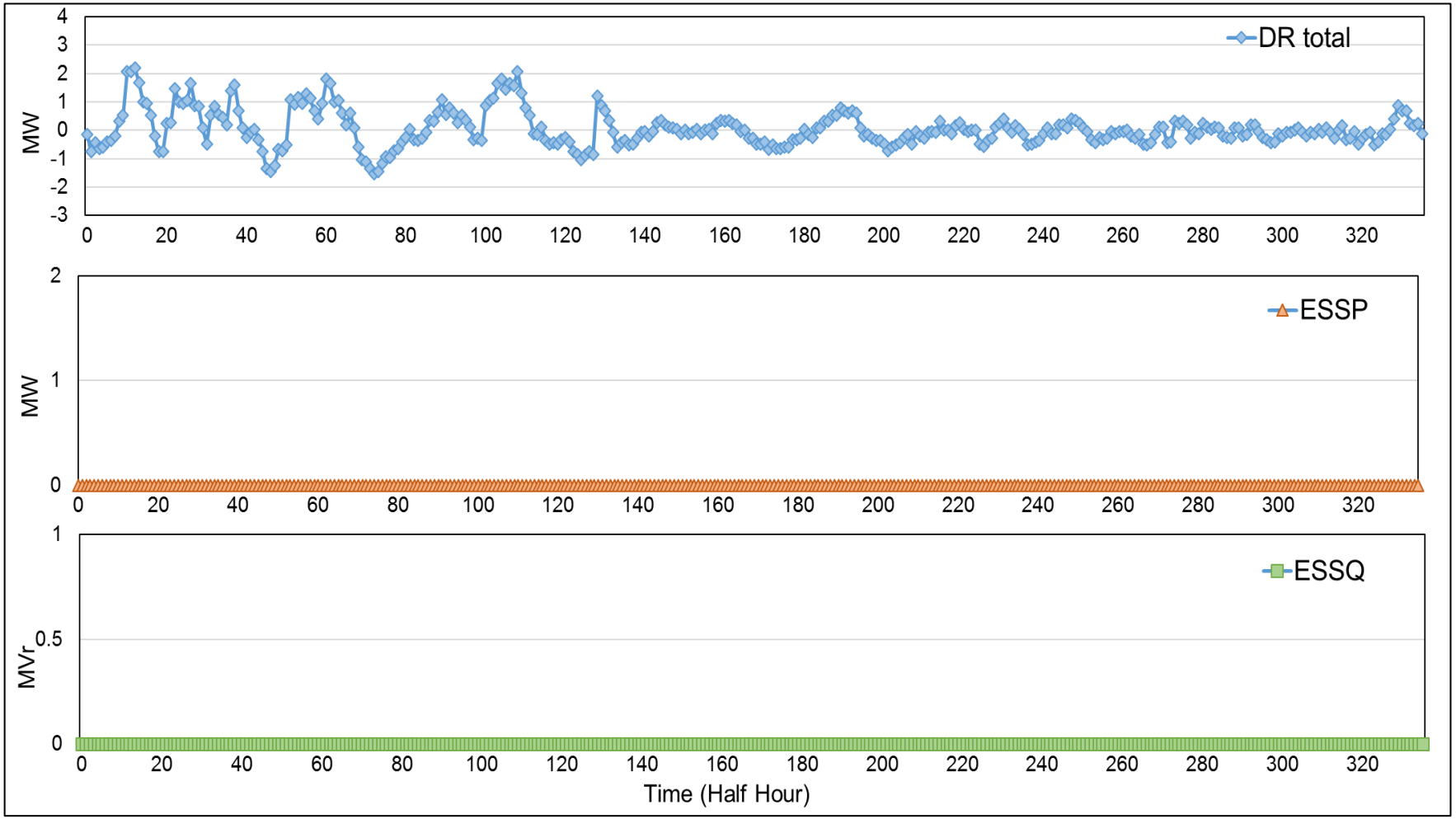

Fig. 5.28 The response from different VESS components in the fourth test period (autumn week).

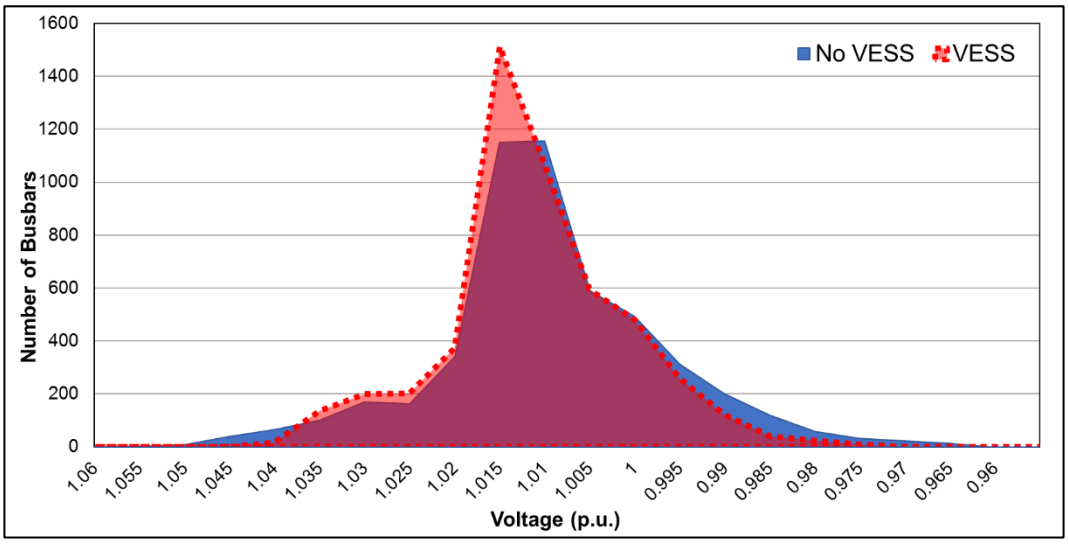

Fig. 5.29 The distribution of the UKGDS busbar voltages in the fourth test period (autumn week).

Figure 5.30 shows the apparent power flowed through the substation of UKGDS with and without the VESS in the first test period. The voltage control scheme of the VESS uses mainly active power, which is obtained by altering the demand response units' power consumption, to mitigate the voltage violation problem. As a result, the maximum power flowed through the substation (i.e. 37.6 MVA) was less than the network firm connection capacity of 37.7 MVA. Accordingly, this can prevent the reinforcements of adding a third 33 MVA transformer and a feeder to the substation. Whereas in the base case, the power flow exceeded (41.9 MVA) the network firm connection.

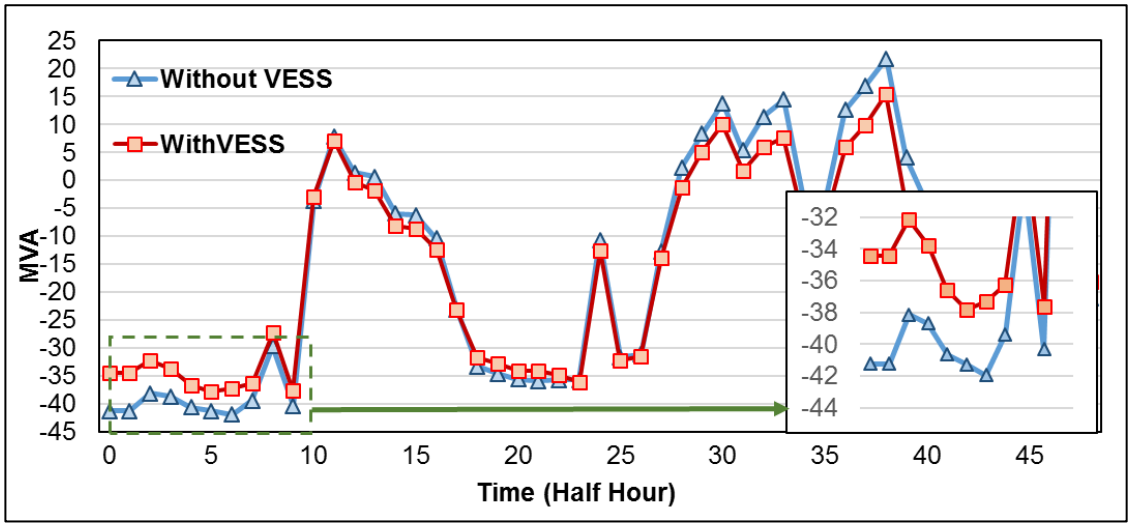

Fig. 5.30 The power flowed through the substation of the UKGDS in the first test period (spring day).

5.4. The economic evaluation

The economic evaluation of the voltage control scheme of the VESS is roughly estimated. The estimation is based on comparing the capital cost of the VESS with the reinforcement cost of the UKGDS.

Table 5.12 shows the estimated investment costs of the VESS and the reinforcement of the UKGDS. The investment costs of the battery energy storage system and the substation reinforcement are based on the smarter network storage project [142]. In that project, a 6 MW/10 MWh battery energy storage system was installed at the 33 kV substation to avoid the reinforcement of adding a 33 kV feeder and a 38 MVA transformer. The cost of the battery energy storage system was £11.2m and the cost of the substation upgrade was £6.2m in 2013 [142]. Based on given costs of that project, the approximate cost of the battery energy storage system (i.e. a VESS component) is £1.6m and the approximate cost of the network reinforcement is £5.4m. The cost of remote monitoring devices of the voltage controller of the battery energy storage system is not considered. The cost of installing voltage controllers on the 245 bitumen tanks is approximately £735 [101]. Therefore, the total cost of the VESS is £1.60735m. Which is much less than the UKGDS reinforcement cost of £5.4m.

TABLE 5.12 THE ESTIMATED INVESTMENT COSTS OF THE VESS AND UKGDS REINFORCEMENT

Case	Unit	Unit price	Capacity or no. of units	Total price	
Network Reinforcement	Feeder and transformer	£0.163m/1 MVA [142]	33 MVA	£5.6m	
VESS	Bitumen tank's controller	£3 [101]	245	£735	£1.607m
	Battery energy storage system	£1.12m/1 MWh [142]	1.4 MWh	£1.6m	

5.5. Summary

A voltage control scheme of the VESS was designed. The voltage control scheme facilitates the connection of more DG by supporting the voltage control of the distribution network. The voltage control of the VESS components were developed and coordinated in order to minimise the voltage deviations and limit it to ±6% of the nominal value (i.e. 1 p.u.).

The voltage control scheme of the VESS coordinates its components and the inherent voltage control equipment of the network, which are the OLTC transformer and the VR, through assigning their controllers different time delay settings. Consequently, the voltage hunting is avoided and a minimum communication is required.

The local voltage control of bitumen tanks alters the power consumption of the flexible loads in response to the voltage deviations. The voltage control has little impact on the primary function of the loads.

The voltage control of the battery energy storage system monitors continuously the voltage of the most vulnerable busbars with respect to voltage violations. After the response from the flexible loads, the voltage controller determines the charging or discharging action from the battery energy storage system. The voltage controller uses a droop control with a droop setting obtained from voltage sensitivity factors. The battery energy storage system voltage control ensures a firm and linear response from the VESS against voltage violations.

Solar panels (i.e. Photovoltaics (PV)), the VESS and optimally sized wind farms were connected to the UKGDS distributed network. Half hourly profiles of DG and loads were adopted. A case study was conducted to evaluate the voltage control scheme of the VESS over different time periods of the year. The results were compared with a base case. In the base case, only the voltage control of the OLTC and the VR transformers were used.

Results showed that voltage controllers of bitumen tanks counteract high voltage deviations most of the time. When voltage violation sustained, mainly reactive power from battery energy storage system was used. The voltage control scheme of the VESS made a significant improvement in the UKGDS busbars voltage and reduced tap changing actions of the OLTC transformer and the VR compared with the base case. The voltage control scheme of the VESS represents an economic, i.e. the cost for setting the VESS is one-third the cost of network reinforcement, and a technical solution to accommodate more with DG in distribution networks without reinforcement.

CHAPTER 6

Conclusions and suggestions for further work

6.1. Conclusions

This research investigated the development of a mathematical model for a Virtual Energy Storage System (VESS). The VESS coordinates demand response and energy storage units, with different physical characteristics, to provide services to the power system operator and the distribution network operator. A frequency control scheme of a VESS to provide frequency response services to the system operator was developed. A voltage control scheme of a VESS to support the voltage control in distribution networks to accommodate DG was also developed.

6.1.1. Modelling the components of a virtual energy storage system

Mathematical models of four components of a VESS were developed. Specifically, the models of the flywheel energy storage system, the battery energy storage system, the domestic refrigerator and the industrial bitumen tank were developed. Models of the flywheels and the refrigerators were used to establish the frequency control scheme of the VESS described in Chapter 4. Models of the battery and the bitumen tanks were used to implement the voltage control scheme of the VESS presented in Chapter 5.

An average model and a simplified model of a flywheel energy storage system were developed. The average model simulates the unit of flywheel energy storage system dynamic performance, while the simplified model facilitates the simulation of a population of units with much shorter simulation time. A velocity limiter was added to the simplified flywheel model to prevent the model from exceeding velocity limits.

A simplified model of a battery energy storage system was designed. A state of charge limiter was added to the model to avoid exceeding the state of charge limits.

A model mimicing the thermodynamic behaviour of a refrigerator was developed and an internal cavity temperature controller was incorporated into the model. Hence, the primary function of refrigerators, i.e. cooling supply, remained intact.

A model representing the thermodynamic behaviour of a bitumen tank was developed and the internal temperature controller was included in the model. Consequently, the key role of bitumen tanks, i.e. heat supply, was maintained.

All the models that were developed, i.e. the average and the simplified flywheel, the simplified battery, the refrigerator and the bitumen tank models, were validated by comparing the simulation results with results of similar equipment from the literature.

Simulation results showed that the simplified models of a flywheel and a battery energy storage systems reflected the performance of these systems and facilitated grid scale studies due to the short simulation time required. The results also showed that, the models of a refrigerator and a bitumen tank produced the thermodynamic behaviour of these demand response units.

Aggregated models, representing a population of units, for each of flywheels, batteries, refrigerators and bitumen tanks, i.e. an aggregated model for each of the four components of a VESS, were modelled. These models preserve diversity amongst the population by randomly initiating the velocity in the population of flywheels, the state of charge in the population of batteries, cavity temperature in the population of refrigerators and tanks temperature in the population of bitumen tanks.

Modelling the components of the VESS assisted in identifying the most suitable components for the targeted applications of the VESS. Flywheels, with a long cycle life, and refrigerators have short-duration responses hence are suitable to provide frequent frequency response services. On the contrary, batteries (i.e. with a moderate cycle life) and bitumen tanks have long-duration responses therefore are suitable to provide voltage support services. The modelling also helped to indicate the critical parameters to be used in the design of control schemes of the VESS. Parameters such as the flywheel velocity and the battery state of charge indicate the ability to charge or discharge the energy storage system. Also, refrigerators and bitumen tanks temperatures indicate the potential to switch ON or OFF the demand response units.

6.1.2. **The frequency control scheme**

A frequency control scheme of a VESS to provide high, low and continuous frequency response services to the power system was developed. The control scheme, which coordinates models of a population of refrigerators and a population of flywheels, provides frequency response services similar to using only a population of flywheels with a higher capability and lower costs. In the frequency control scheme of the VESS, the refrigerators respond to frequency deviations while units of the flywheel energy storage system compensate for the uncertainty of the refrigerators response.

In addition to the internal temperature controller of the refrigerator, a frequency controller was developed and added. The integrated temperature and frequency controller maintains the primary function of refrigerators and mitigates the impact of the reduction in load diversity amongst the population.

A Coordinated Adaptive Droop Control (CADC) for the population of units of flywheel energy storage was developed. The CADC strategy reduces the number of units to be committed during small frequency deviations while delivering a similar response to the Conventional Droop Control (CDC), i.e. where all units are committed. The CADC minimises the charging and discharging cycles of each unit of the flywheel energy storage, hence prolongs their lifetime.

Three case studies were conducted to evaluate the performance of the frequency control scheme of the VESS. The VESS aggregated 3.22 million refrigerators and 400 units of the flywheel energy storage system. The rated power consumption of each of these identical refrigerators is 0.1 kW, hence a total rated power consumption of the aggregated refrigerators is 322 MW. The power and the energy capacities of each of the identical flywheel units are 50 kW and 30 kWh, therefore the total power and energy capacities of all units are 20 MW/12 MWh. The VESS can provide a minimum of 60 MW as a low-frequency response (if the frequency reached 45.5 Hz or below), since refrigerators can provide a minimum power reduction of 40 MW and the flywheels can provide 20 MW. The VESS can also provide a minimum of 180 MW as a high-frequency response (if the frequency reached or exceeded 50.5 Hz), because the refrigerators can provide a minimum power increase of 160 MW and the flywheels can provide 20 MW. The difference between the low and high-frequency response capacities is due to the higher availability of the refrigerators to be switched ON, hence giving a larger high-frequency response. The performance of the VESS was compared to using only 1200

units of the flywheel energy storage system (i.e. a total power and energy capacities of 60 MW/36 MWh), which is 60 MW of high, low and continuous frequency response.

The VESS was connected to a simplified Great Britain power system model with 20 GW demand. The case studies were:

1) The provision of 60 MW of low-frequency response service, following the loss of 1.8 GW of generation.
2) The provision of high-frequency response service, following the loss of 1 GW of demand.
3) The provision of continuous frequency response service. In this case, the VESS responded to a historical frequency profile, which has large frequency deviations, from the Great Britain power system.

Simulation results showed that the VESS delivered 60 MW of low-frequency response when the frequency dropped below 45.5 Hz in Case 1, 140 MW of a high-frequency response when the frequency reached 50.4 Hz in Case 2 and an efficient continuous frequency response in Case 3. Consequently, frequency deviations were reduced and the increase in the power output of generators, which are connected to the power system model, was reduced. The frequency control scheme of the VESS delivered frequency response to the power system similar to the frequency-sensitive generators response.

Based on the results that were obtained, it was concluded that the response from the frequency control scheme of the VESS was small in the context of the GB power system, therefore the improvement in frequency was insignificant (approximately 0.01 Hz when the VESS provided a low-frequency response and 0.05 Hz when the VESS provided a high-frequency response). If the frequency control scheme of the VESS implemented in other demand response and energy storage units, their contribution to the power system frequency control would be substantial. Therefore, a large deployment of the VESS will reduce the frequency response requirements from frequency-sensitive generators.

An economic evaluation was conducted. Based on that evaluation, the VESS is estimated to obtain 50% higher revenues compared with the case that uses only the flywheel energy storage system. These revenues are based on providing frequency response services to the system operator.

6.1.3. **The voltage control scheme**

A voltage control scheme of a VESS was designed. The control scheme coordinates models of bitumen tanks and a battery energy storage system to enhance the voltage control of distribution networks to accommodate Distributed Generation (DG). The control scheme of the VESS coordinates its components and voltage control equipment of the network, which are the On-Load Tap Changing (OLTC) transformer and the Voltage Regulator (VR), through setting their controllers different time delays.

A voltage controller was developed and added to the inherent temperature controller of the bitumen tank. The integrated temperature and voltage controller respond to voltage deviations without undermining the bitumen tanks primary function of heat supply.

A voltage controller for the battery energy storage system was designed. The controller continuously monitors the most vulnerable busbars with respect to voltage violations. When a voltage deviation takes place, voltage controllers of bitumen tanks respond. If the voltage violation persists, the voltage controller of the battery energy storage system responds to the voltage violation. The battery energy storage system responds by the active and the reactive powers exchange where the reactive power is prioritised. This response is determined using a droop control with a droop setting obtained from voltage sensitivity factors.

A case study was undertaken to evaluate the voltage control scheme. The VESS aggregated 245 bitumen tanks (i.e. 9.8 MW) and a 2.3 MW/1.4 MWh battery energy storage system to increase the DG accommodated by the distribution network from 48.45 MW to 60.25 MW. Bitumen tanks were connected to 11 of 14 busbars of the network and a single battery energy storage system was located at busbar 5 based on voltage sensitively factors. Solar panels were connected to 11 of 14 busbars of the network with aggregated rated capacity of 6.55 MW, while 5 wind farms were connected to the end of 5 different feeders and their sizes were optimally found using a Genetic Algorithm.

The control scheme performance was assessed against a base case over four test periods of the year, i.e. a summer week, a winter week, an autumn week and a spring day. In the base case, only the OLTC transformer and the VR were used to control the network voltage. In the base case, voltage violations occurred, i.e. voltage exceeded the ±6% of nominal value, and the number of tap changing of the OLTC transformer and the VR increased in all test periods with the increase of DG penetration.

Results showed that the voltage control scheme of the VESS eliminated all voltage violations and reduced the required number of the OLTC and the VR transformers actions by approximately 30%, hence extends the transformers life.

An economic evaluation was conducted. Based on this evaluation and simulation results, the voltage control scheme of the VESS represents an economic and a technical alternative to substation upgrade to cope with the increasing number of the DG connected to distribution networks.

The following conclusions were drawn, voltage violations occurred due to coincidences of high DG and low demand. The voltage control scheme of the VESS manipulated demand levels and therefore voltage violations were reduced or eliminated. Introducing more DG into the UKGDS network led to increasing tap changes of the OLTC transformer and the voltage regulator. For instance, the number of tap actions of the voltage regulator at busbar 9 rose from 51 to 101, when the voltage control scheme of the VESS introduced it fell to 72.

The results of this thesis assist policy makers to support the transmission and distribution system operators adopting the VESS. Thus, improves the power system efficiency, maintains its high reliability while reduces the dependency on partly loaded fossil fuel generators which cause high carbon emissions.

6.2.Suggestions for further work

A. An integrated control scheme of the VESS

The frequency control and the voltage control schemes of a VESS were developed in Chapter 4 and Chapter 5; it is proposed to combine these two control schemes into a single integrated control scheme. This control scheme would allow the VESS to provide voltage support service to the distribution network operator during small frequency deviations and deliver frequency response services to the power system operator during larger frequency deviations. The control scheme simultaneously facilitates an efficient integration of distributed energy resources into the power system while considering reserve and security requirements. Consequently, this control scheme optimises the VESS revenues from different sectors.

B. A control scheme of the VESS for the Microgrid operation

A voltage control scheme of the VESS applied to the distribution network was designed in Chapter 5; a similar control scheme can be developed and coordinated with the existing controller of a Microgrid. However, a two-way communication network is then required. The proposed control scheme of the VESS includes three objectives executed in the following sequence

1. In a large frequency deviation case, the frequency control scheme of the VESS will supports the frequency control of the Microgrid, similarly to the frequency control scheme developed in chapter 4.
2. In a voltage violation case, the voltage control scheme of the VESS will supports the voltage control of the Microgrid, which is similar to the voltage control scheme developed in chapter 5.
3. In normal operation, a power smoothing control scheme of the VESS will smooths power fluctuations of the intermittent renewable resources at the connection point, i.e. the point connecting the Microgrid to the power system. The control scheme of the VESS continuously monitors the intermittent renewable resources power output to changes its state between charging, discharging and standby modes accordingly.

C. A stochastic unit commitment for optimising the operation of the VESS in power system with significant penetration of intermittent renewable resources

The stochastic nature of the intermittent renewable resources increases the uncertainty in the power system operation. The role of the VESS to maximise the absorbed the generation of intermittent renewable resources by the power system without compromising its economic operation is yet to be explored. The uncertainty associated with the intermittent resources is a key aspect of the proposed unit commitment algorithm. Historical data of the intermittent resources generation and the availability of the elastic demand will be utilised. The required spinning reserve from both conventional generators and the VESS will be considered. The algorithm will also consider network constraints, particularly related to the VESS components connected to distribution networks.

References

[1] N. Jenkins and J. Ekanayake, *Renewable Energy Engineering*, Cambridge University Press, 2017.

[2] Eenergy and Climate Change Committee, "2020 renewable heat and transport targets," House of Commons, UK, 2016.

[3] National Grid plc, "Future energy scenarios," July 2016, [Online]. Available: http://fes.nationalgrid.com/.

[4] R. Harrabin, "Renewables provide more than half UK electricity for first time," in *BBC News*, 8th June 2017.

[5] A. Vaughan, "Record levels of green energy in UK create strange new world for generators," in *The Guardian Newspaper*,17th June 2017.

[6] J. Zhu, *Optimization of power system operation*, John Wiley & Sons, 2015.

[7] National Grid plc, "System operability framework," November 2016, [Online]. Available: http://www2.nationalgrid.com/UK/Industry-information/Future-of-Energy/System-Operability-Framework/.

[8] N. Jenkins *et al.*, *Embedded Generation (IEE power and energy series; 31)*: Institution of Engineering and Technology, 2000.

[9] M. Akmal, B. Fox, J. D. Morrow, and T. Littler, "Impact of heat pump load on distribution networks," *IET Generation, Transmission & Distribution*, vol. 8, pp. 2065-2073, 2014.

[10] UK Power Networks, "Impact of electric vehicle and heat pump loads on network demand profiles," UK, Tech. Rep., September 2014.

[11] U Ofgem,"Project discovery energy market scenario," Cnsul. doc., October 2009.

[12] D. Pudjianto, P. Djapic, M. Aunedi, C. K. Gan, G. Strbac, S. Huang, *et al.*, "Smart control for minimizing distribution network reinforcement cost due to electrification," *Energy Policy*, vol. 52, pp. 76-84, 2013.

[13] National Grid plc, "Electricity ten year statement," November 2016, [Online]. Available: http://www2.nationalgrid.com/UK/Industry-information/Future-of-Energy/Electricity-ten-year-statement/ETYS-Archive/.

[14] J. B. Ekanayake, N. Jenkins, K. Liyanage, J. Wu, and A. Yokoyama, *Smart grid: technology and applications*, John Wiley & Sons, 2012.

[15] G. Strbac, M. Aunedi, D. Pudjianto, P. Djapic, F. Teng, A. Sturt, *et al.*, "Strategic assessment of the role and value of energy storage systems in the UK low carbon energy future," *Report for the Carbon Trust, Energy Futures Lab, Imperial College EDF UK R&D Centre*, p. 9, 2012.

[16] Department for Business, Energy and Industrial, "Digest of United Kingdom energy statistics," July 2016.

[17] B. Drysdale, J. Wu, and N. Jenkins, "Flexible demand in the GB domestic electricity sector in 2030," *Applied Energy*, vol. 139, pp. 281-290, 2015.

[18] M. Cheng, J. Wu, S. Galsworthy, N. Jenkins, and W. Hung, "Availability of load to provide frequency response in the Great Britain power system," in *Power Systems Computation Conference (PSCC), 2014*, 2014, pp. 1-7.

[19] National Grid plc, (accessed June 2017) "*Frequency Response Services-General Description*" [Online]. Available: http://www2.nationalgrid.com/uk/services/balancing-services/frequency-response/.

[20] National Grid plc, (accessed June 2017) *"Mandatory Frequency Response-General description"* [online]. Available: http://www2.nationalgrid.com/uk/services/balancing-services/frequency-response/mandatory-frequency-response/.
[21] National Grid plc, "The grid code," Issue 5, Revision 21, March 2017, [Online]. Available: http://www2.nationalgrid.com/UK/Industry-information/Electricity-codes/Grid-code/The-Grid-code/.
[22] I. Erinmez, D. Bickers, G. Wood, and W. Hung, "NGC experience with frequency control in England and Wales-provision of frequency response by generators," in *Power Engineering Society 1999 Winter Meeting, IEEE*, 1999, pp. 590-596.
[23] National Grid plc, "NETS security and quality of supply standard," Febreuary 2017, [Online]. Available: http://www2.nationalgrid.com/uk/industry-information/electricity-codes/sqss/the-sqss/.
[24] National Grid plc, (accessed June 2017)*"Mandatory Services Policy Note"* [Online]. Available: http://www2.nationalgrid.com/uk/services/balancing-services/frequency-response/mandatory-frequency-response/.
[25] National Grid plc (accessed June 2017) *"Firm Frequency Response-FAQ"* [Online]. Available: http://www2.nationalgrid.com/UK/Services/Balancing-services/Frequency-response/Firm-Frequency-Response/.
[26] National Grid plc (accessed June 2017) *"Frequency Control by Demand Management-General description"* [Online]. Available: http://www2.nationalgrid.com/uk/services/balancing-services/frequency-response/frequency-control-by-demand-management/.
[27] National Grid plc (accessed June 2017) *"Enhanced Frequency Response-General Description"* [Online]. Available: http://www2.nationalgrid.com/Enhanced-Frequency-Response.aspx .
[28] National Grid plc (accessed June 2017) "*Enhanced Frequency Response FAQs*" [Online]. Available: http://www2.nationalgrid.com/Enhanced-Frequency-Response.aspx
[29] UK Government, National Infrastructure Commission, "Smart power," March 2016.
[30] National Grid plc (accessed June 2017) *"Firm Frequency Response-Services Reports"* [Online]. Available: http://www2.nationalgrid.com/UK/Industry-information/Electricity-transmission-operational-data/Report-explorer/Services-Reports/
[31] M. R. Narimani, J.-Y. Joo, and M. L. Crow, "The effect of demand response on distribution system operation," in *Power and Energy Conference at Illinois (PECI), 2015 IEEE*, 2015, pp. 1-6.
[32] Statutory Instruments, "The electricity safety, quality and continuity regulations," 2002.
[33] M. H. Bollen and F. Hassan, *Integration of distributed generation in the power system* vol. 80, John wiley & sons, 2011.
[34] D. R. Patrick and S. W. Fardo, *Electrical Distribution Systems*, The Fairmont Press, Inc., 2009.
[35] N. Hadjsaïd and J.-C. Sabonnadière, *Electrical distribution networks*, John Wiley & Sons, 2013.
[36] National Grid plc, "System Operability Framework" September 2014, [Online]. Available: http://www2.nationalgrid.com/UK/Industry-information/Future-of-Energy/System-Operability-Framework/

[37] Z. Akhtar, B. Chaudhuri, and S. Y. R. Hui, "Smart loads for voltage control in distribution networks," *IEEE Transactions on Smart Grid*, vol. 99, pp. 1-10, 2015.
[38] H. H. Zeineldin, Y. A.-R. I. Mohamed, V. Khadkikar, and V. R. Pandi, "A protection coordination index for evaluating distributed generation impacts on protection for meshed distribution systems," *IEEE Transactions on Smart Grid*, vol. 4, pp. 1523-1532, 2013.
[39] G. Putrus, P. Suwanapingkarl, D. Johnston, E. Bentley, and M. Narayana, "Impact of electric vehicles on power distribution networks," in *Vehicle Power and Propulsion Conference, 2009. VPPC'09. IEEE*, 2009, pp. 827-831.
[40] R. Liu, L. Dow, and E. Liu, "A survey of PEV impacts on electric utilities," in *Innovative Smart Grid Technologies (ISGT), 2011 IEEE PES*, 2011, pp. 1-8.
[41] N. Mahmud and A. Zahedi, "Review of control strategies for voltage regulation of the smart distribution network with high penetration of renewable distributed generation," *Renewable and Sustainable Energy Reviews*, vol. 64, pp. 582-595, 2016.
[42] A. Navarro-Espinosa and L. F. Ochoa, "Probabilistic impact assessment of low carbon technologies in LV distribution systems," *IEEE Transactions on Power Systems*, vol. 31, pp. 2192-2203, 2016.
[43] C. Protopapadaki and D. Saelens, "Heat pump and PV impact on residential low-voltage distribution grids as a function of building and district properties," *Applied Energy*, vol. 192, pp. 268-281, 2017.
[44] C. Wang, J. Wu, J. Ekanayake, and N. Jenkins, *Smart Electricity Distribution Networks*, CRC Press, 2017.
[45] N. Hatziargyriou, *MicroGrids*, wiley-IEEE press, 2014.
[46] P. Lund, "The danish cell project-part 1: Background and general approach," in *Power Engineering Society General Meeting, 2007. IEEE*, 2007, pp. 1-6.
[47] D. Pudjianto, C. Ramsay, and G. Strbac, "Virtual power plant and system integration of distributed energy resources," *IET Renewable Power Generation*, vol. 1, pp. 10-16, 2007.
[48] X. Luo, J. Wang, M. Dooner, and J. Clarke, "Overview of current development in electrical energy storage technologies and the application potential in power system operation," *Applied Energy*, vol. 137, pp. 511-536, 2015.
[49] M. Aneke and M. Wang, "Energy storage technologies and real life applications–a state of the art review," *Applied Energy*, vol. 179, pp. 350-377, 2016.
[50] H. Chen, T. N. Cong, W. Yang, C. Tan, Y. Li, and Y. Ding, "Progress in electrical energy storage system: A critical review," *Progress in Natural Science*, vol. 19, pp. 291-312, 2009.
[51] I. Staffell and M. Rustomji, "Maximising the value of electricity storage," *Journal of Energy Storage*, vol. 8, pp. 212-225, 2016.
[52] A. G. Ter-Gazarian, *Energy storage for power systems*, Institution of Engineering and Technology, 2nd ed., 2011.
[53] D. Rastler, *Electricity energy storage technology options: a white paper primer on applications, costs and benefits*, Electric Power Research Institute, 2010.
[54] A. J. Pimm, S. D. Garvey, and M. de Jong, "Design and testing of Energy Bags for underwater compressed air energy storage," *Energy*, vol. 66, pp. 496-508, 2014.
[55] Beacon Power co., (accessed April 2014)*"Beacon Power Technology Brochure"* [Online]. Available: http://beaconpower.com/resources/

[56] E. Navarro, J. G. Posada, A. Rennie, D. Rogers, G. Strbac, S. P. Villar, *et al.*, "UK research needs in grid scale energy storage technologies," 2016.
[57] D. Steward, G. Saur, M. Penev, and T. Ramsden, "Lifecycle cost analysis of hydrogen versus other technologies for electrical energy storage," *US National Renewable Energy Laboratory (NREL)*, 2009.
[58] M. Korpås and C. J. Greiner, "Opportunities for hydrogen production in connection with wind power in weak grids," *Renewable Energy*, vol. 33, pp. 1199-1208, 2008.
[59] B. Scrosati and J. Garche, "Lithium batteries: Status, prospects and future," *Journal of Power Sources*, vol. 195, pp. 2419-2430, 2010.
[60] F. Díaz-González, A. Sumper, O. Gomis-Bellmunt, and R. Villafáfila-Robles, "A review of energy storage technologies for wind power applications," *Renewable and Sustainable Energy Reviews*, vol. 16, pp. 2154-2171, 2012.
[61] O. S. Popel' and A. B. Tarasenko, "Modern kinds of electric energy storages and their application in independent and centralized power systems," *Thermal Engineering*, vol. 58, pp. 883-893, 2011.
[62] X. Tan, Q. Li, and H. Wang, "Advances and trends of energy storage technology in Microgrid," *International Journal of Electrical Power & Energy Systems*, vol. 44, pp. 179-191, 2013.
[63] T. Oshima, M. Kajita, and A. Okuno, "Development of Sodium-Sulfur batteries," *International Journal of Applied Ceramic Technology*, vol. 1, pp. 269-276, 2004.
[64] P. Taylor, R. Bolton, D. Stone, X.-P. Zhang, C. Martin, and P. Upham, "Pathways for energy storage in the UK," *Report for the Centre for Low Carbon Futures*, York, March 2012.
[65] Y. Morioka, S. Narukawa, and T. Itou, "State-of-the-art of alkaline rechargeable batteries," *Journal of Power Sources*, vol. 100, pp. 107-116, 11/30/ 2001.
[66] P. J. Hall and E. J. Bain, "Energy-storage technologies and electricity generation," *Energy Policy*, vol. 36, pp. 4352-4355, 2008.
[67] D. Sutanto and K. W. E. Cheng, "Superconducting magnetic energy storage systems for power system applications," in *Applied Superconductivity and Electromagnetic Devices, 2009. ASEMD 2009. International Conference on*, 2009, pp. 377-380.
[68] C. A. Luongo, "Superconducting storage systems: an overview," *Magnetics, IEEE Transactions on*, vol. 32, pp. 2214-2223, 1996.
[69] R. Alanen, G. Appetecchi, and M. Conte, "EERA joint programme on smart grids," *European Energy Research Alliance*, pp. 1-111, 2012.
[70] International Electrotechnical Commission, "electrical energy storage - white paper," December 2011.
[71] Dominion Virginia Power. (accessed March 2014). *Bath County Pumped Storage Station*. Available: https://www.dom.com/about/stations/hydro/bath-county-pumped-storage-station.jsp
[72] F. Crotogino, K. Mohmeyer, and R. Scharf, "Huntorf CAES:More than 20 Years of Successful Operation," Solution Mining Research Institute Meeting, Orlando, USA, 2001.
[73] M. Lazarewicz., "Status of flywheel storage operation of first frequency regulation plants," 2011, [Online]. Available: www.beaconpower.com/files/EESAT_2011_Final.pdf
[74] Ø. Ulleberg, T. Nakken, and A. Eté, "The wind/hydrogen demonstration system at Utsira in Norway: Evaluation of system performance using operational data

and updated hydrogen energy system modeling tools," *International Journal of Hydrogen Energy*, vol. 35, pp. 1841-1852, 2010.

[75] W. V. Hassenzahl, D. W. Hazelton, B. K. Johnson, P. Komarek, M. Noe, and C. T. Reis, "Electric power applications of superconductivity," *Proceedings of the IEEE*, vol. 92, pp. 1655-1674, 2004.

[76] China's Great Science and Technology (accessed March 2014) *China to Complete World's First 4 in 1 Hybrid Green Power Station,* [online]. Available: http://www.chinatechgadget.com/china-to-complete-worlds-first-4in1-hybrid-green-power-station.html

[77] Clean Energy (accessed March 2014). *Tomamae Wind Villa Power Plant /Case Study*, [online]. Available: http://www.cleanenergyactionproject.com/CleanEnergyActionProject/CS.Tomamae_Wind_Villa_Power_Plant___Energy_Storage_Case_Study.html

[78] Japan Wind Development Co. (accessed March 2014). *World's 1st Commercial Application of CaFrESS:Rokkashomura-Futamata Wind Power Plant* [online]. Available: http://www.cir-strategy.com/uploads/Kuhrt.pdf

[79] T. Siostrzonek, A. Penczek, and S. Pirog, "The control and structure of the power electronic system supplying the Flywheel Energy Storage (FES)," in *Power Electronics and Applications, 2007 European Conference on*, 2007, pp. 1-8.

[80] H. Hofmann and S. R. Sanders, "Optimal efficiency controller for synchronous reluctance flywheel drive," in *Telecommunications Energy Conference, 1998. INTELEC. Twentieth International*, 1998, pp. 724-731.

[81] S. Talebi, B. Nikbakhtian, A. K. Chakali, and H. A. Toliyat, "Control design of an advanced high-speed FESS for pulsed power applications," in *Industrial Electronics, 2008. IECON 2008. 34th Annual Conference of IEEE*, 2008, pp. 3358-3363.

[82] G. O. Suvire, M. G. Molina, and P. E. Mercado, "Improving the Integration of Wind Power Generation Into AC Microgrids Using Flywheel Energy Storage," *Smart Grid, IEEE Transactions on*, vol. 3, pp. 1945-1954, 2012.

[83] R. Sebastián and R. Peña Alzola, "Flywheel energy storage systems: Review and simulation for an isolated wind power system," *Renewable and Sustainable Energy Reviews*, vol. 16, pp. 6803-6813, 2012.

[84] M. E. Amiryar and K. R. Pullen, "A Review of Flywheel Energy Storage System Technologies and Their Applications," *Applied Sciences*, vol. 7, p. 286, 2017.

[85] B. Biswal (accessed April 2017). *World's Biggest Battery Energy Storage Facilities*, [online]. Available: http://utilitiesretail.energy-business-review.com/news/worlds-biggest-battery-energy-storage-facilities-5781056

[86] SIEMENS, "SIESTORAGE: The modular energy storage system for a sustainable energy supply," Munich, Germany, 2012.

[87] S. Banerjee, J. Chatterjee, and S. Tripathy, "Application of magnetic energy storage unit as load-frequency stabilizer," *IEEE Transactions on Energy Conversion*, vol. 5, pp. 46-51, 1990.

[88] G. Delille, B. Francois, and G. Malarange, "Dynamic frequency control support by energy storage to reduce the impact of wind and solar generation on isolated power system's inertia," *IEEE Transactions on Sustainable Energy*, vol. 3, pp. 931-939, 2012.

[89] D. Kottick, M. Blau, and D. Edelstein, "Battery energy storage for frequency regulation in an island power system," *IEEE Transactions on Energy Conversion*, vol. 8, pp. 455-459, 1993.

[90] N. Hamsic, A. Schmelter, A. Mohd, E. Ortjohann, E. Schultze, A. Tuckey, *et al.*, "Stabilising the grid voltage and frequency in isolated power systems using a flywheel energy storage system," in *The Great Wall World Renewable Energy Forum*, 2006, pp. 1-6.
[91] Renewable Energy Association, "Energy storage in the UK: an overview," 2015.
[92] *YOUNICOS*, (accessed June 2017) *YOUNICOS TO BUILD 49 MW BATTERY SYSTEM IN UK*, [online]. Available: https://www.younicos.com/younicos-deliver-49-mw-battery-system-uk/
[93] M. Kashem and G. Ledwich, "Energy requirement for distributed energy resources with battery energy storage for voltage support in three-phase distribution lines," *Electric power systems research*, vol. 77, pp. 10-23, 2007.
[94] P. Wang, D. H. Liang, J. Yi, P. F. Lyons, P. J. Davison, and P. C. Taylor, "Integrating Electrical Energy Storage Into Coordinated Voltage Control Schemes for Distribution Networks," *IEEE Transactions on Smart Grid*, vol. 5, pp. 1018-1032, 2014.
[95] L. Wang, D. H. Liang, A. F. Crossland, P. C. Taylor, D. Jones, and N. S. Wade, "Coordination of multiple energy storage units in a low-voltage distribution network," *IEEE Transactions on Smart Grid*, vol. 6, pp. 2906-2918, 2015.
[96] UK Power Networks, "Smarter Network Storage - business model consultation," 2013.
[97] B. Li, J. Shen, X. Wang, and C. Jiang, "From controllable loads to generalized demand-side resources: A review on developments of demand-side resources," *Renewable and Sustainable Energy Reviews*, vol. 53, pp. 936-944, 2016.
[98] N. G. Paterakis, O. Erdinç, and J. P. Catalão, "An overview of demand response: Key-elements and international experience," *Renewable and Sustainable Energy Reviews*, vol. 69, pp. 871-891, 2017.
[99] Western Power Distribution, "Project FALCON: Commercial trials final report," UK, 2015.
[100] G. Strbac, "Demand side management: Benefits and challenges," *Energy policy*, vol. 36, pp. 4419-4426, 2008.
[101] M. Cheng, J. Wu, S. J. Galsworthy, C. E. Ugalde-Loo, N. Gargov, W. W. Hung, *et al.*, "Power system frequency response from the control of bitumen tanks," *IEEE Transactions on Power Systems*, vol. 31, pp. 1769-1778, 2016.
[102] Power Responsive, "Demand side flexibility annual report," UK, 2016.
[103] Energyst, "Demand side response report," UK, 2015.
[104] Element Energy, "Demand side response in the non-domestic sector," *Prepared for Ofgem*,UK, 2012.
[105] M. Cheng, J. Wu, J. Ekanayake, T. Coleman, W. Hung, and N. Jenkins, "Primary frequency response in the Great Britain power system from dynamically controlled refrigerators," *22nd International conference and exhibition on electricity distribution*, 2013.
[106] J. A. Short, D. G. Infield, and L. L. Freris, "Stabilization of grid frequency through dynamic demand control," *IEEE Transactions on Power Systems*, vol. 22, pp. 1284-1293, 2007.
[107] M. T. Muhssin, L. M. Cipcigan, N. Jenkins, M. Cheng, and Z. A. Obaid, "Modelling of a population of Heat Pumps as a Source of load in the Great Britain power system," in *Smart Systems and Technologies (SST), International Conference on*, 2016, pp. 109-113.
[108] S. Koch, M. Zima, and G. Andersson, "Active coordination of thermal household appliances for load management purposes," *IFAC Proceedings Volumes*, vol. 42, pp. 149-154, 2009.

[109] N. Lu, "An evaluation of the HVAC load potential for providing load balancing service," *IEEE Transactions on Smart Grid*, vol. 3, pp. 1263-1270, 2012.
[110] M. Cheng, J. Wu, S. J. Galsworthy, N. Gargov, W. H. Hung, and Y. Zhou, "Performance of industrial melting pots in the provision of dynamic frequency response in the Great Britain power system," *Applied Energy*, vol. 201,pp. 245-256, *2017*.
[111] A. Zakariazadeh, O. Homaee, S. Jadid, and P. Siano, "A new approach for real time voltage control using demand response in an automated distribution system," *Applied Energy*, vol. 117, pp. 157-166, 2014.
[112] J. Petinrin and M. Shaaban, "Voltage control in a smart distribution network using demand response," in *Power and Energy (PECon), 2014 IEEE International Conference on*, 2014, pp. 319-324.
[113] P. J. Douglass, R. Garcia-Valle, J. Østergaard, and O. C. Tudora, "Voltage-sensitive load controllers for voltage regulation and increased load factor in distribution systems," *IEEE Transactions on Smart Grid*, vol. 5, pp. 2394-2401, 2014.
[114] D. Wang, S. Ge, H. Jia, C. Wang, Y. Zhou, N. Lu, *et al.*, "A demand response and battery storage coordination algorithm for providing microgrid tie-line smoothing services," *IEEE Transactions on Sustainable Energy*, vol. 5, pp. 476-486, 2014.
[115] A. G. Tsikalakis and N. D. Hatziargyriou, "Centralized control for optimizing microgrids operation," in *Power and Energy Society General Meeting, 2011 IEEE*, 2011, pp. 1-8.
[116] S. Hakimi and S. M. Tafreshi, "Smart virtual energy storage control strategy to cope with uncertainties and increase renewable energy penetration," *Journal of Energy Storage*, vol. 6, pp. 80-94, 2016.
[117] D. Papadaskalopoulos, D. Pudjianto, and G. Strbac, "Decentralized coordination of microgrids with flexible demand and energy storage," *IEEE Transactions on Sustainable Energy*, vol. 5, pp. 1406-1414, 2014.
[118] J. Yi, P. Wang, P. C. Taylor, P. J. Davison, P. F. Lyons, D. Liang, *et al.*, "Distribution network voltage control using energy storage and demand side response," in *Innovative Smart Grid Technologies (ISGT Europe), 2012 3rd IEEE PES International Conference and Exhibition on*, 2012, pp. 1-8.
[119] X. Jin, Y. Mu, H. Jia, J. Wu, T. Jiang, and X. Yu, "Dynamic economic dispatch of a hybrid energy microgrid considering building based virtual energy storage system," *Applied Energy*, vol. 194, pp. 386-398, 2017.
[120] J. T. Hughes, A. D. Domínguez-García, and K. Poolla, "Identification of virtual battery models for flexible loads," *IEEE Transactions on Power Systems*, vol. 31, pp. 4660-4669, 2016.
[121] H.-J. Bullinger, C. Doetsch, and P. Bretschneider, "Smart grids-the answer to the new challenges of energy logistics?," *DICE Report*, vol. 10, p. 29, 2012.
[122] Upside energy co. (accessed Septemper 7th). [online]. Available: https://upsideenergy.co.uk/.
[123] C. Chapelsky, J. Salmon, and A. Knight, "Control of a high-inertia flywheel as part of a high capacity energy storage system," in *Electrical and Computer Engineering, 2007. CCECE 2007. Canadian Conference on*, 2007, pp. 1437-1440.
[124] O. Tremblay, L. A. Dessaint, and A. I. Dekkiche, "A Generic battery model for the dynamic simulation of hybrid electric vehicles," in *2007 IEEE Vehicle Power and Propulsion Conference*, 2007, pp. 284-289.

[125] S. Teleke, M. E. Baran, S. Bhattacharya, and A. Q. Huang, "Optimal control of battery energy storage for wind farm dispatching," *IEEE Transactions on Energy Conversion*, vol. 25, pp. 787-794, 2010.
[126] N. Sforza (accessed April 2017). *How Does a Refrigerator Work?*, [online]. Available: https://www.realsimple.com/food-recipes/tools-products/appliances/how-does-refrigerator-work
[127] Mineral Products Association, "Guidance for safe bitumen tank management," UK, 2013.
[128] Panasonic, "Panasonic batteries: Nickel metal hydride handbook," 2003.
[129] National Grid plc, "Enhance frequency response: invitation to tender for pre-qualified parties," 2016 [Online]. Available: http://www2.nationalgrid.com/Enhanced-Frequency-Response.aspx
[130] T. A. Bopp, "Technical and commercial integration of distributed and renewable energy sources into existing electricity networks," University of Manchester, 2006.
[131] P. Kundur, N. J. Balu, and M. G. Lauby, *Power system stability and control*, vol. 7, New York: McGraw-hill, 1994.
[132] A. J. Wood and B. F. Wollenberg, *Power generation, operation, and control*, 3ed, John Wiley & Sons, 2013.
[133] J. Ekanayake, N. Jenkins, and G. Strbac, "Frequency response from wind turbines," *Wind Engineering*, vol. 32, pp. 573-586, 2008.
[134] Office for national statistics, "Total number of households by region and country of the UK, 1996 to 2016," UK, 2016.
[135] AMDEA (accessed June 2016) "The Time to Change Programme encouraging energy efficiency in UK households" [Online]. Available: http://www.powershow.com/view/126be5-NDIzO/The_Time_to_Change_Programme_encouraging_energy_efficiency_in_UK_households_powerpoint_ppt_presentation
[136] National Grid plc, "Post assessment tender report," December 2014.
[137] National Grid plc, (accessed June 2017) "Services reports FFR market information" [Online]. Available: http://www2.nationalgrid.com/UK/Industry-information/Electricity-transmission-operational-data/Data-explorer/Outcome-Energy-Services/
[138] Y. He, M. Petit, and P. Dessante, "Optimization of the steady voltage profile in distribution systems by coordinating the controls of distributed generations," in *2012 3rd IEEE PES Innovative Smart Grid Technologies Europe (ISGT Europe)*, 2012, pp. 1-7.
[139] Distributed Generation and Sustainable Electrical Energy Centre (accessed June 2017) "United Kingdom Generic Distribution System (UKGDS) [Online]. Available: https://github.com/sedg/ukgds
[140] R. Currie, G. Ault, and J. McDonald, "Methodology for determination of economic connection capacity for renewable generator connections to distribution networks optimised by active power flow management," *IEE Proceedings-Generation, Transmission and Distribution*, vol. 153, pp. 456-462, 2006.
[141] R. D. Zimmerman, C. E. Murillo-Sanchez, and R. J. Thomas, "MATPOWER: Steady-state operations, planning, and analysis tools for power systems research and education," *IEEE Transactions on Power Systems*, vol. 26, pp. 12-19, 2011.
[142] M. Wilcox, "smarter network storage the uk's largest electrical energy storage system," UK, 2014.

[143] A. Yazdani and R. Iravani, *Voltage-sourced converters in power systems: modeling, control, and applications*, John Wiley & Sons, 2010.
[144] L. Wang, *Modeling and Control of Sustainable Power Systems: Towards Smarter and Greener Electric Grids*, Springer, 2011.
[145] O. W. Paul C Krause, Scott D. Sudhoff, *Analysis of Electric machinery and Drive Systems*. USA: John Willy an Sons, 2002.
[146] F. Díaz-González, A. Sumper, O. Gomis-Bellmunt, and R. Villafafila-Robles, "Modeling, control and experimental validation of a flywheel-based energy storage device," *EPE Journal*, vol. 23, pp. 41-51, 2013.
[147] R. Krishnan, *Electric motor Drives modeling, Analysis, and control*, upper saddle river, New Jersey: Prentice Hall, 2001.

An average model of a flywheel energy storage system

As shown in Fig. 3.1, the average model consists of a DC busbar which connects a back to back converters and an electrical machine.

A. Modelling and control of the grid side converter and DC busbar

Figure A.1 shows the model of an ideal (average) three-phase converter used [143, 144] in this research. The ac side is represented by an ideal Voltage Source Converter (VSC). The DC side is represented by an ideal current source connected with the DC busbar capacitance in parallel.

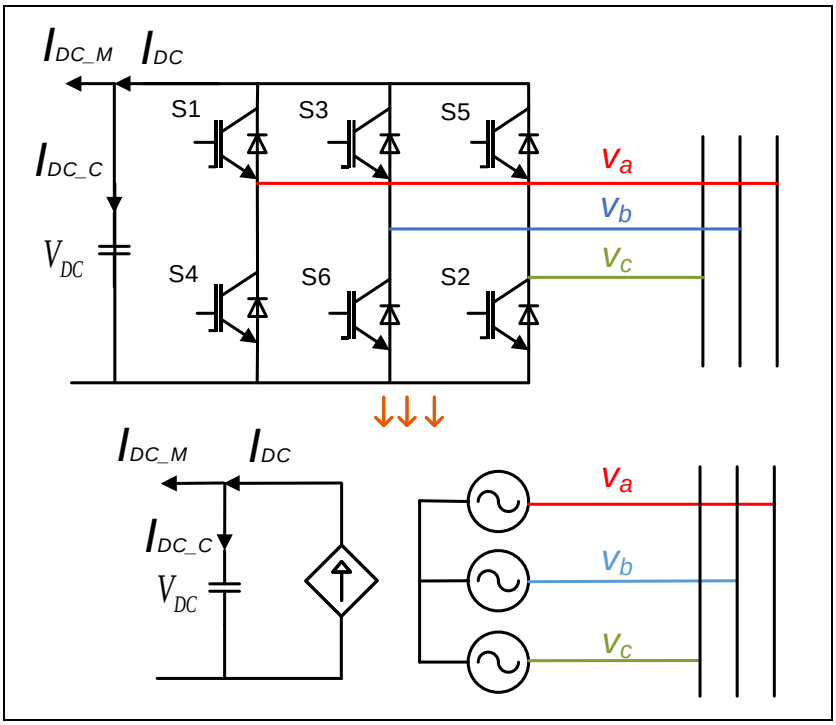

Fig. A.1 A model of an average voltage source converter and the DC busbar.

Neglecting converter losses, the active power on both sides are equal [143]:

$$P_{DC} = P_{ac} \tag{A.1}$$

$$P_{DC} = V_{DC} \times I_{DC} \tag{A.2}$$

$$P_{ac} = v_a \times i_a + v_b \times i_b + v_c \times i_c \tag{A.3}$$

where

P_{DC}, P_{ac}: DC side and ac side powers of the converter (W).

V_{DC}, I_{DC}: Voltage and current of the converter DC side (V, A).

I_{DC_M} : Current flow to the other side of the DC bausbar (i.e. to the machine side) (A).

I_{DC_C}: Current follows through the DC busbar capacitor (A).

$v_{a,b,c}$, $i_{a,b,c}$: Instantaneous voltages and currents of the converter ac side (V, A).

Figure A.2 shows the grid side converter control scheme. The control scheme consists of a phase-locked loop, current controllers and a DC voltage controller.

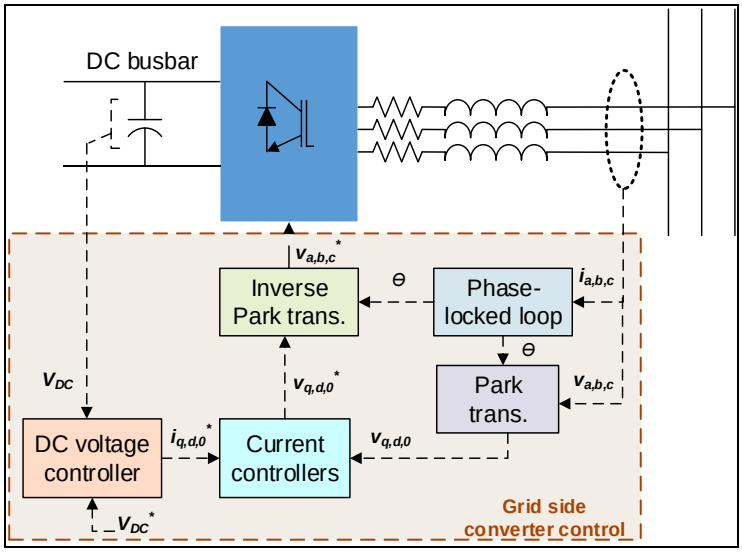

Fig. A.2 The control scheme of the grid side converter.

To simplify the converter control design, a frame of two rotating phases was adopted. Using Park transformation, the three stationary phases (i.e. *abc*) are resolved into two rotating phases; quadratic (*q*) and 90° lag direct (*d*) phases.

1) Park transformation

The three-phase currents in the stationary frame are [131]

$$i_a = i_s \times \sin(\omega t) \quad \text{(A.4.a)}$$

$$i_b = i_s \times \sin\left(\omega t - \frac{2\pi}{3}\right) \quad \text{(A.5.b)}$$

$$i_c = i_s \times \sin\left(\omega t + \frac{2\pi}{3}\right) \quad \text{(A.6.c)}$$

where is is the peak current (A) and ω is the synchronous velocity (rad/sec).

The Park transformation is

$$\begin{bmatrix} q \\ d \\ 0 \end{bmatrix} = K \begin{bmatrix} a \\ b \\ c \end{bmatrix} \quad \text{(A.7)}$$

$$K = \frac{2}{3}\begin{bmatrix} \cos(\theta) & \cos(\theta - \frac{2}{3}\pi) & \cos(\theta + \frac{2}{3\pi}) \\ \sin(\theta) & \sin(\theta - \frac{2}{3\pi}) & \sin(\theta + \frac{2}{3\pi}) \\ 1/2 & 1/2 & 1/2 \end{bmatrix} \quad \text{(A.8)}$$

where *K* is the Park transformation matrix and θ is the angle between the quadratic phase and phase *a*.

Then the two-phase currents in the rotating frame are:

$$i_q = \frac{2}{3}[i_s \times \sin(\omega t) \times \cos(\theta) + i_s \times \sin\left(\omega t - \frac{2\pi}{3}\right) \times \cos\left(\theta - \frac{2\pi}{3}\right) + i_s \times \sin\left(\omega t + \frac{2\pi}{3}\right) \times \cos\left(\theta + \frac{2\pi}{3}\right)]$$

$$i_d = \frac{2}{3}[i_s \times \sin(\omega t) \times \sin(\theta) + i_s \times \sin\left(\omega t - \frac{2\pi}{3}\right) \times \sin\left(\theta - \frac{2\pi}{3}\right) + i_s \times \sin\left(\omega t + \frac{2\pi}{3}\right) \times \sin\left(\theta + \frac{2\pi}{3}\right)]$$

$$i_0 = \frac{2}{3}[i_s \times \sin(\omega t) \times \frac{1}{2} + i_s \times \sin\left(\omega t - \frac{2\pi}{3}\right) \times \frac{1}{2} + i_s \times \sin\left(\omega t + \frac{2\pi}{3}\right) \times \frac{1}{2}]$$

$$i_q = i_s \times \cos(\omega t - \theta) \quad \text{(A.9.a)}$$

$$i_d = -i_s \times \sin(\omega t - \theta) \quad \text{(A.9.b)}$$

$$i_0 = \tfrac{1}{3}(i_a + i_b + i_c) \quad \text{(A.9.c)}$$

In the presence of a balanced three-wire system operation, the third set of variables (*0*-component) should be zero as well.

$$i_a + i_b + i_c = 0 \quad \text{(A.10)}$$

2) Phase-Locked Loop

The Phase-Locked Loop (PLL) determines the angular velocity and the angle θ of the grid, hence synchronises the three-phase frame variables of the converter with the grid three-phase frame variables. The two-phase voltages in the rotating frame are [143]:

$$v_d = v_s \times \sin(\omega t - \rho) \quad \text{(A.11.a)}$$

$$v_q = v_s \times \cos(\omega t - \rho) \quad \text{(A.11.b)}$$

where $v_{d,q}$ are the direct and quadratic voltages, v_s is the pack voltage, ω is the synchronous velocity and ρ is the three-phase stationary frame rotate angle.

The phase-locked loop dynamically synchronises the two-phase rotating frame (A.11) of the converter to the grid three-phase stationary frame by setting direct axis voltage v_d to zero (i.e. $\rho=\omega t$) [143].

Figure A.3 shows the three-phase phase-locked loop control scheme. The direct axis voltage v_d which was obtained by the Park transformation is filtered by a PI controller. The output of the PI controller corresponds to the angular velocity ω and the integration of the angular velocity signal corresponds to the grid angle θ.

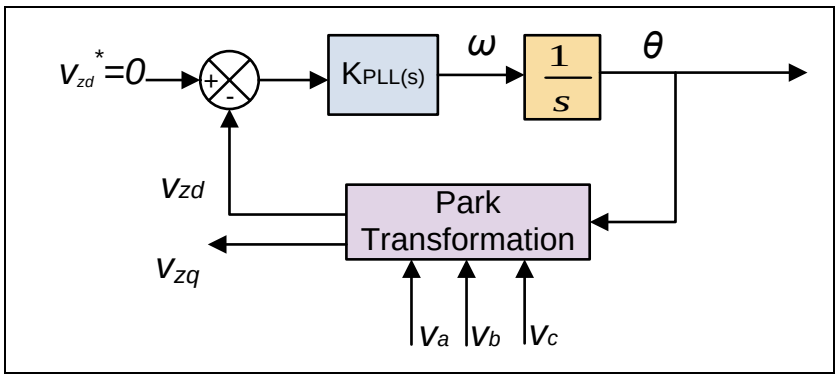

Fig. A.3 The phase-locked loop control.

The PI controller consists of a time constant (τ_{PLL}) and a controller coefficient K_p.

$$K_{PLL} = K_p \times \left(\frac{\frac{1}{\tau_{PLL}} + s}{s}\right) \quad \text{(A.7)}$$

The PI coefficients were tuned to values of K_p=10 and τ_{PLL}=0.01 s.

3) Current loop controllers of the grid-side converter

Figure A.4 shows the model of the ac side of the grid side converter connected to the grid. The two sets of ideal voltage sources are connected through an inductance and a resistance (i.e. RL filter).

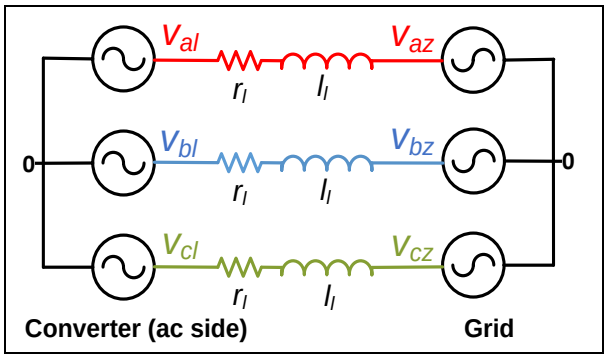

Fig. A.4 A model of the ac side of the converter connected to the grid.

The voltage equations for the converter ac side in the three-phase stationary frame are [144]:

$$\begin{bmatrix} v_{az} \\ v_{bz} \\ v_{cz} \end{bmatrix} - \begin{bmatrix} v_{al} \\ v_{bl} \\ v_{cl} \end{bmatrix} - (v_{0l} - v_{0z}) \begin{bmatrix} 1 \\ 1 \\ 1 \end{bmatrix} = \begin{bmatrix} r_l & 0 & 0 \\ 0 & r_l & 0 \\ 0 & 0 & r_l \end{bmatrix} \begin{bmatrix} i_a \\ i_b \\ i_c \end{bmatrix} + \begin{bmatrix} l_l & 0 & 0 \\ 0 & l_l & 0 \\ 0 & 0 & l_l \end{bmatrix} \frac{d}{dt} \begin{bmatrix} i_a \\ i_b \\ i_c \end{bmatrix} \quad \text{(A.8)}$$

where v_{za}, v_{zb} and v_{zc} are the three-phase instantaneous grid voltages (V), v_{la}, v_{lb} and v_{lc} are the three-phase instantaneous converter voltages (V) in the three-phase frame, i_a, i_b and i_c are the three-phase instantaneous currents (A) in the three-phase frame, r_l is the inductance equivalent resistance (Ω), and l_l is the inductance value (H) of the RL filter.

In three wire balanced systems, the zero-sequence current and voltages are equal zero. Therefore, (A.8) can be rewritten in the two rotating phases frame as follows [144, 145]:

$$\begin{bmatrix} v_{zq} \\ v_{zd} \end{bmatrix} - \begin{bmatrix} v_{lq} \\ v_{ld} \end{bmatrix} = \begin{bmatrix} r_l & -l_l w_e \\ l_l \omega_e & r_l \end{bmatrix} \begin{bmatrix} i_q \\ i_d \end{bmatrix} + \begin{bmatrix} l_l & 0 \\ 0 & l_l \end{bmatrix} \frac{d}{dt} \begin{bmatrix} i_q \\ i_d \end{bmatrix} \quad \text{(A.9)}$$

where v_{zq} ,v_{zd}, v_{lq} v_{ld} are the grid and the converter two rotating phases frame voltages (V), i_q and i_d are two rotating phases frame currents (A) and ω_e is the electrical angular velocity (rad/s).

Equation (A.9) can be rewritten to obtain decoupled linear systems as follows [144]:

$$v_{zq} = v_{lq} + \hat{v_{lq}} - l_l \times \omega_e \times i_{ld} \quad \text{(A.10.a)}$$

$$v_{zd} = v_{ld} + \hat{v_{ld}} + l_l \times \omega_e \times i_{lq} \quad \text{(A.10.b)}$$

where v_{lq}^ and v_{ld}^ are the decoupled terms [144]:

$$\begin{bmatrix} \hat{v_{lq}} \\ \hat{v_{ld}} \end{bmatrix} = \begin{bmatrix} r_l & 0 \\ 0 & r_l \end{bmatrix} \begin{bmatrix} i_q \\ i_d \end{bmatrix} + \begin{bmatrix} l_l & 0 \\ 0 & l_l \end{bmatrix} \frac{d}{dt} \begin{bmatrix} i_q \\ i_d \end{bmatrix} \quad \text{(A.11)}$$

Referring to (A.11) the relationship between the voltage and the current of the current loop controllers is derived in Laplace domain as

$$G_{q,d}(s) = \frac{i_q(s)}{\hat{v_{lq}}} = \frac{i_d(s)}{\hat{v_{ld}}} = \frac{1}{l_l \times s + r_l} \quad \text{(A.12)}$$

where $G_{q,d}$ (s) represents linear systems. PI controllers ($C_{q,d}(s)$) are proposed to control the currents

$$C_q(s) = C_d(s) = \frac{K_p \times s + K_i}{s} \quad \text{(A.13)}$$

Figure A.5 shows the converter current loop controllers. The direct voltage reference value v_{dz}^* is set to zero by the phase-locked loop.

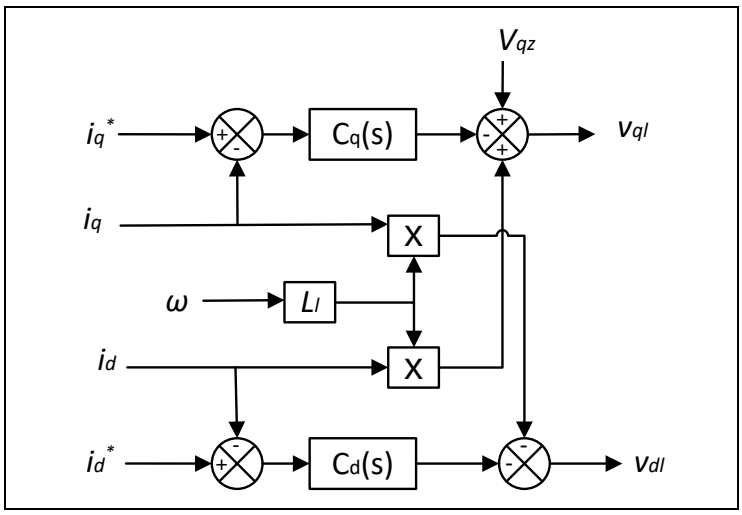

Fig. A.5 Grid converters current loop controllers.

Figure A.6 illustrates the quadratic and the direct currents loops. The internal model control technique is used to calculate the proportional and the integral coefficients of the PI controller [144]. This technique depends on the exact cancellation of the system pole by inserting a controller zero. The resultant system ($M(s)$) would have a first order transfer function.

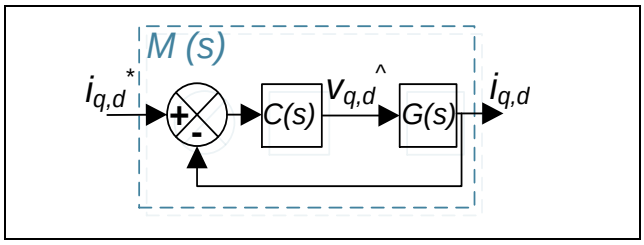

Fig. A.6 The grid side q,d current loops.

The proportional and the integral coefficients (i.e. K_p, K_i) of the PI controllers were computed based on (A.12), (A.13) and $M(s)$ as follows [144]

$$M(s) = \frac{1}{1+\tau \times s} \tag{A.14}$$

$$M(s) = \frac{C(s)\times G(s)}{1+c(s)\times G(s)} \implies C(s)\times G(s) = \frac{M(s)}{1-M(s)}$$

$$\therefore\ K_p = \frac{l_l}{\tau},\ K_i = \frac{r_l}{\tau} \tag{A.15}$$

where τ (s) is the closed-loop time constant of the electrical system. This constant must be chosen considering the converter physical restrictions, it was set to 0.001 second.

The active and the reactive powers (i.e. P_{ac}, Q_{ac}) of the converter *ac* side in the two-phase rotating frame are [143]

$$P_{ac} = {}^{3}/_{2}\,[v_{qz}\times i_q + v_{dz}\times i_d] \tag{A.16.a}$$

$$Q_{ac} = {}^{3}/_{2}\,[v_{qz}\times i_d - v_{dz}\times i_q] \quad \text{(A.16.b)}$$

The study aims to control the active power; hence the reactive power is set to zero and (v_{dz}=0) using the phase-locked loop, $i_d^*$was set to zero. Quadratic current reference value i_q^* is the output of the DC busbar voltage controller.

4) DC busbar voltage controller

Controlling the DC busbar voltage ensures the power balance between the grid and the electrical machine.

Using (A.2), (A.16.a) and (v_{dz}=0), the reference quadratic current (i_q^*) is

$$i_q{}^* = \frac{2}{3}\times V_{DC}\times\frac{I_{DC}}{v_{qz}} \quad \text{(A.17)}$$

The DC busbar voltage (V_{DC}) can by expressed in terms of its currents as

$$I_{DC} = I_{DC\_C} - I_{DC_M} \quad \text{(A.18.a)}$$

$$I_{DC\_C} = C\times\frac{dV_{DC}}{dt} \implies V_{DC} = \frac{1}{Cs}(I_{DC} + I_{DC_M}) \quad \text{(A.18.b)}$$

When the DC voltage is kept constant, the current follow through the capacitor is zero (I_{DC_C}). A PI controller is used to set the reference value of the capacitor current. The DC voltage control is shown in Fig. A.7.

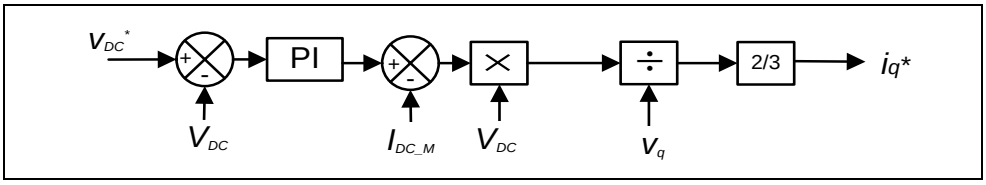

Fig. A.7 The DC busbar voltage controller.

Figure A.8 illustrates the DC busbar voltage loop diagram. In the presence of a much faster current controller loop, its effect on the DC busbar voltage loop is negligible. Referring to (A.17), a linear relationship between (i_q^*) and (I_{DC}) exists; in turn (A.18.b) shows the relationship of the DC voltage to the DC currents.

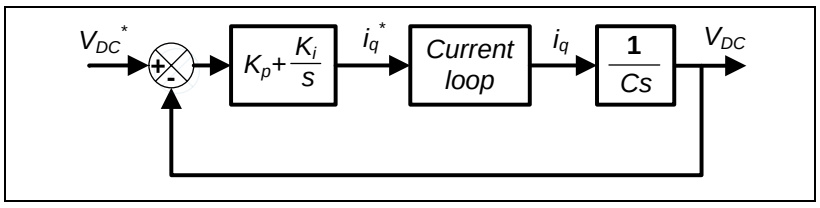

Fig. A.8 The DC busbar voltage control loop.

The closed loop transfer function of the DC busbar voltage controller can be computed as

$$\frac{V_{DC}}{V_{DC}^{*}} = \frac{(K_p+\frac{K_i}{s})\times(\frac{1}{C\times s})}{1+(K_p+\frac{K_i}{s})\times(\frac{1}{C\times s})} \Longrightarrow \frac{\frac{K_p\times s}{C}+\frac{K_i}{C}}{s^2+s\times\frac{K_p}{C}+\frac{K_i}{C}} \quad \text{(A.19)}$$

A typical second order transfer function is

$$\frac{V_{DC}}{V_{DC}^{*}} = \frac{2\times s\times\xi\times\omega_e+{\omega_e}^2}{s^2+2\times s\times\xi\times\omega_e+{\omega_e}^2} \quad \text{(A.20)}$$

where ξ is the system dumping ratio ω_e and is the desired angular velocity of the DC voltage control loop.

Comparing (A. 19) with (A.20) yields

$$K_i = C\times{\omega_e}^2 \, , K_p = 2\times\xi\times\omega_e \quad \text{(A.21)}$$

In this study, tuning the damping ratio to 0.98 and the angular velocity 11.309 rad/sec achieved the desired results.

The grid side converter parameters [146] and controllers' coefficients are listed in Table A.1 below:

TABLE A.1 PARAMETERS OF THE GRID SIDE CONVERTER, INDUCTOR, THE DC BUSBAR AND THE INTERNAL CONTROL COEFFICIENTS

Parameter	Value
phase locked-locked controller proportional gain	10
phase locked-locked time constant (s)	0.01
Inductor (resistance) (Ω)	0.3
Inductor (inductance) (mH)	4.6
DC voltage (V)	650
DC capacitor (mF)	5
q,d-axes current controller proportional gain	46
q,d-axes current controller integral gain	3000
DC voltage controller proportional gain	0.1108
DC voltage controller integral gain	0.6396

B. Modelling and control of the electrical machine

The Permanent Magnet Synchronous Machine (PMSM) was modelled. The flywheel is modelled as an additional mass added to the rotor mass of the machine. The electrical machine is modelled using the stator and the rotor voltage equations in the two rotating phases frame [123, 147]

$$v_{qm} = r_s\times i_q + L_q\times\frac{di_q}{dt} + \omega_r\times L_d\times i_d + \omega_r\times\lambda_m \quad \text{(A.22.a)}$$

$$v_{dm} = r_s \times i_d + L_d \times \frac{di_d}{dt} - \omega_r \times L_q \times i_q \quad \text{(A.22.b)}$$

$$T_e = {}^{3}/_{2}\,{}^{p}/_{2}\,[\lambda_m \times i_q + (L_d - L_q) \times i_q \times i_d] \quad \text{(A.23)}$$

$$T_e = J \times \frac{d\omega_m}{dt} \quad \text{(A.24)}$$

where

v_{dm} ,v_{qm}: Direct and quadratic voltages of the machine (V).

i_d, i_q: Direct and quadratic currents of the machine (A).

r_s: Stator winding resistance (Ω).

L_d,L_q: Direct and quadratic inductances of the machine (H).

ω_m,ω_r: Mechanical and electrical velocities of the machine (rad/sec).

λ_m: The permanent magnets flux (wb).

T_e: Electromagnetic torque developed by the machine (N.m).

J: Inertia of the machine's rotor plus the flywheel (kg.m^2).

Since this study aims to capture the active power exchanged between the machine and the grid, only the electrical machine was modelled. The active power of the machine was directly fed into the DC busbar as shown in Fig. A.9. The reactive power of the machine was set to zero.

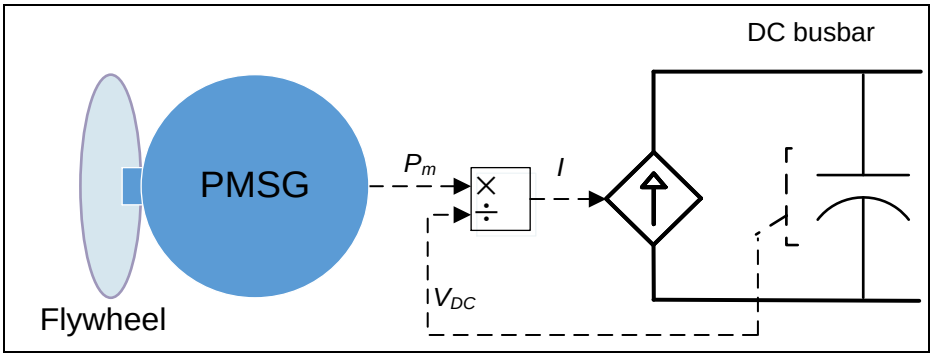

Fig. A.9 The electrical machine connection to the DC busbar.

Figure A.10 shows the electric machine control scheme. The control scheme consists of current loop controllers and the active and the reactive powers controller.

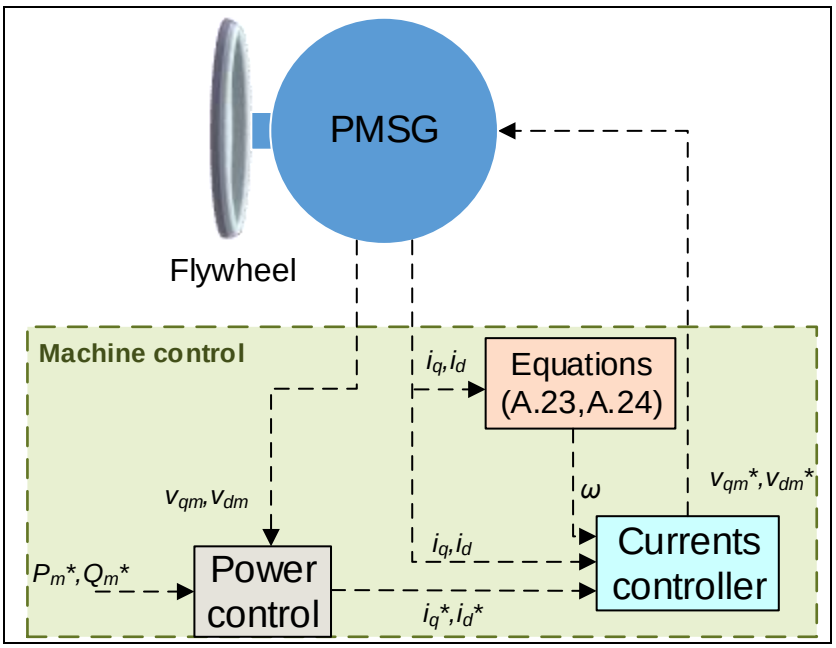

Fig. A.10 The electrical machine control scheme.

1) Current loop controllers of the machine

The same procedure and design criteria used in the grid side current loop controllers was employed in the machine side current loops controllers. Voltage equations (A.22) can be rewritten to obtain decoupled linear systems as follows

$$v_{qm} = \hat{v_{qm}} + \omega_r \times L_d \times i_d + \omega_r \times \lambda_m \quad \text{(A.25.a)}$$

$$v_{dm} = \hat{v_{dm}} - w_r \times L_q \times i_q \quad \text{(A.25.b)}$$

where $\hat{v}_{qm}$ and $\hat{v}_{dm}$ are the decoupled terms:

$$\begin{bmatrix} \hat{v_{qm}} \\ \hat{v_{dm}} \end{bmatrix} = \begin{bmatrix} r_s & 0 \\ 0 & r_s \end{bmatrix} \begin{bmatrix} i_q \\ i_d \end{bmatrix} + \begin{bmatrix} L_q & 0 \\ 0 & L_d \end{bmatrix} \frac{d}{dt} \begin{bmatrix} i_q \\ i_d \end{bmatrix} \quad \text{(A.26)}$$

Referring to (A.26) the relationship between the voltage and the current of the current loop controllers are

$$G_{qm}(s) = \frac{i_q(s)}{\hat{v_{qm}}} = \frac{1}{L_q \times s + r_s} \quad \text{(A.27.a)}$$

$$G_{dm}(s) = \frac{i_d(s)}{\hat{v_{dm}}} = \frac{1}{L_d \times s + r_s} \quad \text{(A.27.b)}$$

A PI controllers ($C_{qm,dm}(s)$) were proposed to control the currents

$$C_{qm}(s) = \frac{K_{pqm} \times s + K_{im}}{s} \quad \text{(A.28.a)}$$

$$C_{dm}(s) = \frac{K_{pdm} \times s + K_{im}}{s} \quad \text{(A.28.b)}$$

where K_{pdm}, K_{pqm}, K_{im} are the proportional and the integral coefficients of the PI controllers.

Figure A.11 shows the machine current loop controllers. Current reference values i_{qm}^* and i_{dm}^* are obtained from the active and the reactive powers controller.

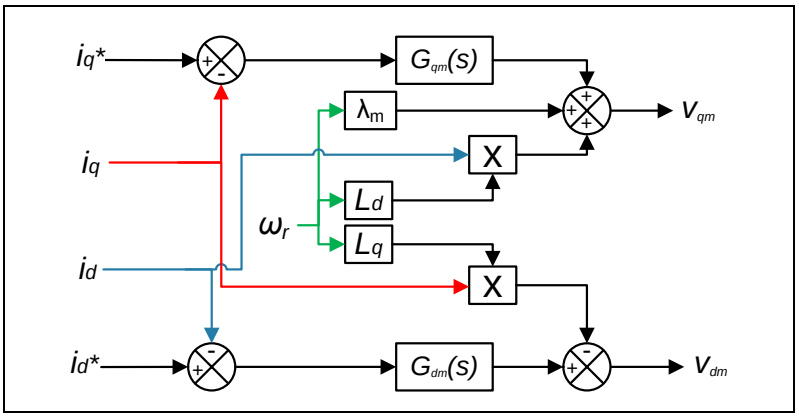

Fig. A.11 The machine current loop controllers.

Figure A.12 shows the machine currents loops diagram. A PI controller ($C_{qm,dm}(s)$) was used to control the machine $G_{q,d}(s)$. The internal model control technique was used to calculate the proportional and the integral coefficients of the PI controllers [144]. The resultant system ($N(s)$) has a first order transfer function.

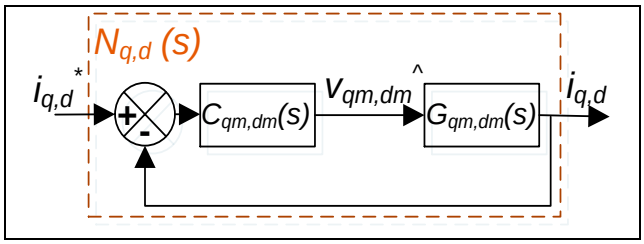

Fig. A.12 Currents control loops of the machine.

The proportional and the integral coefficients of the PI controllers were obtained from (A.27), (A.28) and $N_{q,d}(s)$ as follows:

$$N_{q,d}(s) = \frac{1}{1+\tau \times s} \tag{A.29}$$

$$N_{q,d}(s) = \frac{C_{qm,dm}(s) \times G_{qm,dm}(s)}{1+C_{qm,dm}(s) \times G_{qm,dm}(s)} \Rightarrow C_{qm,dm}(s) \times G_{qm,dm}(s) = \frac{N_{q,d}(s)}{1-N_{q,d}(s)}$$

$$K_{pqm} = \frac{L_q}{\tau} \tag{A.30.a}$$

$$K_{pdm} = \frac{L_d}{\tau} \tag{A.30.b}$$

$$K_{im} = \frac{r_s}{\tau} \tag{A.30.c}$$

where τ is the closed loop time constant. The time constant was set to 0.001 s.

The direct and the quadratic currents reference values i_d^*,i_q^* are the output of the active and the reactive powers controller.

2) Active and reactive powers controller of the machine

The electrical machine active and reactive powers controllers were directly derived from the active and reactive powers equation. The electrical machine active and reactive powers are [123]:

$$P_m = {}^{3}/_{2}\,[v_{qm}\times i_q + v_{dm}\times i_d] \quad \text{(A.31.a)}$$

$$Q_m = {}^{3}/_{2}\,[v_{dm}\times i_q - v_{qm}\times i_d] \quad \text{(A.31.b)}$$

The direct and quadratic currents reference values can be determined by rewriting the set of equations (A.31.a) and (A.31.b) as [123]

$$i_q{}^{*} = \frac{2}{3}\left[\frac{P_m\times v_{qm}+Q_m\times v_{dm}}{v_{qm}{}^{2}+v_{dm}{}^{2}}\right] \quad \text{(A.32.a)}$$

$$i_d{}^{*} = \frac{2}{3}\left[\frac{P_m\times v_{dm}-Q_m\times v_{qm}}{v_{qm}{}^{2}+v_{dm}{}^{2}}\right] \quad \text{(A.32.b)}$$

Figure A.13 shows the active and reactive power controllers of the machine.

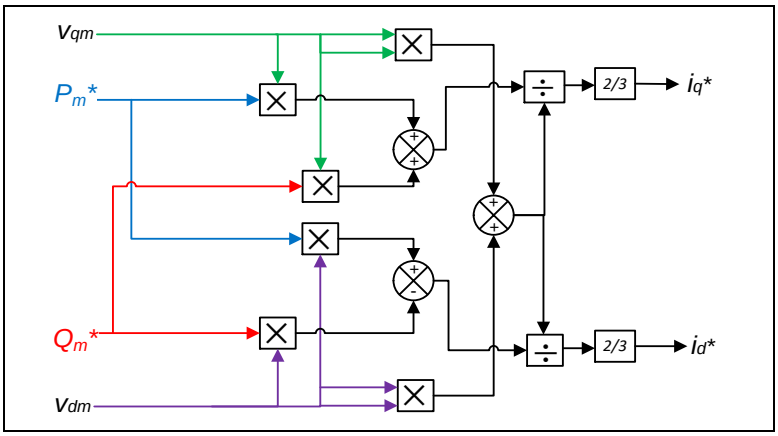

Fig. A.13 The active and the reactive powers controllers of the electrical machine.

The parameters of the electrical machine model [123] and the control coefficients used are listed in Table A.2 below.

TABLE A.2 THE MACHINE AND ITS CONTROL LOOPS COEFFICIENTS

Parameter	Value
Rated Power (kW)	50
Energy stored (kWh)	1
Flux created by the magnets (Wb)	0.0608
Rotating disc inertia (kg.m^2)	0.862
Frequency range (Hz)	515-1030
Velocity range (krpm)	15.5-31
Resistance (L-N) (mΩ)	8
Inductance on q-axis (μH)	75
Inductance on d-axis (μH)	68.5
q-axis current controller proportional gain	0.075
d-axis current controller proportional gain	0.0685
q,d-axes current controller integral gain	8

The machine model has an energy density of 1 kWh and a rated power of 50 kW (i.e. 50 kW for approximately one minute). While the grid side converter model has a rated power of 7.5 kW. Consequently, the machine power output was limited to 1.6 kW (i.e. 1.6 kW for approximately 35 minutes). The model power output to the grid was scaled up to 50 kW (i.e. by multiplying it by a factor of 31.25) to replicate the commercial flywheel energy storage system in [55].